INVESTIGATION OF PERCOLATION IN BOROSILICATE GLASS MATRIX COMPOSITES CONTAINING CONDUCTING SEGREGATED NETWORKS

A Dissertation
Presented to
The Academic Faculty

by

Timothy L. Pruyn

In Partial Fulfillment
of the Requirements for the Degree
Doctor of Philosophy in the
School of Materials Science and Engineering

Georgia Institute of Technology
May 2013

INVESTIGATION OF PERCOLATION IN BOROSILICATE GLASS MATRIX COMPOSITES CONTAINING CONDUCTING SEGREGATED NETWORKS

Approved by:

Dr. Rosario A. Gerhardt, Advisor
School of Materials Science and Engineering
Georgia Institute of Technology

Dr. Jason Nadler
Georgia Tech Research Institute
Georgia Institute of Technology

Dr. Robert Speyer
School of Materials Science and Engineering
Georgia Institute of Technology

Dr. Tom Quantrille
Advanced Composite Materials, L.L.C.

Dr. Joe Cochran
School of Materials Science and Engineering
Georgia Institute of Technology

Date Approved: March 25, 2014

"It's a magical world, Hobbes ol' buddy. Let's go exploring!"
-Calvin

ACKNOWLEDGEMENTS

I'd like to express my appreciation and sincere thanks to my advisor, Dr. Gerhardt, for her guidance and support throughout my time here at Georgia Tech. Her support, encouragement, and hard work on her end did not go unnoticed and I benefited as a result of this. I want to express my gratitude to my committee members to Dr. Speyer, Dr. Cochran, Dr. Nadler, and Dr. Quantrille for all their knowledge, support, and advice throughout this thesis process.

I would like to acknowledge the funding and financial support from the National Science Foundation via DMR-060421 and DMR-1207323 for this project over the years. The author was fortunate enough to also be supported by the Boeing and Presidential fellowship over the years as well as the SMART scholarship. A special thanks is necessary to Advanced Composite Materials and their support through the years with the use of their hot press and their expertise. In particular Kevin Fox and Lew Short who went out of their way to be helpful and supportive of my work. The assistance of Todd Walters with the variable pressure SEM and EDS is also greatly appreciated.

I want to acknowledge and recognize my fellow graduate students who have taught me much and also made graduate school an enjoyable experience. To my labmates Brian Bertram, Chunqing Peng, Salil Joshi, Justin Brandt, and Rachel Muhlbauer for all their help over the years. Many days here at Tech would have been unbearable if not for the friendship and laughter I received from my friends Rachel Muhlbauer and Jarod Gagnon. I am certainly deeply appreciative and thankful for the many lasting friends and colleagues that I have come to know or have gotten to know better along the course of my PhD.

Finally, I am endlessly thankful and indebted to my family, especially my parents,

Lori and Lansing Pruyn and grandparents Leota and Louis Trapasso, who have always been so supportive and encouraging throughout my education.

TABLE OF CONTENTS

LIST OF TABLES

LIST OF FIGURES

LIST OF SYMBOLS AND ABBREVIATIONS

ρ_c/f_c	Percolation threshold
PVA	Poly(vinyl alcohol)
ATO	Antimony tin oxide
CNT	Carbon nanotubes
SWCNT	Single-walled carbon nanotubes
MWCNT	Multi-walled carbon nanotubes
UHMWPE	Ultrahigh-molecular-weight polyethylene
SEM	Scanning electron microscopy
PMMA	Polymethymethacrylate
CB	Carbon Black
AFM	Atomic force microscopy
I-AFM	Current atomic force microscopy
PVC	Polyvinyl chloride
Vol%	Volume percent
Phr	Parts per hundred, resin/glass
HPD	Hot pressing direction
SiC_w	Silicon carbide whiskers
ITO	Indium tin oxide
η	Viscosity
VFT	Vogel-Fulcher-Tamman equation
T_m	Melting Temperature
df/dt	Densification rate (1/s)
P_E	Effective Pressure
f	Fractional density
f_G	Fractional green density
ε	Fractional Porosity
IS	Impedance Spectroscopy
*Z**	Complex impedance (Ω)
Z'	Real part of impedance (Ω)
Z''	Imaginary part of impedance (Ω)
I	Current (Ampere)
V	Voltage(Volts)
Θ	Phase Angle
j	The imaginary unit
ε*	Complex dielectric permittivity (F/m)
ε’	Real part of dielectric Permittivity (F/m)
ε’’	Imaginary part of dielectric Permittivity (F/m)
*M**	Complex electric modulus (m/F)
M'	Real part of electric modulus (m/F)
M''	Imaginary part of electric modulus (m/F)
*Y**	Complex admittance (siemens)
Y'	Real part of admittance (siemens)

Y''	Imaginary part of admittance (siemens)
Tan δ	Tan delta
R	Resistance(Ω)
C	Capacitance(F)
T_g	Glass transition temperature
CPE	Constant phase element
σ_m	Property of a material
ρ	Probability of a filler site
s	Exponent insensitive to microstructure (percolation)
A	Proportionality constant
B	Proportionality constant (VFT equation)
T_o	Proportionality temperature (VFT equation)
T	Temperature
TiN	Titanium nitride
Al_2O_3	Aluminum oxide
SiC	Silicon carbide
EDS	Energy dispersive spectroscopy
nm	Nanometer
Å	Angstrom
F	Farad
H	Henry
L	Inductor
R	Resistor
C	Capacitor
SPS	Spark plasma sintering

SUMMARY

In this research, borosilicate (Pyrex®) glass-matrix composites were fabricated using a processing method to create segregated networks with low concentrations of conducting fillers. The fillers used were antimony tin oxide (ATO) and silicon carbide whiskers (SiC_w). The conducting fillers were hot pressed with the glass microspheres at temperatures near the glass transition temperature (550°C) and halfway to the softening point (675°C), using various pressures. Upon hot-pressing at these low temperatures, the glass microspheres deformed into faceted polyhedra and the fillers were displaced to the edges of the glass particles due to the relatively low hot pressing temperatures used (i.e. at high glass viscosity) and the added pressure.

The result of this processing technique was the formation of segregated percolated networks of the conducting filler used, which decreased the electrical resistivity of the composites. Both the ATO and SiC_w have electrical resistivities many orders of magnitude lower than that of the glass, so the formation of the connected filler networks resulted in substantial decreases in the electrical resistivity as the concentration of the filler was increased. In some cases, this decrease was 12-13 orders of magnitude in the resistivity. Using a non-destructive electrical measurement technique, ac impedance spectroscopy (IS), the changes in the electrical properties were tracked as the conducting networks developed. Using IS in conjunction with other techniques, correlations were made between the electrical properties and the development of the percolation networks within the composites.

By comparing the impedance behavior of the pure filler material in various states, an equivalent circuit model was developed that describes the development of the filler networks as the concentration increased. The model was also able to elucidate the different types of

interfaces that can develop in these types of composites based on factors such as the temperature and pressure. Some of these interfaces were formed by a physical point contact between ATO and/or SiC_w particles at low temperatures (550°C), and others were partially reacted/sintered contacts at the higher temperatures (675°C).

This project showed that the processing method used in this study was able to bypass many of the current issues associated with the creation of percolated networks in glass composites. It was also shown that even when using the same materials, varying the temperature and/or pressure can cause different types of interfaces between the fillers which can affect the electrical response obtained and thus may lead to fabrication of glass composites with many different functionalities, that may be useful for a wide range of applications.

CHAPTER 1

INTRODUCTION

With composites containing an insulating and a conducting phase, the interactions between these phases can result in a large range of potential electrical property behaviors. This is especially true for composites where the conducting phase forms a continuous network throughout the composite, which is known as percolation.[1, 2] When percolation happens, a significant shift in the electrical properties is observed: the properties of the composite change from insulating phase-dominated to conducting-phase dominated.[3] Much research has been done studying percolation behavior within polymer composites, and a technique has been developed which can achieve the large change in electrical properties utilizing very low concentrations of the filler (conducting) phase. [4-6] This processing technique involves the compression molding of large particulates of the polymer matrix material with finely-sized conducting filler particles.[4-6] The polymer is pressed at specific temperatures and pressures in order to control the viscosity such that as the polymer particles deform into a faceted polyhedra, the filler particles are pushed primarily to the edges of the filler particles instead of penetrating into the polymer particles.[4] As a result, the filler forms a percolated network at low concentrations.

The concepts used to create percolated segregated networks in polymer composites should also be applicable to ceramic glass composites; however, this processing methodology and composite microstructure has not yet been applied to ceramic glasses. The benefit with glass composites is that they have higher application temperatures than polymer composites and the processing involved with glass can result in a greater range of electrical properties. Glass is not typically produced through powder processing since glass is often just melted and shaped

instead. As a result information about the temperatures, pressures, and hot pressing conditions needed to create this type of segregation is rather limited with powder processing of glass. These glass composites also have an additional complexity compared to polymer composites since these composites are processed at a temperature much higher than the polymer composites. With this higher temperature is the possibility of the filler and glass materials reacting or sintering, which can influence percolation in ways not entirely known.

Successfully creating glass composites with segregated networks of percolated filler using very low concentrations of filler could have a great deal of potential applications and uses. Typically, glass for electronic applications is used primarily for its insulating properties and is often found as a substrate material or as sealing glasses[7, 8]. With this percolated microstructure, the application of glass in electronic applications can be expanded to anti-static shields[9], transparent conductors and electrodes[10-12], IR shielding[13], and EMI shielding[14] to just name a few. Also, compared to polymer composites, glass composites can be used at much higher temperatures. The application will determine the type of filler, but this processing method should be relatively independent of the filler material. In addition, the technique should be primarily glass composition independent, which bypasses many of the issues with percolated networks in glasses today.

As mentioned, this processing idea has not been applied to glass, but it has a great deal of potential. This project will focus on whether it is possible to create percolated networks in glasses using the segregated network processing technique employed for polymer composites, as well as how many of these processing variables can influence both percolation and the overall electrical properties. In particular, the behavior of the filler particle interfaces will be explored

since this can highly influence the electrical properties. A great number of potential interfacial interactions can occur with this processing technique and the temperatures involved.

The background literature is sumarized in Chapter 2. A detailed description of the processing techniques used to create these composites along with the several characterization techniques utilized in this study are given in Chapter 3. Chapter 4 describes several techniques that were used to verify the segregation, percolation, and spatial arrangements of the materials in the composite. The focus of chapter 5 is to show how the electrical resistivity changes due to this spatial arrangement of the materials. Chapter 5 also explores some of the processing parameters such as temperature, pressure, particle size, and particle shape that can influence the resistivity and the onset of percolation.

In chapter 6 many of the ideas already presented are combined with an in-depth analysis of the information extracted from impedance spectroscopy to provide a description of the filler networks that formed, and how they influence the overall electrical properties. This discussion is aided by the development of an equivalent circuit model to help explain what is occurring within the composite. The influence that the processing variables (i.e. temperature, pressure, particle size and shape) have on the percolated networks, particle interfaces, and resulting electrical properties are also discussed. Chapter 7 will conclude the dissertation and will suggest possible future ideas that can be explored that will further develop this research.

CHAPTER 2

LITERATURE SURVEY

2.1. Percolation in Composites

Percolation in general terms refers to the movement of a material or signal throughout a system. This concept has numerous applications such as the spread of forest fires through trees, the flow of fluids in soil, and the spread of disease in a population.[2, 15, 16] For composite materials, percolation refers to when the added phase, or filler, forms some sort of contact with one another and results in an interconnected network in the composite.[17] When this network forms, which is typically three-dimensional, this results in a property change in the composite as the filler's properties are imparted to it.[17] For example, the addition of an electrically conducting filler to a composite that has an electrically insulating material as the matrix will eventually result in percolation. This will result in a rapid increase in the electrical conductivity of the composite.

Figure 2.1 shows a simplified experiment of percolation in a composite material. Figure 2.1(a) shows a glass jar full of glass marbles, which are the white spheres. At the top and bottom of this jar is an electrode. In its current state there will be no flow of electricity from the top of the jar to the bottom since the glass marbles are electrically insulating. Suppose that one of these glass marbles was replaced with a sphere made out of aluminum, which is electrically conducting. An example of this situation is given in Figure 2.1(a). Overall there won't be a change in the electrical properties of the contents of the jar, which is the "composite" in this scenario. As more aluminum spheres are added to the jar, the aluminum spheres start to become closer to one another, such as what is shown in Figure 2.1(b). At a certain point, the concentration of aluminum will be high enough that aluminum particles will start to touch and

eventually, form a continuously touching pathway from the bottom electrode to the top electrode. An example of this is shown in Figure 2.1(c). The conducting percolated network is depicted with a parallel arrow. When this occurs the "composite" has percolated and the conductivity of the jar will be much closer to the electrical conductivity of aluminum. The concentration at which the aluminum or filler forms this continuous network is known as the percolation threshold (ρ_c).[1, 2, 18]

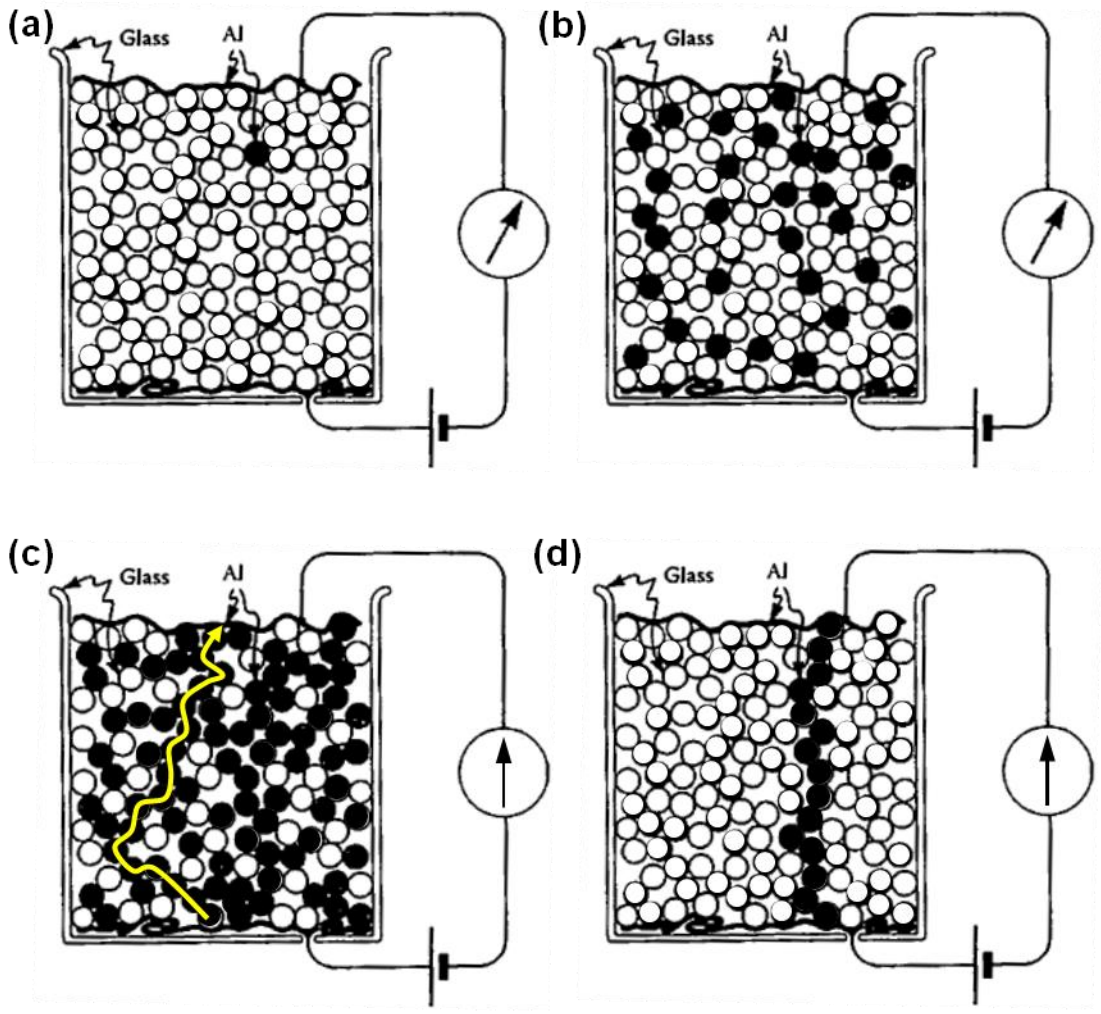

Figure 2.1. Percolation experiment using conducting (aluminum) and insulating (glass) spheres at (a) low concentrations and (b) mid-range compositions. (c) Percolation through a random distribution of aluminum spheres. (d) Percolation through a segregated distribution of aluminum spheres. Modified from references [19, 20].

Percolation in composites, especially with materials with a large disparity in the properties such as the electrical conductivity, have been studied extensively.[5, 6, 21-26] The reason they have been studied so much is due to the potential composite properties that can result, which is dependent on numerous factors. One of the most commonly used equations to describe percolation in composites is listed below in equation (2.1).

$$\sigma_M \propto A(\rho - \rho_c)^s \tag{2.1}$$

Where σ_M is the property of the mixture, A is proportionality constant, ρ is the probability of a site being filled, ρ_c is the percolation threshold, and s is an exponent that is insensitive to the microstructure.[3, 24, 27] This model has several limitations, especially at the higher concentrations when percolation has occurred, but it does show that the concentration of conductive material and the percolation threshold are a critical part of the composite property.[3, 28] While the concentration of filler material is important for percolation, there are many other factors that can influence percolation in a composite.

2.2. Influence of Microstructure on Percolation

For insulator-conductor composites, the onset of percolation has a dramatic influence on the overall composite properties. The onset of percolation in these composites and the overall properties will be dependent on how the added filler percolates and the resulting microstructure in the composite. There are two models that are often used to describe the types of microstructure that can lead to percolation, which are the random and segregated models. As the name would suggest, the random model describes the filler being randomly or homogenously dispersed throughout the microstructure of the glass. At high enough concentrations the filler will form clusters and eventually these clusters will be large enough to span the composite.[29] The jar example in Figure 2.1 (a-c) with the glass marbles and aluminum spheres is an example

of this random model. The other type of microstructure is described by the segregated model. An example of which is shown in 2.1(d). For the glass jar full of glass marbles and aluminum spheres, instead of randomly placing the aluminum spheres the placement of the spheres will be limited to a certain area/volume. Since the aluminum is limited to where it can be placed, it will be more likely that the aluminum will span across the composite with less material. This is shown in Figure 2.1(d).

For Figures 2.1(c) and (d), there is a large difference in both the concentration of conducting material/filler and the percolation threshold between these two models. As a result the percolation behavior will be quite different. The random model results in a high percolation threshold, while the segregated model has a lower percolation threshold than a random model.[4, 28, 30] Some examples of a random and segregated network are shown in Figure 2.2. The microstructure containing randomly placed filler is shown in Figure 2.2(a), which is a composite consisting of poly(vinyl alcohol) (PVA) as the matrix and antimony tin oxide (ATO) as the filler material. The composite was fabricated by solution blending the ATO with the PVA and casting the solutions.[31] The filler (ATO) in this micrograph is the bright spots located homogeneously throughout. An example of a segregated percolated network is shown in Figure 2.2(b). This composite has carbon nanotubes (CNT), which are the dark phase, segregated in an ultrahigh-molecular-weight polyethylene (UHMWPE) composite matrix along with some silica. A close up of these segregated CNT networks is shown in Figure 2.2(c).[32]

For many conventional composites a random or homogeneous distribution is often the common type of percolation that occurs. The main drawback to this method is that it requires a much higher concentration of the filler material in order to percolate, which can increase the cost, create processing issues, and make reproducing a specific property difficult.[1, 20, 33, 34] The

advantage in the creation of a segregated network is that it can result in percolation at concentrations substantially lower than a random distribution, which means that the cost can be reduced and many of the properties of the matrix material can be maintained, such as the mechanical[32] or optical properties[22].

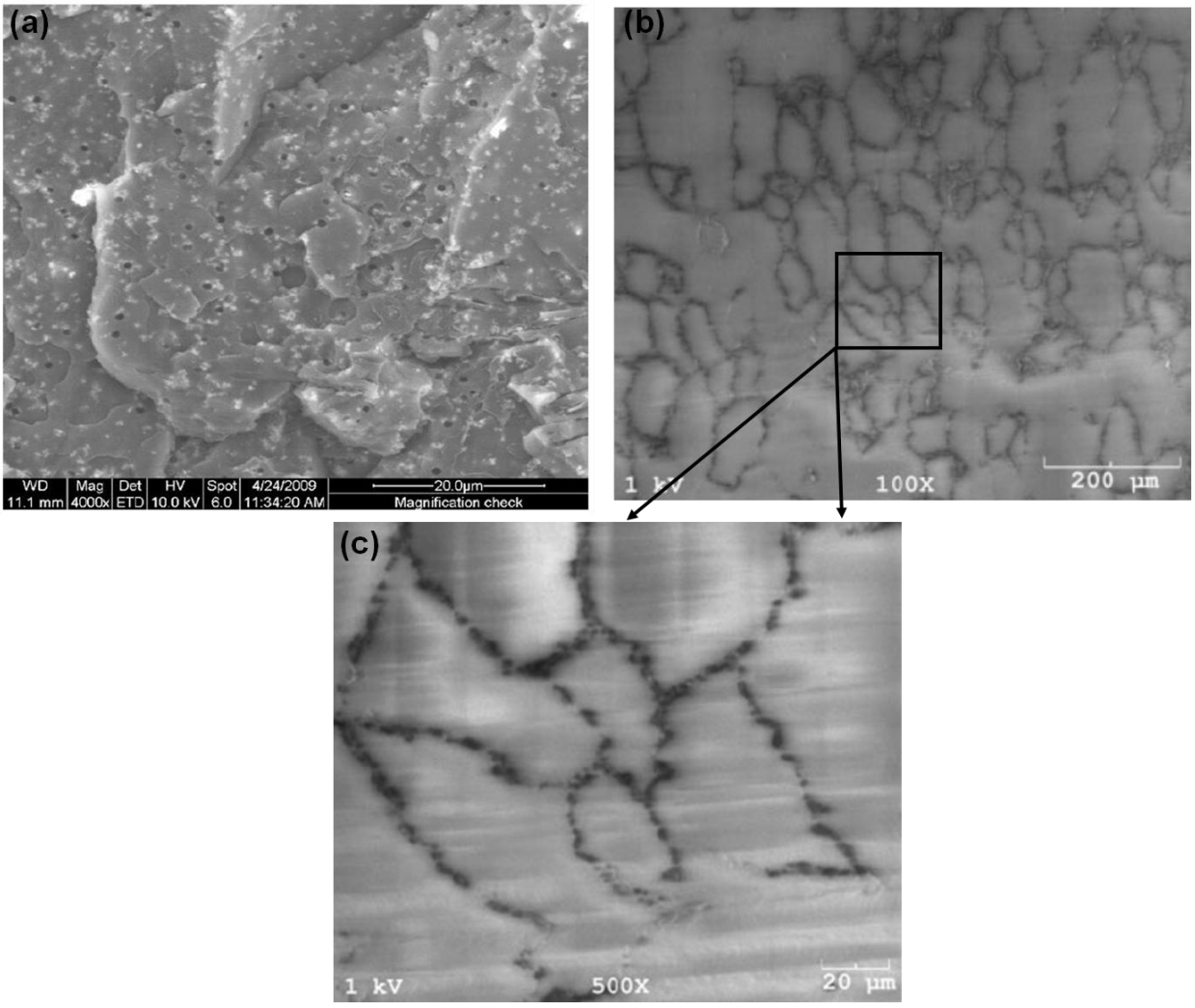

Figure 2.2. (a) SEM micrograph of PVA/ATO composite with 5 wt% ATO resulting in a random or homogeneous distribution. The ATO particles are the bright specks.[31] (b) SEM micrograph of polyethylene composite (gray) with 5 vol% segregated networks of SWCNT (black). (c) Higher magnification of (b) of these segregated networks.[32]

The creation of percolated networks of filler through segregation method has primarily been studied through polymer composites.[1, 4, 5, 16, 30, 35] Typically there are three main methods to

create these segregated networks that utilize structural, thermodynamic, and physical properties.[28] Structural property segregation is where the polymer is partially crystallized, and as the polymer is crystallized the added filler is segregated to the amorphous regions of the polymer.[36, 37] Segregation using thermodynamic properties involves an immiscible blend of matrix polymers.[38] The added filler is located in one of these blends, or depending on the wettability, the polymer can be segregated at the interface between the two immiscible polymers.[39] The final method of segregation is achieved through adjusting the particle size ratio of the matrix and filler particles and then compression molding/hot pressing the powder mixture using specific processing conditions.[28, 35, 40] The particle size ratio between the filler and matrix particles typically involves combining a fine-sized conducting filler with a coarse-sized insulating powder.[5, 6, 24] This physical method results in the most amount of segregation and also relies on the processing parameters. This means that it isn't materials dependent like the previous two methods.[28] This type of method was used to create the composite in Figure 2.2 (b and c)[32] as well as numerous types of segregated composites with different matrix and filler materials.[4, 35, 41-44] Along with controlling the particle size ratio, the consolidation during hot pressing is essential to preserve the segregated spatial arrangement promoted by the particle size difference. The influence of the hot pressing is shown in Figure 2.3. The figure shows the fracture cross-sections of polymethylmethacrylate (PMMA) matrix composites containing carbon black (CB) with increasing amounts of CB.[4] With no filler/CB in the composite (Figure 2.3(a)) the composite fractures like a ductile polymer. With the addition of the CB and the use of this hot pressing method, the polymer particles become faceted polyhedral, shown in Figure 2.3 (b and c). The CB is on the edges and somewhat on the faces of these polyhedra. At the higher

concentrations, 10 phr CB in Figure 2.3(d), the CB can be seen to be primarily forming percolated networks on the edges.[4]

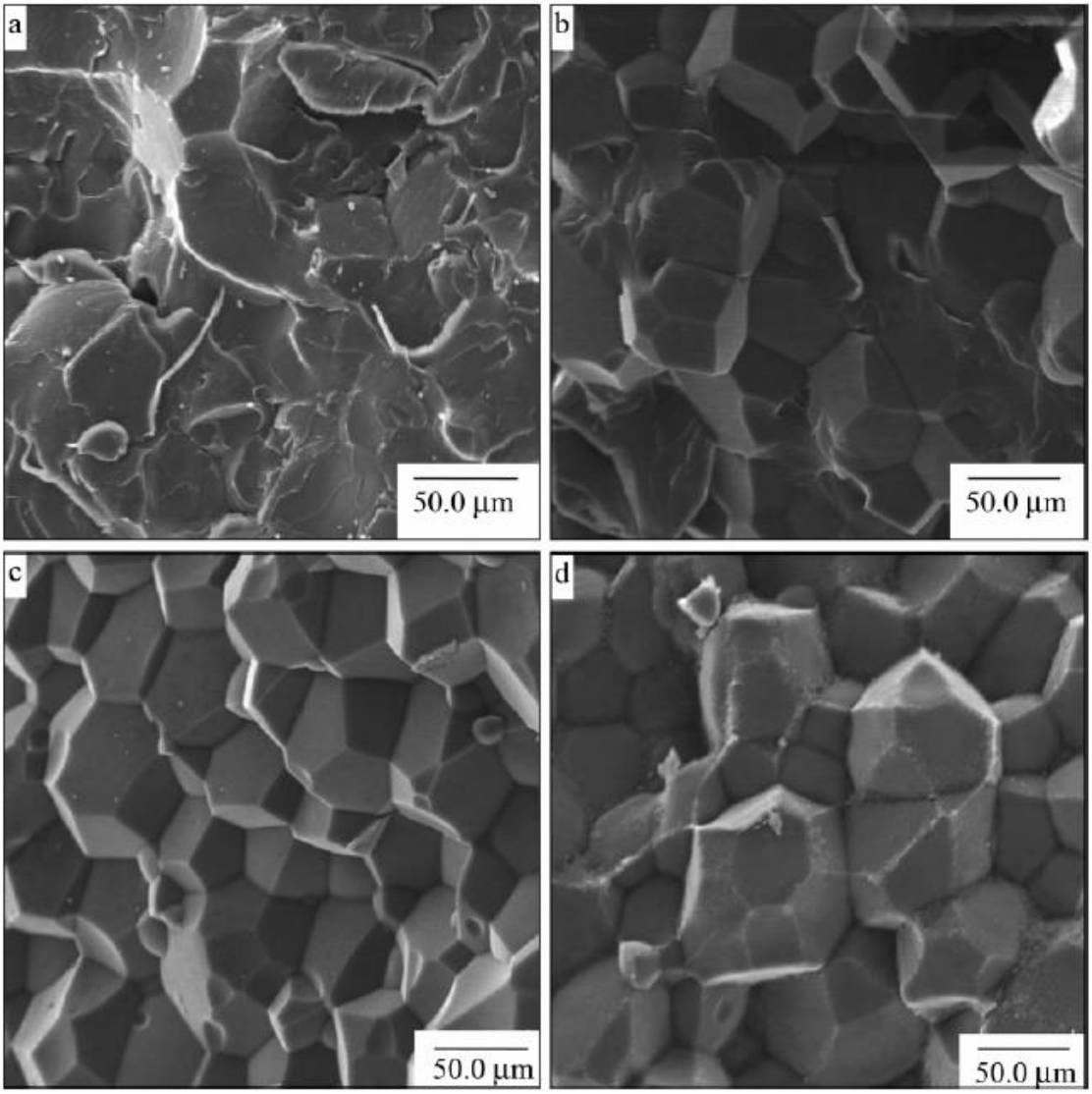

Figure 2.3. SEM micrographs of fractured cross sections of PMMA/CB specimens with CB concentrations of (a) 0 phr CB, (b) 0.1 phr CB, (c) 1 phr CB, and (d) 10 phr CB.[4]

2.3. Influence of Percolation Microstructure on Electrical Properties

The advantage of this type of segregated network is that it can result in an improvement of the electrical properties as well have a much lower percolation threshold compared to a random network.[4] An example of this is shown with PMMA composites containing carbon

black, which were fabricated using two different processing methods. The first method was through dissolving the PMMA in solution and adding the carbon black.[4] A similar method was used to create the composite in Figure 2.2(a).[31] Similar to the microstructure in Figure 2.2(a), this PMMA/CB composite also had a homogeneous dispersion of the filler.[4] An example of this microstructure is in Figure 2.4(a). This micrograph shows the topography of a PMMA/CB composite with a random distribution using atomic force microscopy (AFM).[6] The CB particles can be detected by the brighter regions in the micrograph, which using the z-axis scale are the raised areas. This composite is percolated but the corresponding current-AFM (I-AFM) micrograph in Figure 2.4(b) shows very little current change (current is the z-axis scale) throughout the microstructure because it is difficult to detect the low current across the thickness of the composite. The influence of this distribution of filler, and the lack of faceted particles with the polymer matrix, on the electrical resistivity as a function of carbon black concentration is shown in Figure 2.5.

An example of this segregated network is shown with the AFM(Figure 2.4(c)) and I-AFM(Figure 2.4(d)) micrographs. The CB particles in Figure 2.4(c) are located at the edges of the particles and resemble grain boundaries. The I-AFM micrograph in Figure 2.4(d) is the same area but is showing areas of high current through the thickness of the composite instead of the topography.[6, 45] The areas of high electrical current are the same as the boundary areas in Figure 2.4(c). So by changing the distribution of the carbon black, these composites percolated at a much lower concentration of carbon black and had resistivity orders of magnitude lower than the composites with a homogeneous distribution.

The solution mixing method (shown with the diamond symbol in Figure 2.5) with the random distribution of carbon black resulted in percolation around 2.7 vol% carbon black and in

total the resistivity dropped about 12 orders of magnitude at the highest reported concentration of carbon black. The other type of composite was fabricated using carbon black that was much smaller in size than the PMMA particles and compression molding the powder mixture at temperatures around the melting point of PMMA (170°C).[4] When compression molding, the temperature and pressure were controlled so the viscosity of the polymer is low enough to consolidate the composite but high enough that it doesn't allow the polymer to penetrate the polymer, but is instead pushed to the polymer particle edges and triple points. This was how the composite in Figure 2.2 (b and c) were also fabricated. This was also the method used for the mechanical mixing data (triangle symbol in Figure 2.5). As a result of this method, percolation occurred at 0.26 vol % carbon black and the total resistivity dropped over 15 orders of magnitude at the highest concentration of carbon black.[4]

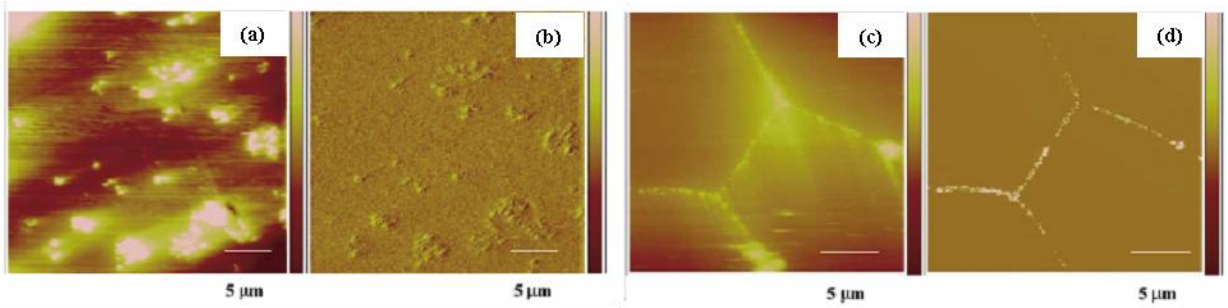

Figure 2.4. (a) AFM micrograph of a distributed network of carbon black in a PMMA composite. **(b)** I-AFM micrograph of the same area of microstructure as (a) showing the low amount of current passing through the carbon black in the composite. **(c)** AFM micrograph of a segregated network of carbon black in a PMMA composite. **(d)** I-AFM micrograph of the same area of microstructure as (c) showing that the segregated carbon black is percolated due to the high amount of current passing through it.[6]

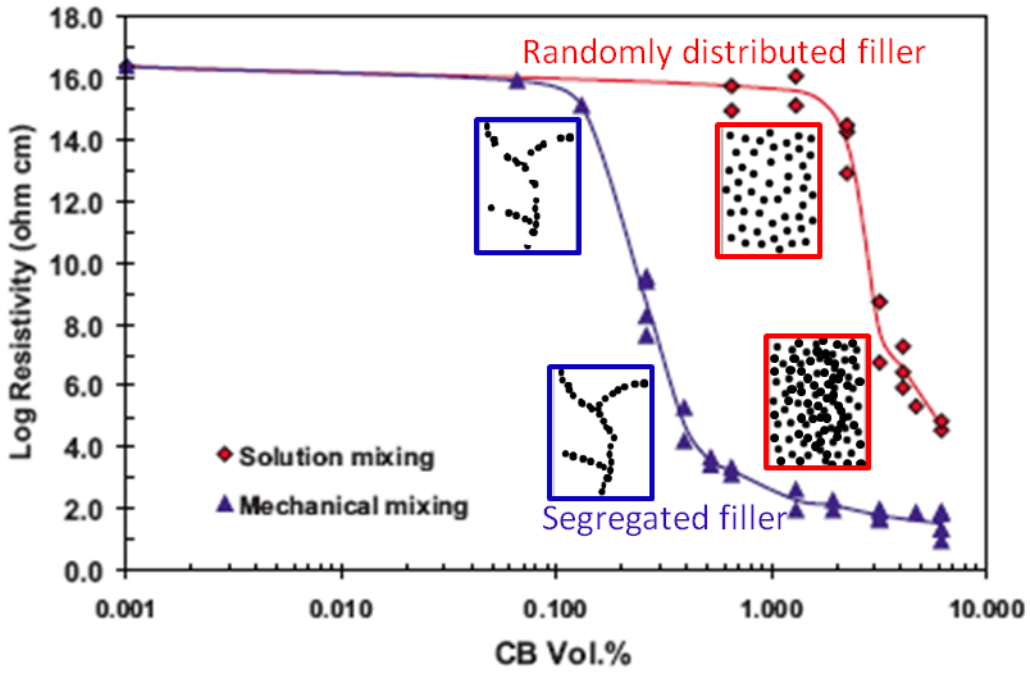

Figure 2.5. Log resistivity vs. volume fraction of carbon black (CB):PMMA composites with mechanical mixing of segregated network and solution mixing random network. Modified from reference [4, 6].

Other polymer systems have also shown evidence of formation of segregated networks through similar methods although not as ordered as the composites previously discussed. Kusy and Turner created segregated polymer composites of polyvinyl chloride (PVC) and nickel by controlling the temperature and pressure during processing such that the flow of polymer was controlled enough that the spatial arrangement of the particles remained. This resulted in a segregated microstructure with a percolation threshold around 6 vol%. Similar composites with a random distribution of filler had the percolation threshold around 35 vol%.[25] Grady formed segregated microstructures using polyethylene, silica, and single-walled carbon nanotubes (SWCNT) through heated compression molding that resulted in a percolation threshold of 0.14 wt%. An example of these composites was shown in Figure 2.2 (b and c).[32] Lisunova et al. reported percolation as low as 0.04 vol% in a polyethylene and multi-walled carbon nanotube

(MWCNT) composite through hot pressing.[46] Numerous more composites have been reported with various types of polymer matrices and conducting filler particles, which shows how this physical processing method not only results in a low percolation threshold, but also that it is applicable to a large range of matrix and filler types and compositions.

2.4. Processing Factors that Influence Segregated Percolation

The physical method, which controls the particle size and viscosity of the polymer, typically results in the most amount of filler segregation and the lowest percolation threshold. This method however, is dependent on many factors that can either reduce or raise the percolation threshold and influence the percolation network.

2.4.1. Influence of Particle Size

When creating a segregated percolated network, the percolation threshold tends to decrease with a larger particle size ratio between the matrix and filler particles. The general relationship between the percolation threshold and particle size ratio of the matrix material radius (R_1) and the filler material radius (R_2) is shown in Figure 2.6.[1] The use of smaller glass particles will result in smaller particle size ratio between the matrix and filler, which will result in a more homogeneous dispersion. This means that a higher filler loading will be needed to achieve percolation, which is what is shown in Figure 2.6. A larger particle size ratio, with the glass particle being much larger than the filler, would create an excluded volume in which the filler cannot occupy. As a result, the filler would be segregated between the larger glass particles. This will result in a lower percolation threshold.[47] Ideally for segregated composites, the matrix particle will be relatively coarse (micron-sized) and the filler will be as small as possible (nano-sized). The influence of the filler size on the percolation threshold can be seen in Figure 2.7 for size ratios far larger (>1,000) than the ones shown in Figure 2.6 (< 80).[6]

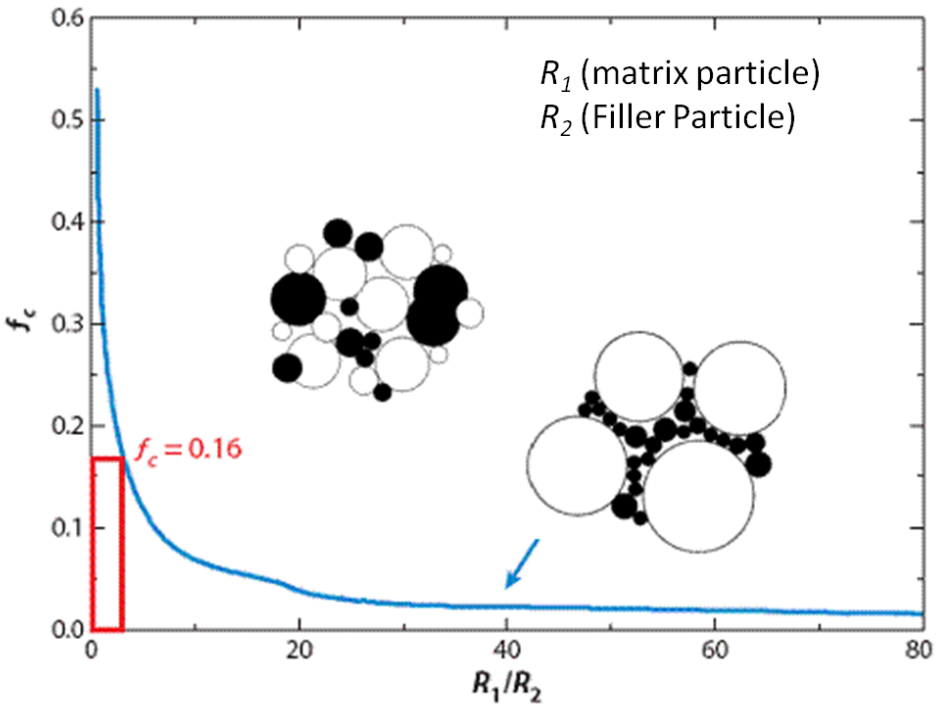

Figure 2.6. Variation of the percolation threshold (f_c) due to the ratio between the matrix phase particle radius (R_1) and the filler particle radius (R_2).[1] A cartoon depiction of the difference in particle size of the matrix and filler has been added.

The filler sizes in figure 2.7 are 100nm or smaller and the polymer matrix size is kept constant at 75 μm. This figure also shows different shapes of the polymer matrix (truncated octahedral and tetrahedral) and the percolation for edges (1D) and faces(2D).[6] From this figure, the percolation threshold, which is given in phr (parts per hundred, resin), decreases to extremely small concentrations of filler as the filler size decreases.[6] This figure shows how little filler material is needed to potentially result in percolation, while creating a noticeable change in the composite properties.

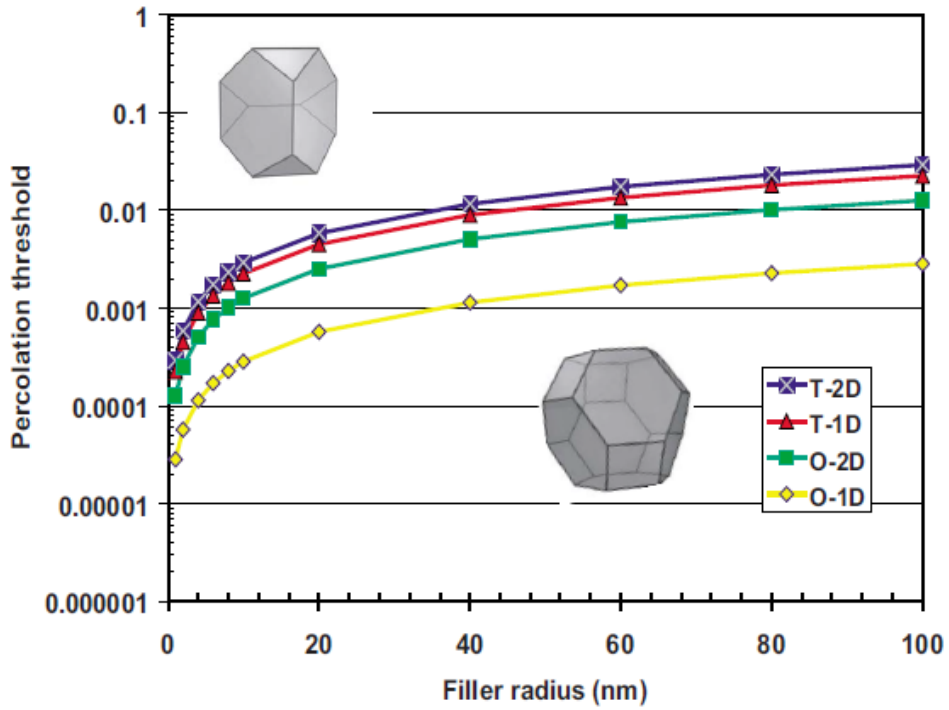

Figure 2.7. Simulated percolation threshold as a function of filler size for filler placement on the edge (1D) and face(2D) for matrix particles. The matrix particles are 75µm and have either a truncated octahedral (O) or a truncated tetrahedral (T) shape.[6]

2.4.2. Influence of Particle Shape

From Figure 2.7 the shape of the matrix particle can influence the percolation threshold since this will change the length of the edge networks and the length of the percolation network. With the previous models in Figure 2.6 and 2.7, the influence of the particle size had the assumption that the filler particles were close to spherical and had an aspect ratio close to 1. As the filler changes from spherical to more ellipsoidal, the chance for the filler to connect with one another is higher, especially if there is some sort of texture or preferred orientation in the composite.[1, 48, 49] Fillers with different shapes and aspect ratios can have different percolation behavior than just spherical particles, which is what is shown in Figure 2.8.[1] From this figure, it can be seen that as the aspect ratio increases for the filler particle, the percolation threshold is

lowered. This was shown with both simulated composites and polymer composites containing carbon and aluminum fibers in this figure.[1]

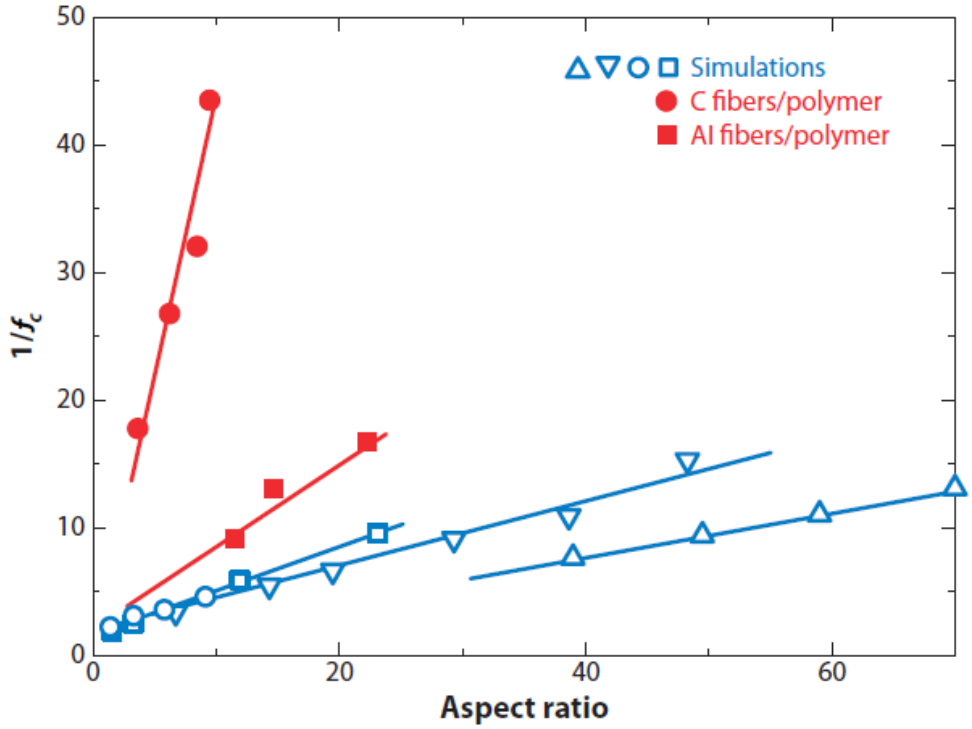

Figure 2.8. Variation of the percolation threshold (f_c) due to the aspect ratio of the filler particles. Both experimental and simulation data are presented.[1]

There are several other factors with the percolation threshold with elongated filler that this figure does not show. Due to the shape, there will likely be more variation in the types of interfaces and how these filler particles contact each other. For example, the electrical properties of the percolated network may vary if the filler particles are aligned end-to-end or side-by-side.[48, 50] The processing temperature and conditions can also have a strong influence when filler particles with a large aspect ratio are involved. This is especially the case when the composites are hot pressed, which is the method to be used in this study and the method used to create many of the polymer composites previously mentioned that had segregated networks.[4-6,15,32,38] As the composite is hot pressed, the elongated filler has the tendency to orient perpendicular to the hot

pressing direction.[48, 49, 51] The degree of orientation depends on many factors, especially the viscosity of the polymer or glass, but if the hot pressing consolidates the composite, it will also likely result in an orientation of the filler particles.

Schematic of orientation obtained due to hot pressing of anisotropic fillers is shown in Figure 2.9. When viewing parallel to the hot pressing direction (∥ HPD)[49], such as in Figure 2.9(a), where the hot pressing direction is into the paper, the elongated fibers or whiskers appear to be randomly placed and oriented. When viewing the composite perpendicular to the hot pressing direction (⊥HPD)[49], as depicted in Figure 2.9(b), shows the whiskers will have some horizontal alignment with the hot pressing direction. With these types of alignment, the percolation threshold for the ∥ HPD and ⊥ HPD will be different. Not only will the percolation threshold be different, but the properties will be different along each direction. An example of this is shown in Figure 2.10 which shows the thermal conductivity of aluminosilicate glasses containing silicon carbide whiskers (SiC_w) that were hot pressed. The temperature used to hot press these composites was quite high (>1300°C) compared to the temperatures that will be involved with creating segregated networks, so the microstructure is not expected to be the same. With the fluid glass, the whiskers oriented perpendicular to the hot pressing direction.[52] The thermal conductivity perpendicular to the hot pressing (Figure 2.10(a))direction was noticeably higher than the parallel (Figure 2.10(b)) to the hot pressing direction due to this alignment. Similar behavior has been observed with the electrical conductivity with composites of alumina and SiC_w.[48, 53, 54]

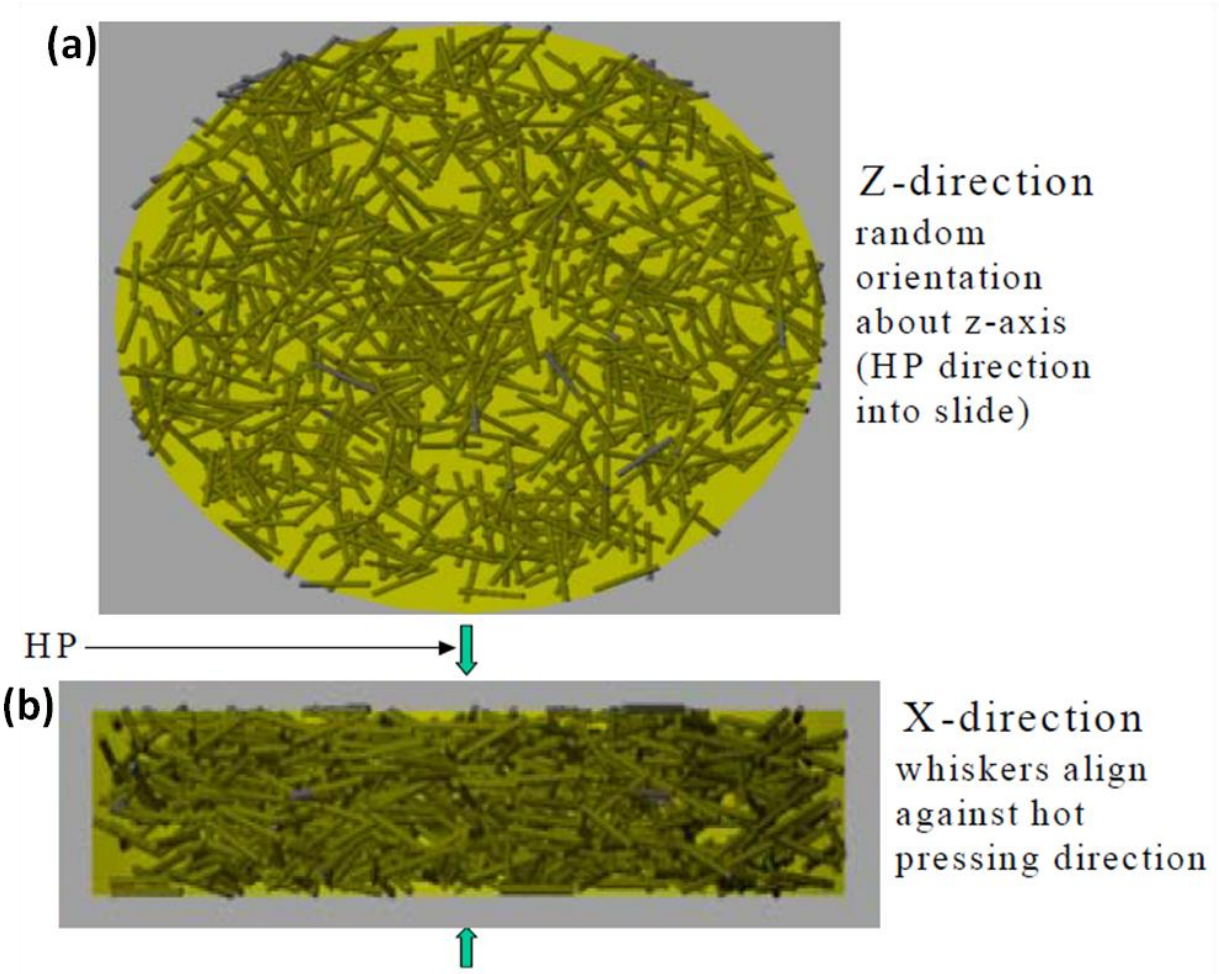

Figure 2.9. Whisker alignment of SiC_w from hot pressing (a) parallel to the hot pressing direction and (b) perpendicular to the hot pressing direction.[53]

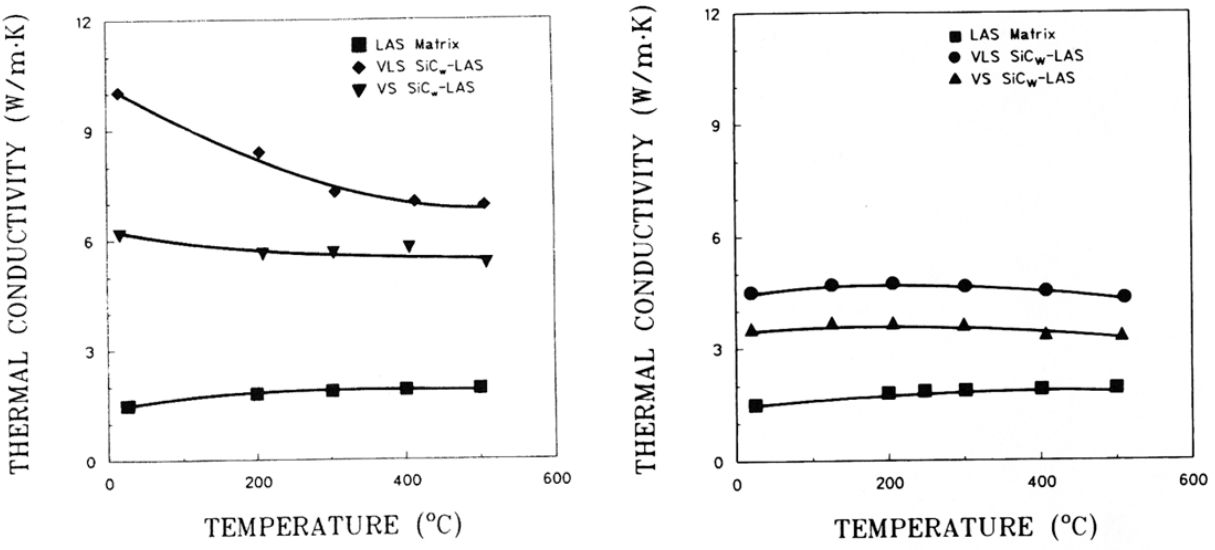

Figure 2.10. Thermal conductivity for lithium aluminosilicate glass matrix composites containing small diameter (VS, ~ 0.7 μm) and large diameter (VLS, 5-8 μm) for silicon carbide whiskers (SiC_w) along the (a) perpendicular direction to hot pressing and (b) parallel to hot pressing. [52]

2.4.3. Influence of Processing Temperature on Segregated Percolation

From the orientation effects with hot pressing, the processing variables during hot pressing have been found to influence the percolation threshold and resulting properties with segregated networks in polymer composites.[21, 55, 56] The temperature during hot pressing is significant since this will influence the viscosity of the glass or polymer. For these segregated composites, it is preferable to have the viscosity as high as possible to prevent the filler particles from penetrating into the matrix and instead to be displaced to the polymer particle edges and interfaces. The viscosity will still have to be low enough to consolidate the composite so a range of temperatures can be used to create this microstructure. With many polymer composites, an increase in temperature results in an increase of penetration of the filler into the matrix, which will break up the network.[55, 56] At a critical temperature or with long enough times, the resistivity increases sharply due to the matrix polymer being fluid enough to penetrate and break up the percolated network.[55] Higher temperatures can also result in improved packing and

consolidation of the matrix around the filler particles, which will improve the packing of the filler and likely result in a decrease in the resistivity. An example of this is shown in Figure 2.11 which shows the resistivity of polymer composites containing a percolated network at different processing times and temperatures.[55] At short processing times (<30 mins in Figure 2.11) the composites are densifying and the filler particles in the network are forming betters contacts with one another. The composites pressed at higher temperatures (T_m+40°C = 162°C) had a lower resistivity even at higher temperatures due to the improved network packing. At longer times however (< 30 mins), the composite will be consolidated and the matrix will begin to penetrate the network. With enough time or with an excess of temperature, the matrix material can interdiffuse between the filler and break up the network, which is what is commonly seen.[55, 56]

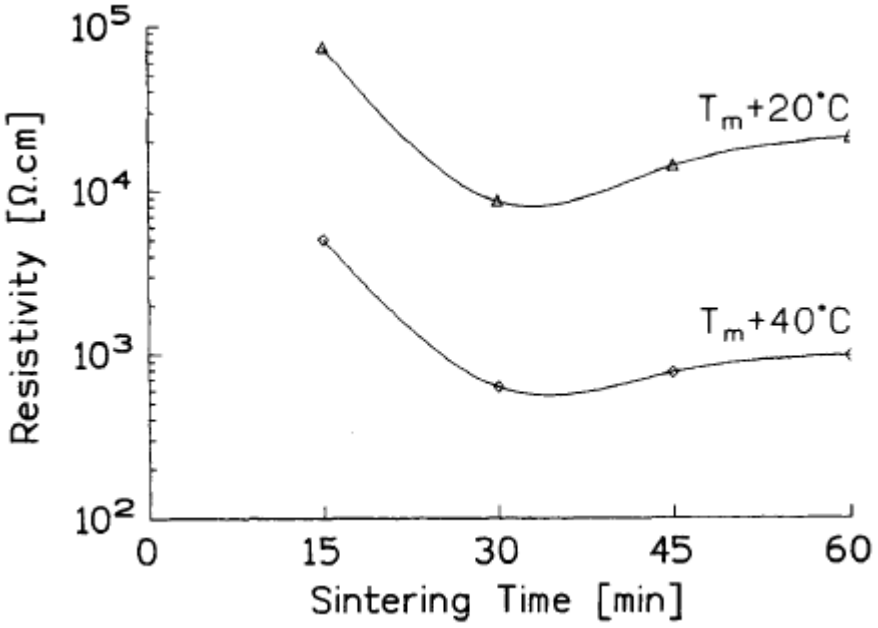

Figure 2.11. (a) Log resistivity vs. time for select composites containing polyethylene and 13 vol% TiN at two different temperatures. T_m for the polymer was estimated at 142°C.[55]

2.4.4. Influence of Processing Pressure on Segregated Percolation

Along with the influence of temperature, an increase in the pressure can influence this segregated percolation in various ways. For some composite systems, the increased pressure could improve the contact between filler particles and result in better electrical conductivities. [55] The pressure can also be detrimental to the percolation network with high enough pressures, since the added pressure can allow the polymer to flow into the capillaries between filler particles and break up the network.[21, 55] An example of this is shown in Figure 2.12 with composites of PMMA/ITO.[21] As the pressure is increased from 6.4 to 25.6 and 51.3 MPa, the conductivity of the composites decrease and for high enough pressures, the percolation threshold shifts to higher concentrations. [21]

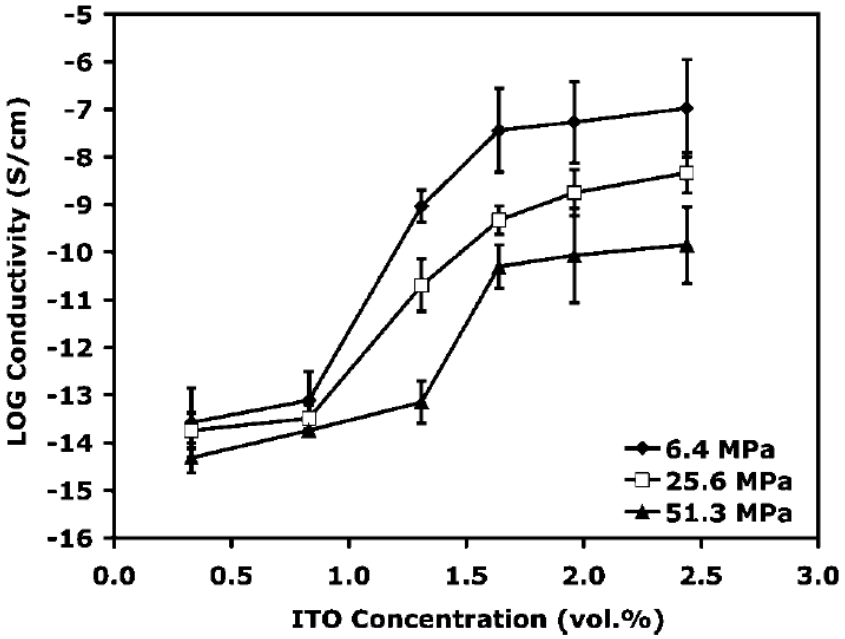

Figure 2.12. The dc conductivity vs. ITO concentration (vol. %) for PMMA/ITO nanocomposites molded using three different compaction pressures while maintaining the same hot pressing temperature.[21]

While with many of these polymer composites, an increase in the pressure and temperature results in the matrix breaking up the percolated network, this may not be the case for

the glass composites to a point. Since the glass is being processed at much higher temperatures than the polymer composites, there is the chance that filler particles can react with one another at the higher temperatures so the temperature and pressure influence could be much more complicated for these composites.

2.5. Percolation in Glass Composites

All the methods used to create segregated percolated networks in polymer composites should be applicable to glass composites, especially the physical method which has little composition dependence. The majority of glass composites that are designed to result in a change in the electrical properties have used a homogeneous or random distribution of the filler. Examples of this have included the addition of fillers such as: copper, silver, ZnO, TiO_2, and ferroelectric crystals.[10, 26, 45, 57-59] There are few examples in the literature of percolation in ceramic glass composites with segregated networks.

2.5.1 Thick Film Resistors

One of the few types of ceramic glass composites that utilizes a segregated network are thick film resistors. The name thick film resistor is actually misleading since it doesn't refer to the thickness of the composite but to how it is made.[60] These composites are often fabricated with a lead borosilicate glass and RuO_2 particles.[61, 62] The glass particles are mixed with a paste containing the RuO_2, which are often much smaller than the glass particles, and is then screen printed. After being screen printed the composites are dried and fired to removed the organics. The final step involves sintering around 700-900°C.[60, 63] The main variables in controlling the sheet resistance of these films are the particle size distribution and firing temperature.[61, 63]

After processing, these thick film resistors have a relatively low percolation threshold. The exact concentration of RuO_2 will vary upon several factors including the desired resistivity

of the composite, the composition[62, 64, 65], the size of the glass frit[63], and the processing temperatures[61, 66]. The resistivity can often vary from 10^0 to 10^5 $\Omega \cdot cm$.[61, 64, 65] These resistors can approach the limit of pure RuO_2, 10^{-4} $\Omega \cdot cm$, but this is at high concentrations of filler (~60 vol% RuO_2).[64] The reason for the low threshold is the interface that forms between the RuO_2 particles. These RuO_2 particles are actually not physically touching. Between these particles is a glassy film (~1 nm) which wets and penetrates in between the RuO_2 particles.[64] An example of this is shown in the SEM micrographs in Figure 2.13. Even though the RuO_2 particles are not physically touching (Figure 2.13(a)), percolation is still occurring due to tunneling across these thin glass regions.[62] This is also aided due to the RuO_2 reacting with the lead based glass, which results in a conducting glass region around the conducting filler particles. An example of this conducting glass region is shown in Figure 2.13(b). With certain additives to the glass or with certain heat treatments during sintering, the size of this region can be controlled[62], which will result in a change in the composite resistivity.[64] These regions around the glass are critical for the onset of percolation and the drop in resistivity but this also makes these thick film resistors highly composition dependent on both the glass and filler material. RuO_2 is an expensive filler and the glass used is commonly one of the "heavy" glasses, such as a lead or bismuth based glass, which often can have health or corrosion concerns.[60, 65] These glasses are hard to avoid since the RuO_2 has some solubility in lead or bismuth based glass that helps form the conductive region around the RuO_2 particles and the flattening that occurs with the RuO_2 after sintering and heat treatment.[64, 67]

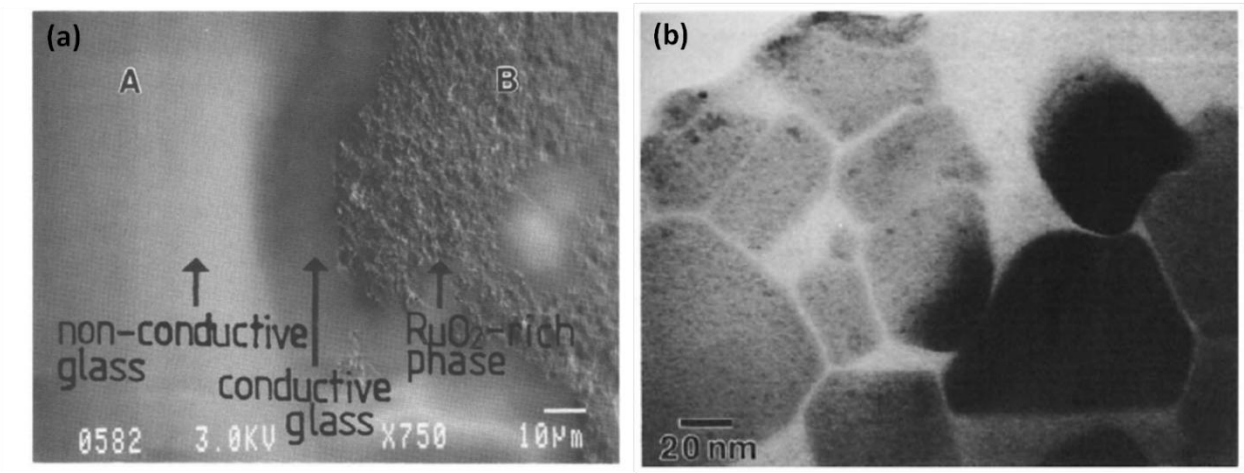

Figure 2.13. (a) Backscatter micrograph of a thick film resistor showing the region of glass that has a high concentration of RuO_2 solute in it.[66] **(b)** RuO_2 particles network that has a gap between the particles where tunneling occurs.[64]

2.6. Glass Viscosity and Sintering

The reason why more percolated glass composites with segregated networks haven't yet been created is due to several factors with processing and sintering. Typically, the manufacture of glasses occurs through a melting process due to the relative ease and shaping this method allows.[68] Recently, interest in glasses produced from powders and sintering have increased in areas such as creating porous glass filters, glass composites, and advanced glass ceramics.[69] The benefit of glass sintering is that glasses are less susceptible to processing flaws in particle packing than polycrystalline ceramics.[70] Unlike its crystalline counterparts, the primary mechanism of sintering for glasses is viscous flow.[69, 71] Because of this, the viscosity behavior as a function of temperature is a critical factor when sintering with glass. One of the most common models to describe the viscosity of glass as a function of temperature for any glass is the use of the Vogel-Fulcher-Tamman(VFT) equation, which is listed as equation (2.2).[69, 72]

$$\log \eta = A + B(T - T_0)^{-1} \qquad (2.2)$$

The variables *A*, *B*, and T_0 are constants while *T* is the temperature in °C. The variables *B* and T_0 are in units of °C or K while *A* can be in poise or Pa·s.[73] The constants can be determined using specific points in viscosity such as the softening point ($\eta=10^{7.6}$ Poise) and the working temperature ($\eta=10^4$ Poise).[68] A viscosity vs. temperature curve for many commercial glasses is shown below in Figure 2.15. As the VFT equation suggests, the viscosity of glass is highly temperature and composition based. In order to achieve glass sintering, the viscosity has to be in the glass transition range or higher. Generally the glass transition region is around 10^{11}-10^{12} Pa·s. This region is shown with the highlighted box region in Figure 2.14. The glass transition range is the lower limit for glass sintering. The top limit is the working point, which has a viscosity of about 10^3 Pa·s. This limit is marked off with the solid black line in Figure 2.14. Below this viscosity the glass is fluid enough to deform under its own weight.[68] While this range for glass sintering may seem quite large, especially glasses with a large working range, in actuality this range is much smaller. This is because in order to sinter glasses to full densities, the viscosity should be in the range of 10^6 Pa·s[74], which is shown with the dashed line. For glasses such as Pyrex®, this reduces the potential sintering range from >600°C to about 300°C or less.

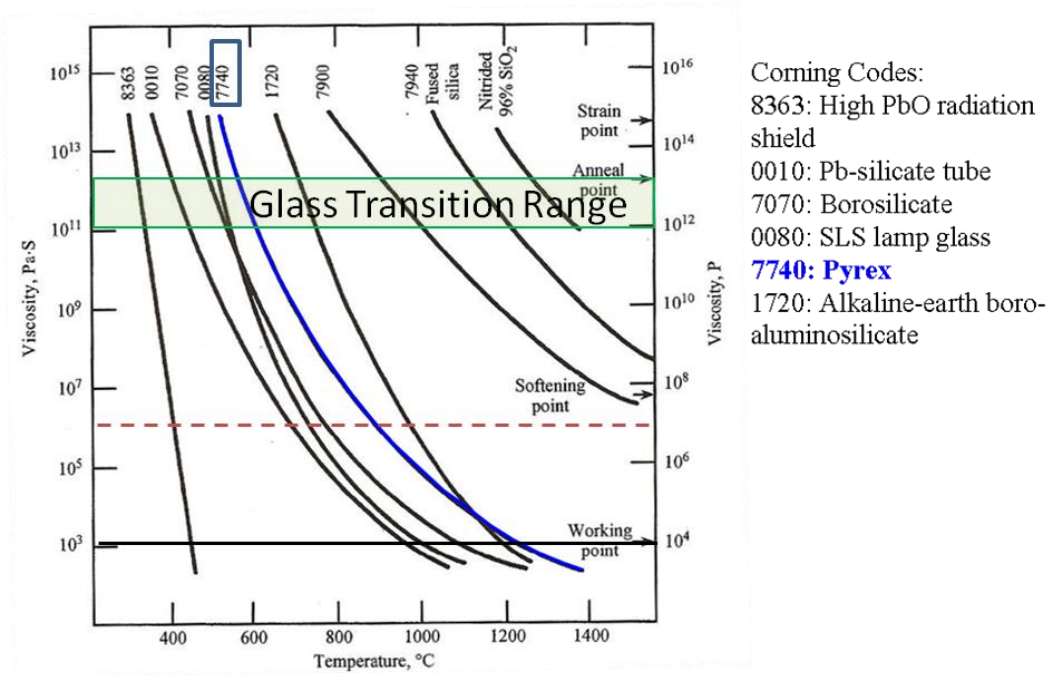

Figure 2.14. Viscosity vs. temperature for several commercial glass compositions. Figure was modified from reference.[68]

This is one of the advantages of a lead based glass, such as 0010 in Figure 2.14. Sintering for lead glasses can occur at several hundred degrees less than many other types of glasses such as Pyrex®. Ideally if there was a way to fabricate composites at viscosities above 10^6 Pa·s, it would allow the fabrication of many types of glass systems to be used as well as allow for many types of fillers that typically cannot tolerate the higher temperatures.

2.6.1. Glass Sintering with an Applied Pressure

Much like the polymer composites, the glass composites in this study will be hot pressed at certain temperatures and pressures to create these segregated networks. This should allow the temperature range, such as the ones in Figure 2.14, to be larger since it would allow viscosities potentially up into the glass transition range(η~10^{11}-10^{12} Pa·s). The reason this is possible is due to the added pressure. While the added pressure to a glass composite won't change the viscosity, it will improve the densification rate. A model that explains the relationship between viscous

flow in pressure-assisted sintering from Scherer[75] and modified by German and Park[76] is shown below in equation 2.3.

$$\frac{df}{dt} = \frac{3P_E\varepsilon}{4\eta} \tag{2.3}$$

Where *df/dt* is the densification rate (1/s), P_E is the effective pressure (MPa), ε is the fractional porosity (dimensionless, 0 to 1), and η is the viscosity (Pa·s).[75, 76] The effective pressure is not the same as the applied pressure (P_A) since it factors in the concentrations of the forces at the point of contact between particles. The relationship between effective pressure and applied pressure is shown in equation 2.4.

$$P_E = P_A \frac{(1 - f_G)}{f^2(f - f_G)} \tag{2.4}$$

Where f is the fractional density (dimensionless, 0 to 1), and f_G is the fractional green density (dimensionless, 0 to 1).[76] At high enough pressures, the densification rate will be controlled by the pressure part of the equation and the viscosity will not matter as much. The pressure is also more significant at the lower fractional densities and its influence will reduce as the composite consolidates, which at this point the viscosity will play a more significant role.[75] For this study a balance between the two is likely necessary to obtain the desired microstructures.

2.6.2. Glass Sintering with Rigid Inclusions and Networks

The viscosity of glass is a very important factor when sintering a glass composite, but the influence that the added filler has on the viscosity and the processing is also very important. The addition of filler or a rigid inclusion to a glass system is considered a type of constrained sintering.[77-79] The influence this has on the viscosity is dependent on several factors including: particle size, particle size distribution, distribution of rigid inclusions, wetting and chemical

interaction between the glass and rigid inclusions.[78, 80] With all these factors however, the viscosity will increase with the addition of filler or rigid inclusions, which will cause a deviation from the viscosity in Figure 2.14 and the VFT equation.[78] For this study, the most important factor with the addition of rigid inclusions or filler is the interaction the filler has with one another. This leads to the reason why thick film resistors are one of the few inorganic glass composite systems with a segregated percolated network.

The addition of filler to a glass composite will increase the viscosity and result in the difficulties when pressureless sintering a composite. This has been shown in various glass systems with fillers ranging from silicon carbide (SiC)[81, 82], alumina (Al_2O_3)[83], and aluminum borate whiskers[84]. The key parameter that influences sintering is the volume fraction of inclusions, which has been shown theoretically by Jagota and Scherer[85] and experimentally by Rahaman and De Jonghe[77]. While these models are able to describe the influence added filler has on the viscosity, they are more appropriate for composites with a homogeneous distribution of filler because these models are unable to predict the influence of filler interaction, which will be prominent in segregated percolated networks.[79, 85, 86] The influence of filler particle interaction and percolation can be seen in Figure 2.15. In this figure, the densification rate of the composite is normalized to the densification rate of the pure glass or ceramic matrix and is plotted as a function of volume fraction of filler/inclusions (SiC). For the polycrystalline based composite, which is ZnO, there is a large drop in the densification rate due to the back stress from the SiC that is resisting the sintering forces of the ceramic.[20, 82] This is one of the advantages of using glass as the matrix since it is more forgiving with the addition of filler. This can be seen at low concentrations with SiC as a filler in Figure 2.15 as it follows the rule of

mixture line. A sudden deviation from this behavior occurs at around 0.16 vol% SiC, which correlates to the onset of percolation and filler interactions.

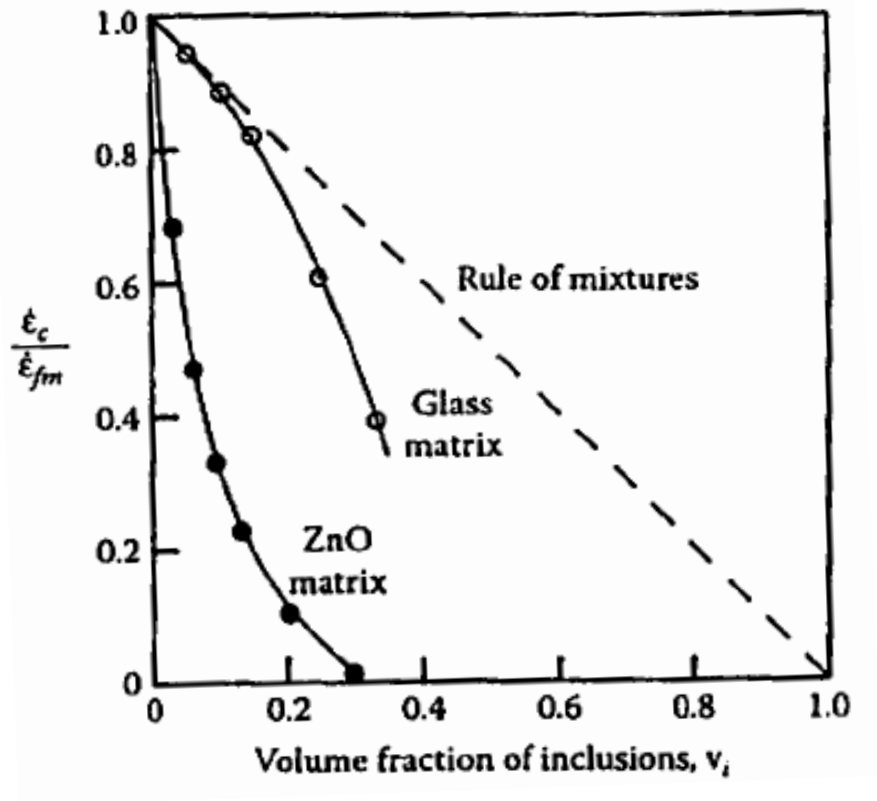

Figure 2.15. Comparison of the densification rate ($\dot{\varepsilon}_c / \dot{\varepsilon}_{fm}$) of the composite relative to that for the free matrix plotted vs. the volume fraction of SiC filler/inclusions for a glass matrix and ZnO matrix composite.[20]

The cause of this deviation is due to something known as the rigidity threshold. The rigidity threshold in composites is similar to the percolation threshold since it involves filler particles forming an interconnected network throughout the composite.[43, 87, 88] The filler particles in the rigidity threshold have a type of contact known as hard-hard. Hard-hard contacts typically involve particles that are bonded/sintered together or are "locked" together due to surface roughness.[20, 87] This rigid contact allows for the transfer of loads and moments as well as rendering the composite rigid.[85, 89] This network will be mechanically rigid, which will resist

deformation and densification forces during sintering.[82, 86, 88] The reason thick film resistors are able to have these percolated networks is because they have a contact known as soft-soft.[87] This type of interface does not have the particles physically touching and usually have the matrix material in between the filler particles, which will act like a lubricant and allow for the particles to move and rearrange, which allows them to be sintered through isothermal sintering.[85] This is why thick film resistors are so composition dependent because a change in the glass or filler material will not result in this conducting glass region and the composite will either have a very high resistivity or will form hard-hard contacts in the composite and not sinter properly. Based on this, it would be quite advantageous to have a method that can result in segregated percolation networks in glass composites that does not rely on composition and can either have hard-hard or soft-soft contacts in the percolation network.

2.7. Impedance Spectroscopy

The electrical properties of a material system involve multiple microstructural processes such as the movement, concentration, and hopping of charge carriers like electrons and ions, that will contribute to the overall properties. These properties can change if additional features are present in the material, such as defects and interfaces.[90] For composites with these percolated networks, this will be a useful method to characterize the filler particle interfaces and the percolated networks in these composites. When measuring with a direct current (dc) it is assumed that the system is time-invariant and that the electrical measurement is at a steady state.[91] As a result, many of these microstructural processes that contribute to the overall properties are lost out in the dc measurement. Impedance spectroscopy (IS) on the other hand, is often able to show the influence of these processes. Impedance is the ac term for resistance since

it is a complex quantity (Z^*). With impedance spectroscopy the complex impedance is determined by the current(I), voltage(V), and the phase angle (Θ) between the current and voltage over a frequency range. The relationship between current, voltage, and phase angle with the complex impedance is defined in the equations below[92]:

$$Z^* = Z' - jZ''$$
$$|Z| = \left[(Z')^2 + (Z'')^2\right]^{1/2}$$
$$\theta = \tan^{-1}\left(\frac{Z''}{Z'}\right)$$
$$Z' = |Z|\cos\theta$$
$$Z'' = |Z|\sin\theta$$

Where Z' is the real part of the impedance and represents the energy that passes through the material, and Z'' is the imaginary part of the impedance and represents energy lost or stored in the material.[93] The term j is $\sqrt{-1}$ and the real and imaginary part of each of these complex functions are designated with a prime and double prime respectively. The impedance magnitude is defined as $|Z|$.[92]

2.7.1. Frequency Dependent and Independent Plots

The real and imaginary components of the impedance are often plotted with the real component along the x-scale and the imaginary component on the y-scale. The convention with the imaginary component is to have the negative values along the y-axis in the first quadrant. These types of plots are complex plane plots but can also be known as frequency independent/implicit plots. While the frequency is not shown explicitly, for impedance behavior with a semicircle the frequency is increasing from right to left.[92] Some examples of some of the types of complex impedance behavior are shown in Figure 2.16 (a-d). Figure 2.16(a) is a semicircle in the first quadrant (Z' vs. $-Z''$), which is often a common type of impedance behavior. The resistance (R) can be estimated by the intercept of the complex impedance

semicircle with the real axis (Z').[92] In this case and for Figure 2.16(b) this is also the diameter of the semicircle. For Figure 2.16(c and d) the resistance would be where the lines intercept the Z' axis.[92]

A great deal of other information can be gathered from these plots. For example a capacitance can be extracted from Figure 2.16(a) by using the impedance and frequency at the apex of the semicircle. A similar method can be used to calculate the inductance in Figure 2.16(b). The shape of the curves is also telling. If the complex impedance has curves resembling semicircles, such as Figure 2.16(a and b) then this shows that there are elements in parallel. On the contrary, if the complex impedance is linear, such as 2.16(c and d) then it will have elements in series.[92]

Representing impedance data often comes in the form of frequency dependent plots, often know as Bode plots. Frequency dependent plots, or Bode plots, involves the log frequency with either the real or imaginary part of an impedance function. These plots are particularly useful since they can show the onset of a relaxation, through an increase or decrease with the real part of the component, or with a peak in the imaginary part.[92, 93] The plots are also useful in determining the type of element behavior in the impedance. This element behavior is especially explicit in the Bode plot of the phase angle. A phase angle of -90° is purely capacitive behavior, 0° is purely resistor behavior, and 90° is purely inductive behavior. When the impedance has multiple behaviors, the shift from one element to the other can occur at certain frequencies.[92] All of these types of behaviors are displayed in Figure 2.16(e). The impedance magnitude can also provide this element behavior. For example, a decrease in the impedance magnitude with frequency is indicative of capacitive behavior and an increase with frequency is inductive

behavior. When the curve flattens out at lower frequencies and becomes independent of frequency, then it is a resistor. All of these behaviors are shown in Figure 2.16(f).

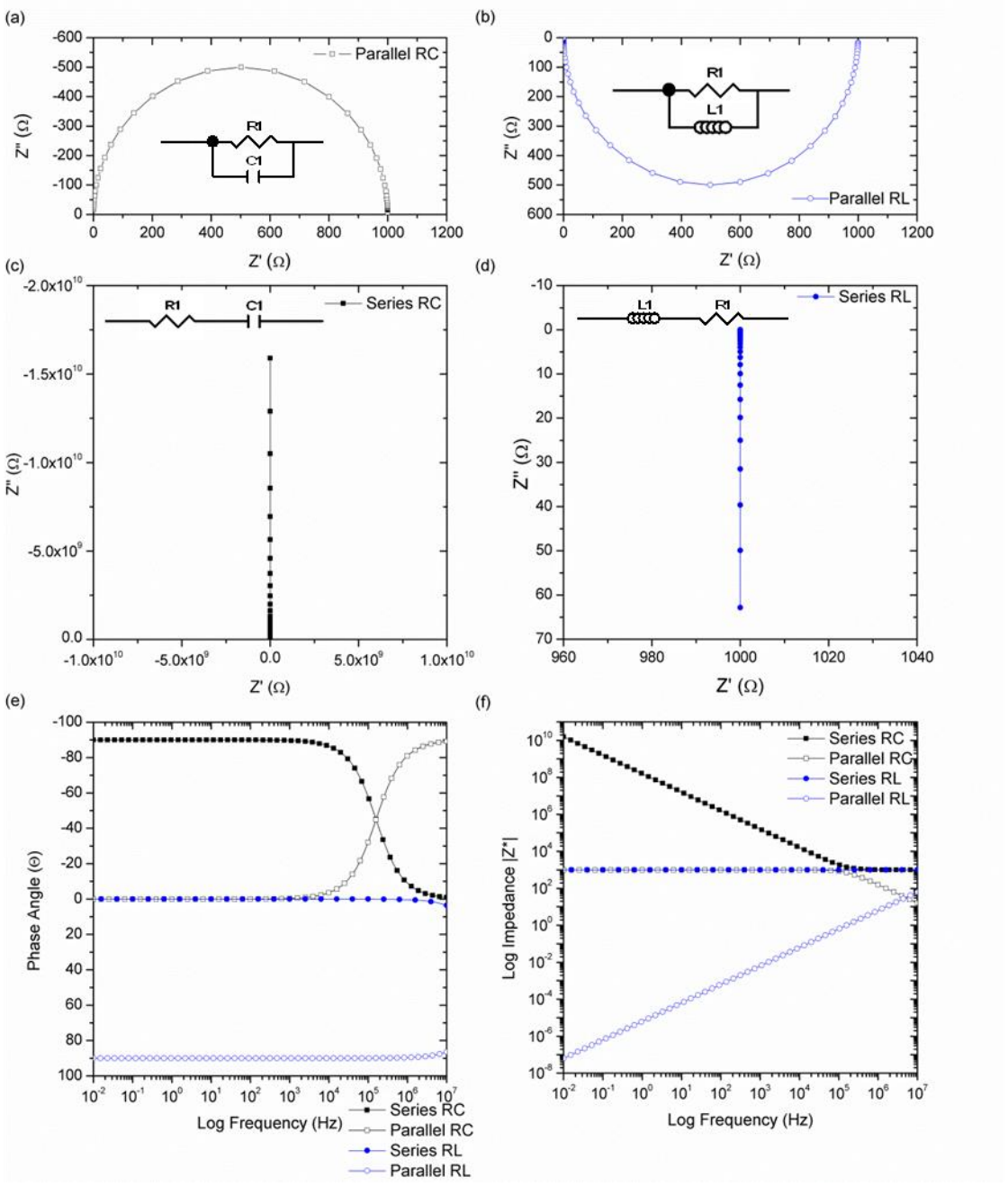

Figure 2.16. (a) Complex impedance for a resistor (1000 Ω) and capacitor (1 n*F*) in parallel. (b) Complex impedance for a resistor (1000 Ω) and inductor (1 μ*H*) in parallel. (c) Complex impedance for a resistor (1000 Ω) and capacitor (1 n*F*) in series.(d) Complex impedance for a resistor (1000 Ω) and inductor (1 μ*H*) in series. (e) Phase angle Bode plot of the circuit impedance from (a-d). (f) Impedance magnitude of the circuits from (a-d). Plots were created using the complex impedance equations of the circuits.[92]

2.7.2. Calculation of Additional Immitance Functions

Impedance spectroscopy allows for additional information besides the dc resistivity, such as the capacitance and loss tangent (*tan δ*). The use of this information can be used to calculate several types of immitance functions that highlight and emphasize different responses in the material and electrical behavior. So a comparison of all these functions would allow for the identification of different types of materials and processes.[23] A conducting material will behave very differently than an insulating material with these functions. These immitance functions include the impedance (*Z**), permittivity (*E**), dielectric modulus (*M**), and the admittance (*Y**). The equations to calculate these functions are shown below.[23, 92]

$$Z^* = Z' - jZ''$$
$$\varepsilon^* = \varepsilon' - j\varepsilon''$$
$$M^* = M' + jM''$$
$$Y^* = Y' + jY''$$
$$\tan\delta = \frac{\varepsilon''}{\varepsilon'} = \frac{M''}{M'} = \frac{Z'}{Z''} = \frac{Y'}{Y''}$$

2.7.3. Equivalent Circuit Modeling

All of the impedance spectra presented in Figure 2.16 are simulations of different types of circuits. For example Figure 2.16(a) was made with a resistor (1000 Ω) and capacitor (1n*F*) in parallel (parallel RC). When a material is measured using impedance spectroscopy, it often will exhibit similar, or a mix of behavior of the impedances displayed in Figure 2.16(a-f). In order to help to properly analyze this material impedance information, a circuit is often created that matches the impedance data for the material. This will allow for the material impedance data to be analyzed and also allow for the different processes that are occurring in the material to be explained with a circuit element.[92-94] A classical example of this is a polycrystalline ceramic having an equivalent circuit fit of two parallel RCs in series.[95] One of these RCs can be

attributed to the material behavior while the other parallel RC is due to the added resistance and capacitance of the grain boundary.[94-96] One of the common pitfalls with equivalent circuit modeling is that most people only use the complex impedance for the equivalent circuit fitting.[92, 97] Multiple circuits can be used to fit the same complex impedance data so it is important to use the other immitance functions in conjunction with the complex impedance to obtain as accurate of an equivalent circuit fit as possible.

2.8. Background on Materials to be Made Into Composites

The materials in this study will focus on a borosilicate glass as the matrix material, which in this case is the majority phase of the composite, and antimony tin oxide (ATO) and silicon carbide whiskers (SiC_w) as the added phase/filler materials.

2.8.1. Overview of Borosilicate Glass

Borosilicate glass is often utilized for its, low thermal expansion (30-60 x 10^{-7}/°C), chemical durability, glass transition temperatures ranging from 500-600°C, and relatively low melting temperature.[68] Pyrex® is one of the more commercial compositions of borosilicate glass[72] and is the glass used in this study. The name Pyrex® in this study will refer to the composition originally based from Corning, and not the new Pyrex® from World Kitchen, LLC which is a soda lime silicate glass. The composition of Pyrex® places it on the edge of immiscibility. For Pyrex, the immiscibility leads to nucleated phase droplets, which are kept small (20-50 Å) through rapid cooling.[68] These droplets are rich in boron which means they are surrounded by a silica rich matrix. This silica rich matrix improves the chemical durability and the low thermal expansion, which is why this glass composition is often used for laboratory glassware.[68]

2.8.2. Overview of Antimony Tin Oxide

The primary filler for this study will be antimony doped tin oxide, which is often referred as ATO. Like ITO, ATO is a transparent conducting oxide.[11] ATO has been garnering more attention lately since it is seen as a potential replacement for ITO due to the much lower cost.[98] There are a few reasons why ITO is currently being used more than ATO. ITO has a higher conductivity, so for solar cell and transparent conductors, this is highly desirable. Also in order to create ITO films, a common method to create these films is magnetron sputtering, which requires a high quality target.[13] ITO targets have been sintered to full density relatively easily, but ATO targets cannot be made easily made dense. This is due to some dominant nondensifying sintering mechanisms which includes surface diffusion, evaporation-condensation, and especially for ATO, a high vapor pressure for temperatures over 1000°C, which are temperatures needed for sintering.[13]

Tin oxide (SnO_2) itself is a wide-band-gap semiconductor (~3.6eV at RT) with a rutile structure (tetragonal cassiterite).[99] The tin atoms are located at the corner and center position of the unit cell, and the oxygens are located at the tetrahedral interstitials.[99, 100] When doped with antimony, the antimony replaces the tin at these positions. The addition of dopants such as antimony can greatly decrease the electrical resistivity (from 10^7 to 10^{-4} $\Omega \cdot cm$).[9, 12, 98] This resistivity for ATO is highly dependent on the amount of antimony doping. There are several theories as to the cause of the dependency but one of the leading theories is the possibility of two different oxidation states for antimony. Sb^{5+} is the main oxidation state at low levels of doping (<10%), which results in a decrease in the resistivity.[9] The Kroger-Vink notation for this doping is shown below.

$$2Sb^{5+} \rightarrow 2Sb_{Sn}^{\cdot\cdot} + 2e'$$

The Sb^{5+} oxidation state leads to n-type behavior with the free electrons it produces. As a result the conductivity for the material increases significantly. With this doping the material acts as a degenerate semiconductor exhibiting metallic conduction properties.[98] This change in the electrical properties can be seen in Figure 2.17 with a current-voltage curve of various doping concentrations of ATO and pure SnO_2. From these nonlinear curves, the tin oxide behaves like a semiconductor, but the addition of the antimony to SnO_2 has led to these materials to act like an ohmic resistor since they follow ohm's law.[98] Most of the ATO has a concentration between 1 and 10% antimony in order to get the lowest resistivities.[9, 12, 31]

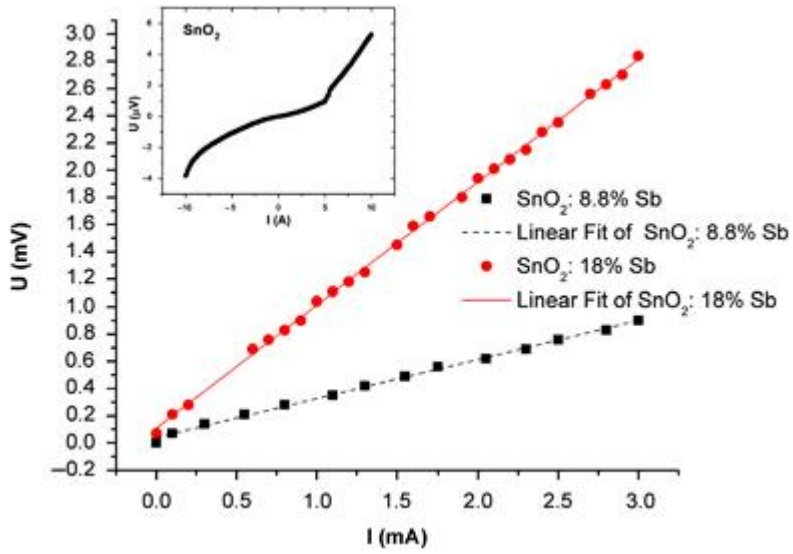

Figure 2.17. Room temperature current and voltage measurements for SnO_2, 8.8% antimony doped SnO_2, and 18% antimony doped SnO_2.[92]

At a certain concentration of antimony doping, Sb^{3+} will start to appear, which will be detrimental to the conductivity created by the Sb^{5+} state. This is due to a switch to p-type and the loss of these free electrons.[98] The defect reaction for this oxidation state is shown below.

$$2Sb^{3+} \rightarrow 2Sb'_{Sn} + V_O^{\cdot\cdot}$$

2.8.3. Overview of Silicon Carbide Whiskers

The other type of filler to be used in this project are silicon carbide whiskers (SiC_w). The term whisker refers to a small single crystalline rod. These whiskers are typically a micron or less in diameter and usually have an aspect ratio much greater than one.[101] Whiskers are often used in composites for their mechanical and thermal properties such as cutting tools, since the addition of whiskers often leads to an increase in fracture toughness.[102] They are also being used more for microwave heating applications. This is because the whiskers have a high dielectric loss factor[48, 103], which means with the application of a microwave the whiskers will heat up quickly.[104]

These whiskers can be produced from several different methods including chemical vapor deposition, plasma deposition, and pyrolysis of agricultural waste such as rich hulls and sugarcane leaf. SiC has numerous polytypes but the material for this study will focus on the form which is a β-cubic zinc blende structure.[105]

CHAPTER 3

EXPERIMENTAL PROCEDURES

This section provides details concerning the main fabrication steps used to obtain the composites described in this thesis and the methods used to characterize them. Additional experimental details of some of these methods, particularly the hot pressing conditions, are noted in the subsequent relevant chapters.

3.1 Composite Fabrication

Several batches of composites containing borosilicate glass, that had a composition equivalent to Pyrex®[68], and a variety of filler materials, with different shapes, and sizes were made in this study. The various types of glass and filler used in this study are listed in Table 3.1. below. The shape and sizes were estimated by the optical and SEM images shown in Figure 3.1. and 3.2 together with information provided by the manufacturers.[106-109]

Table 3.1. Details Concerning the Various Types of Matrix and Filler Materials used in These Composites Provided by the Manufacturer and Details Extrapolated by SEM.[106-109]

Matrix Type	**Particle Size**	**Shape**	**Manufacturer**
GL0179S	34-50 μm	Spherical	Mo-Sci
GL0179L	212-250 μm	Spherical	Mo-Sci
Filler Type	**Particle Size**	**Shape**	**Manufacturer**
ATO(nm)	~40-70nm	Roughly Spherical	Alfa Aesar
ATO (μm)	~0.5-2 μm	Roughly Spherical	Sulzer
SiC_w (SC-9M)	0.5-0.8 μm (Diameter) ~10 μm (length)	Rod	Advanced Composite Materials L.L.C.

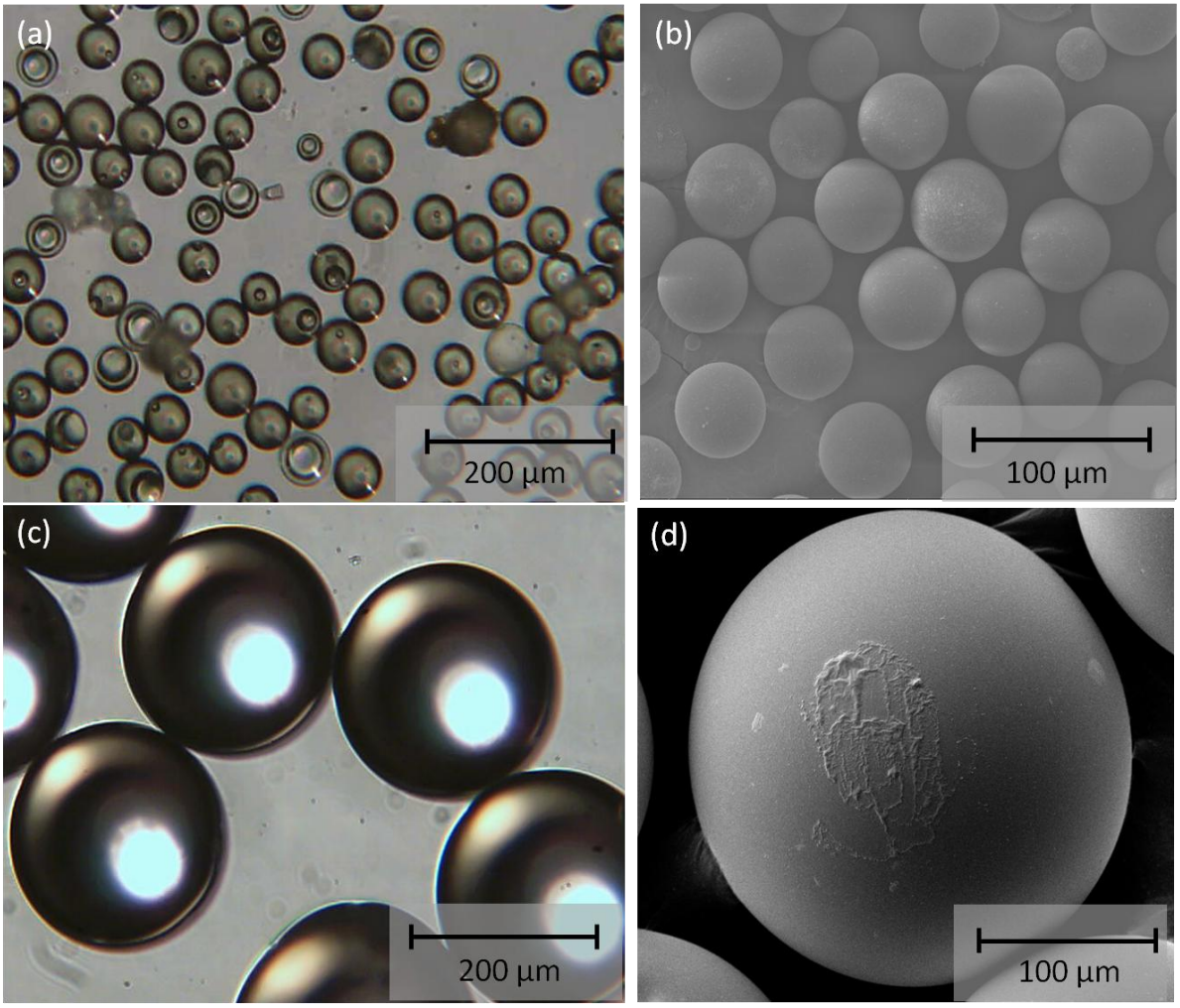

Figure 3.1. Micrographs of the borosilicate glass microspheres used in this study. (a) Optical[110] and (b) SEM micrographs of GL0179S. (c) Optical and (d) SEM micrographs of GL0179L.

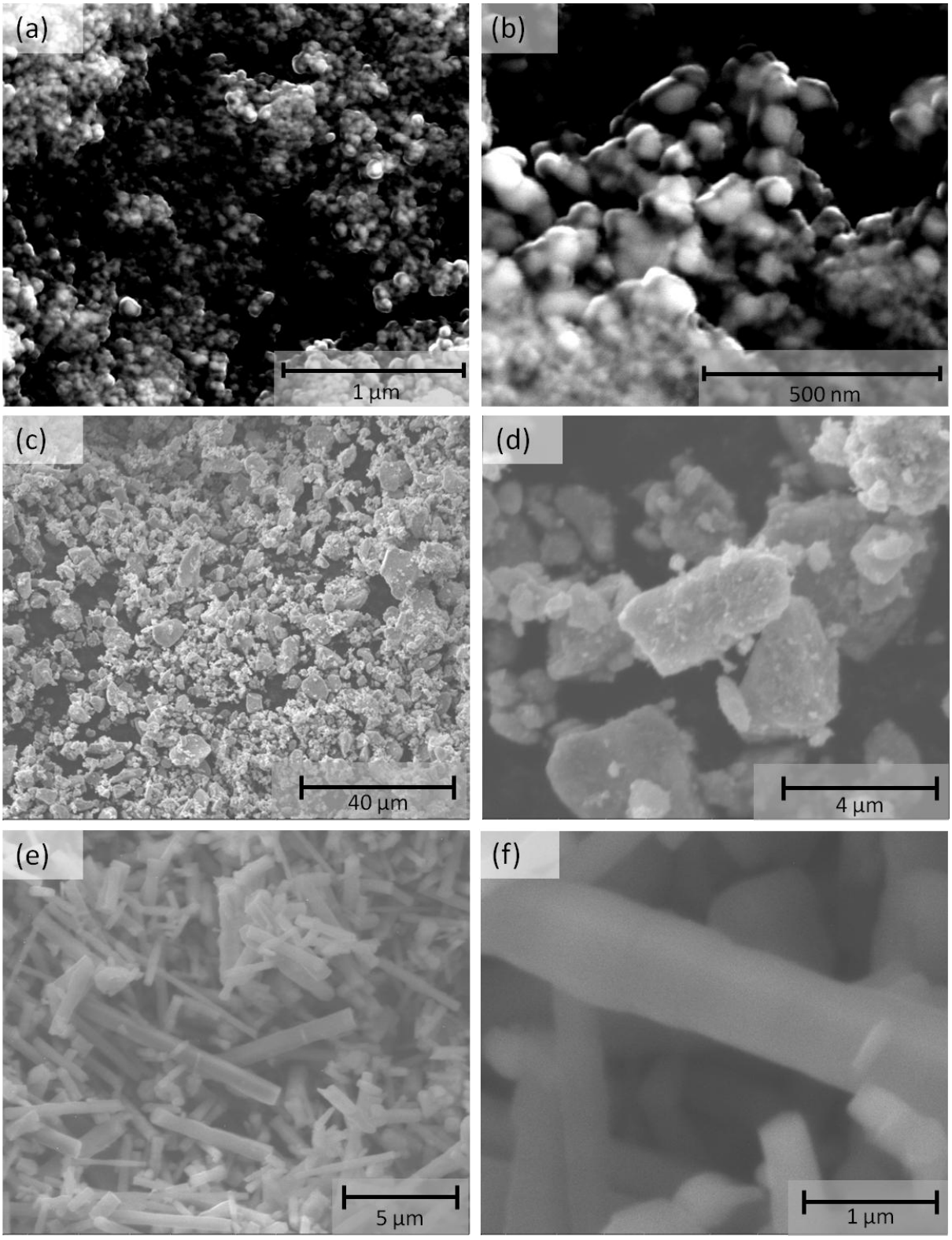

Figure 3.2. SEM micrographs of the various fillers used in this study. (a) Low magnification[110] and (b) high magnification of ATO(nm). (c) Low magnification and (d) high magnification of ATO(µm). (e) Low magnification and (f) high magnification of SiC_w (SC-9M)[111].

3.1.1. Mixed Powder Processing

For all the compositions in the sets, the matrix and filler powders were mixed using a rotary ball mill with 5mm alumina media(99.5%), although the glass microspheres appeared to contribute in dispersing the ATO and SiC_w. Table 3.2. summarizes the matrix and filler used in each set of composites made. The concentration of filler in these composites ranged from 0.001 to 12.5 parts per hundred, glass (phr). The filler compositions for each set are summarized in Table 3.3. The mechanical blending from the ball mill, which lasted about four hours for each composition, seemed to be sufficient at coating the glass particles with the filler. In Figure 3.3. it can be seen that the ATO(nm) in particular adhered to the glass microspheres quite well. Some ATO seemed to have come off during SEM sample preparation but for most of the particles, and especially the higher concentrations, the coating of ATO on the glass particles was very consistent.

Table 3.2. Summary of Glass Composite Sets that Describes the Matrix and Filler Material Used, the Peak Hot Pressing Temperature, and the Peak Hot Pressing Pressure.

Set	Matrix Type	Filler Type	Peak HP Temp (°C)	Peak HP Pressure (MPa)
1	GL0179S	ATO(nm)	550	23.4
2	GL0179S	ATO(nm)	675	23.4
3	GL0179L	ATO(nm)	675	23.4
4	GL0179S	ATO(µm)	675	23.4
5	GL0179S	SiC_w (SC-9M)	675	11.7
1-T	GL0179S	ATO(nm)	610	23.4
2-P1	GL0179S	ATO(nm)	675	11.7
2-P2	GL0179S	ATO(nm)	675	6.5

Table 3.3. Concentration in Phr (Parts Per Hundred, Glass) and Vol % of ATO and SiC_w Fillers in Glass Matrix Composites. Compositions that were Made in Each Set are Marked with an "x".

Phr	ATO								SiC_w	
	Vol% ATO	Set#1	Set#2	Set#3	Set#4	Set #1-T	Set#2-P1	Set#2-P2	Vol% SiC_w	Set#5
0	0	x	x	x	x	-	-	-	0	x
0.001	3.24×10^{-4}	x	x	x	x	-	-	-	1.10×10^{-3}	x
0.01	3.24×10^{-3}	x	x	x	x	-	-	-	1.10×10^{-2}	-
0.05	1.62×10^{-2}	x	-	-	-	-	-	-	5.50×10^{-2}	-
0.1	3.24×10^{-2}	x	x	x	x	-	-	-	0.11	x
0.25	8.10×10^{-2}	x	x	-	-	-	-	-	0.27	x
1	0.32	x	x	x	x	-	-	-	1.09	-
1.5	0.48	-	x	-	-	-	-	-	1.64	-
2.5	0.82	x	x	x	x	-	-	-	2.63	x
5	1.67	x	x	x	x	x	x	x	5.20	x
7.5	2.43	x	x	x	-	-	-	-	7.60	x
10	3.24	x	x	x	x	-	-	-	9.88	x
12.5	4.05	-	-	-	-	-	-	-	12.10	x

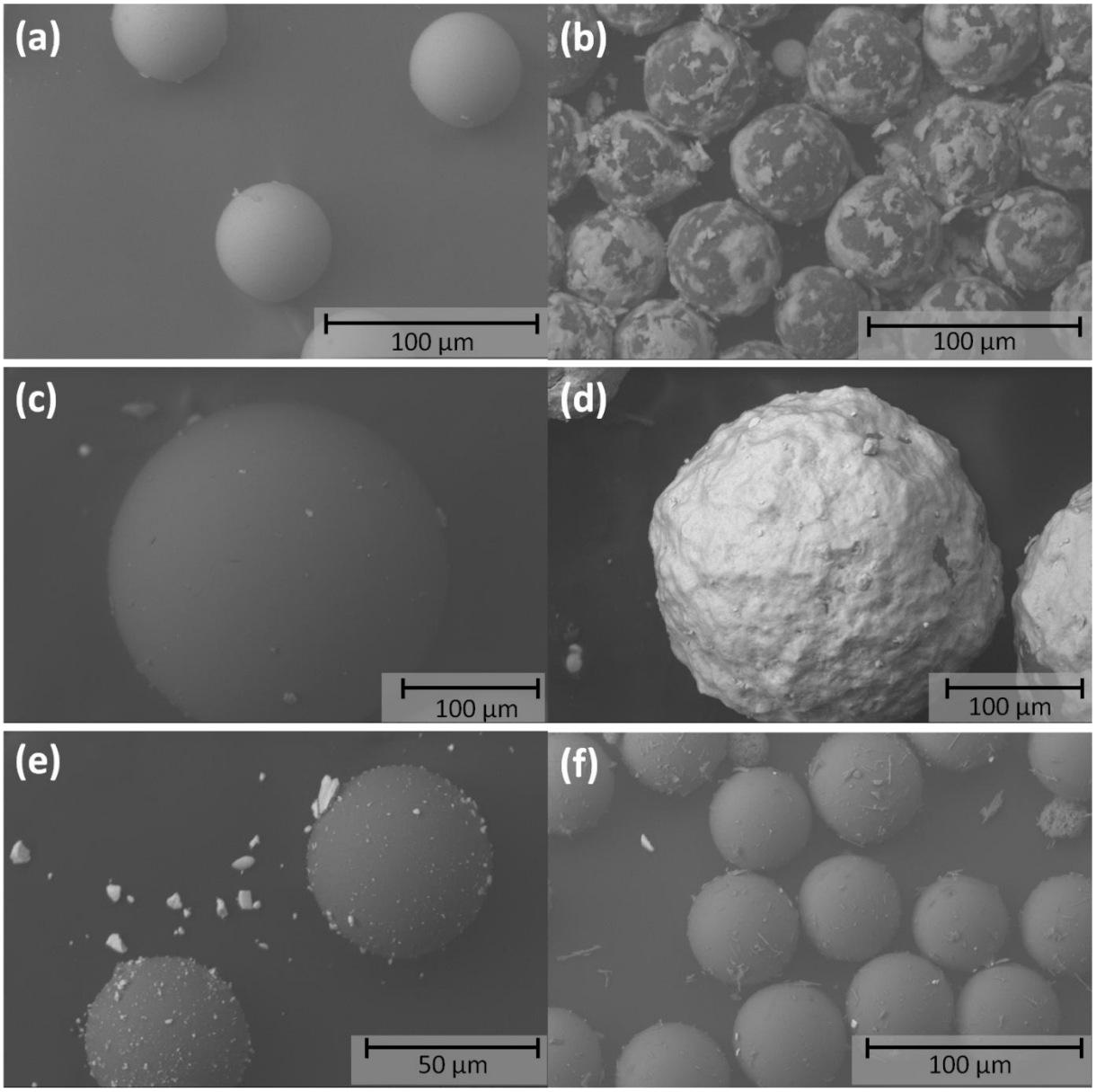

Figure 3.3. Micrographs of low and high concentrations of filler mixed with glass microspheres. (a) Low concentration(0.01 phr) and (b) high concentration(7.5 phr) of ATO(nm) coating GL0179S. (c) Low concentration (0.01 phr) and (d) high concentration (10 phr) of ATO(nm) coating GL0179L. (e) 2.5 phr of ATO(µm) coating GL0179S. (f) 7.5 phr SiC_w (SC-9M) coating GL0179S. Both the ATO and SiC_w have a higher density than the glass so they are the brighter particles in the micrographs.

3.1.2. Hot Pressing

The powder mixtures were hot pressed using an Astro Press located at Advanced Composite Materials (ACM) L.L.C.. The powder was placed in a graphite die lined with graphite foil (grafoil). Three samples for each composition were pressed within a die, which were separated by a graphite spacer lined with grafoil. A schematic of the loading and the die is shown in Figure 3.4. The grafoil was located at all the exposed faces of the graphite die in order to prevent the glass from adhering to the die and making removal difficult during post processing.

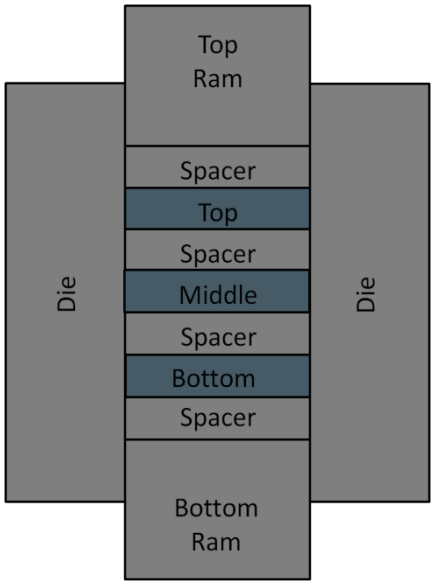

Figure 3.4. Schematic of the mixed powder (blue rectangles) in the graphite die(gray) during hot pressing.

Before the mixed powder was placed in the die, the grafoil was wiped down in order to help prevent excess graphite from entering the glass. The powder was poured into each section of the die (Figure 3.4) and the die was tapped to create an even layer of the powder. Once all the powder was loaded, the graphite die was dry pressed using an uniaxial press to about 100MPa.

Higher pressures were avoided during dry pressing to avoid fracturing the glass microspheres. During each hot press run, the die was placed within the hot press shell and vacuum was pulled before a flowing N_2 atmosphere was introduced. Several heating and pressure curves were used for these composite and the details of these curves will be discussed in the subsequent chapters. All of the composites had processing parameters, described in Table 3.2., that consisted of a peak temperature between 550° and 675°C and a max pressure between 6.5-23.4 MPa. At the end of the peak temperature run, the hot press was water cooled to 300° C. After this temperature the outer shell of the hot press was raised and the die was allowed to air cool to room temperature. The glass composites, once stripped of the graphite dies, were lightly sandblasted to remove any excess carbon or grafoil that may have remained on the surface of the glass. The thickness of the composites ranged from about 5-10 mm. The densities of the specimens were then determined via the Archimedes method using water.

3.2. Sample Surface Preparation

3.2.1 Sectioning and Polishing

For the various electrical and microstructural characterization methods, the specimens were sectioned using a diamond blade. Composites with an excessive amount of carbon along the edges had the carbon-rich regions sectioned off to minimize any carbon influence on the electrical properties. For all the hot-pressed specimens, SiC grit paper (Buehler, Lake Bluff, IL) was used to smooth out the sample surface for both electrical measurements as well examination by microscopy. This grinding also helped to remove any excess carbon that may have remained on the surface. Grits of 180, 320, 600, and 1200 were used. Cross sections that were observed in

the SEM were further polished to a mirror finish with 0.25 µm alumina polishing media (Buehler).

3.2.2. Electrode Deposition

For all the electrical characterization methods, an electrode was deposited onto the large polished flat faces (parallel-plate configuration). Before deposition, all the sample surfaces were cleaned first with distilled water then with isopropyl alcohol (IPA). The samples were dried with compressed air to remove any residual water or IPA. The electrode was applied by sputtering Ag (nominal purity of 99.9%-Alfa Aesar) with an argon plasma in a Denton Vacuum Desk II Turbo Sputter Coater. To prevent deposition onto the side wall of the sample, which would cause a short, Scotch® tape was used to cover the sides and act as a mask during deposition.

3.3. Microstructural Characterization

The primary microstructural characterization methods (SEM and optical microscopy) are discussed below. Atomic force microscopy (AFM) and current-atomic force microscopy (I-AFM) are discussed in Chapter 3.

3.3.1. Optical Microscopy

Optical micrographs of polished cross sections (both parallel and perpendicular to the hot pressing direction) were acquired using a XSB 411 and a LEICA DMRX microscope. All optical photographs were taken with the XSB 411 primarily at 4x and 10x. The LEICA is a stereographic microscope and was particularly useful in looking through the deformed glass particles to confirm the shape of the glass particle and the location of the filler.

3.3.2. Scanning Electron Microscopy (SEM)

Several different SEM microscopes were used to study these composites, primarily using a backscatter detector. The microstructure of these composites were primarily viewed with a FEI Quanta 600 and 200 ESEM (FEI, Hillsboro, OR) and a Hitachi 3700 variable pressure SEM (Hitachi, Dallas, TX). An accelerating voltage of about 10-15 kV was typically used. When the sample was sputter-coated with some type of conducting thin film, the filler in the glass was difficult to resolve so most of the images obtained were taken without a conducting film. The Hitachi 3700 variable pressure SEM was advantageous in this regard since a pressure of about 40 Pa (air) inside the microscope dissipated all charging and allowed the microstructure to be observed. The 3700 also had an EDS detector which was also used in this study to help identify the compositions at different regions in these composites.

3.4. Electrical Characterization

3.4.1. Alternating Current (ac) Impedance Spectroscopy Measurements

Electrical characterization through the thickness of the composites was performed using impedance spectroscopy. The dimensions of the composite samples, which were used for resistivity calculations, were taken with a digital caliper (Mitutoyo Corp., model 500-196). Since the composites were expected to have a wide range of electrical behavior, a Solartron 1260 analyzer was used in conjunction with a Solartron 1296 Dielectric Interface (Solartron Analytical, Farnborough, Hampshire, U.K.). All scans were taken with a 500mV ac voltage and a frequency range of 10MHz-0.1 Hz with the electric field generally applied parallel to the hot pressing direction (||-HPD). Measurements perpendicular to the hot pressing direction ($\perp$-HPD) were also made, but this was significant only for the samples with SiC_w as the filler. A

schematic of this is shown in Figure 3.5. Samples were scanned soon after the electrodes were ready in order to avoid any aging effects.

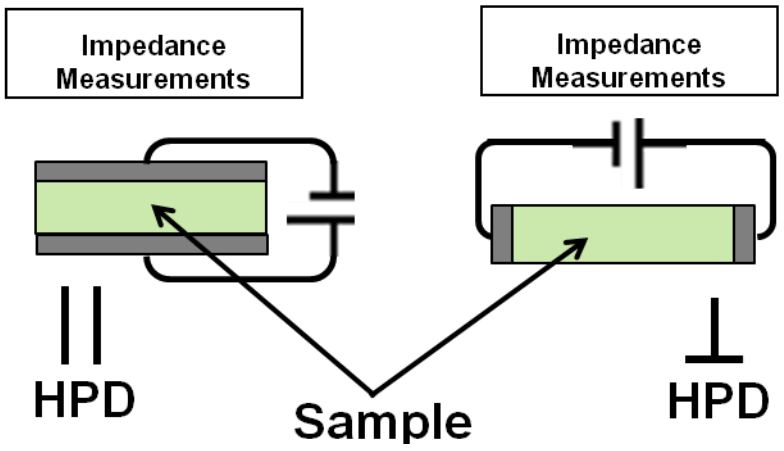

Figure 3.5. Schematic of the electrical characterization set up used for both ac and dc measurements with the composite and electrode arranged (a) parallel to the hot pressing direction and (b) perpendicular to the hot pressing direction.

3.4.2. Direct Current (dc) Calculations and Measurements

The dc resistance, which can be used to calculate the dc conductivity or resistivity, can be taken from this impedance data from the intercept of the impedance data with the real axis intercept (Z'_{int}) in the complex impedance plot (Z" v. Z').[92] The calculation for the dc resistivity is shown in equation (3.1) below where A and t are the cross-sectional area and thickness of the composite. In order to confirm the correct value of Z'_{int} from the impedance data, dc resistance measurements were also made with a Keithley 6430 (Keithley Instruments, Cleveland, OH) using the set-up in Figure 3.5 (a).

$$\rho_{dc} = \frac{A \cdot Z'_{int}}{t} \tag{3.1}$$

3.4.3. Electrical Characterization of Powders

In order to know an expected impedance that these fillers and mixes may have, a method was created to measure the impedance of powders by using a special die that was designed and

custom made for this study. A schematic of the die used is shown in Figure 3.6. below. The concept behind this die is to allow impedance spectroscopy measurements to be made on powders that are under an applied load. At high enough pressures, the compacted powder should have a good contact with one another and as a result, provide a good estimate of the expected electrical properties for the filler. As mentioned before, impedance spectroscopy can be used to calculate a dc resistivity which can be used to predict a limit that these composites can reach. Impedance spectroscopy however, has a great deal of additional information that can come from it. One of the additional bits of information that can come from this method is the expected impedance behavior for the filler that is physically contacting one another. This will provide a good comparison to the hot pressed composites in order to determine the type of contact a given filler has with one another inside the hot pressed composite.

A 12-ton model-C uniaxial Carver press (Carver Inc., Wabash, IN) was used to apply the pressure. A two-probe connection was used that connected to the top and bottom pieces of the steel pistons. The steel pistons were insulated from the Carver press, in order to prevent the impedance measurement to be made on the press, by using highly insulating paper and electrical tape. The impedance measurements will be made through the pistons and the compacted powder. For the filler particles (ATO and SiC_w) the impedance was measured at pressures between 0 MPa to 300 MPa, typically in increments of 50 MPa. Powder mixtures of the glass and filler were also used but the max pressure was 50 MPa in 5 MPa increments in order to prevent any glass microspheres from breaking.

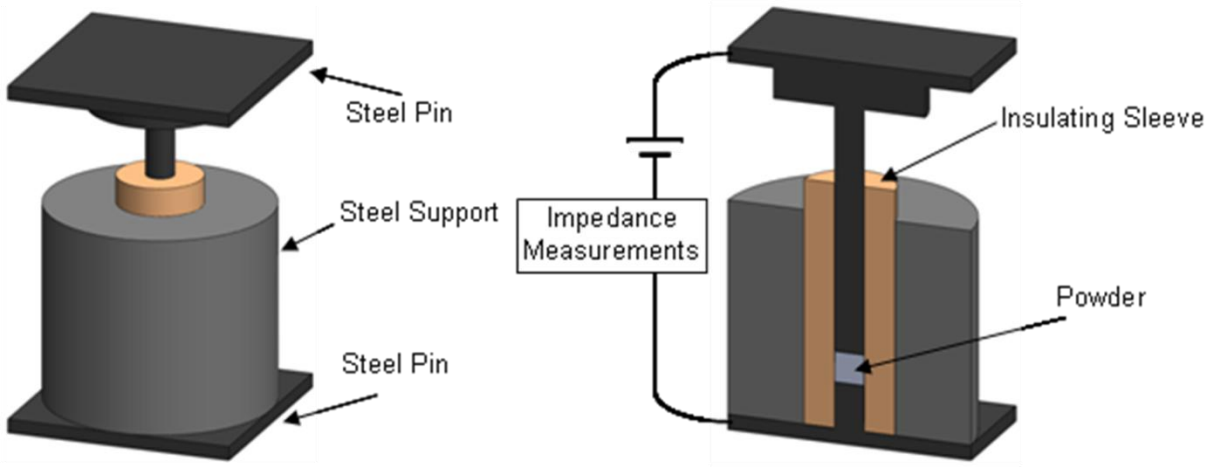

Figure 3.6. Schematic of the electrical characterization set up created for this study to measure the electrical properties of particulate materials under an applied pressure.

CHAPTER 4

CONFIRMATION OF ELECTRICALLY CONDUCTING SEGREGATED ATO NETWORKS

In this chapter the results obtained by using the various characterization methods described in the previous chapter are presented and discussed. Since this study is heavily dependent on using the segregation method to make glass composites, it is important to confirm the location of the filler and if this processing method produced consolidated composites with the desired microstructure.

4.1. Processing of Set #1 and #2

As described earlier, in order to create composites with a segregated network, the viscosity has to be controlled so the filler particles will be pushed to the interface and segregate to the particle edges. Because of this, the processing temperature has to be lower than normal sintering temperatures so the viscosity is high enough that it prevents the filler from penetrating into the glass. At the same time the composite will still need to be consolidated so the temperature has to be high enough to allow for viscous flow to consolidate the composite. Figure 4.1 shows the heating curves used in set #1 and #2, which had a max temperature ranging from 550°C (set #1) to 675°C (set #2). These max temperatures are in the range of the glass transition temperature and halfway to the softening point of this borosilicate glass. In terms of viscosity, this range is about 10^{13}-10^{11} Pa·s which is a very high viscosity when attempting to consolidate a composite through sintering.[74] Typical temperatures and viscosity requirements to fully consolidate borosilicate glass through sintering are normally >900°C and $<10^{6}$ Pa·s.[68, 74] Even

though the processing temperature is several hundred degrees less than the conventional temperatures, the application of a uniaxial pressure should help offset this.

Listed below in Table 4.1 are the densities for the ATO composites (sets#1 and #2). The primary difference between these sets is the maximum processing temperature used. From the table it can be seen that for most of the concentrations of ATO, the relative densities are quite high, even though the temperatures used were about 300° C less than conventional sintering temperatures.

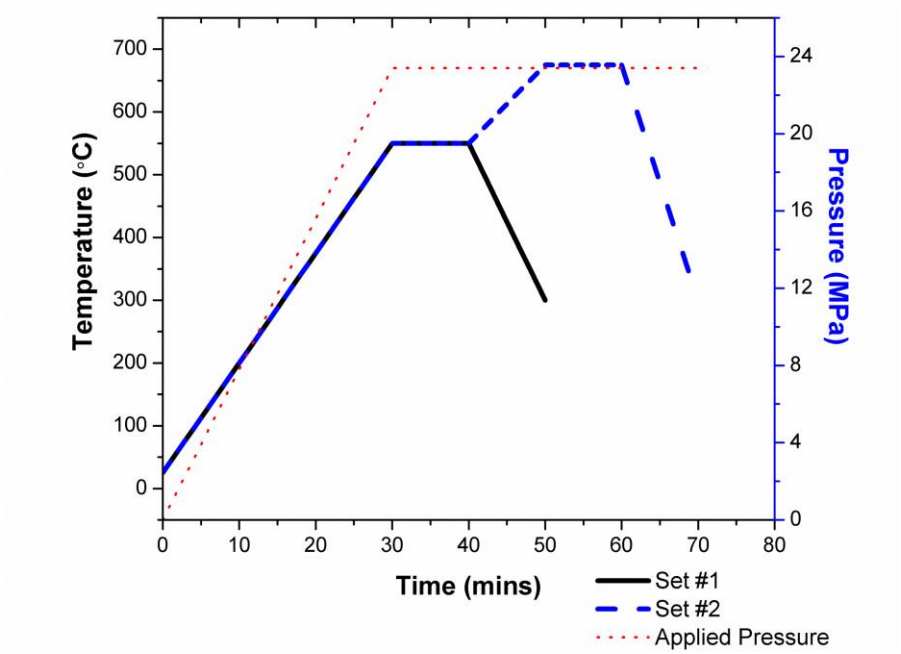

Figure 4.1. Heating and pressure curve for ATO(nm)-GL0179S glass composites for sets #1 (550°C peak temperature) and set #2 (675°C peak temperature hold). Both sets had a maximum pressure of 23.4 MPa applied during the peak temperature holds. Figure modified from reference [110].

Table 4.1. Relative Densities for Set#1 and #2 after Hot Pressing. Modified from Reference [110].

Powder Composition (ATO phr)	Relative Density-Archimedes Set#1	Relative Density-Archimedes Set#2
0.0	**99.47 ± 0.03**	
0.001	**99.49 ± 0.32**	**99.72 ± 0.02**
0.01	**98.89 ± 0.64**	**99.58 ± 0.06**
0.05	**99.66 ± 0.06**	**-**
0.1	**99.69 ± 0.10**	**99.67 ± 0.04**
0.25	**99.65 ± 0.08**	**99.47 ± 0.04**
1.0	**99.56 ± 0.27**	**99.33 ± 0.06**
1.5	**-**	**97.27 ± 0.19**
2.5	**99.25 ± 0.11**	**98.81 ± 0.24**
5.0	**98.95 ± 0.10**	**98.70 ± 0.08**
7.5	**98.16 ± 0.10**	**98.81± 0.25**
10.0	**96.91± 0.33**	**97.37± 0.19**

4.2. Confirmation of ATO Networks

Shown in Figure 4.2 are SEM micrographs of the general microstructures for several compositions for set #2. Since the ATO has a density about three times higher than that of the glass (6.8 g/cc v. 2.2 g/cc) the ATO will show up brighter when using a backscatter detector.[13, 68] There are distinct regions of the ATO that resemble grain boundaries in polycrystalline ceramics. Although for most of these composites the volume fraction of the ATO is quite small, for example the composition of 1.0 phr (Figure 4.1 (d)) has about 0.32 volume % ATO.

The actual composites are shown in Figure 4.3 (a-f). From this figure it can be seen that for low concentration samples from 0.1 to about 1.0 phr ATO (Figure (a-d), the composites are somewhat translucent. The composites have some coloration likely due to some carbon from the graphite die. The lower the concentration of ATO, the more susceptible the glass transparency was to the carbon impurities. This can be seen with 0.001 phr ATO compared to 0.01 phr ATO in Figure 4.3 (a) and (b). Past 1.0 phr ATO, the composites have a bluish hue to them due to the high concentrations of ATO, shown in Figure 4.3 (e and f).

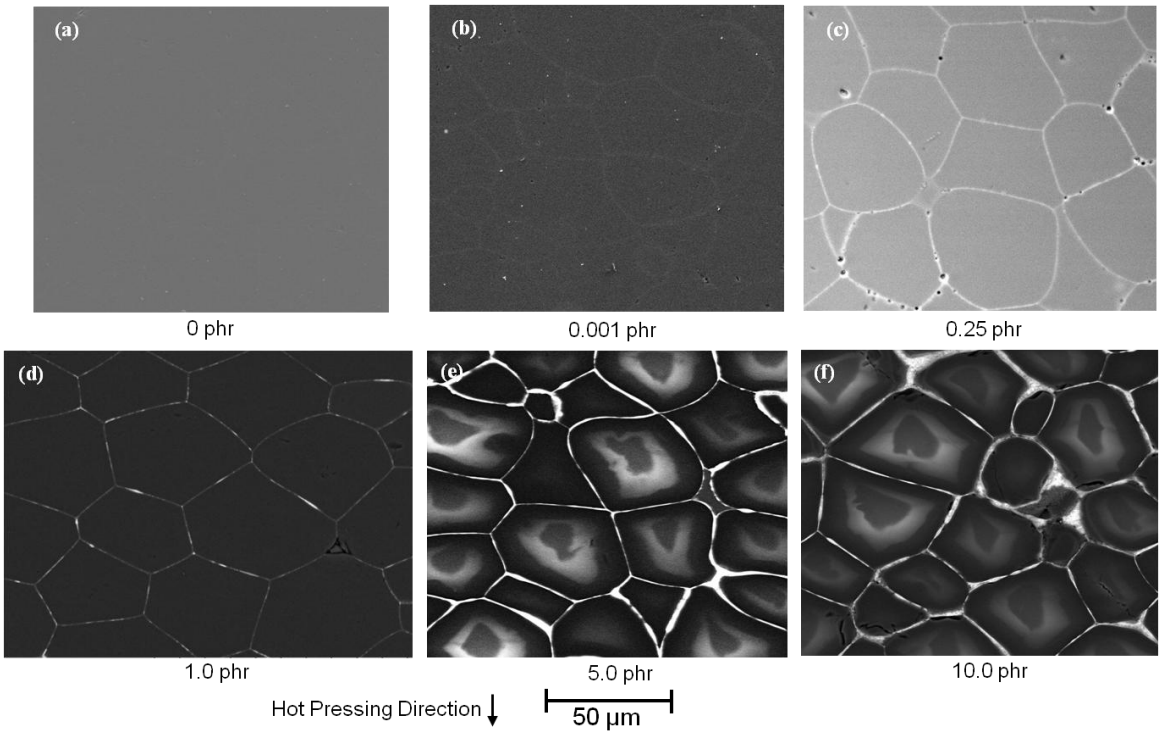

Figure 4.2. Selected microstructures of hot pressed glass composites from set #2 with the following compositions: (a) 0phr, (b) 0.001 phr, (c) 0.25 phr, (d) 1.0 phr, (e) 5.0 phr, and (f) 10.0 phr. Figure modified from reference [110].

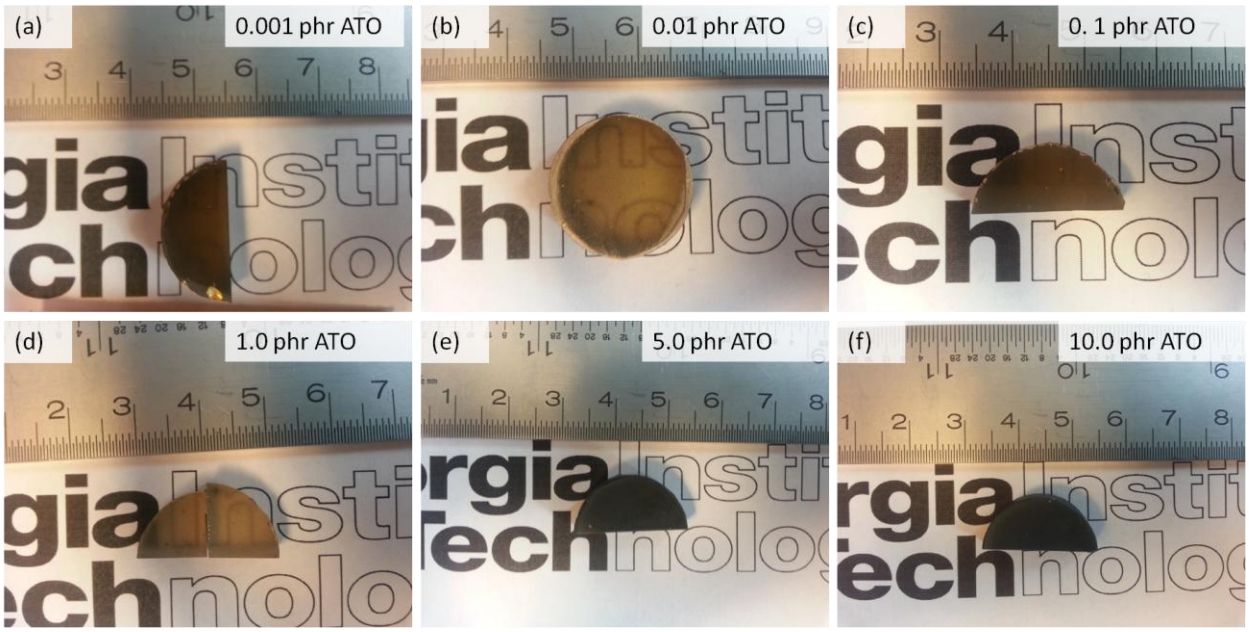

Figure 4.3. Optical images of hot pressed glass composites from set #2 with the following compositions: (a) 0.001phr, (b) 0.01 phr, (c) 0.01 phr, (d) 1.0 phr, (e) 5.0 phr, and (f) 10.0 phr.

The ATO is located in the regions at the boundaries of the deformed glass particles, which for the most part have a faceted shape. As a result the microstructure greatly resembles a polycrystalline ceramic microstructure. This microstructure was consistent throughout the composite for all of the compositions. Shown in Figure 4.4 below are several magnifications of the same composite showing that this distribution of the networks occurs throughout the entire composite and is not only in isolated regions.

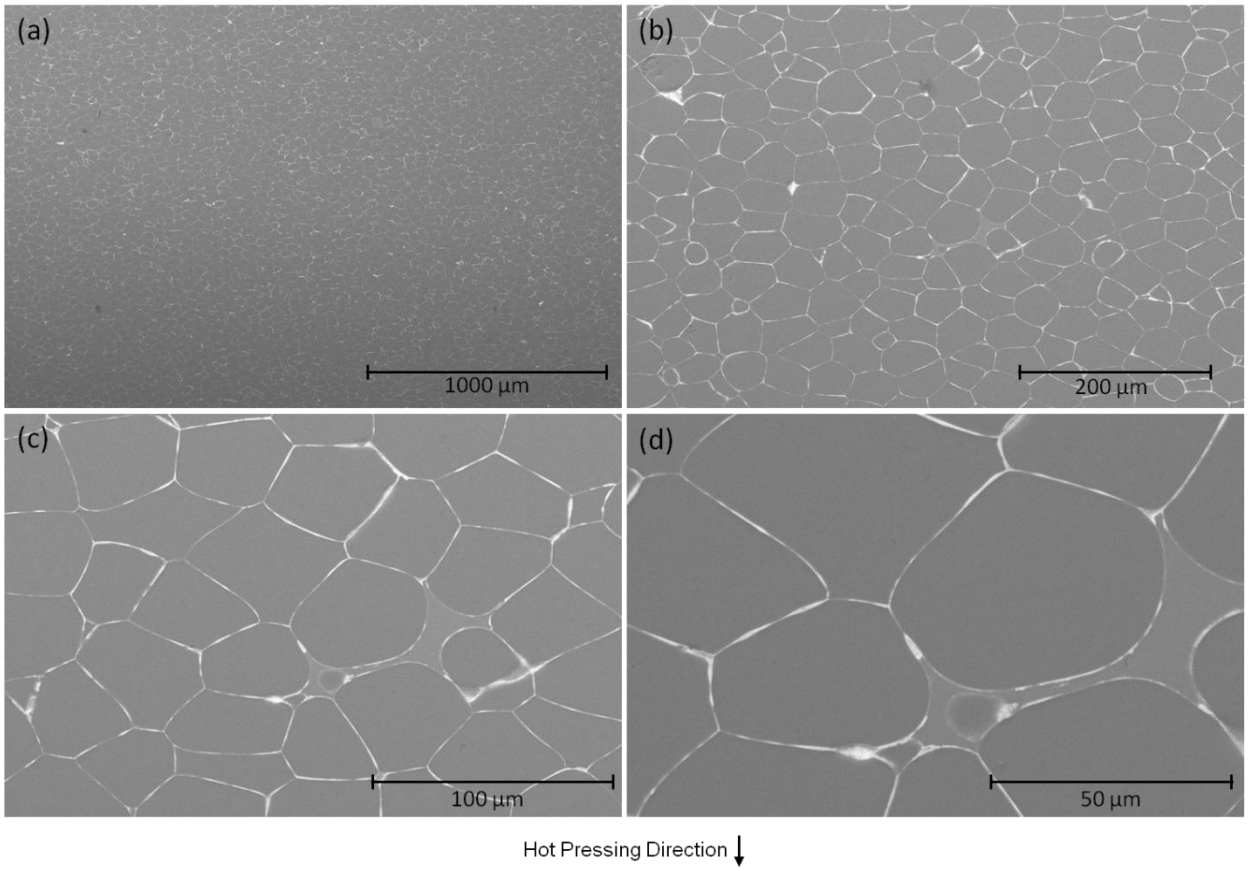

Figure 4.4. Microstructure of 5.0 phr from set#2 at magnifications ranging from 50x-1000x showing the consistent microstructure throughout.

The shape of the glass was quite consistent throughout the composite and any anisotropy that sometimes appeared with the glass particle was more due to the location in the composite than the orientation to the hot pressing direction. For example, particles near the edge and in

contact with the die had more orientation/alignment of the glass particles than in the center (which is the area shown in Figure 4.4). This orientation near the edge is due to the friction with the die wall. These regions of slight anisotropy did not seem to have a great influence on the overall properties of the ATO/glass composites.

However, the network of the ATO can also show some variability. At low concentrations of ATO, such as what is shown for the 0.1 phr ATO sample displayed in Figure 4.5(a), the ATO is located in between the glass particles and there seems to be some intermingling of the ATO and the glass at the very edge. At 0.1 phr, the concentration is not high enough which causes a gap. As the concentration increases, the ATO boundary becomes thicker and it appears to consist of two parts. Along the edge one can see glass and ATO, which is likely due to some penetration of the glass into the ATO. An example of this is shown in Figure 4.5(b). Towards the center of this ATO boundary, it appears to consist of just ATO. During polishing it appears that some of the ATO in the center was removed, likely due to the pure ATO in the center being more loosely bound than at the ATO/glass edges.

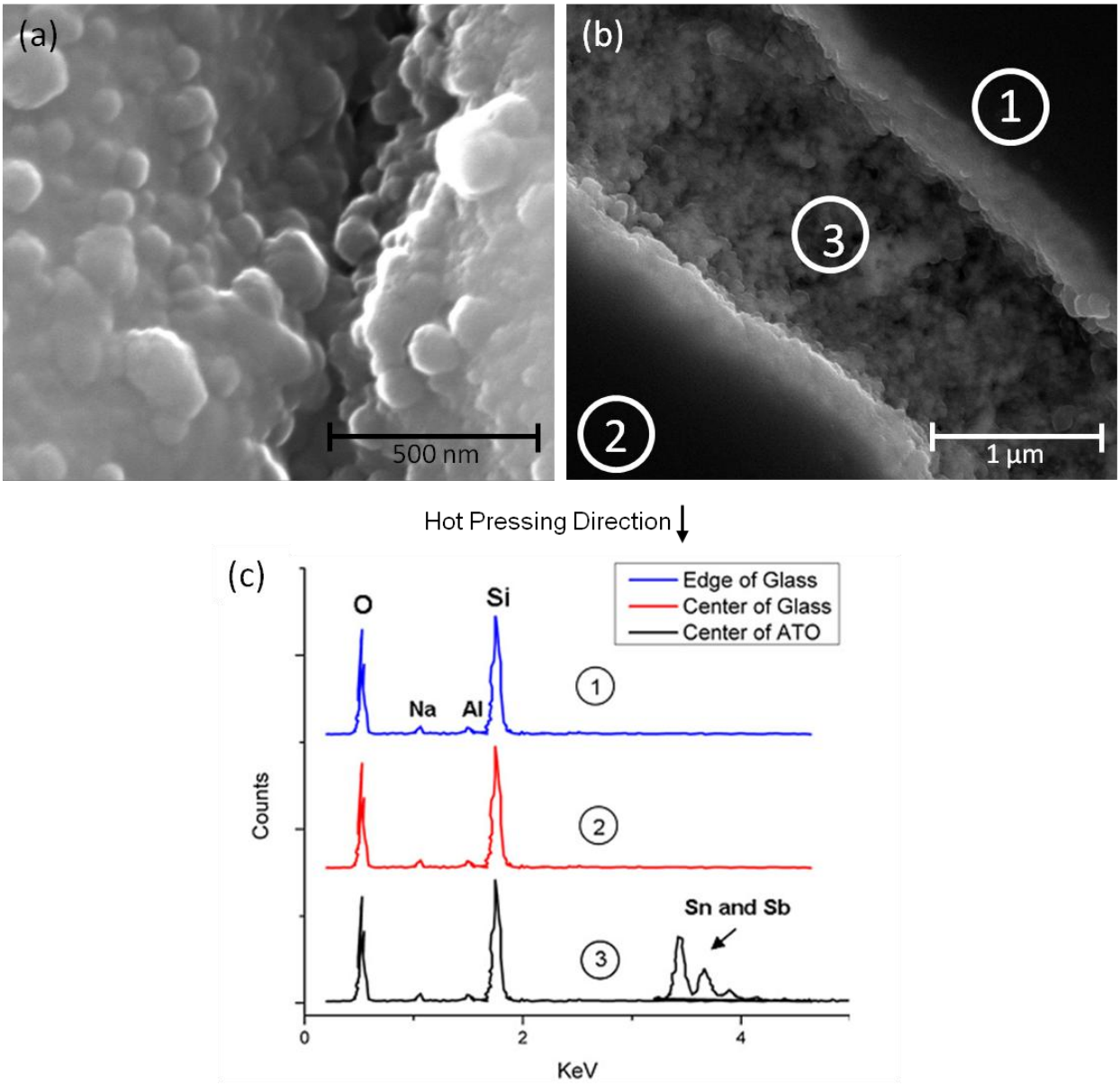

Figure 4.5. High magnification images of the ATO network in (a) 0.1 phr sample from set#1[112], (b) 2.5 phr from set#2, and (c) EDS spectra for the areas labeled in (b)[110].

In order to confirm the location of the ATO, EDS was performed on these composites. Both EDS and point scans were used to detect the location of the ATO. With the EDS point scans, the resulting spectra was dependent on the location of the scan. An example of this is shown in Figure 4.5(c) which is the resulting EDS spectra of areas shown in Figure 4.5(b). Several point scans of this area included the edge of the glass particle (1), at the center of the

glass particle (2), and at the center of the ATO network(3). It can be seen in Figure 4.5(c) that the only location that had any detectable ATO content was at the center of the ATO networks (3).

SEM images and the corresponding EDS maps of the 1.0 phr and 5.0 phr (set#2) samples are shown in Figure 4.6 (a) through (d). The SEM micrograph of 1.0 phr is displayed in Figure 4.6.(a) and the corresponding EDS map of the area is shown in Figure 4.6(b). For 5.0 phr ATO, the SEM micrograph and corresponding EDS map are in Figure 4.6(c) and (d), respectively. The EDS maps in Figure 4.6 (b) and (d) show the location of high concentrations of tin, which is the most distinguishing element that makes up the ATO.[113] The red/dark regions in Figure 4.6 (c) and (d) are these concentrated regions of tin, which match the bright areas in Figure 4.6 (a) and (b)[113]. The bright areas in Figure 4.6 (a) and (c) are the regions that are believed to be where all the ATO was segregated to. There also appears to be some slight coloration inside the glass particles. It is believed that this is mostly noise and possibly some ATO located beneath the particles. Numerous point scans of these areas, such as the ones in Figure 4.5(c) also indicates that these slight colorations inside the glass particles is just noise.

While SEM and EDS were able to confirm the location of the ATO at the boundaries, it is important to identify how much coverage the ATO has at these boundaries. Based on this processing method, the ATO should be located at the edges and triple points, but even with composites made using a similar process there is also the chance that the ATO could be located at the faces of the glass particles. In Figure 4.7(a) there is a schematic of a tetrakaidecahedron typically used in sintering models. Due to the processing method used, the glass goes from spherical shaped to a faceted polyhedral, similar to the tetrakaidecahedron. An ideal formation

in these composites is in the ATO is located at the gaps located at the boundaries (Figure 4.7 (b)) and not on the faces like in Figure 4.7 (a).

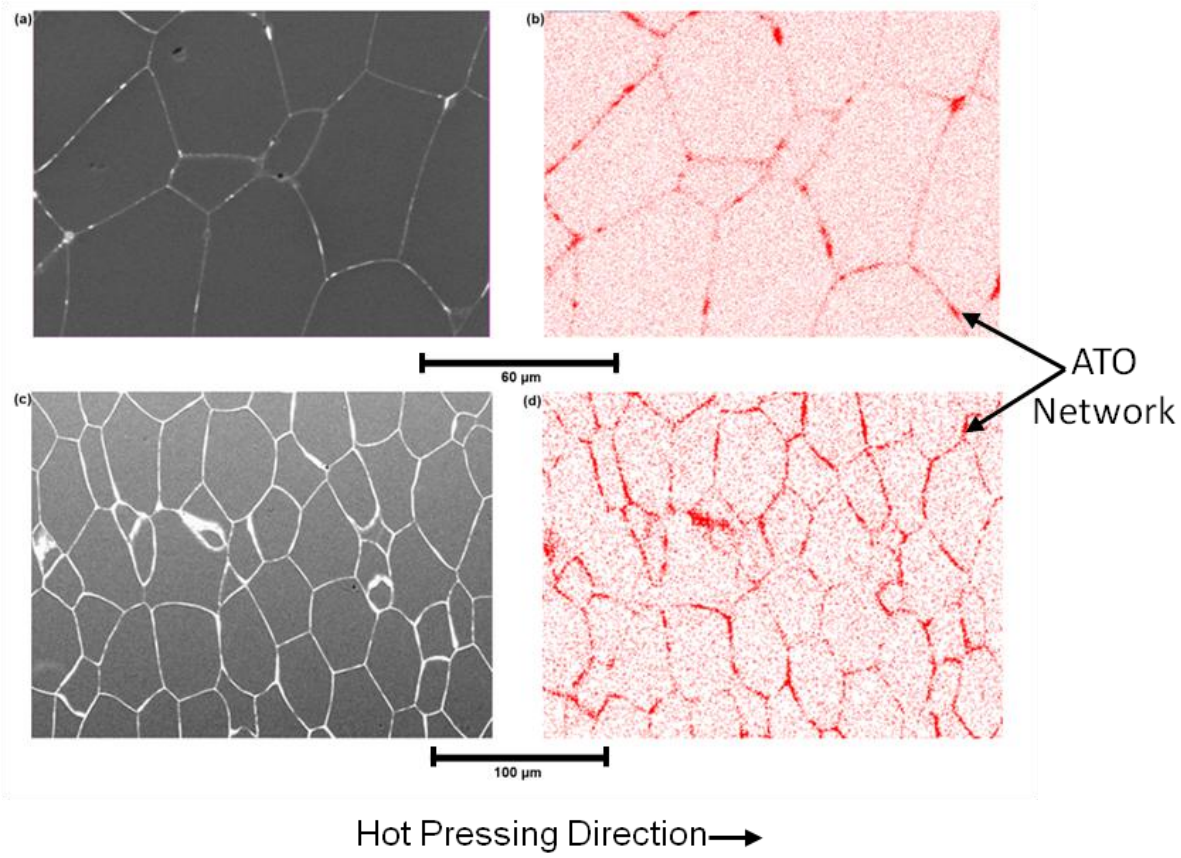

Figure 4.6. (a) SEM micrograph of 1.0 phr ATO (set#2) and (b) the same region but detecting the high concentrations of tin (red/dark regions). (c) SEM micrograph of 5.0 phr ATO (set#2) and (d) the corresponding EDS map. Image modified from reference [113].

Since the glass particles are transparent, a more convenient way to confirm the exact location of the ATO particles is to use optical microscopy. By either using a stereographic microscope and changing the depth of field on individual particles in the composite, the exact location of the ATO can be seen. An example of this technique is shown in Figure 4.6(c-d) with the 10phr sample from set #3 at different depths of field. The images shown here were taken with the larger glass (GL0179L) particle size because it is easier to see through these glass particles with the optical microscope and take an image. While some of the depth of the image is

lost when converting it to a 2-d image, the glass particle can be still resolved. The top of the particle is shown in Figure 4.7(c) and the bottom of the particle is shown in Figure 4.7(d). At the bottom is one of the edges of this faceted glass polyhedron and the ATO can be seen to be located all along the edge. Based on the contour of the glass particle from the optical images, the glass does have a polyhedral shape similar to Figure 4.7(b). This was also confirmed with sets#1 and #2 in the stereographical microscope, which is not shown here because the microscope did not have a camera and pictures were not able to be collected.

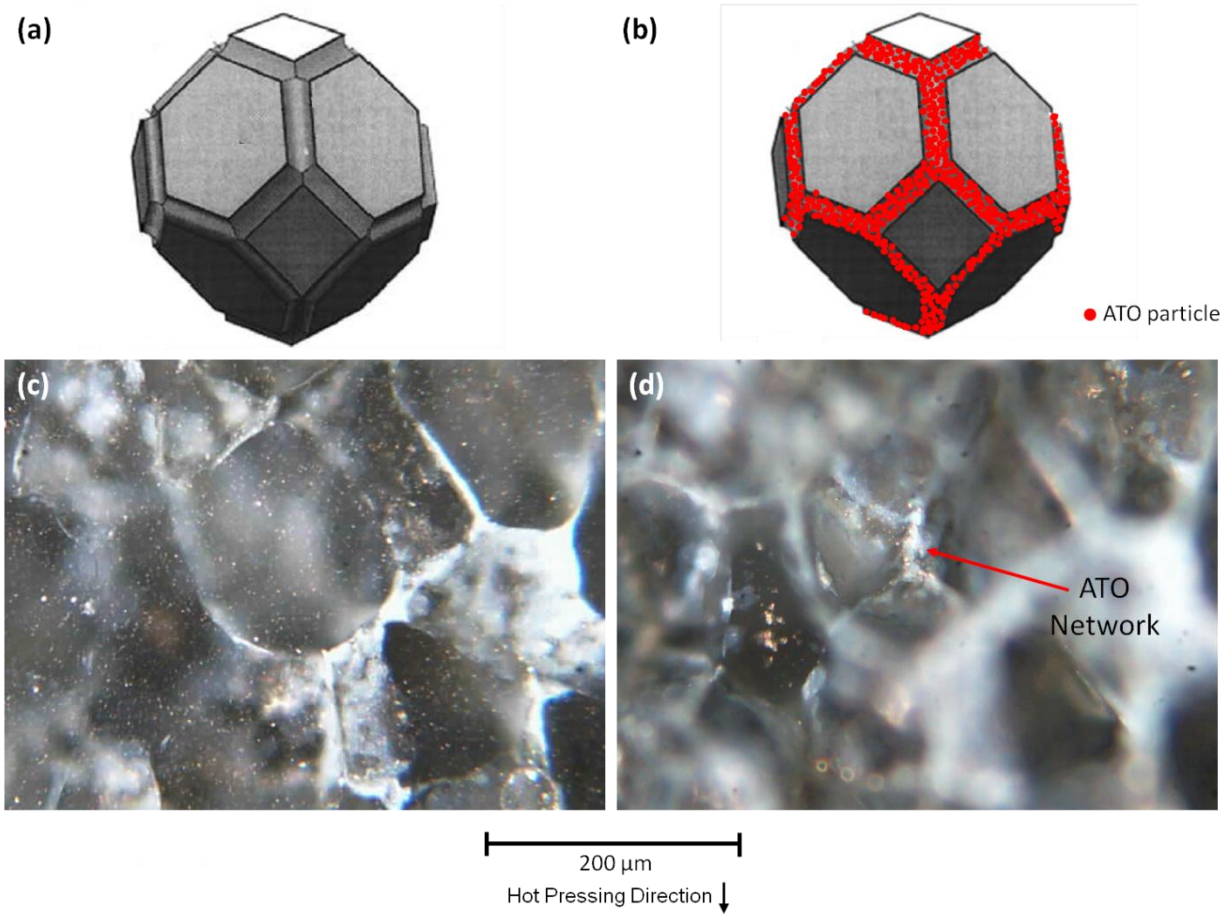

Figure 4.7. (a) Model of a tetrakaidecahedron that resembles the shape of the deformed glass particles in these composites. (b) Adapted image of a tetrakaidecahedron with added ATO located at the boundaries based on the evidence from optical microscopy. Both images in (b) and (c) were modified from reference[20]. (c) Optical micrograph of 10.0 phr ATO sample (set#4) and (d) the same region but the working distance of the microscope changed in order to focus on the bottom of the glass particle.

The only time that ATO had a more complete coverage on the glass occurred when the glass particles did not deform during the hot pressing process. These were rare and are likely due to the glass having a slightly different composition. It is speculated that this was probably related to the amount of sodium in the glass. The amount of sodium would change the viscosity and if the viscosity is too high, these particles wouldn't deform as much.

4.3. Confirmation of Electrically Conducting Network

Before the electrical properties are studied in further detail, it is important to confirm and identify the main conduction paths. This way the cause of any substantial changes in the electrical properties can be correctly attributed to certain microstructural features. Based on the SEM micrographs presented in several of the previous figures, the ATO does seem to be percolated, which also means it should be electrically conducting. There are indications of this when these glass composites are imaged in the SEM when not using the variable pressure SEM or a coated specimen. In Figure 4.2 (e and f), it can be seen that inside of the glass particles charging was occurring. This is expected since the glass is highly insulating. Towards the edge of the glass particles this charging dissipates so it appears that the ATO network is preventing the charging to a degree, which can be attributed to an electrically conducting network.

A more precise method to confirm a percolated electrically conducting network is to use current atomic force microscopy (I-AFM).[6, 114] An atomic force microscope (AFM, XE-100E, Park Systems, Santa Clara, CA) was used to obtain both topography and current images of the composite samples. An applied bias was applied to the bottom of the composites and a current amplifier is attached to the cantilever. In Figure 4.8 (a) a schematic of the I-AFM setup is shown. Electrical current will go from the tip to the applied bias at the bottom of the composite if there is

a conducting pathway through the sample. This particular method is quite useful in detecting percolated pathways and the electrically conductive regions in these composites.[6] So for these ATO-glass composites, a high current signal should be detected when the AFM tip is in contact with a percolated ATO network. In Figure 4.8(b) is a typical topography microstructure of these composites in the AFM. In these images the dark regions are the ATO networks and the light regions are glass. The same region is shown in Figure 4.8 (c) except it is in current mode.[110] The brighter/white regions are areas of higher current flow, which in order to have high current flow this network has to be percolated throughout the composite thickness as depicted in Figure 4.8(a).[110]

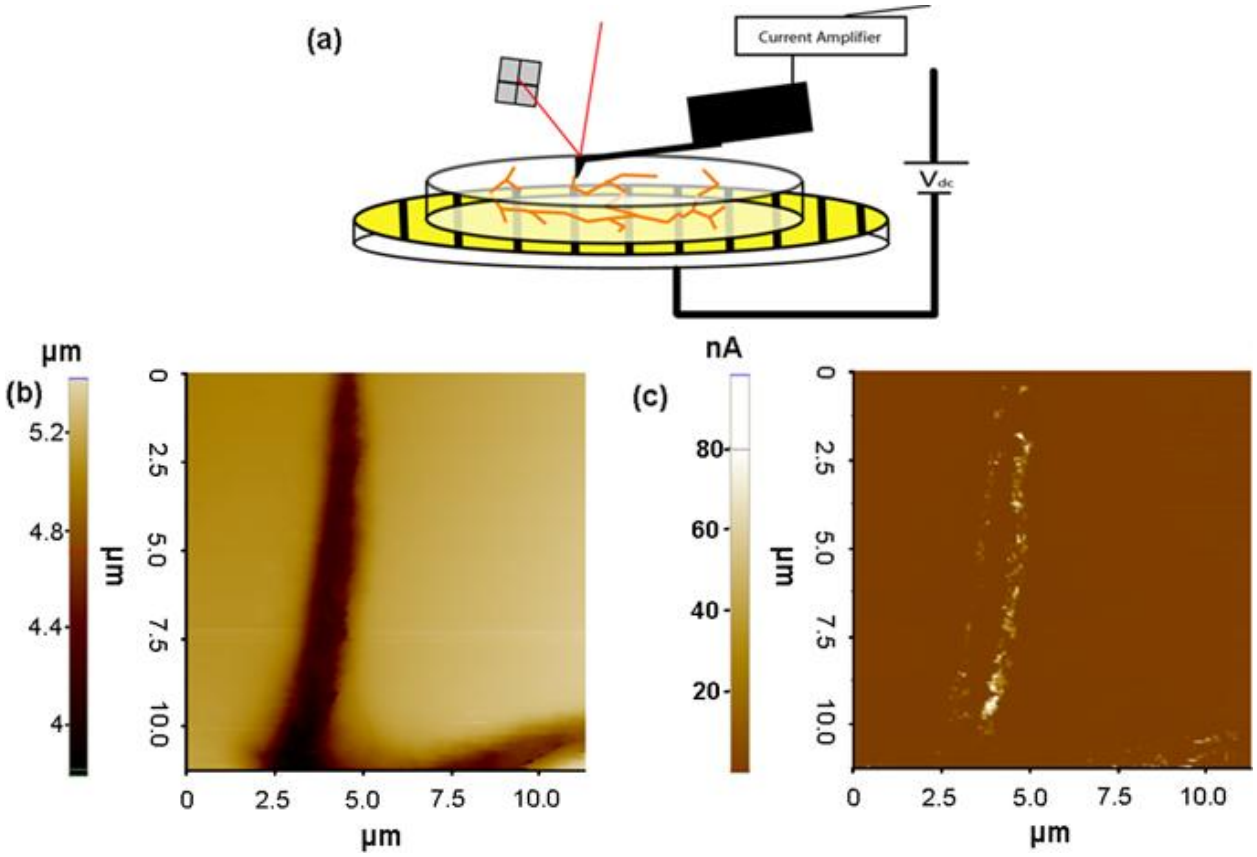

Figure 4.8. (a) Schematic of I-AFM measurement of an insulator-conductor composite containing percolated network paths. (b) Atomic force topography micrograph of a 10.0 phr ATO-glass sample (Set#2). The bar to the left of the image is the z-axis scale. (c) Atomic force current image of the same area as (b). The bar to the left of the image is the current scale.[110]

Since the network is confirmed to be electrically conducting, it is important to know how conducting these networks are and if there is any influence on the concentration of ATO or the processing method (i.e. the differences in set#1 vs. set#2). The electrical resistivity of these sets for all the compositions is shown in Figure 4.9. The dc electrical resistivity values in Figure 4.9 were obtained using the low frequency intercept of the real ac impedance and the geometry of the samples. For set#1 (hot pressed at 550°C), the resistivity for the lower concentrations of ATO (~ 0.001-1.0 phr), the composite resistivity is lower than that of set#2 (hot pressed at 675°C). The onset of percolation is around 0.1 phr ATO since there is a large drop in the resistivity of several orders of magnitude after this composition. The onset of percolation for set#2 is also around 0.1 phr but the resistivity at this composition was over an order of magnitude higher than the set#1 counterpart. Past 0.1 phr for set #2, the drop in resistivity is much more dramatic than set#1 and the resistivity is lower than set #1 at concentrations of 2.5 phr ATO and higher. There are several interesting behaviors at these concentrations, i.e. at 2.5 phr ATO and higher. The first is the difference in resistivities between set#1 and #2. Once a percolated network is formed, the resistivity for both sets is expected to be comparable. However comparing these two sets demonstrates that the processing method must have had a significant influence on the electrical properties. This is especially true for 5.0 phr ATO. Even though this composition is well above percolation there is about a 3-4 order of magnitude difference in resistivity between samples in set #1 and set #2, which is a substantial difference. This concentration for set #2 also had the lowest resistivity of all the composites made and, compared to the resistivity of pure borosilicate glass, is about 11-12 orders of magnitude lower in resistivity. For concentrations above 5.0 phr ATO for set #2, the average resistivity increases which was unexpected.

In order to help determine the disparities between the two sets as well as the increasing resistivity for the high compositions of set #2, several of the microstructures were compared. The microstructure for sets#1 and #2 for 2.5, 5.0, 7.5, and 10.0 phr ATO samples are compared in Figure 4.10. For the lower compositions (2.5 and 5.0 phr ATO), the microstructures between the sets are similar with the glass particles taking on a faceted polyhedral shape. For 7.5 phr and 10.0 phr ATO in set #2 (Figures 3.9 (f) and (h)), the microstructure is very different compared to the microstructures in set#1 and for 2.5 phr and 5.0 phr ATO in set #2. The glass particles are more flattened and the shape is much more random. The boundaries are more curvy and less faceted compared to the other microstructures. It is likely that these more tortuous boundaries are contributing to the increase in resistivity. The cause of the disparity between 5.0 phr ATO with set#1 and #2 is not as clear, but it is important to understand the cause since the small differences in processing has led to a significant difference in the electrical properties between the sets when it is at a composition where there shouldn't be a large difference.

Understanding how the processing influences the ATO network and the overall electrical properties is very important in further design and optimization of these composites. This will be the subject for the next couple of chapters. A strong focus will be made on the 5.0 phr ATO composition to help elucidate the source of the differences.

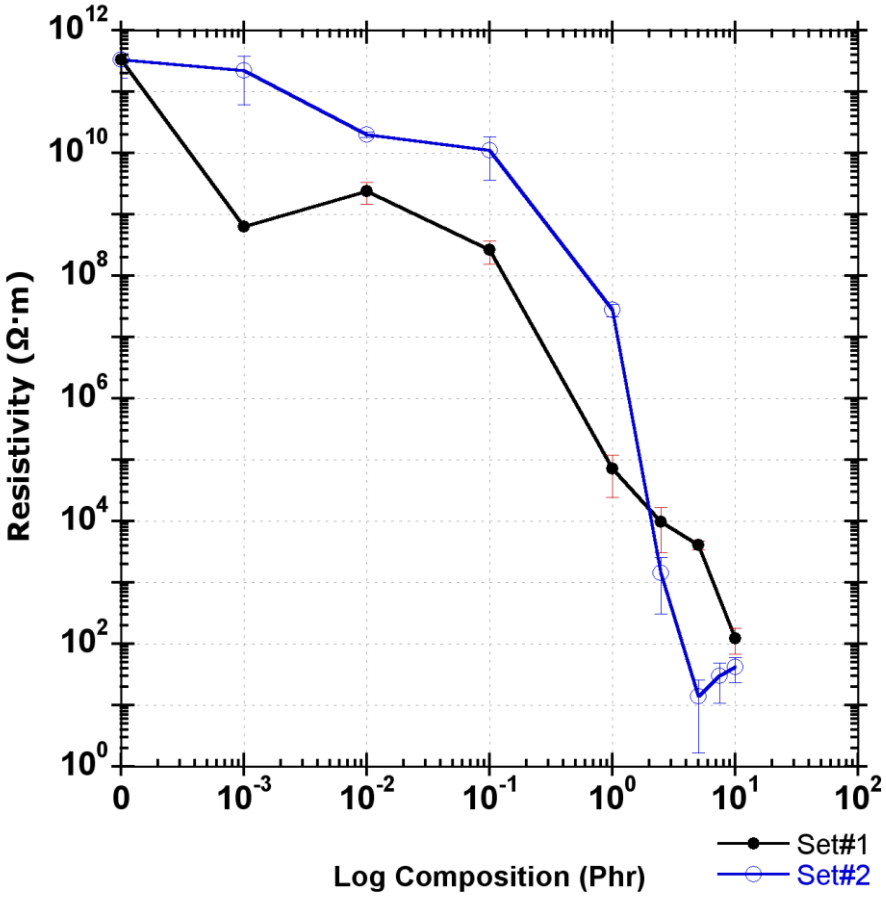

Figure 4.9. Comparison of the low frequency ac resistivity versus the concentration of ATO in ATO/glass composites for sets #1 and #2.[110]

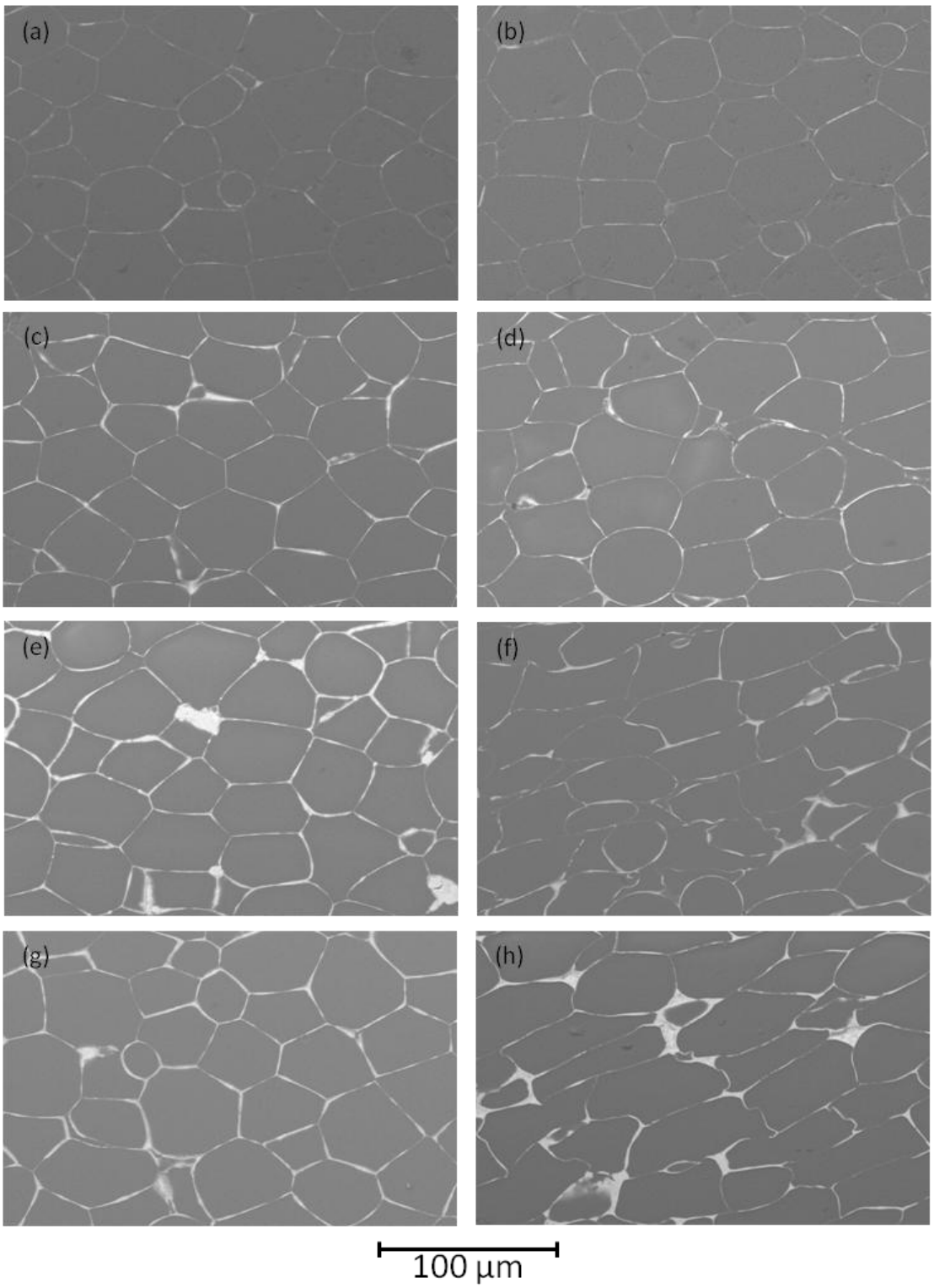

Figure 4.10. SEM micrograph of 2.5 phr ATO set#1(550°C) (a) and set#2(675°C) (b). SEM micrograph of 5.0 phr ATO set #1 (c) and set #2 (d). SEM micrograph of 7.5 phr ATO set#1 (e) and set#2 (f). SEM micrograph of 10.0 phr ATO set#1 (g) and set#2 (h). The hot pressing direction is in the top to down direction.

CHAPTER 5

INFLUENCE OF PROCESSING VARIABLES ON ELECTRICAL RESISTIVITY

At the end of chapter 4 it was shown that even after the percolation threshold was reached, set #1(ATO(nm)-GL0179S hot pressed at 550°C) and #2(ATO(nm)-GL0179S hot pressed at 675°C) had some large and unexpected discrepancies in the resistivities after percolation. For both of these composite sets, the percolation threshold was around 0.1-1.0 phr ATO. Past these concentrations of ATO, the resistivity dropped for both sets substantially (8-12 orders of magnitude) but the difference in resistivity between the sets was quite large. A large difference was unexpected because once percolation occurs, it is assumed the composites would converge to a low resistivity. Instead, the sets had very different resistivities at concentrations past the percolation threshold and even had the resistivity increase with concentration.

These discrepancies and differences are shown in Figure 5.1 with the resistivities for ATO(nm)-GL0179S glass composites (set #1 and #2) at concentrations of 2.5 phr ATO and higher. These concentrations presented in this figure are either at (2.5 phr ATO) or past(>5.0 phr ATO) the percolation threshold for sets #1 and #2. Once percolation occurs, the resistivity between the two sets should be comparable and this behavior is shown with 7.5 phr and 10.0 phr ATO with the two sets. The behavior at 5.0 phr however, acts very differently from what is expected during post-percolation. Although percolation has occurred, the difference in resistivity between sets #1 and #2 is about 3-4 orders of magnitude, which is a substantial difference at this concentration. The only difference between these two sets is the temperature processing parameter.

The focus of this chapter will be on the various processing parameters that can influence the composite percolated network and help explore the cause for these large differences and deviations from expected behavior**.** Since 5.0 phr ATO exhibits large variation in the electrical properties, seemingly due to the processing, it is a prime candidate to study the influence of temperature, pressure, and other processing variables.

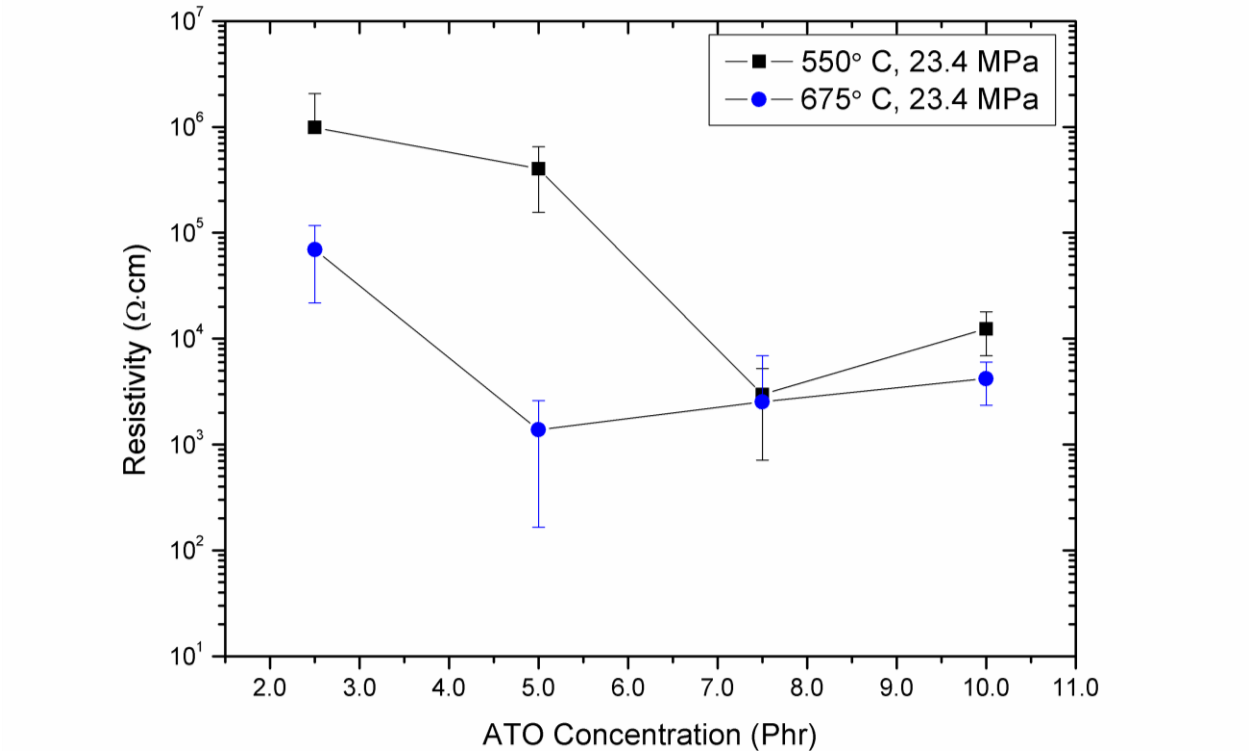

Figure 5.1. Resistivity curve for 2.5-10 phr for set#1 (ATO(nm)-GL0179S hot pressed at 550°C) and #2(ATO(nm)-GL0179S hot pressed at 675°C).

5.1. Processing Parameters that Influence Viscous Flow

The influence of processing, primarily temperature and pressure, on pressure-assisted sintering of glass can be seen in the viscous flow in pressure-assisted sintering and model in section 2.6.1. From the viscous flow in pressure-assisted sintering model, the two primary factors are the viscosity, controlled by the temperature, and the effective pressure, which is controlled by the applied pressure.[75, 76] The equations for the densification rate as a function of

viscosity and the effective pressure as a function of applied pressure were shown in section 2.6.1. A modified version of the model that describes viscous flow in pressure-assisted sintering, which combines the equations in section 2.6.1 and replaces the viscosity variable with the VFT equation, is presented below in equation (5.1).[75, 76]

$$\frac{df}{dt} = \frac{3P_A(1-f)(1-f_o)}{4\left(10^{\left(A+\frac{B}{T-T_o}\right)}\right)f^2(f-f_o)} \qquad (5.1)$$

Where *df/dt* (1/s) is the densification rate, T is the temperature (K),[75] P_A is the applied pressure (MPa), f is the fractional density (dimensionless [0 to 1]), f_o is the fractional green density (dimensionless [0 to 1]),[75, 76] and A, B, and T_o are empirical fit parameters for the VFT equation.[69, 72] The primary variables in this equation are the temperature (T) and the applied pressure (P_A) . The particle size and particle size ratio of the materials involved can also be a factor in this model, since it can control the packing of the particles (f_o).

5.2. Influence of Temperature on the Electrical Properties

From equation 5.1., the temperature should have a large influence on the processing of the composite since it controls the viscosity of the glass, which controls viscous flow. The difference in viscosity at 550°C and 675°C corresponds to a change of about ~10^{13} to ~10^9 Pa·s.[69] A more precise method to estimate these viscosities at this temperatures is to use the VFT equation, shown in equation 2.2 in section 2.6, and the empirical fit values for Pyrex® (A= -2.37, B = 8077, and T_o = 282).[115] These viscosities from the VFT equation at 550°C and 675°C are about 3.6 x 10^{12} and 5.7x 10^9 Pa·s, respectively. In order to study the influence of temperature on the electrical properties, an additional temperature set at 610°C (set #1-T) and a viscosity of ~1 x 10^{11}Pa·s was investigated for samples made with 5.0 phr ATO. Shown in Figure 5.2 is the

heating curve for this additional temperature study. For all of the temperature studies, the pressure was held constant at 23.4 MPa.

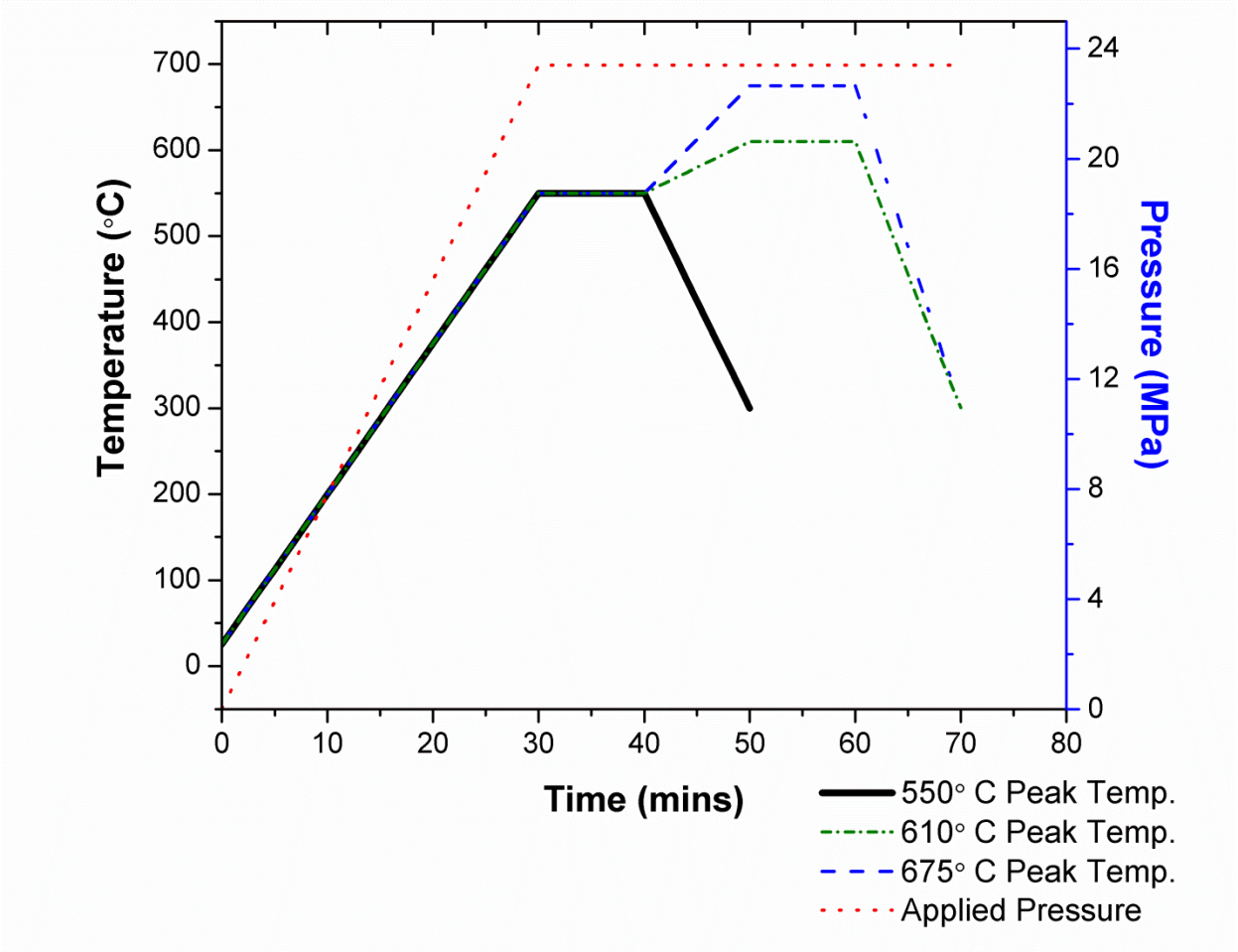

Figure 5.2. Heating and pressure curve for ATO(nm)-GL0179S glass composites for sets #1 (550°C peak temperature), set #1-T (610°C peak temperature hold), and set #2 (675°C peak temperature hold). All sets had a maximum pressure of 23.4 MPa applied during the peak temperature holds (shown by the dotted line).

Using these three temperature sets and the constant pressure of 23.4 MPa, the different densification rates for each set are presented in Figure 5.3. For this model, the values for the fractional density (f) were derived from the displacement of the ram during hot pressing, and an assumption was made that the starting fractional density (f_o) was 0.60 and the final fractional

density was 1.0. From this model, the influence of varying the temperature plays a significant role towards the end of the processing (~2,500 seconds and higher). At this point in the processing, the composite typically has densified to about 90% relative density or higher, so it seems that changing the peak temperature will likely primarily influence how the composite is further consolidated once the ATO networks have already been formed.

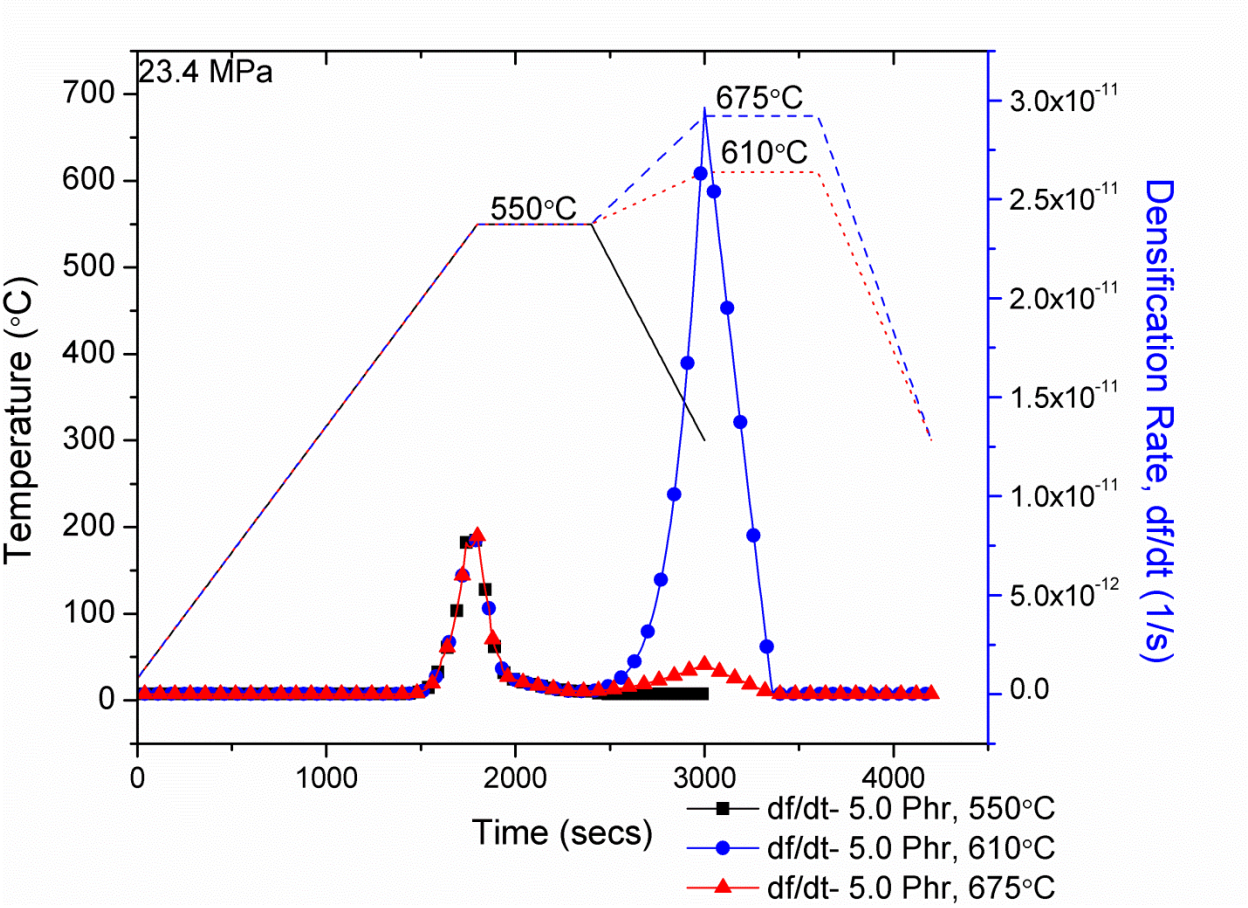

Figure 5.3. Densification rate, based on equation 5.1, as a function of time and temperature for composites hot pressed at 550°C (set #1), 610°C (set #1-T), and 675°C (set #2).

The average relative density for samples in set #1-T (ATO(nm)-GL0179 hot pressed at 610°C) containing 5.0 phr ATO was 98.89% ± 0.14%. The densities for these composites were quite high, which was expected since set#1 and set#2 both had high relative densities at this

composition. Since the densities are comparable between all the sets, the electrical behavior should depend primarily on the ATO network.

Shown in Figure 5.4 are the complex impedance (Z' vs. Z'') plots for samples in sets #1 (550°C), #1-T (610°C), and #2 (675°C) along with a representative SEM microstructure for each set. The impedance has been normalized to the geometry of the sample. Several differences are apparent in the electrical behavior for each composite set.

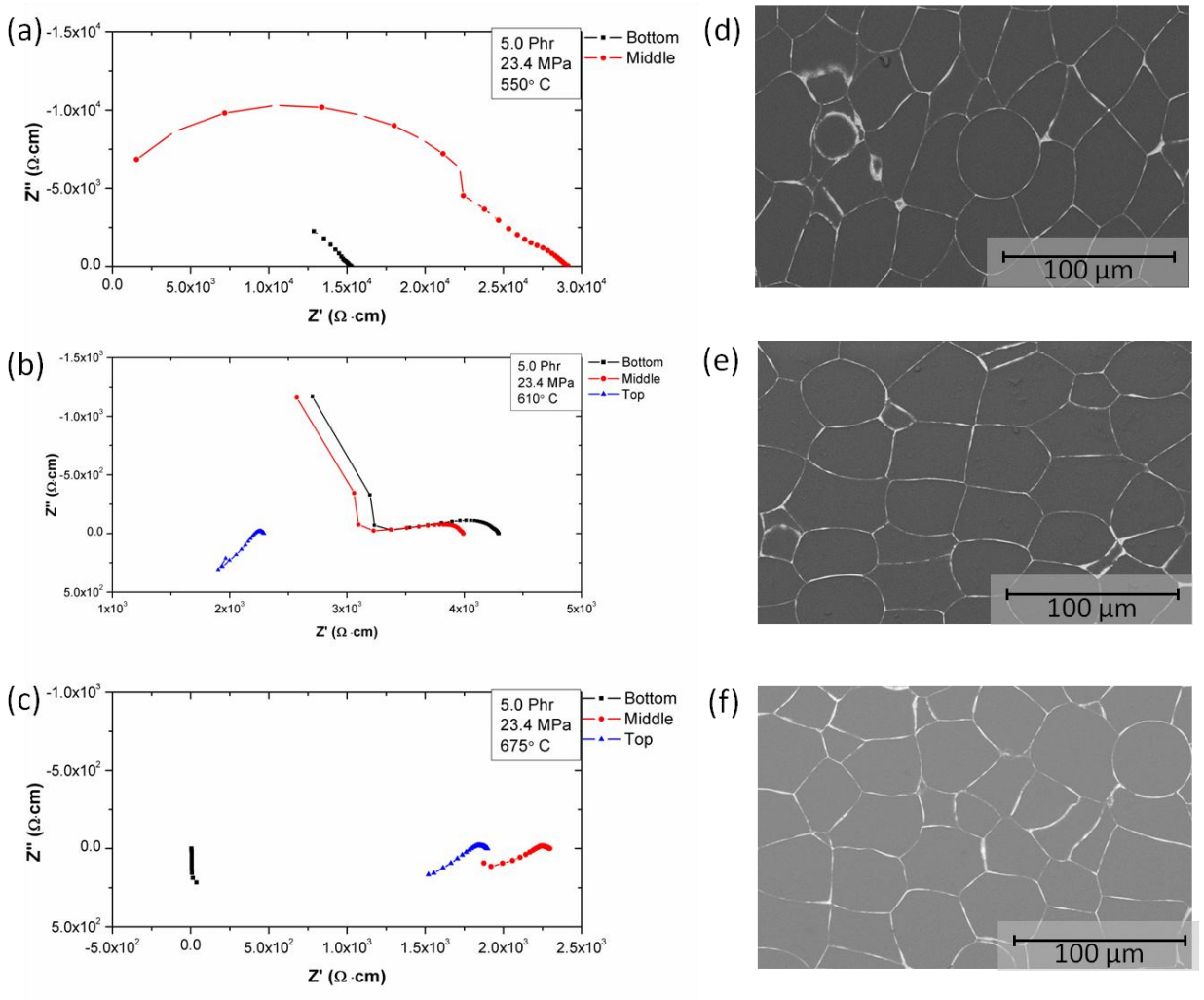

Figure 5.4. Complex impedance for 5.0 phr samples for (a) set #1 (550°C), (b) set #1-T (610°C), and (c) set #2 (675°C). All sets were made at a constant pressure of 23.4 MPa. Corresponding representative microstructures for 5.0 phr samples for (d) set #1, (e) set #1-T, and (f) set #2 are also shown.

Figure 5.4(a) shows the complex impedance for set #1 (hot pressed at 550°C) and it can be seen that the impedance is the highest for this set. The impedance is also entirely in the first quadrant (Z' and $-Z''$) which is due to a combination of resistive and capacitive behavior.[92] A detailed approach to fitting an equivalent circuit model to each impedance response will be discussed in the subsequent chapter. For set #1-T (610°C) the impedance starts to exhibit a change of behavior from set #1(550°C), which is shown in Figure 5.4(b). Not only is the impedance smaller, but it is also more suppressed along the Z'' scale, which suggests that the impedance is primarily influenced by a resistive element with some contribution from a capacitor.[91, 92] There is also some inductance behavior in one of the samples (set #1-T top), which can be seen as the tail of the data extending into the fourth quadrant (Z' vs. Z'').[92] Such behavior have been characteristic of a percolated conducting network.[41, 92, 116]

For set#2 (675°C), in Figure 5.4(c), all of the samples have impedance characteristics in both the first and fourth quadrant. The most conducting sample (bottom) can be modeled primarily using inductance and resistive behavior. So the general trend when increasing processing temperature is that the complex impedance changes from resistive and capacitive behavior to resistive and inductive behavior. Figure 5.4(d-e) shows the typical microstructure seen for each of these sets. The faceted microstructure previously presented is apparent in all three microstructures. As the temperature increases, the glass particles are slightly more rounded at the edges, but between the sets, the microstructure still appears to be similar at a macro scale. From the impedance data, it is known that these composites exhibit different behavior, so it is likely that there are some differences in the microstructure of the ATO network that is causing the electrical behavior differences observed.

The differences in behavior can be summarized by the resistivity curve as a function of temperature, shown in Figure 5.5. As mentioned before with the complex impedance, as the temperature increases, the resistivity of the composites decreases once percolation has occurred. The highest temperature also seems to have the most variability of all the sets.

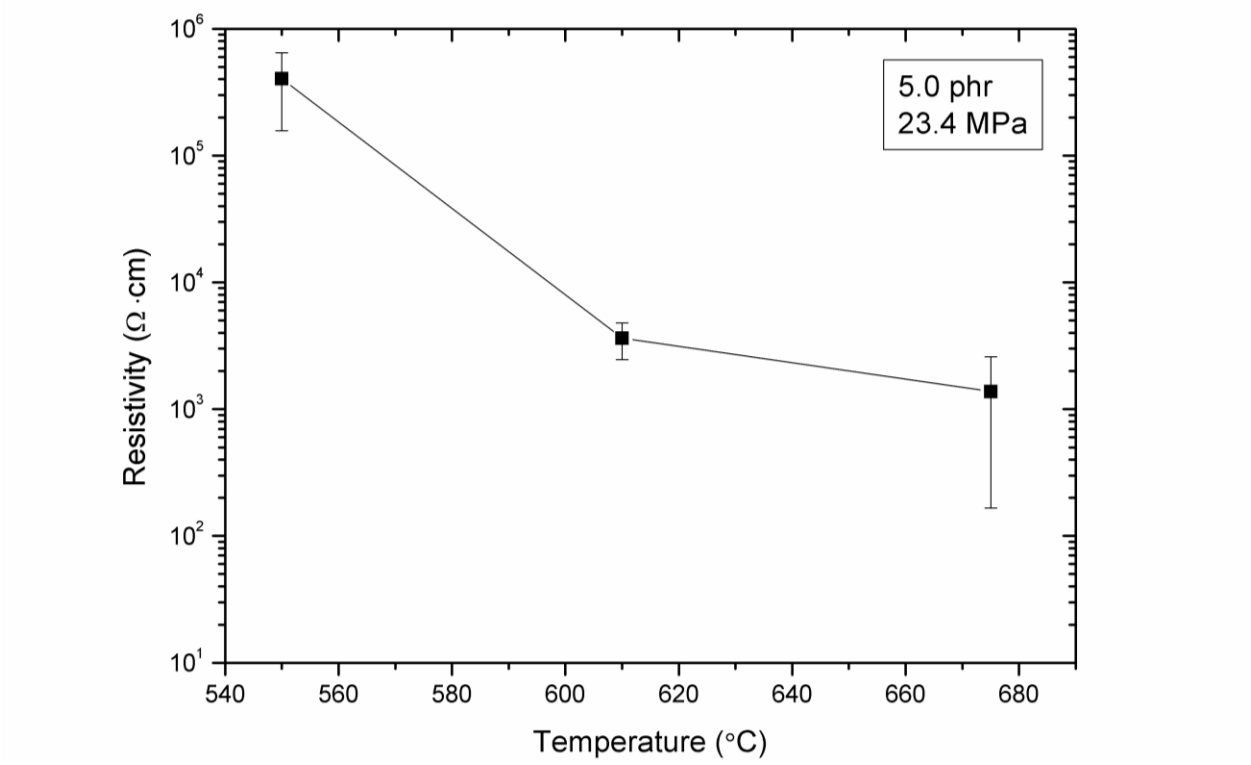

Figure 5.5. Resistivity curve for 5.0 phr ATO(nm)-GL0179S as a function of hot pressing temperature used during processing.

All of these samples were subjected to a 550°C hold prior to reaching the maximum temperature and both the model (equation 5.1) and the actual displacement recorded during hot pressing shows that most of the densification and compaction occurs during the first hold at 550°C. An example of the typical fractional density during processing is presented in Figure 5.6. For the additional hold at 610°C and 675°C for set#1-T (610°C) and #2 (675°C), respectively, there is some additional densification at these temperatures but most of the composite has already been consolidated by this point. As the temperature increases, the densification rate

increases due to a lower viscosity even though the overall effective pressure is lower due to a high fractional density at this point. This increase explains how the temperature can have a large influence on the formation of the ATO network even during the late stages of the pressure-assisted sintering. From the high resolution images presented in Figure 4.4(b) of the ATO network, it appears that this additional hold is likely resulting in some penetration of glass into the ATO network. Although this penetration is occurring, the ATO network is still becoming less resistive with temperature.

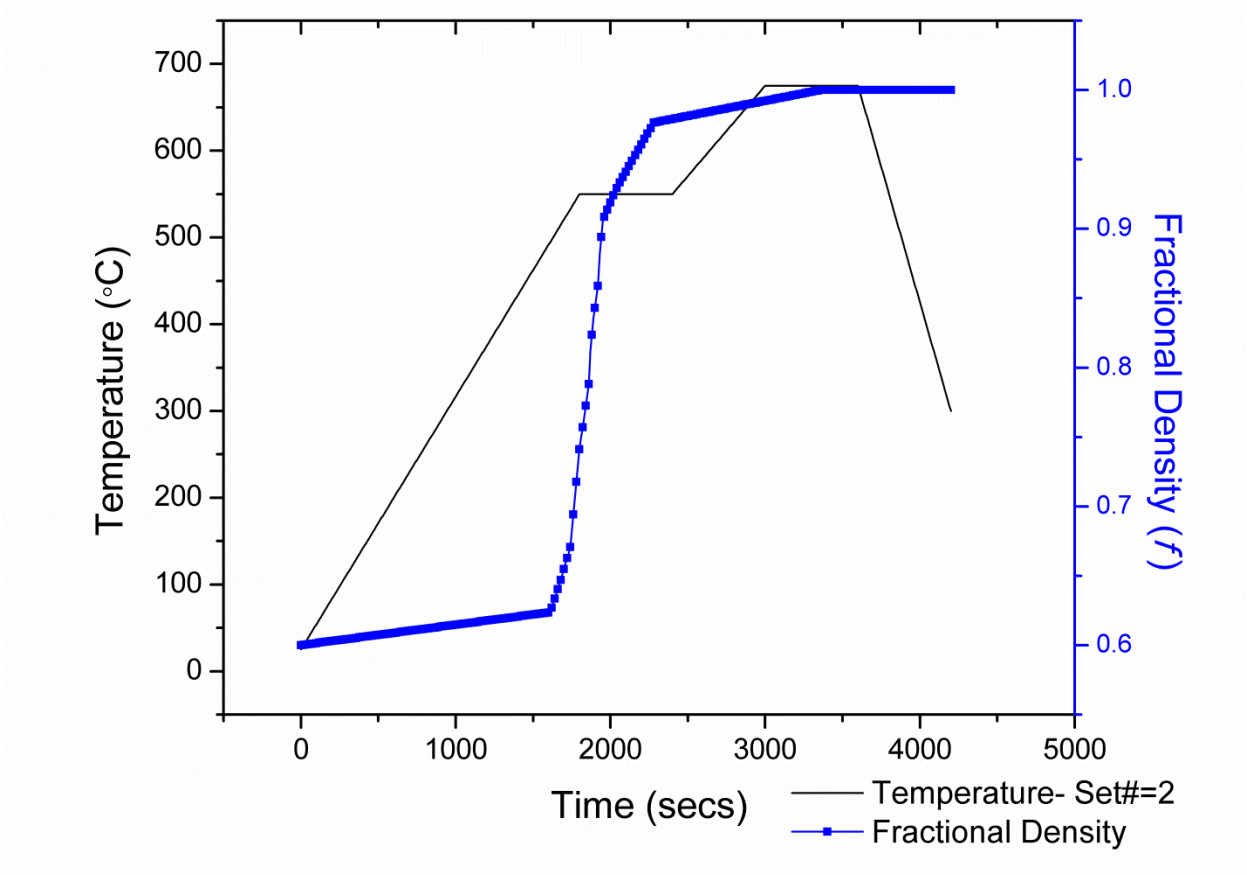

Figure 5.6. The typical fractional density of set #2 composites as a function of temperature and time.

The temperature dependence behavior of the segregated network composites in these glass composites presented here is quite different from the behavior of polymer composites when the matrix material penetrates into the network.[55, 56] Typically, with the intrusion of the polymer

matrix beginning to disrupt the percolation networks in the composites, the resistivity increases with increasing temperature.[55, 56] The more fluid the polymer is, the more it is able to flow in-between the filler particles and disrupt the network. While this seems to partially occur with the glass composites at the higher temperatures (675°C), the resistivity still decreases because the microstructure is different. The processing temperature used to create these glass composites is also significantly higher compared to polymer composites. With these glass composites, there is the factor that with the higher processing temperature, the inorganic filler particles can potentially react or sinter, which typically isn't the case with polymer composites since the temperature used is relatively low.

5.3. Influence of Pressure on Electrical Properties

Since temperature was shown to have an influence on the electrical properties for the same composition, it is important to investigate the influence of the other major parameter when hot pressing glass, which is the pressure. The use of applied pressure in these composites is essential since the additional force used contributes to the segregation effect at the glass boundaries. For the pressure study, the peak temperature was held constant at 675°C and the pressure was varied from 23.4 MPa to 5.8 MPa. The pressure was not increased beyond 23.4 MPa due to issues with the graphite dies cracking during processing. The heating curves for this study are shown in Figure 5.7. It appears that even with the low pressure of 5.8 MPa, the pressure was enough to consolidate these composites since the relative density, shown in Table 5.1, were still high and very similar to all of the other sets.

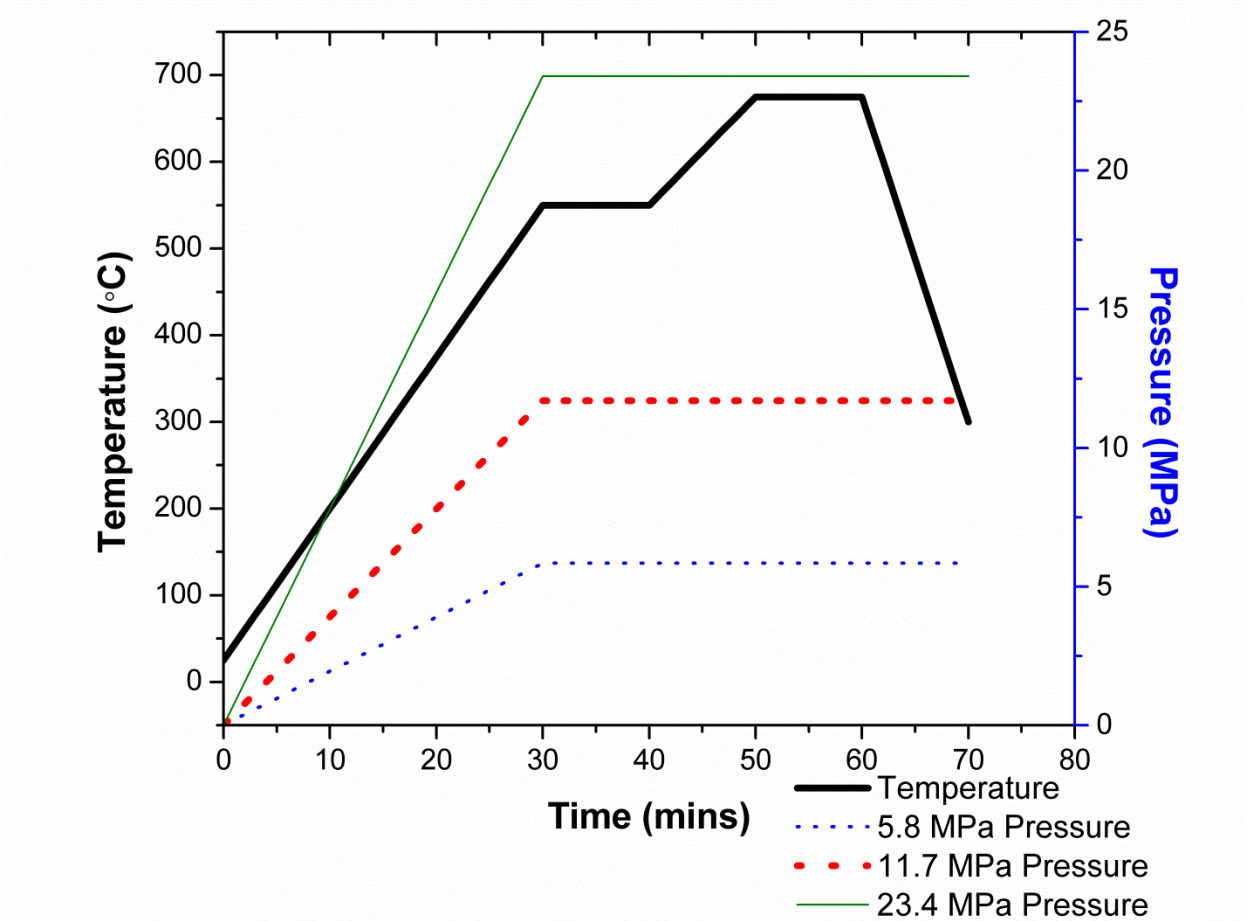

Figure 5.7. Heating and pressure curve for ATO(nm)-GL0179S glass composites for sets #2-P1 (5.8 MPa), set #2-P2 (11.7 MPa), and set#2 (23.4 MPa). All sets were exposed to a maximum temperature of 675°C applied during the peak temperature holds (shown by the solid lines).

Table 5.1. Average Relative Densities for Specimens Containing 5.0 Phr That Were Processed at Different Pressures at 5.8 MPa (Set #2-P1), 11.7 MPa (Set #2-P2), and 23.4 MPa (Set #2).

Set #	Relative Density-Archimedes
2-P1	**98.82 ± 0.29**
2-P2	**98.64 ± 0.14**
2	**98.70 ± 0.08**

Since the applied pressure is the other key parameter in the densification model in equation 5.1, it is important to show how it can influence the processing. The densification rate for all three cases is shown in Figure 5.8. The overall effective pressure, shown in equation 2.3,

is dependent on the applied pressure and the fractional density. At lower fractional densities, the higher the effective pressure will be, so a reduction in pressure will be more significant during the earlier stages of hot pressing when the composites have a low fractional density. This is what is shown in Figure 5.8, where the densification rate is initially much lower than the rates shown in Figure 5.3. As the temperature reaches its peak, which occurs at about 2,500 seconds and higher, the densification rate from the model increases much more rapidly due to the lower viscosity. Based on this, it appears that the composite consolidates at a later time compared to the sets in the temperature study, which can influence the behavior of the electrical properties.

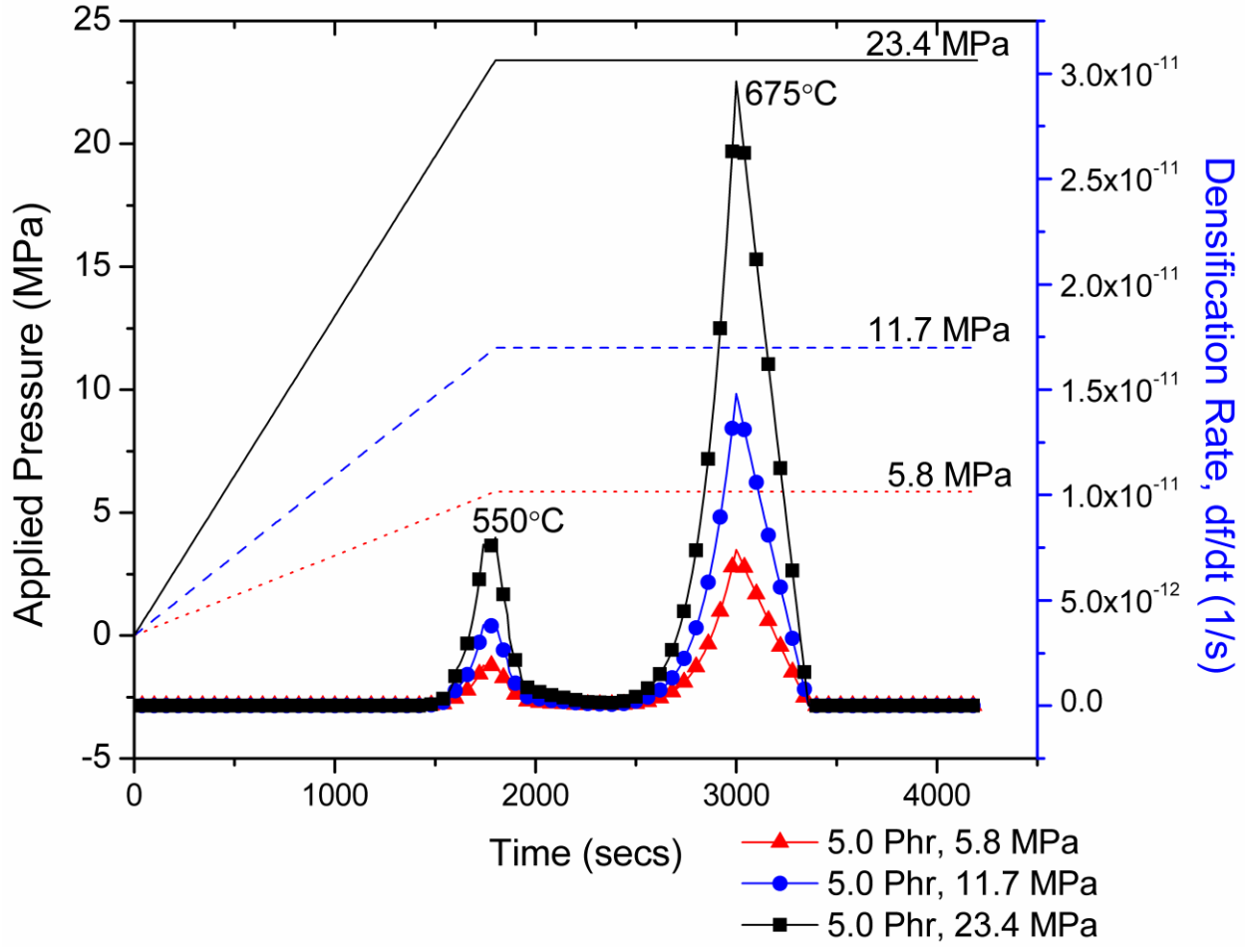

Figure 5.8. Densification rate for 5.8 MPa (Set #2-P1), 11.7 MPa (Set #2-P2), and 23.4 MPa samples (Set #2) based on equation 5.1 as a function of time and pressure.

Figure 5.9 shows the complex impedance and corresponding microstructures for the 5.0 phr samples made at these different pressures. Even though these composites likely consolidated at different times when compared to the temperature study, this pressure study exhibited similar electrical behavior to those samples, whose complex impedance was presented in Figure 5.4. The impedance at the lowest pressure, shown in Figure 5.9(a), is entirely in the first quadrant and has an impedance almost as high as a composite made at 550°C (see Figure 5.4(a)). As the pressure is increased to 11.7 MPa, the impedance, shown in Figure 5.9(b), decreases and starts to exhibit some behavior in the fourth quadrant. This is very similar to the behavior of the composites at 610°C (Figure 5.4(b)). At the maximum pressure of 23.4 MPa in Figure 5.9.(c) the impedance is quite low and has shifted to primarily the fourth quadrant. The microstructures of samples made at these pressures and shown in Figure 5.9(e-f) do have some differences compared to Figure 5.4. (e-f), which is likely related to when consolidation occurred during hot pressing. For the 5.8 and 11.7 MPa samples, the glass particles are not as faceted and are more rounded along the edges. Since they are more curved along the edges, these particles likely did not deform even though they were all sintered at 675°C. This supports the model presented in Figure 5.8 since at lower pressures, the densification rate is much lower compared to 23.4 MPa.

The densification rate is representative of the viscous flow in these composites so with less viscous flow, the glass particles are less likely to deform. For several polymer composites, a decrease in pressure has benefitted the electrical conductivity due to a decrease in the viscous flow.[21] For many polymer composites, a lower pressure often resulted in less penetration of the filler into the polymer matrix, which would decrease the conductivity if this occurred.[21] In some cases a higher pressure led to better lower resistivity due to better packing of the filler[55], but once the polymer begins to penetrate into the network, higher pressures would exacerbate the break up

of the network.[21] For glass composites described here the opposite is seen even though there is evidence of the glass penetrating into the filler network. It seems that with the glass composites there are other variables that are contributing to the overall electrical properties that can compensate for this penetration of glass into the network.

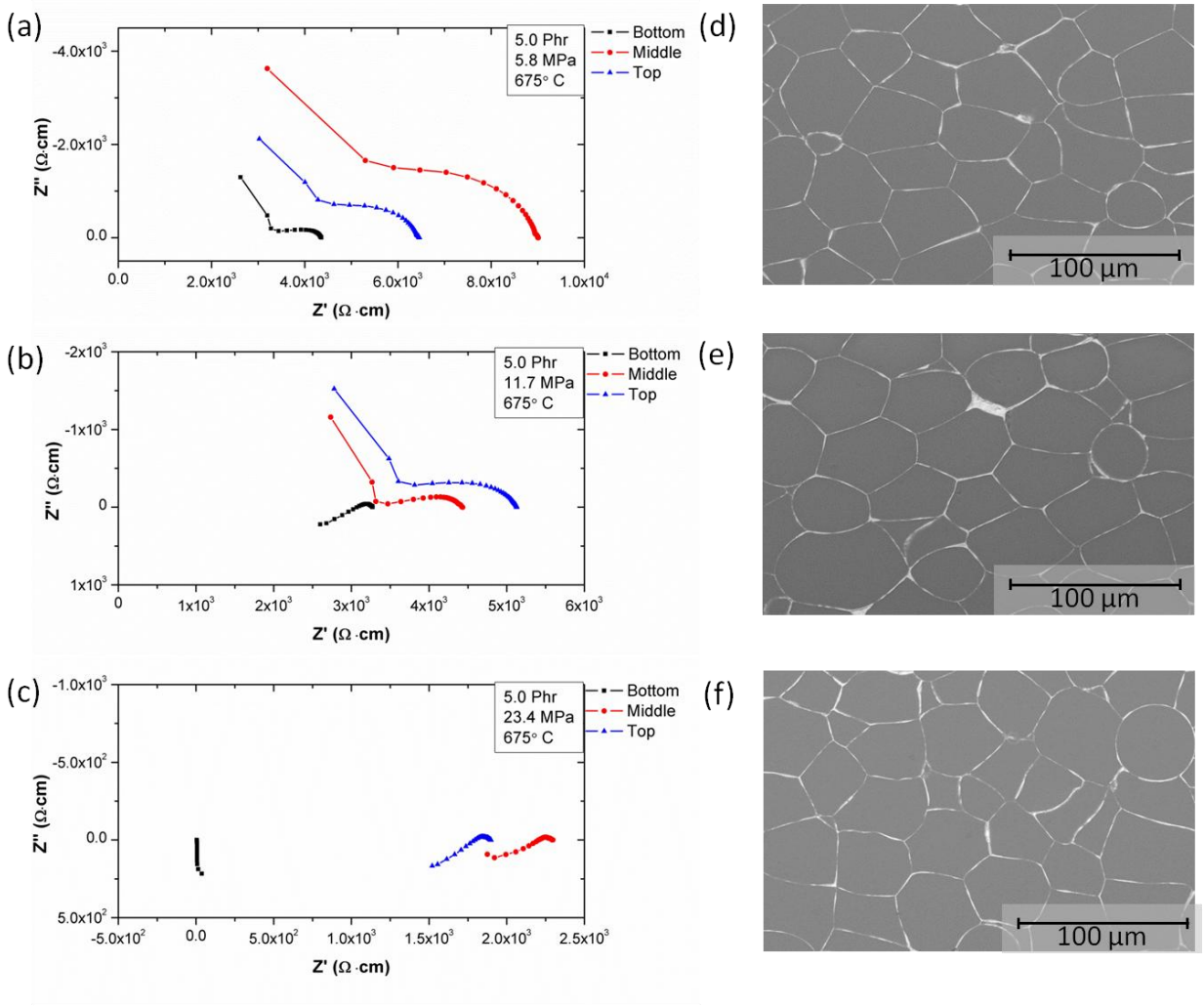

Figure 5.9. Complex impedance for 5.0 phr samples for (a) set #2-P1, (b) set #2-P2, and (c) set #2. All of these samples were made at a constant peak temperature of 675°C. Corresponding microstructures for the 5.0 phr ATO samples for (d) set #2-P1, (e) set #2-P2, and (f) set #2 are also shown.

Both the temperature and pressure dictated the compaction of the ATO, which as a result, influenced the contact between ATO particles. The type and extent of contact between particles

is referred to as quality of contact, and depending on this quality of contact the electrical properties can vary.[50, 117] This has been observed in other insulator-conductor composites depending on the method of processing.[48, 118] Since it appears that the quality of contact inside the ATO network can heavily dictate the overall electrical properties, it is important to investigate other variables that can possibly control the percolation network. These variables include particle size ratio and filler particle shape.

5.4. Influence of Particle Size Ratio on Electrical Properties

The particle size ratio between the matrix and filler particles is one of the largest influences in the creation of a segregated percolated network.[1, 16, 24, 25, 28, 40, 119] The primary influence it has is controlling the concentration of filler particles at which the percolation threshold occurs. Typically, the larger the disparity between the matrix particle and filler particles, with the filler particles as the smaller of the two, the lower the percolation threshold. [1, 4-6, 16, 24, 25, 40, 49, 119] This is because the larger particles create larger excluded volume in which the filler can't occupy so it is segregated to the surfaces of the larger matrix particle. The particle size ratio can also influence the densification in pressure-assisted viscous sintering, since it can influence the packing of the particles(f_o), which was shown in equation 5.1.[76]

Additional composites were fabricated by varying particle size ratios between the glass and the ATO. The same processing parameters were used for set #2, which was a peak temperature of 675°C and a peak pressure of 23.4 MPa. The heating curve was given in Figure 4.1. The additional sets used in this study had a particle size ratio of ~3500:1 (set #3) and ~25:1(set #4) with the glass being the larger particle in both. Set#1 and #2 had a particle size ratio of ~700:1. Listed below in Table 5.2 are the compositions for sets #3 and #4 used for this

study along with the relative densities after hot pressing. These relative densities are quite high, which is expected since the heating procedure used produced close to fully dense composites with set #2 (see Table 4.1 in Chapter 4).

Table 5.2. Concentration of ATO and Relative Densities for Set #3 and #4 After Hot Pressing.

ATO Concentration (Phr)	Relative Density (%) Set #3	Relative Density (%) Set #4
0.001	99.81 ± 0.09	99.74 ± 0.05
0.01	99.65 ± 0.12	99.63 ± 0.25
0.1	99.37 ± 0.04	99.59 ± 0.12
1.0	99.82 ± 0.16	98.63 ± 0.22
2.5	99.54 ± 0.14	95.96 ± 0.09
5.0	99.63 ± 0.24	99.19 ± 0.57
7.5	99.53 ± 0.41	97.80 ± 0.27
10.0	99.62 ± 0.52	97.66 ± 0.52

Based on several percolation size models,[1, 28, 40, 42, 119] the percolation threshold for set#3 should be much lower than that of set #1 and #2. Set #4 should have the highest percolation threshold of all the sets. The actual percolation curves based on the electrical resistivity for set #3 and #4 are shown in Figure 5.10. The resistivity for set #2 is also included for comparison. Even though set #3 had a particle size ratio about five times higher than set #2, the percolation threshold for set #3 is around 1-2.5 phr ATO, which is actually a little bit higher than the percolation threshold in set #2, which was around 0.1-0.25 phr. Past the percolation threshold for set #3, the resistivity continues to decrease and the resistivity at the highest concentration, 10 phr, is the lowest of all the sets at that concentration. The percolation threshold for set #3 is unexpectedly high and will need further examination. An examination of the microstructure at the concentrations near the percolation threshold, shown in Figure 5.11 provides some details as to the potential cause for this.

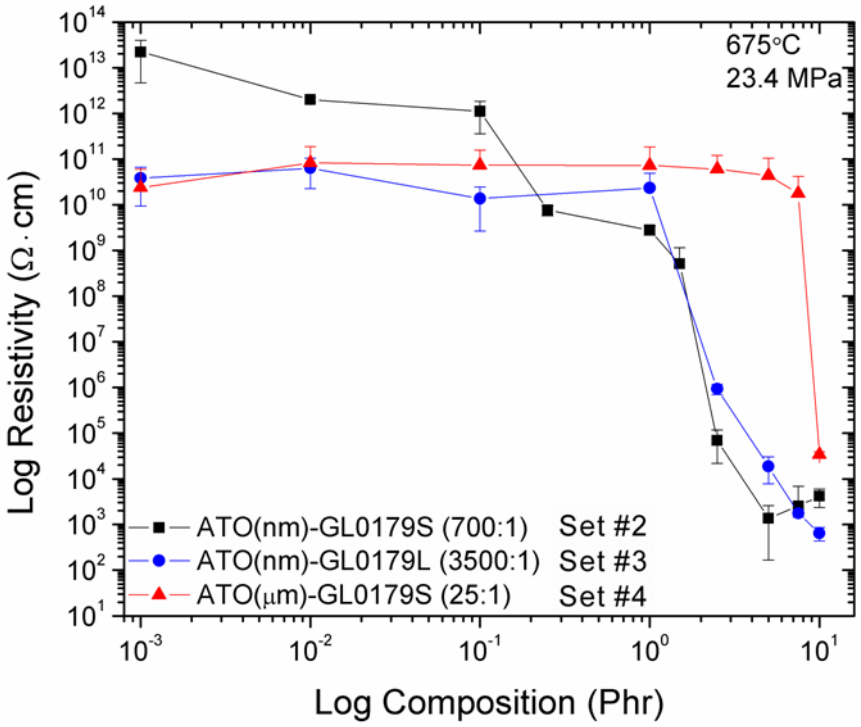

Figure 5.10. Resistivity, obtained from the real impedance low frequency intercept, for various particle size ratios of glass:ATO composites.

From Figure 5.11(a) and (b) the potential cause in the higher-than-expected percolation threshold can be seen. At 1.0 phr ATO, shown in Figure 5.11(a), the ATO network seems to be broken up by voids that are also at the interface. As a result, the resistivity for this concentration is over 10^{10} Ω·cm which is quite high for these composites. At the next highest concentration, 2.5 phr ATO, the percolation threshold has been reached. In Figure 5.11(b) the voids that were prevalent in (a) are gone so it seems that ATO networks are forming. There seems to still be breaks in the network due to varying concentrations of ATO, which is likely contributing to the variations in resistivity. For the higher concentrations, shown in Figures 5.11(c) and (d), the ATO networks have fewer of these breaks and they are overall thicker on average. As a result, the resistivities are lower.

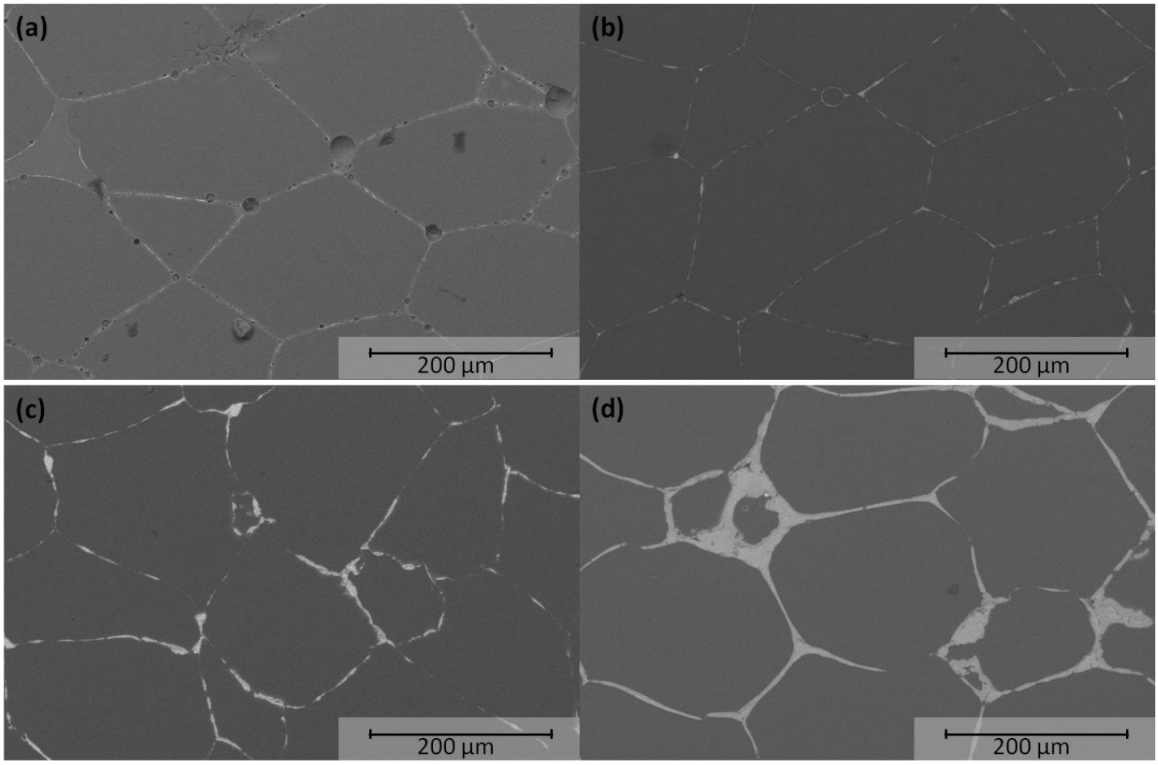

Figure 5.11. SEM micrographs for (a) 1.0, (b) 2.5, (c) 5.0, and (d) 10.0 phr ATO(nm) for Set#3.

In order to verify that the microstructures in 5.11 are indicative of the entire composite, several different magnifications of the same microstructure (5.0 phr ATO for set #3) are shown in Figure 5.12. From this figure, it can be seen that the microstructure is consistent throughout the composite. It can also be seen at the higher magnifications that even for a high concentration such as 5.0 phr ATO, there are breaks in the network due to variations in the concentrations of ATO.

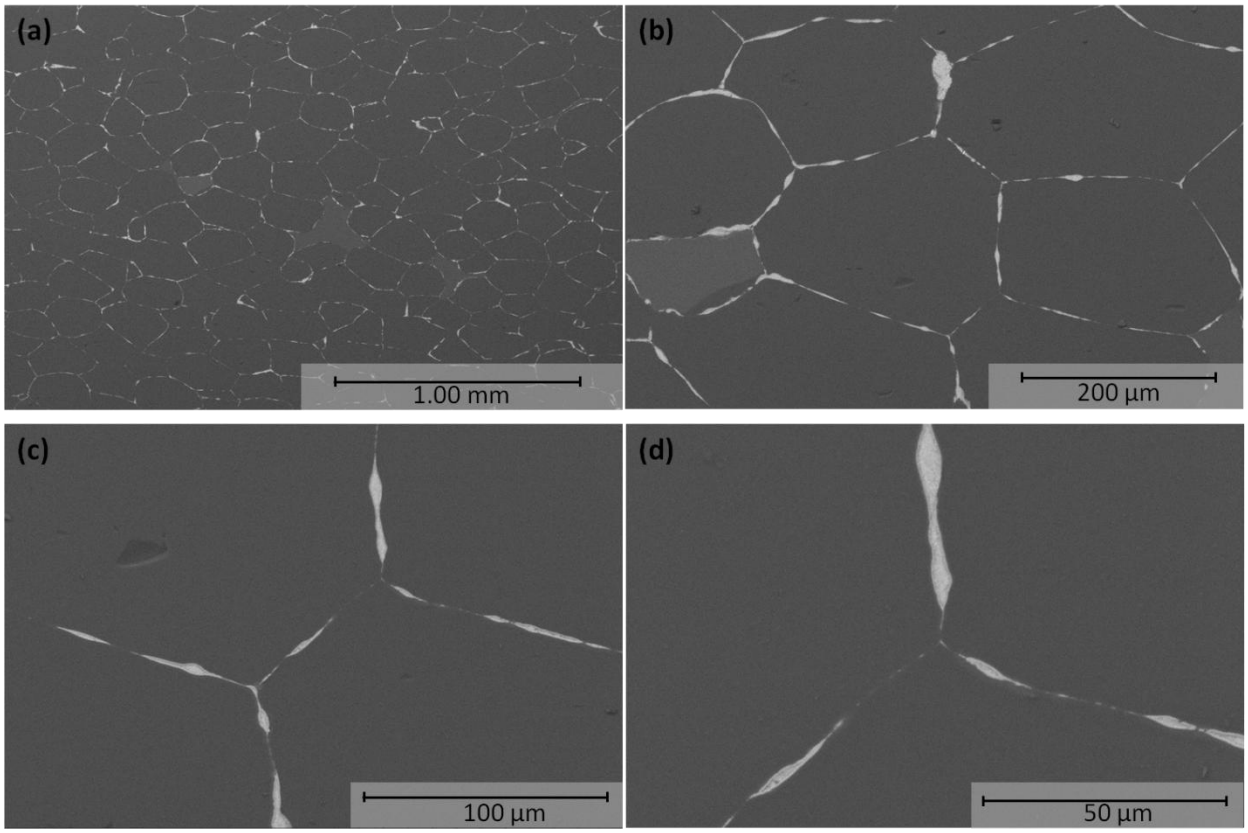

Figure 5.12. Several different micrographs for 5.0 phr ATO/large glass specimen from set #3 taken at different magnifications.

While set #4 has the smallest particle size ratio (~25:1) for all the ATO composites, the percolation threshold based on a model of particle size ratio on the continuity of aggregates (percolation) should be at about 3-5 vol% filler. [1, 28, 40, 42, 119] From Figure 5.10, this model prediction is fairly accurate for this composite set since percolation seems to occur at around 7.5-10 phr ATO, which is equivalent to ~2.5-3.5 vol% ATO. The percolation threshold for set #4 is likely slightly lower than what is predicted due to the additional segregation from the processing method since the model relies on just the particle size difference to account for percolation.[28, 119] This segregation can be seen in the microstructures presented in Figure 5.13. The ATO particles are the brighter regions in this composite, but at first glance the microstructure appears to be different from the ones in sets #1-3. A reason for this difference is likely due to the size of the

ATO used in this case (micron range rather than nanometer). Since the ATO is larger in this composite, the ATO is likely easier to remove during polishing since the glass isn't holding the ATO together as well. It can be seen in both images that there are gaps at the edges of the glass particles, which were likely occupied by ATO particles before they were removed during polishing. Using these gaps, it can be seen that this composite is near the percolation threshold. While it is partially percolated on the surface, it is hard to distinguish ATO below the surface gaps, which indicates that these composites aren't as interconnected through the thickness of the composite. This results in a high resistivity which eventually decreases when the ATO concentration reaches 10 phr.

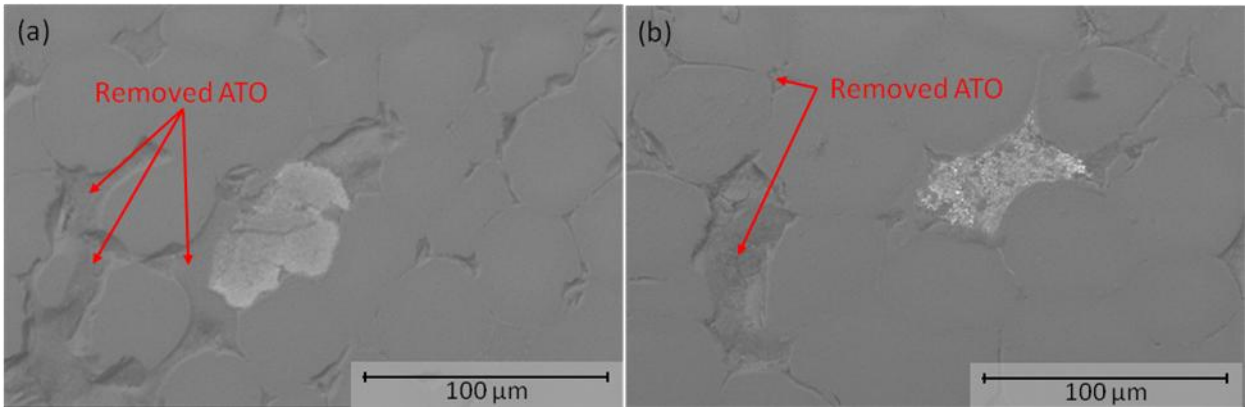

Figure 5.13. Several different views of the same microstructure for 7.5 phr set #4.

5.5. Influence of Particle Shape on Electrical Resistivity

Since the temperature, pressure, and particle size have all shown unexpected results based on the typical behavior in polymer composites, it is important to also examine the particle shape. Also since this processing method should in theory be applicable to a broad range of filler types, it is important to see if this method can be applied to a filler material other than ATO. For this study, silicon carbide whiskers (SiC_w) were used instead of ATO.

The compositions made for this study, set #5, are listed in Table 5.3. This composition set focused more on higher concentrations since it was predicted that these composites would require higher amounts of SiC_w, based on other composites containing this material.[48-50, 53, 117] Also listed in this table are the relative densities after hot pressing. The hot pressing conditions were the same as those used for set #2-P2 (11.7 MPa hot pressed at 675°C) from Figure 5.7.

Table 5.3. Concentration of SiC_w and Relative Densities for Set #5 Samples after Hot Pressing.[111]

SiC_w Concentration		**Relative Density (%)**
Phr	*Vol %*	
1.00×10^{-3}	1.10×10^{-3}	99.78 ± 0.02
1.00×10^{-1}	1.10×10^{-1}	99.85 ± 0.09
2.50×10^{-1}	2.73×10^{-1}	99.37 ± 0.04
2.50×10^{0}	2.63×10^{0}	98.43 ± 0.49
5.00×10^{0}	5.20×10^{0}	97.88 ± 1.59
7.50×10^{0}	7.60×10^{0}	95.43 ± 0.29
1.00×10^{1}	9.88×10^{0}	94.10 ± 0.39
1.25×10^{1}	1.21×10^{1}	93.81 ± 1.16

Presented in Figure 5.14 are optical micrographs that show the typical microstructure of these composites containing SiC_w. It appears that the processing method also resulted in a microstructure that resembles the microstructures observed with ATO(nm) and glass microspheres with the ATO residing at the boundaries between the glass particles.[110, 112] Even though this microstructure does appear to be similar to the ATO composites, there are a few large differences. One of these differences with the SiC_w composites is that it appears that some of the whiskers are still on the faces of the glass particles as well as on the edges, while the ATO(nm) and glass composites in the other studies have formed networks almost exclusively on the edges.[110, 112] This is likely due to the larger size of the whiskers as well as their shape, which make them harder to be segregated to the boundaries compared to the nanoparticles. At the same time, the whiskers aren't completely surrounding the glass since the glass would crumble if it

did. Instead, they form small whisker agglomerates. These clusters of whiskers are likely the reason for the residual porosity, based on the relative densities in Table 5.3, in the higher composition composites since the glass likely can't flow completely into these clusters.[111]

The other difference is that there seems to be some anisotropy between the parallel hot pressing direction (∥-HPD) and the perpendicular hot pressing direction (⊥-HPD)[49] in the whisker composites. An example of this is shown in Figure 5.15. Both the perpendicular and parallel direction do have some of the whisker network along the glass boundary as well as what appears to be breaks in the SiC_w network, which is likely a combination of both breaks in the network and the whiskers only being partially visible on the surface.

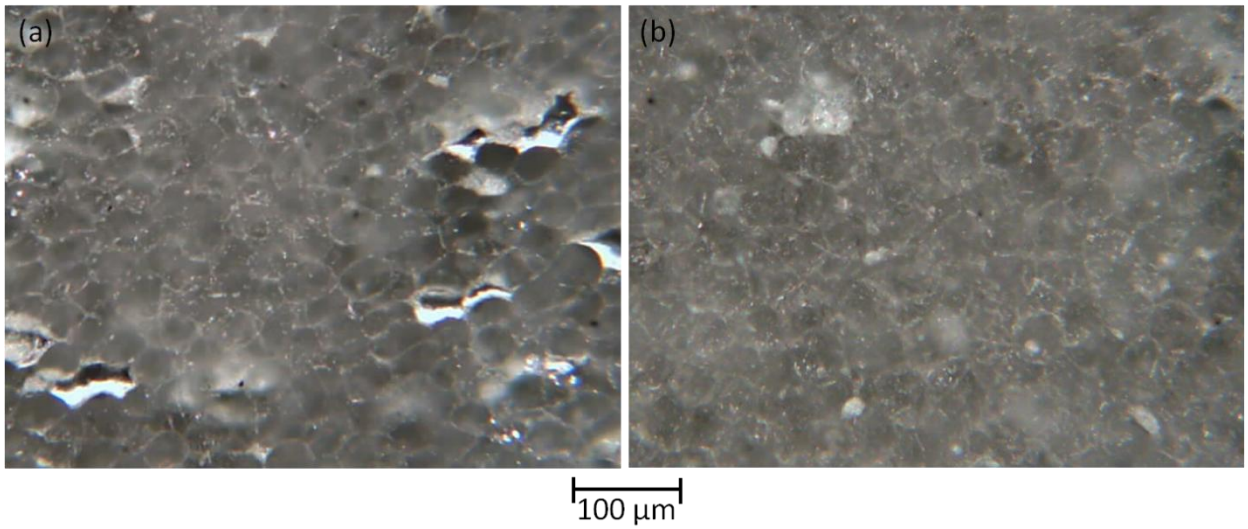

Figure 5.14. (a) Optical micrograph of 2.5 phr SiC_w/ Glass composite perpendicular to the hot pressing direction. (b) Optical micrograph of 2.5 phr SiC_w/ Glass composite parallel to the hot pressing direction.[111]

From both Figure 5.14 and 5.15, it appears that the whiskers are more visible and concentrated along the perpendicular direction than the parallel direction. This was commonly seen all over the microstructures of these composites. Examples of this at other concentrations are shown in Figure 5.16.

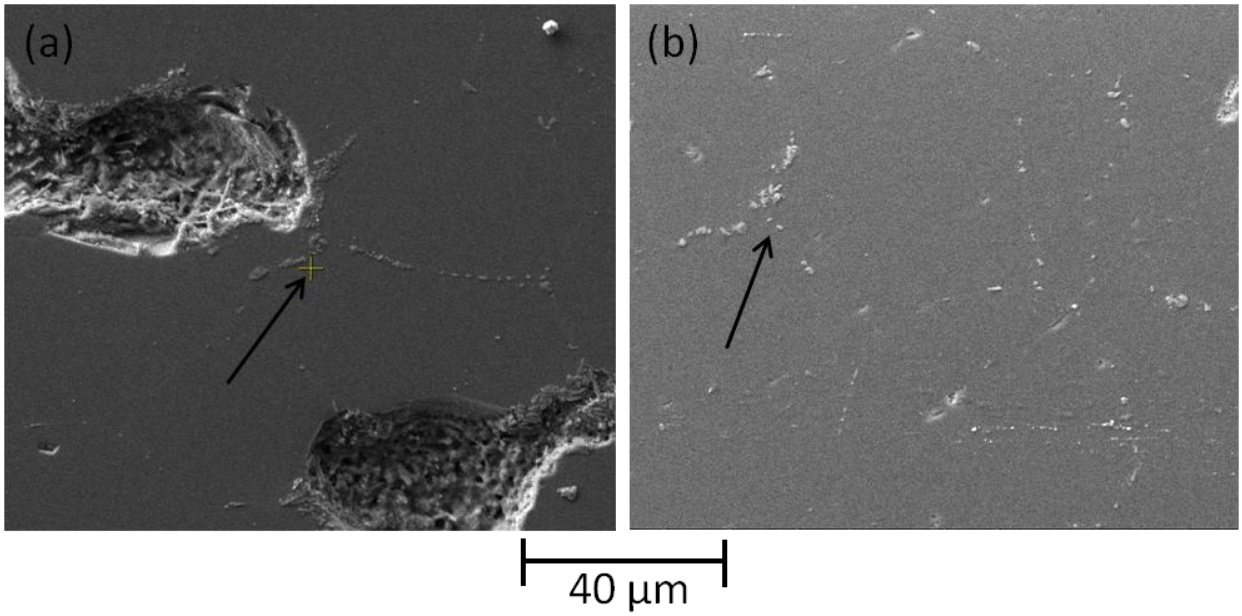

Figure 5.15. (a) SEM micrograph of 2.5 phr SiC_w/ Glass composite perpendicular to the hot pressing direction. An arrow is used to point towards some of the whisker networks. The large gaps are due to glass particles that were pulled out during polishing, but from the shape it suggests a slight flattening of the glass particles. (b) SEM micrograph of 2.5 phr SiC_w/ Glass composite parallel to the hot pressing direction. An arrow points towards a cluster of the SiC_w.[111]

Along with what appears to be a higher concentration of whiskers, the glass particles particle shape also seems to have a dependency on the hot pressing direction. In Figure 5.15(a) and Figure 5.16 (d) the depressed indentations are areas where the glass was removed. From these removed areas, the whiskers are quite visible, and for some of these, the shape of the glass particle appears to be slightly flattened, likely due to the uniaxial force during hot pressing. Some of this flattening along the ⊥-HPD direction can also be seen in Figure 5.14(a), while in Figures 5.14(b), 5.15(b), 5.16(a) and (c) the particle shape doesn't appear to have caused as much of this flattening.[111]

Since there are whiskers along the glass boundary this would likely result in a noticeable change in the electrical resistivity. The resistivity was estimated using the real part of the impedance, Z', at the low frequency intercept as has been described before.[92]

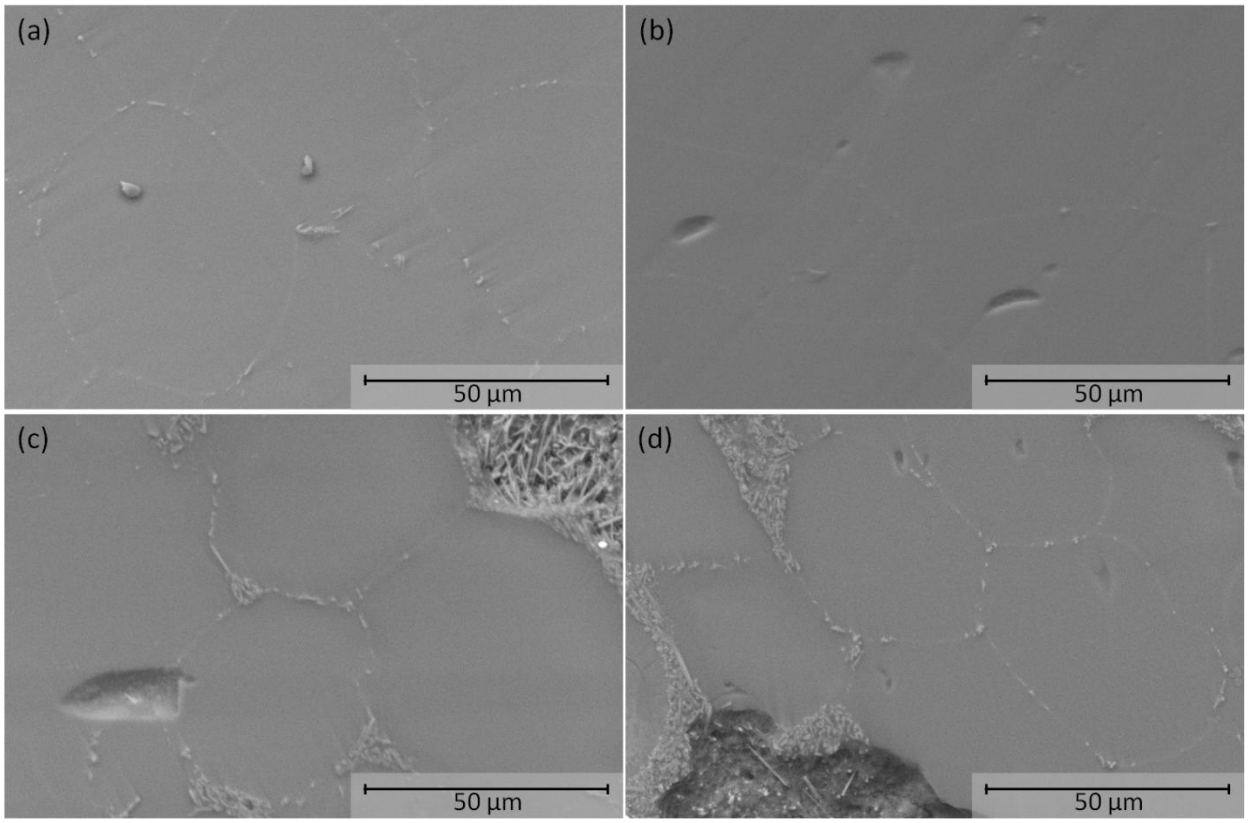

Figure 5.16. SEM micrographs for 0.25 phr SiC_w along the (a) parallel and (b) perpendicular hot pressing direction. SEM micrographs of 12.5 SiC_w along the (c) parallel and (d) perpendicular hot pressing direction.

Figure 5.17 shows the resistivity percolation curves associated with measurements taken with the electric field being applied parallel and perpendicular to the hot pressing direction. Typically with filler material that has a large aspect ratio, there tends to be some preferential orientation that occurs when a force is applied uniaxially during processing.[48, 49, 53] For both directions; however, the onset of percolation was around 5-7.5 phr, which was in the same range for the percolation threshold obtained in hot pressed Al_2O_3-SiC_w composites.[48] The final resistivity at 12.5 phr is about 5-6 orders of magnitude less than that of a pure borosilicate glass.[72] While this is not as large a drop in the resistivity as compared to the ATO segregated network system, which had a 12-13 orders of magnitude drop in resistivity, it is in the range that is expected with these whiskers, which are less conducting than ATO. The resistivity values are

very comparable to the values that were reached with hot pressed Al_2O_3-SiC_w composites.[48, 49] At the same time, the glass composites reported here were fabricated at the third of the hot pressing temperature[48] and at about a fraction of the time it takes to hot press the Al_2O_3-SiC_w composites.

While there was a slight difference in the resistivity, with the $\perp$-HPD direction having a slightly lower resistivity, the difference was not that large and not what was expected with filler particles that have a large aspect ratio. This is likely due to the processing temperature being quite low, so the glass was not nearly fluid enough to allow for the whiskers to rearrange perpendicular to the hot pressing direction. Instead, they were segregated and had a more random distribution at these segregated areas. The small difference detected is likely due to the slight flattening of the glass particles in the hot pressing direction and the slightly higher concentration along the $\perp$-HPD direction. Because of this flattening, the percolation network would be expected to be less tortuous in the $\perp$-HPD direction, which could account for the small difference in the resistivity.[111] From these removed areas in Figure 5.15(a) and 5.16(c) and (d) it can be seen that the whiskers are random in their orientation along the glass boundary, which accounts for why the network isn't as visible in the SEM since whiskers that are either arranged vertically or at an angle and would likely penetrate onto the surface while other whiskers are likely just below.[111] A more in-depth discussion of the impedance spectroscopy results and how the network influences the electrical properties will be provided in the next chapter.

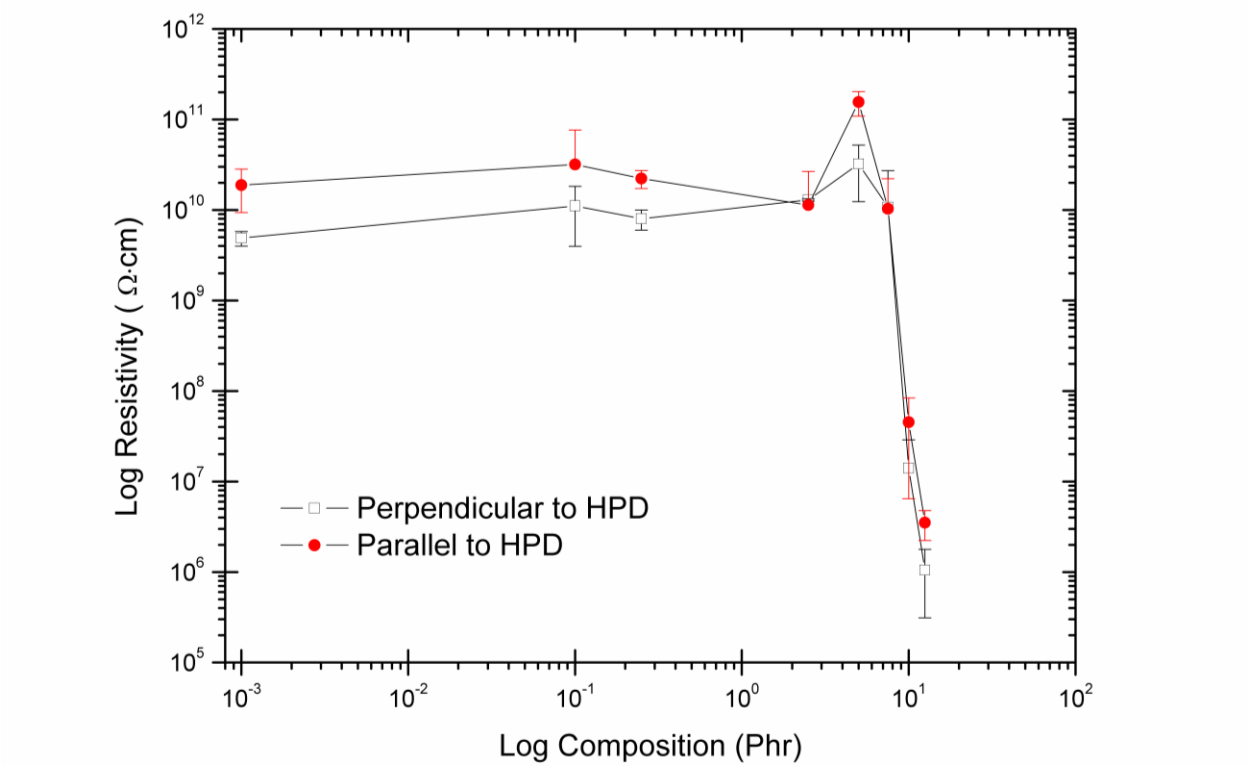

Figure 5.17. Log Resistivity vs. log composition (phr) of SiC_w/borosilicate glass composites and the large drop in resistivity characteristic of percolation. Results measured along the perpendicular and parallel to the hot press directions are shown.[111]

From all these processing variable studies, the influence that the processing has on the resulting segregated network has been presented. It appears that the quality of contact between the ATO or SiC_w filler inside these percolated network heavily influences the electrical properties of the composite. Non-ideal contact likely varies from a mix of physical contacts and partially sintered contacts. Compared to many percolated polymer composites made by a variety of methods, this hasn't been reported as a strong factor in the electrical properties. So processing at these elevated temperatures has included another variable in controlling the electrical properties. The next chapter will provide a discussion on the influence of how these processing variables influence the percolated network through an examination of electrical impedance and immitance functions.

Chapter 6

IMPEDANCE SPECTROSCOPY ANALYSIS OF NETWORK FORMATION

All the composites fabricated in this study resulted in percolation of segregated filler networks, which shows the flexibility and potential of this processing method through controlling the particle size and viscosity during hot pressing. Since several variables were examined in this study, the percolation threshold and composite resistivity exhibited a range of behaviors. This variability is due to small differences in the percolation network of similar samples that are affected by the interfaces, such as those between filler particles that exist in this network. Since this processing method allows for a range of temperatures and pressures to be used to fabricate a percolated composite, this method has the potential to create a large variety of interfaces between filler. This range of potential interfaces can result in a variety of electrical properties, so it is important to understand how the processing influences the filler interfaces, their interaction, and resulting electrical properties. A way to help further understand the cause of this variability and the potential interfaces is with an in-depth impedance spectroscopy analysis and equivalent circuit fitting.

Schematics of some of the potential interfaces that can arise in these types of composites due to the various processing temperatures and pressures used are shown in Figure 6.1. At lower temperatures, it is expected that the composite would have physically contacting filler, which is often the type of contact in segregated percolated polymer composites.[4, 17, 22, 116] At relatively high temperatures the glass is much more fluid so it is much more likely to penetrate the filler network resulting in either tunneling, like in thick film resistors, or an insulating glass barrier penetrating the network.[17, 27, 64, 66, 116, 120-122] This can also occur in polymer composites.[21, 123, 124]

With these glass composites, the potential also exists for the interfaces to be partially sintered, fully sintered, or sintered with residual porosity due to the higher temperatures involved. Figure 6.1 depicts several potential equivalent circuit models for the expected impedance behavior at the interface. From these schematics, many of the potential interfaces could appear to have similar impedance and equivalent circuit behavior. In order to help decipher the difference in the impedance and electrical property behaviors, it is first important to examine them independently, such as whether they are physically touching filler or sintered filler. It is also important to obtain the impedance and electrical properties of the materials involved. All of these impedance behaviors of the materials and interfaces will provide details on the creation of an accurate equivalent circuit model that describes the microstructure and processes in these composites and percolated networks.

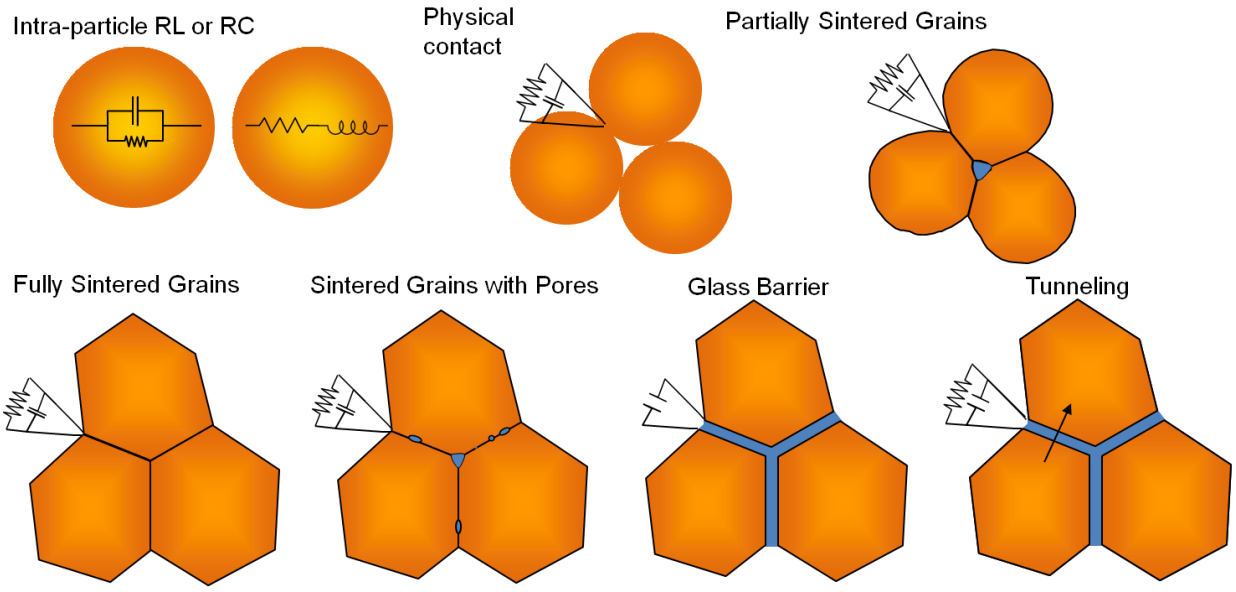

Figure 6.1. Schematics of the possible filler interfaces in these composites along with their expected impedance equivalent circuit behavior. Schematics inspired by reference[125].

6.1. Estimation of the Material and Interface Impedance for ATO

Before the impedance behavior of the various glass/ATO composites can be modeled, an estimate of the electrical properties of the filler particles is needed to create as accurate of an equivalent circuit model as possible, as well as determine the type of interfaces that are dominant in a given sample. In order to get a sense of the expected resistances and impedance behaviors once the composite has percolated, the impedance of the filler itself was measured. Since both ATO and SiC_w are difficult to get in a bulk form[13], a method was developed to measure the impedance of the particulate filler using a custom die.[126] By adjusting the applied pressure, the particle point contact resistances can be minimized so the impedance behavior will be material dominated. This method will be useful to act as a baseline in which the composite behavior can be compared to. The dry pressing impedance will provide an estimate of the impedance behavior of the ATO material as well as the influence of a physical point contact between ATO particles can have on the impedance response. The same is true for the SiC_w.

6.1.1. Dry Pressed Impedance of ATO(nm)

Since ATO(nm) hot pressed at 550°C did not seem to sinter at all, the behavior of the dry pressed ATO should provide a good estimate of the ATO behavior in set #1 as well as potentially set #2. Figure 6.2(a) shows the complex impedance for dry pressed ATO(nm) at pressures ranging from 5 MPa to 250 MPa. For all of these pressures, the complex impedance of the pressed powder samples all reside in the fourth quadrant, which based on this and the other immitance functions, suggests the complex impedance can be fit with a resistor and an inductor in series. As the pressure increases, the equivalent circuit type stays the same, the main difference is that the resistance decreases as the pressure increases. The inductance also slightly increases but the main influence of the pressure is the change in the resistance. This can also be

seen for the sample pressed with 5 MPa. At the low frequencies, there is some variance with the low frequency intercept of the real impedance, which is likely due to fluctuations in the contact resistance due to the low pressure and the movement of ATO particles. As the pressure increases this variance decreases. So it appears that with a physical contact, the influence on the impedance is primarily the location of the *Z'* intercept. This can especially be seen in Figure 6.2(b) which is a frequency dependent, or Bode plot, of the impedance magnitude (*Z**). An estimate of the resistance can be made by taking the low frequency value at 0.1 Hz. From Figure 6.2(b) the resistance ranges from about 10^3 Ω for loosely compacted ATO at no pressure to 10^{-1} Ω at 250 MPa. This is a large range in the electrical properties for the same material. It appears that the amount of contact for physically touching particles can cause a wide range of resistances. All the fit parameters for the various pressures shown in Figure 6.2 (a) are listed in Table 6.1. From this table, the decrease in the resistance due to ATO contacting particles can be seen. An expected intra-particle or material impedance of the ATO can be estimated by the highest pressure impedance at 250 MPa.

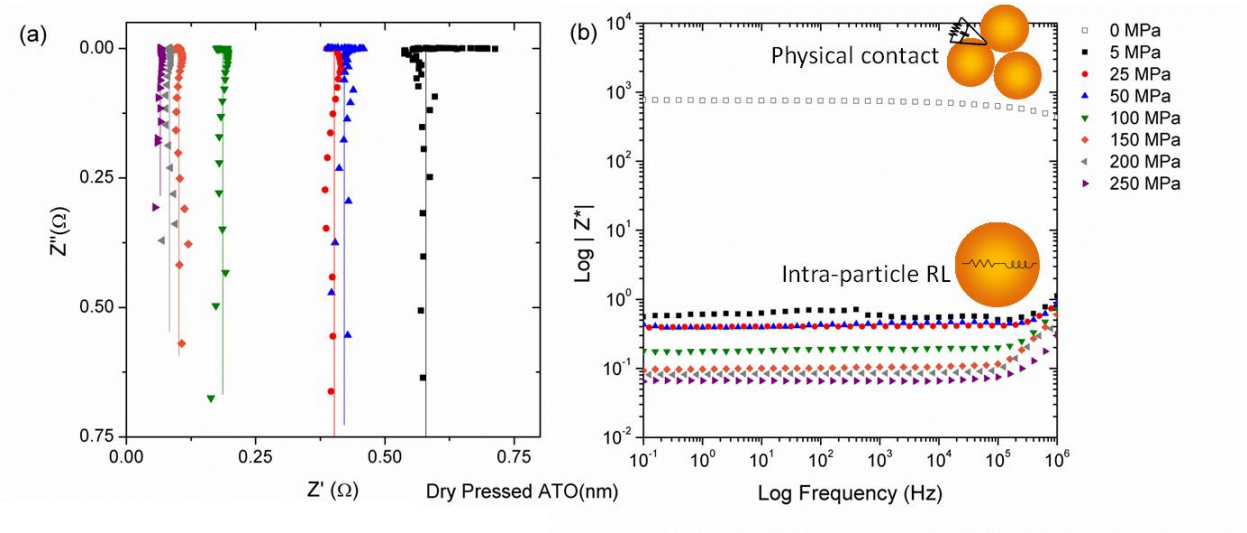

Figure 6.2. (a) Complex impedance of dry pressed ATO(nm) at select pressures. (b) Impedance magnitude of select pressures for dry pressed ATO(nm).

Table 6.1. Equivalent Circuit Fits for Dry Pressed ATO(nm) at Various Pressures.

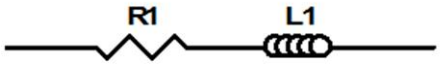

Pressure (MPa)	R1 (Ω)	L1 (H)
5	0.58	1.58×10^{-7}
25	0.40	1.37×10^{-7}
50	0.42	1.16×10^{-7}
100	0.19	1.06×10^{-7}
150	0.10	9.44×10^{-8}
200	0.08	8.69×10^{-8}
250	0.05	4.53×10^{-8}

The complex impedance of the loosely compacted ATO subjected to no pressure is shown in Figure 6.3. This impedance is shown separately from Figure 6.2(a) since the impedance is substantially larger and the impedance behavior is located in a separate quadrant (first). Instead of having series RL behavior, the complex impedance shows that the samples behaves as a resistor and capacitor in parallel (parallel RC) that is in series with a second parallel RC. For this fit and the subsequent fits, a constant phase element (CPE) will be used instead of a capacitor to account for some variation in the capacitance.[92] This is based off the semicircular behavior in the Z' and $-Z''$ quadrant and the behavior in the other immitance functions (not shown). The equivalent circuit fit for this behavior is also shown in Figure 6.3. Overall, it appears that with physically touching ATO, the contact resistances can range from 10^{3}-10^{-1} Ω and have a capacitance with loosely touching ATO and an inductance with tightly compacted ATO. The intra-particle or material impedance seems to behave as an inductor and resistor in series with a resistance around 0.05 Ω.

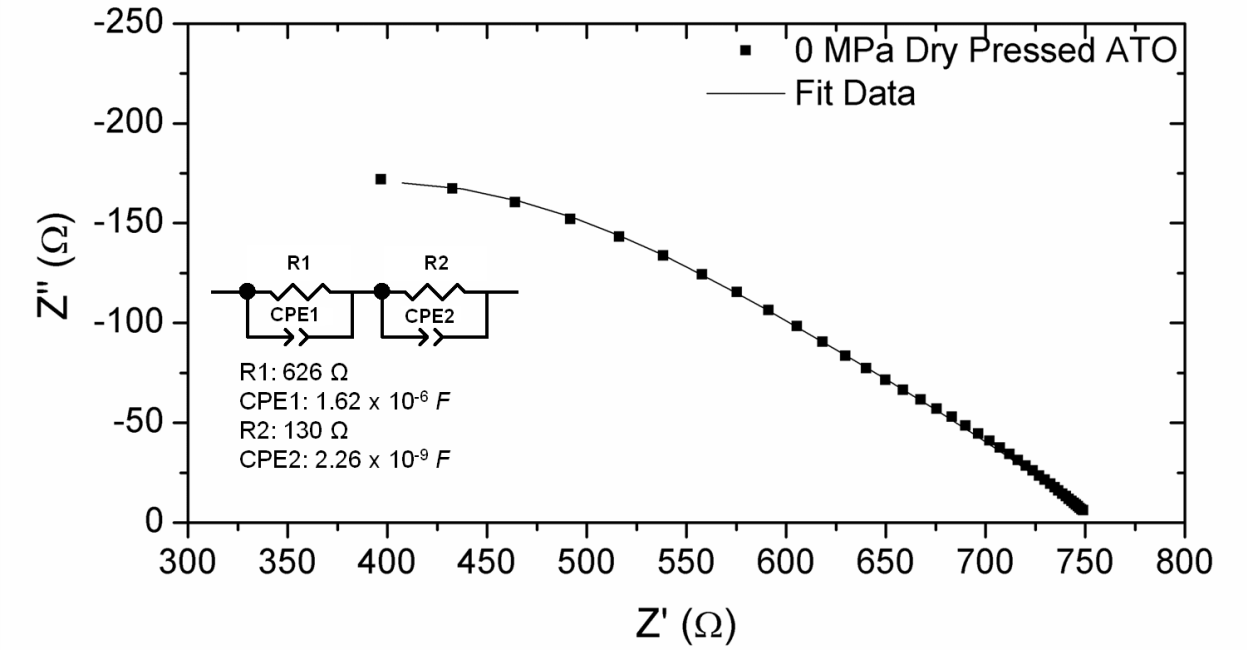

Figure 6.3. Complex impedance of dry pressed ATO(nm) at no applied pressure. The ATO was loosely compacted.

6.1.2. Impedance of Hot Pressed ATO(nm)

The dry pressed ATO(nm) does provide a good estimate of the material and physical contact behavior of this filler, but it would also be informative to have a measurement of just the hot pressed ATO(nm). The hot pressed ATO samples made at 675°C would help show if these particles had reacted or had partially sintered with one another, with resulting influence on the impedance. For the ATO(nm) that was hot pressed at 675°C, the complex impedance behavior had some differences compared to the dry pressed ATO(nm). From Figure 6.4, one can see that the complex impedance for the hot pressed ATO(nm) samples was also in the fourth quadrant, similar to the high pressure impedance of the dry pressed ATO, but the complex impedance had much more curvature compared to the behavior of the dry pressed ATO (nm). This curvature is indicative of a parallel equivalent circuit, either a resistor in parallel with an inductor or with a negative capacitor.[92, 114, 117]

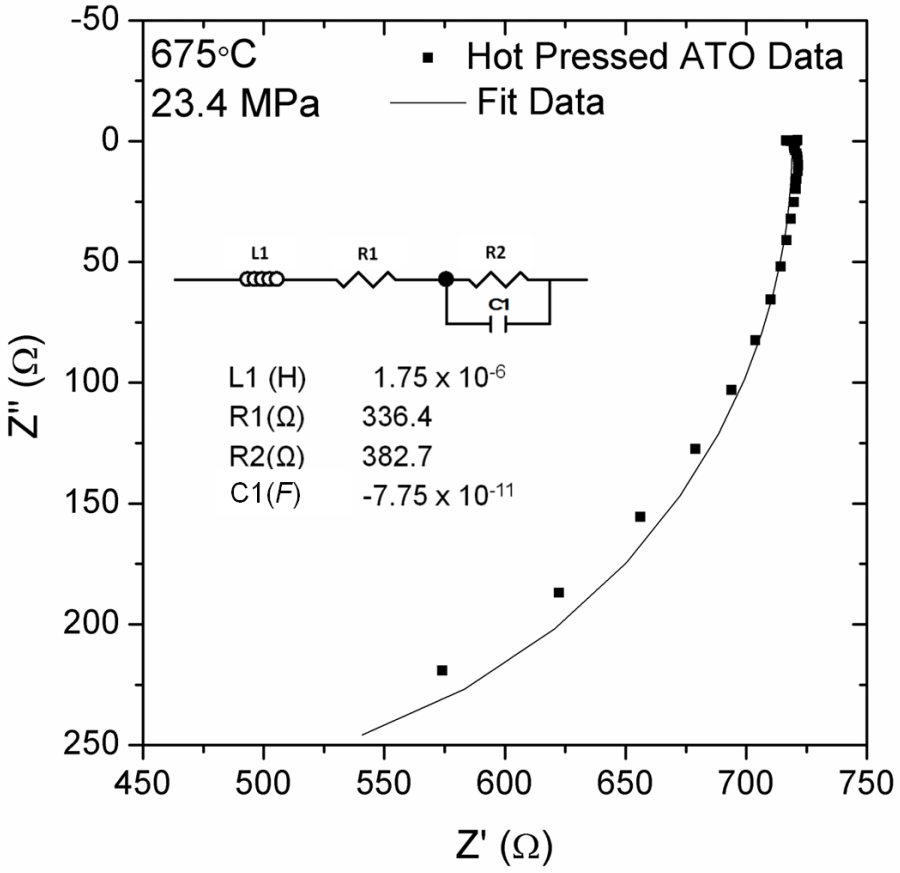

Figure 6.4. Complex impedance for hot pressed ATO(nm).

The complete circuit is similar to the dry press circuit with the addition of a resistor and capacitor in parallel. The resistor (R1) contains the ATO(nm) resistance, which was estimated at around 0.05 Ω from the previous section, and a particle contact resistance which was relatively quite high. Since these resistors were in series they consolidated to the value in R1 (~336 Ω). The ATO(nm) did not exactly consolidate well (only had 60-70% relative density) which helps explain why this impedance (R1) was much higher than expected. Sintering of bulk ATO has been reported to be extremely difficult by several investigations. Methods apart from spark plasma sintering (SPS) have reported difficulties in sintering due to nondensifying mechanisms.[13] For the values with the parallel RC (R2 and C1) in the equivalent circuit fit, the

value of the capacitance (C1) in this circuit was negative. Negative capacitance is a phenomenon that has been reported to occur in numerous types of materials and composites[127-129], including glass composites containing antimony-doped tin oxide.[130] For this study, the possible processes to explain this negative capacitance will not be discussed in detail. The reason it is mentioned here is to help show a characteristic behavior of the hot pressed ATO, so that in more complex impedance fits, this distinguishing behavior of hot pressed ATO can be described with a negative capacitance.

6.1.3. Impedance of Hot Pressed Borosilicate Glass (GL0179)

Now that the expected behavior of the conducting materials has been established, the insulating behavior should also be examined. Figure 6.5 shows the complex impedance of hot pressed borosilicate glass (GL0179). The entire impedance is within the first quadrant (-*Z*'' and *Z*') and has the beginnings of a curve of a semicircle. The impedance is very high for the entire frequency range (10^{7}-10^{-1} Hz) measured, and as a result does not result in a low frequency intercept. In order to estimate the expected resistances and capacitance of the glass alone, an equivalent circuit was created using the curvature of the complex impedance curve. The result was a high resistance (~1 x10^{12} Ω) and a capacitance in the picofarad range. This resistance corresponds to a resistivity value ~10^{13} Ω·cm so this measured impedance seems to accurately describe the electrical properties of the glass.[72]

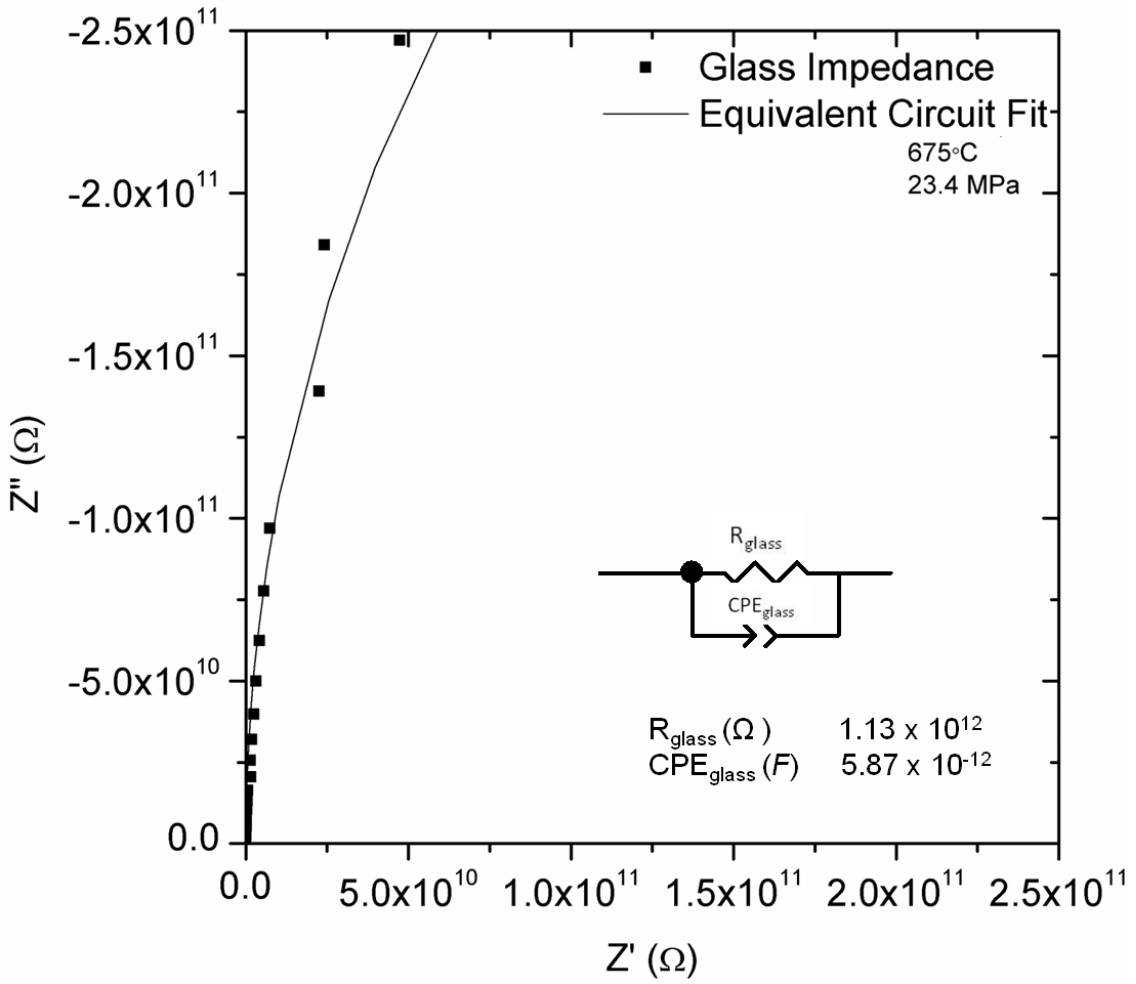

Figure 6.5. Complex impedance for hot pressed borosilicate glass (GL0179).

6.2. Development of An Equivalent Circuit Model for the Network Formation

From section 6.1, a range of behavior was shown with the glass, hot pressed ATO, and compacted ATO. Based on the heat treatments, the impedance and equivalent circuit will likely involve a combination of these various material impedance behaviors. This assumption is made on the relatively low hot pressing temperatures of 550 and 675° C and the pressure ranging from 5.8-23.4 MPa. Now that the material impedance behavior and some of the interfaces has been established, it is important to look at the composite microstructure to develop an equivalent circuit model. An SEM image of an ATO network from set #2 (ATO(nm)-GL0179S hot pressed

at 675°C) is shown in Figure 6.6. This network exhibits several features. The center of the network features a lot of removed ATO from polishing and grinding, so the ATO located at the core of the network was clearly held together loosely. This suggests that the ATO located here had a physically touching or partially sintered interface. In terms of equivalent circuit fitting, such a microstructure would lead to be a resistor and capacitor/CPE in parallel, based on the impedance behavior from Figure 6.3 and 6.4. Since there is the possibility of multiple interfaces in this core network, the behavior of this core network will be estimated with a parallel R-CPE in series with another parallel R-CPE. These two parallel R-CPEs will be designated with R_{grain1} and CPE_{grain1} for the first parallel R-CPE, and R_{grain2} and CPE_{grain2} for the second parallel R-CPE. These two circuit elements can be seen on top of the core of the ATO network in Figure 6.6. The ATO network in Figure 6.6 also had some different behavior along the edges. There was little to no material removed at these edges, which indicates that the ATO here is more tightly held together to withstand all the grinding and polishing. This is likely due to glass penetrating into this network. This is supported by the fact that the networks hot pressed at a peak of 675°C had thicker boundaries like this compared to the ones hot pressed at just 550°C. Since there is a large amount of glass intermixed with the ATO, an interface with a glass barrier such as the one in Figure 6.1 is quite likely. For this interface, the glass behavior will dominate so it is estimated that the impedance behavior will be similar to the hot pressed glass from Figure 6.5, which could be modeled with a parallel R-CPE. Since this edge behavior is not part of the core of the ATO network, this impedance behavior will be in parallel with the two series parallel R-CPEs. This is shown in Figure 6.6(a) with the glass/ATO boundary designated with a parallel R-CPE with R_{glass} and CPE_{glass}.

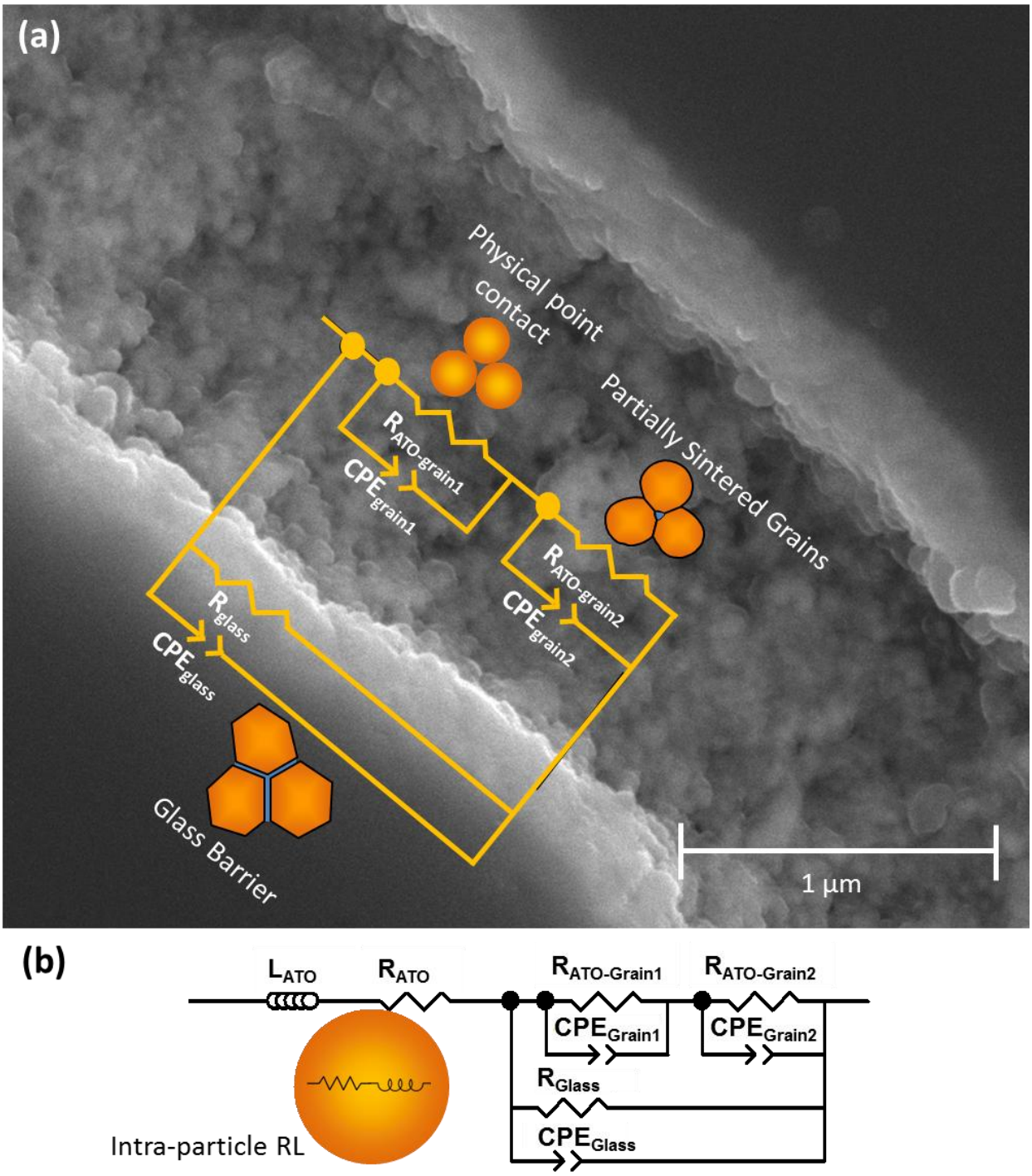

Figure 6.6. (a) Equivalent circuit model basis using the microstructure of an ATO network (2.5 phr ATO(nm)-GL0179S hot pressed at 675°C) along with schematics of the possible circuit elements that are present in this network. (b) Proposed equivalent circuit using the microstructural features in (a) and the impedance behavior/models in Figure 6.3-6.5.

The last part of this proposed equivalent circuit model is to account for the intra-particle or filler material behavior. From the dry pressed impedance study in Figure 6.2, this behavior is likely a resistor and inductor in series, which for this model was denoted L_{ATO} and R_{ATO}. This series RL was placed before the other circuit elements since any of these potential interface behaviors will also include the material behavior. The assembled equivalent circuit model is shown in Figure 6.6(b). This circuit will be applied to the impedance behavior to the composites containing ATO(nm) to help explain the development of the ATO networks and the change in the electrical properties.

6.3. Application of Equivalent Circuit Model

In the previous section, an equivalent circuit model based on the microstructural features of the ATO network and the individual impedance behavior of the materials and interfaces involved was developed. The next step is to apply this equivalent circuit model to the composites containing ATO(nm), particularly set #1 and #2, in order to help determine how the processing influenced the ATO network and electrical properties.

6.3.1. Equivalent Circuit Modeling of Set #1

The impedance behavior for sets #1 varied greatly depending on the composition of the composites. A range of behaviors was observed at concentrations before percolation, during percolation, and after percolation. This variation in the impedance behavior can be seen in Figure 6.7. Figure 6.7(a) shows the impedance for 0.05 phr ATO, which is a composition before percolation. For the pre-percolation composites, the impedance behavior had a large resistance and semicircular behavior in the first quadrant ($-Z''$ vs. Z'). Applying the proposed circuit from 6.6(b) to set #1 yielded interesting results. From Figure 6.7(a) the equivalent circuit from Figure

6.6(b) was able to model the behavior for the pre-percolation composites. The values for these fits are shown in Table 6.2.

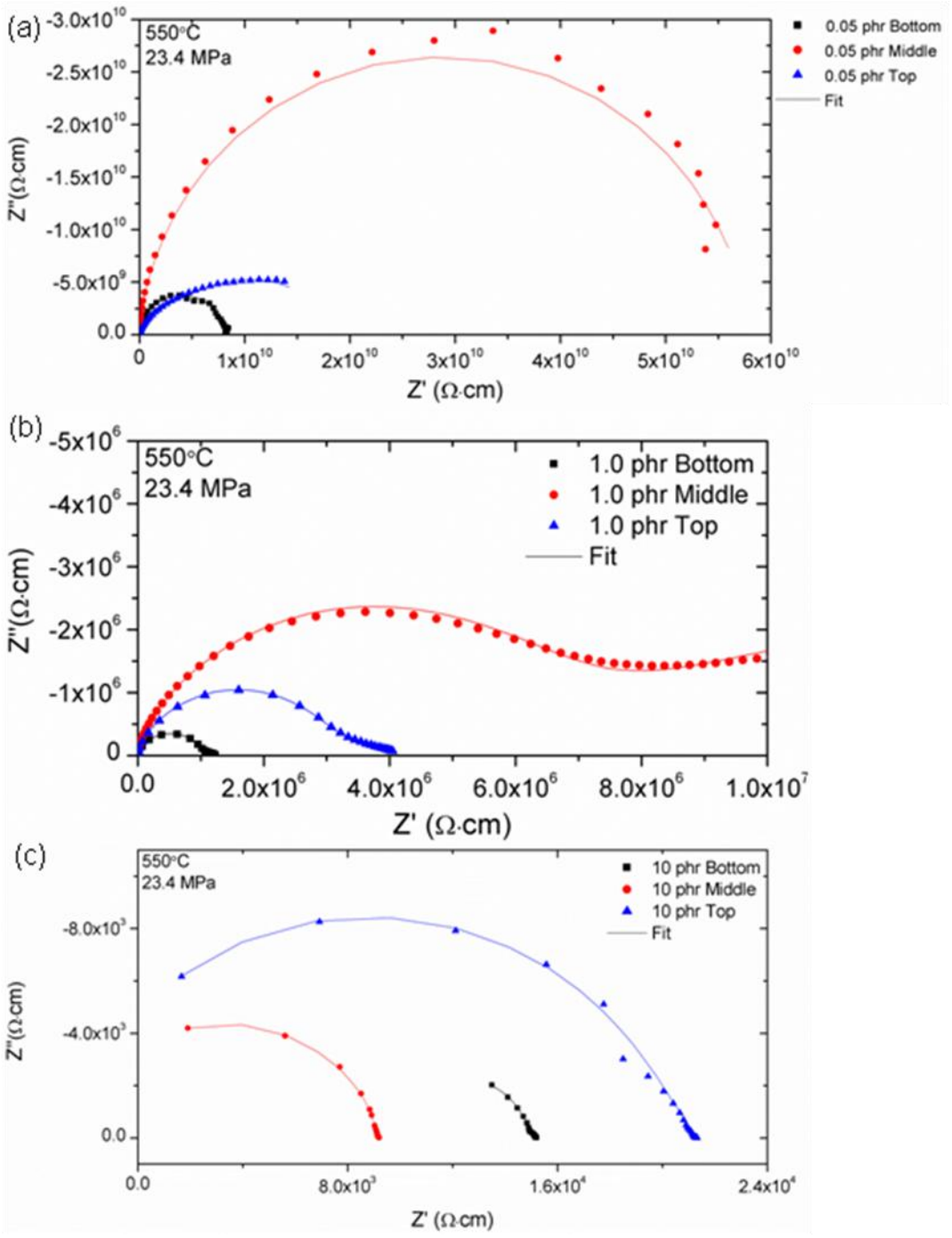

Figure 6.7. Complex impedance for (a) 0.05, (b) 1.0, and (c) 10 phr set#1 (ATO(nm)-GL0179S hot pressed at 550°C) with the applied equivalent circuit fits from Table 6.2 (shown as solid lines).

Table 6.2. Equivalent Circuit Fits For Set#1 (ATO(nm)-GL0179S Hot Pressed at 550°C).

Composition (phr)	L1 (μH)	R_{ato} (Ω)	R_{grain1} (Ω)	CPE1 (*F*)	R_{grain2} (Ω)	CPE2 (*F*)	R_{glass} (Ω)	CPE_{Glass} (p*F*)
0.001	33.75	0.05	1.44×10^{9}	2.14×10^{-11}	1.86×10^{10}	8.53×10^{-11}	2.75×10^{10}	0.26
0.01	37.10	0.05	7.78×10^{8}	3.11×10^{-11}	7.96×10^{8}	1.07×10^{-8}	3.58×10^{9}	2.22
0.05	20.74	0.05	7.66×10^{9}	6.21×10^{-11}	5.02×10^{11}	3.37×10^{-7}	2.11×10^{13}	2.59
0.1	15.06	0.05	2.92×10^{10}	1.24×10^{-10}	2.36×10^{11}	2.47×10^{-10}	3.34×10^{11}	1.54
0.25	18.17	0.05	7.50×10^{9}	2.24×10^{-11}	9.31×10^{8}	3.99×10^{-7}	6.40×10^{9}	0.43
1.0	44.74	0.05	1.18×10^{6}	6.42×10^{-7}	6.88×10^{5}	3.69×10^{-10}	4.71×10^{12}	0.45
2.5	18.92	0.05	1.08×10^{5}	4.19×10^{-6}	1.43×10^{5}	6.11×10^{-10}	4.47×10^{12}	5.71
5	46.07	0.05	3.53×10^{3}	3.00×10^{-7}	7.30×10^{2}	1.26×10^{-6}	4.34×10^{4}	84.29
7.5	36.58	0.05	4.29×10^{4}	1.71×10^{-6}	2.77×10^{4}	4.19×10^{-7}	3.06×10^{11}	30.15
10	25.51	0.05	7.75×10^{4}	8.52×10^{-7}	2.80×10^{4}	2.55×10^{-8}	1.19×10^{6}	99.62

For the pre-percolation range, which was from 0.001 to about 0.25 phr ATO the equivalent circuit fits all had a high resistance for both R_{grain1} and R_{grain2} in the equivalent circuit from Figure 6.6(b). The corresponding capacitances, CPE_{grain1} and CPE_{grain2}, for these resistance elements are around 10^{-11} *F*, which is close to that of the capacitance of the pure glass. Based on this and the high resistance it appears that there are likely large regions of glass that are breaking up the ATO network. During percolation, which was around 1.0 phr, a large drop in the resistance occurred. This can be seen in both Figure 6.7(b) and Table 6.2. From Figure 6.7(b) multiple impedance semicircles can be seen which supports an equivalent circuit containing multiple elements, such as the one being used to fit the data. The equivalent circuit fits from the circuit in Figure 6.6(b) and Table 6.2 are shown with the solid line in Figure 6.7(b). Examining the fit data shows that not only did the resistance drop for both R_{grain1} and R_{grain2}, but their corresponding capacitances increased to about 10^{-7} *F* and 10^{-9} *F* respectively. These capacitance values resemble that of the loosely compacted ATO particles from Figure 6.3. So during percolation it appears that the glass breaking up the network has primarily been replaced with loosely touching ATO particles with point contacts. As the concentration increases to past the

percolation threshold (2.5 phr or higher) the resistance continues to decrease for R_{grain1} and R_{grain2} but their corresponding capacitances remain relatively the same around 10^{-7} *F*. The main difference between the resistances is likely a difference between contact and slight distribution in the contacts between particles. The increased amount of ATO seems to have increased the number of contacts in the network, which accounts for the drop in the resistances of these composites, but overall the ATO is loosely touching in the composite. Figure 6.7(c) shows the complex impedance and fits for 10 phr ATO/glass for set #1. The shape and behavior of the curves resembles that of the loosely compacted ATO in Figure 6.3, which supports the equivalent circuit models since it had similar values to the loosely packed ATO impedance.

Overall the equivalent circuit created in Section 6.1 worked well with all the compositions for set #1, even though the impedance behavior covered a large range of resistances and capacitances. The inductance and ATO resistance (series RL) was consistent with the estimated ATO behavior as well as the glass/ATO boundary (R_{glass} and CPE_{glass}) behavior being consistent with the pure glass impedance.

6.3.2. Equivalent Circuit modeling of Set #2

The composites that were fabricated at a peak temperature of 675°C showed a greater range of impedance behaviors and resistivities compared to set #1, which was hot pressed at 550°C. Figure 6.8 contains the various complex impedance behaviors for composites before(a), during(b) and after percolation(c).

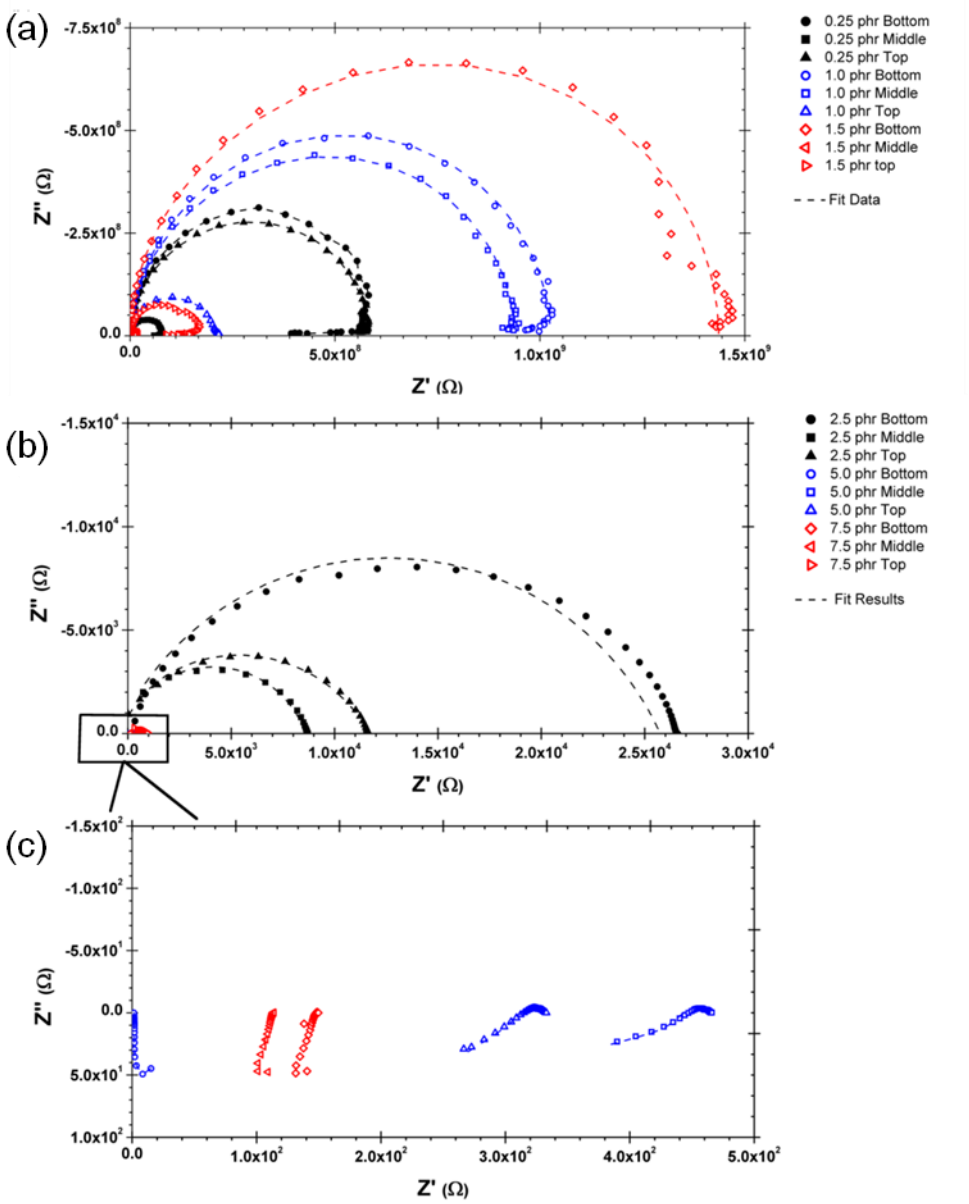

Figure 6.8. Complex impedance for (a) 0.25, 1.0, 1.5 (b) 2.5, and (c) 5.0 and 7.5 phr set#2 (ATO(nm)-GL0179S hot pressed at 675°C) with the applied equivalent circuit fits from Table 5.3.

The impedance behavior in set #2 was similar to Set #1 except for a large exception, which occurred after the percolation threshold. Figure 6.8(c) shows the complex impedance for 7.5 phr and 5.0 phr ATO samples. Unlike their counterparts in Set#1, the behavior for these high

concentrations has curvature in the fourth quadrant very similar to that observed with the hot pressed ATO(nm) presented in Figure 6.4.

Figure 6.8 also shows the fit values from Table 6.3, based on the equivalent circuit from Figure 6.6(b). For set#2 the equivalent circuit takes into account the behavior of the ATO(nm) material, represented by a resistor and inductor in series, the glass and ATO encased glass at the boundary, and the behavior of the ATO(nm) network. For compositions before percolation, the resistance for R_{grain1} was quite high and is within the resistance range for glass. The capacitance (CPE_{grain1} or CPE1 for short) associated with the resistance R_{grain1} is also in the same range as the capacitance for the pure glass impedance from Figure 6.3. The resistance for R_{grain2} was slightly smaller for 0.01 and 0.1 phr ATO(nm), which seems to be more associated with a highly resistive ATO network. This is supported by the capacitances for CPE_{grain2}, or CPE2 for short, which was closer to the range for the loosely touching ATO. At these concentrations, the ATO clusters will be quite small and will likely be intermingled with glass.

Table 6.3. Equivalent Circuit Fits For Set#2 (ATO(nm)-GL0179S Hot Pressed At 675°C).

Composition (phr)	L1 (μH)	R_{ato} (Ω)	R_{grain1} (Ω)	CPE1 (*F*)	R_{grain2} (Ω)	CPE2 (*F*)	R_{glass} (GΩ)	CPE_{Glass} (p*F*)
0.001	N/A	N/A	N/A	N/A	N/A	N/A	2.65	1.38
0.01	42.54	0.05	$9.47x10^{11}$	$4.72 x10^{-12}$	$1.75 x10^{9}$	$1.84 x10^{-8}$	0.01	0.16
0.1	44.06	0.05	$1.32 x10^{13}$	$5.17 x10^{-12}$	$8.06 x10^{10}$	$6.95 x10^{-8}$	2.83	0.35
0.25	18.30	0.05	$3.96 x10^{9}$	$1.17 x10^{-11}$	$5.18E x10^{7}$	$-4.37 x10^{-9}$	0.01	5.15
1	46.37	0.05	$9.84 x10^{8}$	$2.02 x10^{-11}$	$2.93 x10^{11}$	$-2.19 x10^{-11}$	0.73	2.99
1.5	24.41	0.05	$3.95 x10^{8}$	$5.48 x10^{-11}$	$2.42 x10^{11}$	$-8.58 x10^{-11}$	1.24	3.54
2.5	15.70	0.05	$1.13 x10^{4}$	$8.95 x10^{-9}$	$1.83 x10^{4}$	$-1.1 x10^{-8}$	5.84	1.01
5*	1.30	0.05	$2.18 x10^{2}$	$5.49 x10^{-7}$	$7.32 x10^{1}$	$-1.51 x10^{-7}$	1.56	491.51
7.5	1.36	0.05	$2.49 x10^{2}$	$5.08 x10^{-8}$	$1.60 x10^{2}$	$-3.99 x10^{-9}$	2.83	1.03
10	3.29	0.05	$5.91 x10^{2}$	$2.14 x10^{-7}$	$1.72 x10^{2}$	$-1.30 x10^{-7}$	3.02	59.38

As the concentration of ATO(nm) increases in the composites, an interesting switch occurs with the equivalent circuit fits. For compositions around 0.25-1.5 phr (Figure 6.8(a)), which was around the percolation threshold, the resistance for R_{grain1} was very high and the

capacitance is still in the range of that of the pure glass. At these concentrations it appears that long range conductivity is impeded by segments of glass breaking up the network. The values for CPE_{grain2} at these concentrations exhibit a change as the capacitance becomes negative, much like it did with the hot pressed ATO in Figure 6.4. At these concentrations the ATO clusters are likely larger and reacting with one another such that they can be detected in the impedance response.

Once the percolation threshold was reached, which was at concentrations of 2.5 phr and higher, the large drop in resistance associated with percolation was modeled with the equivalent circuit for both R_{grain1} and R_{grain2}. For the capacitance, CPE1, which was associated with R_{grain1}, the capacitance increases to the same range ($\sim 10^{-9}$ *F*) as the loosely pressed ATO. So for this parallel R-CPE, R_{grain1} and CPE_{grain1}, the impedance behavior suggests that some of the ATO network involves a physical point contact. Unlike set #1, the behavior for the second parallel R-CPE, R_{grain2} and CPE_{grain2}, did not indicate ATO that had a physical point contact. Instead, the capacitance for this part of the circuit, CPE_{grain2}, has a negative capacitance value similar to that of the hot pressed ATO. So it appears that this part of the circuit models ATO that has reacted at the higher temperatures and have likely partially sintered. So the ATO network for these composites hot pressed at 675°C showed a mixed behavior of physically touching ATO and partially reacted or sintered ATO. Both contribute to the overall conductivity of the composite.

For the highly conducting samples, which are compositions ranging from 5.0-10.0 phr, the final impedance behavior of these composites can be seen. This is shown in Figure 6.8(c). These composites have impedance behavior in both the first and fourth quadrant. The behavior in the fourth quadrant has curvature very similar to the hot pressed glass. Unlike the hot pressed glass however, these composites also exhibit semicircular behavior in the first quadrant. Based

on the equivalent circuit model the fourth quadrant behavior is due to the partially sintered ATO, and the semicircular behavior in the first quadrant can be contributed to the physically touching ATO.

The inductor and resistor that represent the ATO material stay relatively the same value The same occurs for the R-CPE (R_{glass} and CPE_{glass}) circuit to represent the glass and the glass at the boundary of the ATO(nm) network. The main variation in the circuit as the concentration increases is modeled by the two parallel R-CPE's in series. The main ATO(nm) network is represented by the first parallel R-CPE (R1 and CPE_{grain1}). The R1 is the more resistive element of the network so it will influence the overall composite properties. As the concentration increases, the network capacitance also increases (CPE_{grain1}). The second parallel R-CPE is more representative of the ATO(nm) as it is hot pressed. This is because the capacitor in this part of the circuit (CPE_{grain2}) becomes negative around the same concentration as the percolation threshold. With percolation the ATO(nm) filler particles are starting to come into contact with one another and at this temperature the ATO(nm) seem to be reacting with one another, just like the hot pressed ATO(nm) did at this temperature. The resistance also drops when percolation occurs. Past the percolation threshold, the resistance is quite low compared to all the other resistances from the equivalent circuit fits in Table 6.3.

So this second R-CPE (R2 and CPE_{grain2}) seems to be the distinguishing element between set #1 and #2 due primarily to this capacitor (CPE_{grain2}) and also the lower resistance. Negative capacitances have been reported in glasses containing antimony-doped tin oxide so the antimony might be also reacting somewhat with the glass, along with one another.[130] This would help explain the differences in magnitude between the negative capacitances in these composites and the hot pressed ATO(nm).

6.3.3. Equivalent Circuit Modeling for Variable Temperature and Pressure Study

From the equivalent circuit modeling for set #1 and #2, it was shown that the ATO network behavior influences the electrical properties through both physically touching and partially sintered interfaces of the ATO. For set#1 the physically touching contacts of the ATO determine the electrical properties behavior at the higher concentrations. With set #2, the higher temperature processing conditions resulted in an additional behavior of the interfaces and contacts with partially sintered ATO. Since the difference between these sets was the processing temperature, examining both pressure and temperature variations for samples containing the same amount of ATO (5.0 phr) could help show the influence processing has on the network and the interfaces within this network.

Table 6.4. Equivalent Circuit Fits For the Processing Parameter Study for 5.0 Phr (ATO(nm)-GL0179S).

Variable Temperature Study

Peak Temperature (°C)	L1 (μH)	R_{ato} (Ω)	R_{grain1} (Ω)	CPE1 (*F*)	R_{grain2} (Ω)	CPE2 (*F*)	R_{glass} (Ω)	CPE_{Glass} (p*F*)
550	46.07	0.05	3.53×10^{3}	3.00×10^{-7}	7.30×10^{2}	1.26×10^{-6}	4.34×10^{4}	84.29
610	23.06	0.05	3.22×10^{2}	5.73×10^{-8}	7.22×10^{1}	-6.59×10^{-9}	2.72×10^{12}	3.03
675	1.30	0.05	2.18×10^{2}	5.49×10^{-7}	7.32×10^{1}	-1.51×10^{-7}	1.56×10^{12}	491.51

Variable Pressure Study

Peak Pressure (MPa)	L1 (μH)	R_{ato} (Ω)	R_{grain1} (Ω)	CPE1 (*F*)	R_{grain2} (Ω)	CPE2 (*F*)	R_{glass} (Ω)	CPE_{Glass} (p*F*)
5.8	18.92	0.05	5.66×10^{2}	4.93×10^{-9}	1.78×10^{2}	-1.85×10^{-7}	3.44×10^{12}	1.00
11.7	75.53	0.05	1.94×10^{2}	2.13×10^{-7}	1.81×10^{2}	-2.31×10^{-7}	1.80×10^{12}	4.20
23.4	1.30	0.05	2.18×10^{2}	5.49×10^{-7}	7.32×10^{1}	-1.51×10^{-7}	1.56×10^{12}	491.51

Table 6.4 shows the equivalent circuit fits for the impedance results obtained for both the variable temperature and pressure study on the 5.0 phr ATO/glass composites using the equivalent circuit in Figure 6.6(b). With the variable temperature study, the behavior of R_{grain1} and CPE1 were consistent for all the temperatures. Like the previous sets, the capacitance is similar to the loose dry press ATO powders, so for all three temperatures they exhibited

physically touching ATO. With R_{grain2} and CPE2 the transition from positive to negative capacitance can be seen from 550°C to 610°C. For the temperature study, the composites at 610°C also had a negative capacitance for CPE2. The value is lower than that of the values obtained for the same composition for set #2 (hot pressed at 675°C) so the ATO is likely not reacting as much at the lower temperature (610°C).

The influence the pressure has on the network is a little more complicated. All of these composites were processed at 675°C. It appears that the temperature is the cause of the negative capacitance since all the composites hot pressed at the various pressures had very similar negative capacitances and resistances for R_{grain2} and CPE2. The pressure seemed to primarily influence R_{grain1} and CPE1. As the pressure increases from 5.8 MPa to 11.7 MPa the resistance decreases slightly and the capacitance increases to values similar to the loosely compacted ATO(nm). The pressure is likely influencing the physical point contact, but has likely reached a limit since there is little change in R_{grain1} when increasing the pressure from 11.7MPa to 23.4 MPa. Since for the variable pressure study the concentration was held constant at 5.0phr ATO, further improvements in the ATO network's resistance is also likely due to the number of point contacts along with the force at which the particles are physically touching.

6.3.4. Equivalent Circuit Modeling for Set #3

Set #3 (ATO(nm)-GL0179L (large glass microspheres) hot pressed at 675°C) was processed at the same temperature, pressure, and time as set #2. As a result, the equivalent circuit used for set #3 should be similar to the one used for set #2 (small glass microspheres). Figure 6.9 shows SEM micrographs of the ATO(nm) network in these composites. It appears that the boundary between the ATO(nm) and the glass has a region of glass and ATO, which are marked off with the arrows. Within these boundaries, the ATO network looks partially recessed,

likely due to this section of the impedance network being loosely held together that resulted in ATO being removed during polishing. This was similar to what occurred in set #2 so the equivalent circuit used in set #2 was applied to this large glass particle composite study. The complex impedance for select compositions and their corresponding fit parameters for this composite set are shown in Figure 6.10 and Table 6.5 respectively. Figure 6.10(a) has a large semicircle in the first quadrant for compositions before the percolation threshold. Just before percolation, the networks are cut off since the resistance is very high($\sim 10^{10}$ Ω). While the percolation networks are starting to be linked, such as with 2.5 phr ATO in Figure 6.10(b), the resistance drops significantly (4 orders of magnitude) and also the semicircle becomes stretched along the horizontal axis. This suggests that multiple processes are involved during this stage.

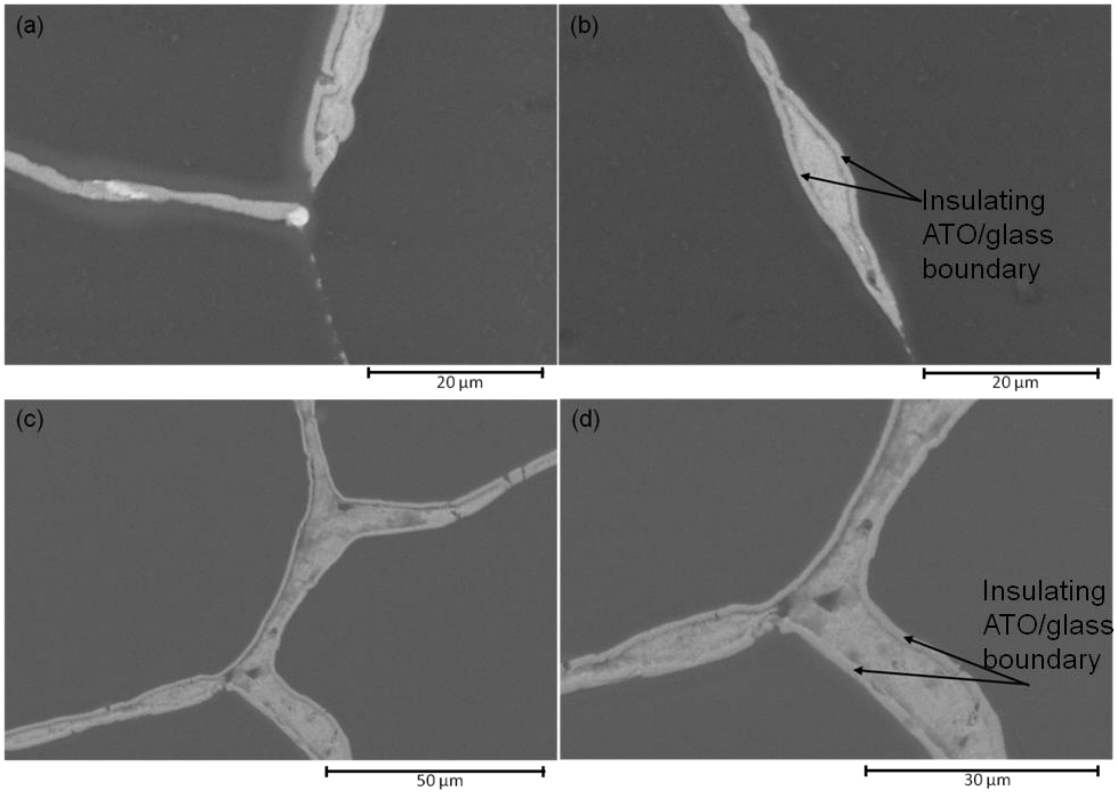

Figure 6.9. SEM micrographs of 5.0 phr (a and b) and 10 phr (c and d) for set #3 (ATO(nm)-GL0179L hot pressed at 675°C). Arrows were added to show the insulating glass/ATO boundaries, which also appeared in the microstructures in set #2 (ATO(nm)-GL0179S hot pressed at 675°C).

For the post-percolation compositions of 7.5 and 10.0 phr in Figure 6.10(c), the impedance behavior is very similar to the complex impedance of the post-percolation composites of set#2 (Figure 6.8(c)). For all of the complex impedance in Figure 6.10(c), all the compositions have a noticeable tail trailing into the fourth quadrant, much like the complex impedance of the hot pressed ATO in Figure 6.4. The primary difference between these two figures is that for the composites, especially for 7.5 phr, the complex impedance also has some activity in the first quadrant. This suggests that an additional process is occurring in these composites that aren't in the hot pressed ATO. Like set #2, the capacitance and resistance that represent the glass/glass boundary and the ATO(nm) material was relatively constant for all the compositions and comparable to the fit values in set #2. The difference between this larger sized-glass and set #2 is primarily the resistances of R_{grain1} and R_{grain2}. The resistance for R_{grain1}, which previously was identified as an ATO-ATO contact resistance, was lower for set #3 compared to set #2. The capacitance (CPE1) is still within the range for loosely packed ATO(nm) so the quality of contact between the ATO(nm) particles is similar to that of set#1 and set #2. The reason R_{grain1} is lower for set#3 compared to set#2 is likely the number of contacts. For composites with the same composition, set#3 will likely have a higher number of contacts within the percolated network since there aren't as many glass boundaries as there are in set#2. This is due to the larger sized glass particles. As a result the ATO would be more heavily concentrated within these networks. Examples of this can be seen in Figure 6.9 where the ATO networks have a much larger thickness compared to the networks in set#1 and #2. For the second parallel R-CPE, which was used to model the negative capacitance and partially sintered ATO, this set also had negative capacitances but overall was smaller than set #2 and more similar to the hot pressed ATO from Figure 6.4.

What is surprising about set #3 is that with a fewer number of boundaries and a higher amount of ATO clustered at these networks these samples didn't percolate at lower phr (before set #1 or #2). Set #1 and #2 had a percolation threshold around 0.1-1.0 phr, while set #3 percolated around 1.0-2.5 phr ATO. From Figure 6.9 and 5.11 the ATO networks tend to be the largest at the triple points but towards the center of the edges they are much thinner. With the large glass initially the glass particles are touching each other at a point and spread out from this point. Since the ATO isn't penetrating into the glass, the ATO will also be pushed away from this point. For low concentrations the ATO will tend to accumulate more at the triple points. Set #3 seems to be more susceptible to this because with a fewer number of networks compared to set #1 and #2, a relatively high number of these breaks can be detrimental to the electrical properties. Set #1 and #2 have a higher number of networks, so there will be more parallel paths for the current to go through if there is a break in one section of the network.

From the complex impedance and equivalent circuit model for set #3 the onset of percolation showed a change in not only the resistance but for the capacitance. Like set #2 CPE-2 exhibited negative capacitance behavior for the reacted ATO, but CPE-1 increases from 10^{-11} *F* to 10^{-7} *F*. It appears that this part of the circuit is showing the network overcoming these breaks due to the glass (indicated by the 10^{-11} *F* capacitance) and percolating throughout the entire composite.

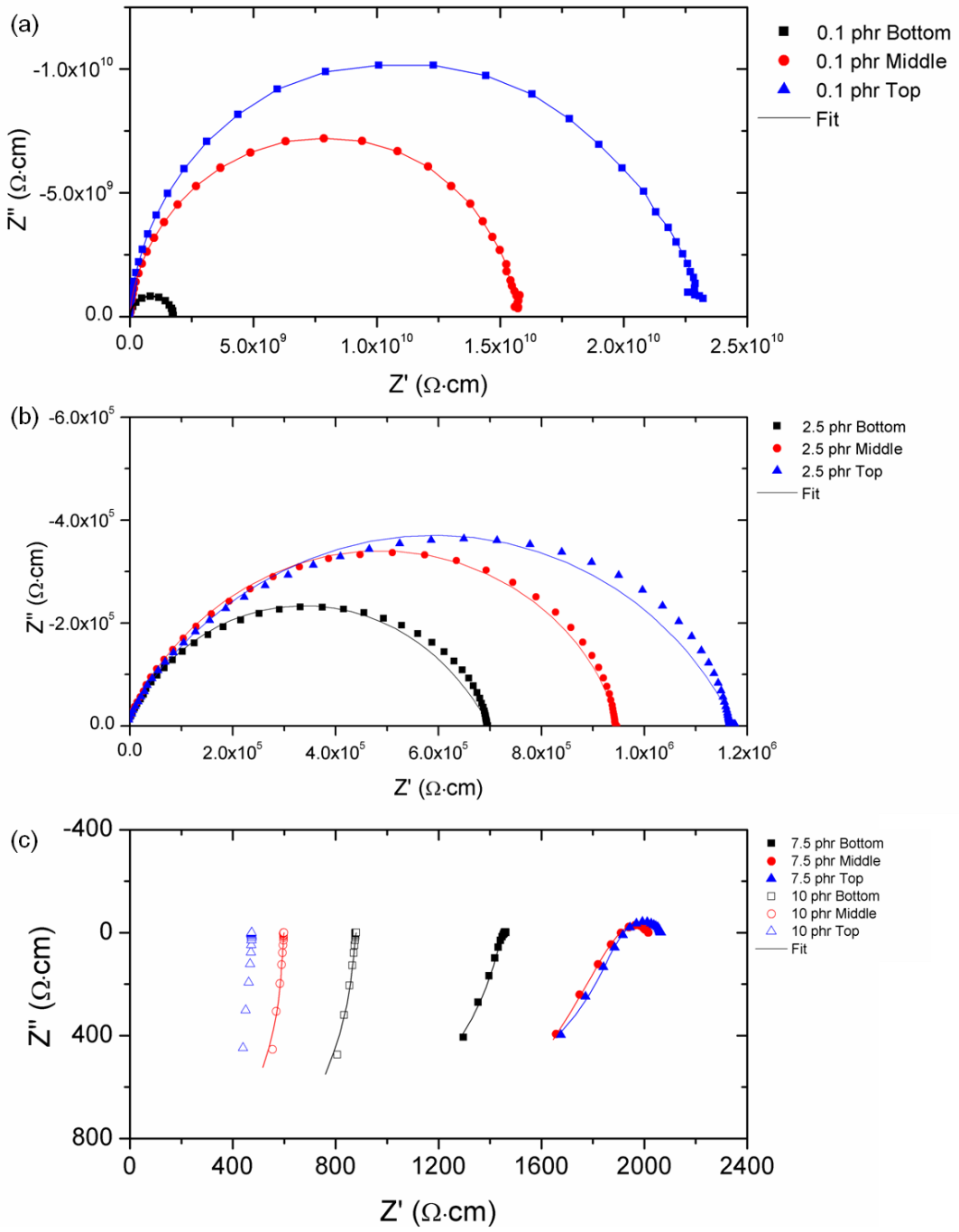

Figure 6.10. Complex impedance and fits for (a) 0.1, (b) 2.5, and (c) 7.5 and 10 phr for set #3 (ATO(nm)-GL0179L hot pressed at 675°C). The fits were applied using the equivalent circuit fits from Table 6.5.

Table 6.5. Equivalent Circuit Fits For Set#3 (ATO(nm)-GL0179L Hot Pressed at 675°C).

Composition (phr)	L1 (μH)	R_{ato} (Ω)	R_{grain1} (Ω)	CPE1 (*F*)	R_{grain2} (Ω)	CPE2 (*F*)	R_{glass} (Ω)	CPE_{Glass} (p*F*)
0.001	29.20	0.05	4.03×10^{9}	7.01×10^{-12}	2.19×10^{5}	2.67×10^{-8}	6.87×10^{12}	0.20
0.01	19.50	0.05	4.17×10^{9}	9.58×10^{-12}	2.17×10^{5}	1.47×10^{-7}	4.29×10^{12}	0.17
0.1	24.08	0.05	2.41×10^{9}	1.27×10^{-11}	4.90×10^{8}	-3.92×10^{-11}	5.23×10^{11}	4.29
1.0	0.37	0.05	1.52×10^{9}	2.00×10^{-11}	4.54×10^{7}	-1.76×10^{-10}	1.00×10^{12}	6.12
2.5	23.05	0.05	9.17×10^{4}	1.09×10^{-7}	7.63×10^{4}	-1.09×10^{-7}	4.18×10^{12}	1055.74
5	2.79	0.05	7.45×10^{2}	3.90×10^{-8}	6.69×10^{2}	-7.25×10^{-9}	1.00×10^{12}	5.34
7.5	0.37	0.05	1.89×10^{1}	2.35×10^{-6}	1.29×10^{2}	-2.38×10^{-10}	2.33×10^{13}	1294.52
10	0.57	0.05	2.45×10^{0}	3.41×10^{-6}	5.13×10^{1}	-3.47×10^{-9}	1.81×10^{2}	1.91

From the temperature and pressure study, it is expected that the ATO would sinter in these composites. Also expected in these composites is the glass behavior at the edges of the ATO network, which was prominent in set #2 and this set of composites. This border resistance was consistently high for all the compositions so for the equivalent circuit the influence this had was that the majority of the conducting processes would go through the two parallel RCs in series. The important influence this glass barrier would have is the capacitance associated with it, which was consistently in the range of that of the pure glass (~p*F*).

6.4. Frequency Dependent Behavior

The application of the equivalent circuit model to sets #1-3 and the variable temperature and pressure study yielded very promising results. Overall the general trend was that at low concentrations the ATO network starts as small clusters isolated by regions of glass. As the concentration increases and these clusters start to span throughout the composite, this glass behavior starts to go away and is replaced by the behavior of the ATO network. The network behavior is heavily influenced by the fraction of physically touching ATO, partially sintered ATO, or a combination of the two.

It appears that for these composites, many of the processes that are occurring are the same, so the primary difference is the extent to which they contribute to the overall impedance at

different stages of ATO concentrations. A way to help verify that these processes are similar is to examine the frequency behavior of some specific impedance functions. This will also help verify if many of the trends observed in the equivalent circuit fits were accurate.

While the impedance is useful in determining the electrical behavior, the other dielectric functions: permittivity, modulus, and admittance are also important in gathering information on the electrical behavior.[93, 131] When a peak appears in an imaginary part of one of these functions, this often represents a relaxation that is occurring, but which pairs occur together determine what type of relaxation is occurring, whether it is caused by a bound dipole or one caused by long-range conductivity.[93, 112] Figures 6.11 show Bode plots that have a comparison between the imaginary impedance (*Z*") and the imaginary modulus (*M*") for select compositions in set #1. Both have been normalized to unity based on the largest peak. These plots are useful since they emphasize the conductivity relaxation time, so the peak positions are highly dependent on the material conductivity. The peak height in *Z*" will be dominated by the most resistive element.[132] With the pre-percolation composition at 0.001 phr, all of the peaks occur at lower frequencies ($<10^1$ Hz) and the peak in *Z*" is close to matching with the peak in *M*" around 10^0 Hz. This means that there is one primary dominant process that is occurring in the composites, which at these concentrations is due to the highly insulating glass breaking up the ATO network. This supports what is modeled with the equivalent circuits in Table 6.2. For a composition close to the percolation threshold, which is 0.01 phr ATO for set #1, interesting behavior can be seen. With *Z*" at 0.01 phr ATO, the peak is very similar to the one that was observed with 0.001 phr ATO at 10^0 Hz. A matching peak in *M*" is also seen at this frequency, which means that the composite electrical properties are controlled by this process. However, with M" there is a secondary peak at a much higher frequency. This peak in M" occurs at about 10^4 Hz. This

secondary peak indicates that there is an additional process that is occurring within the composite but since there is no matching peak in *Z*", this means that this process is not contributing to the long range conductivity of the composite. Instead this process is occurring on a short range.

With compositions above the percolation threshold, such as 2.5 and 10.0 phr for set #1 in Figure 6.11, both the *Z*" and *M*" peaks have shifted to about 10^6 Hz or higher. With this frequency shift, the main conducting mechanism in the composite is much less resistive than before. For 2.5 phr ATO, there is a mismatch of the peaks in *Z*" and *M*" which is often an indication of the material or composite not being an ideal conductor.[110] For this composition this is occurring around the percolation threshold as the ATO networks are forming. The contact between the ATO particles in the network at this concentration will have a weak point contact with one another, which is likely the cause of this non-ideal behavior. As the concentration increases, these contacts must improve, since with 10.0 phr ATO in Figure 6.11 the *Z*" and *M*" peaks partially shift to outside the frequency range and they appear to be more in-sync. As the contacts improve, the composite overall behaves as a better conductor.

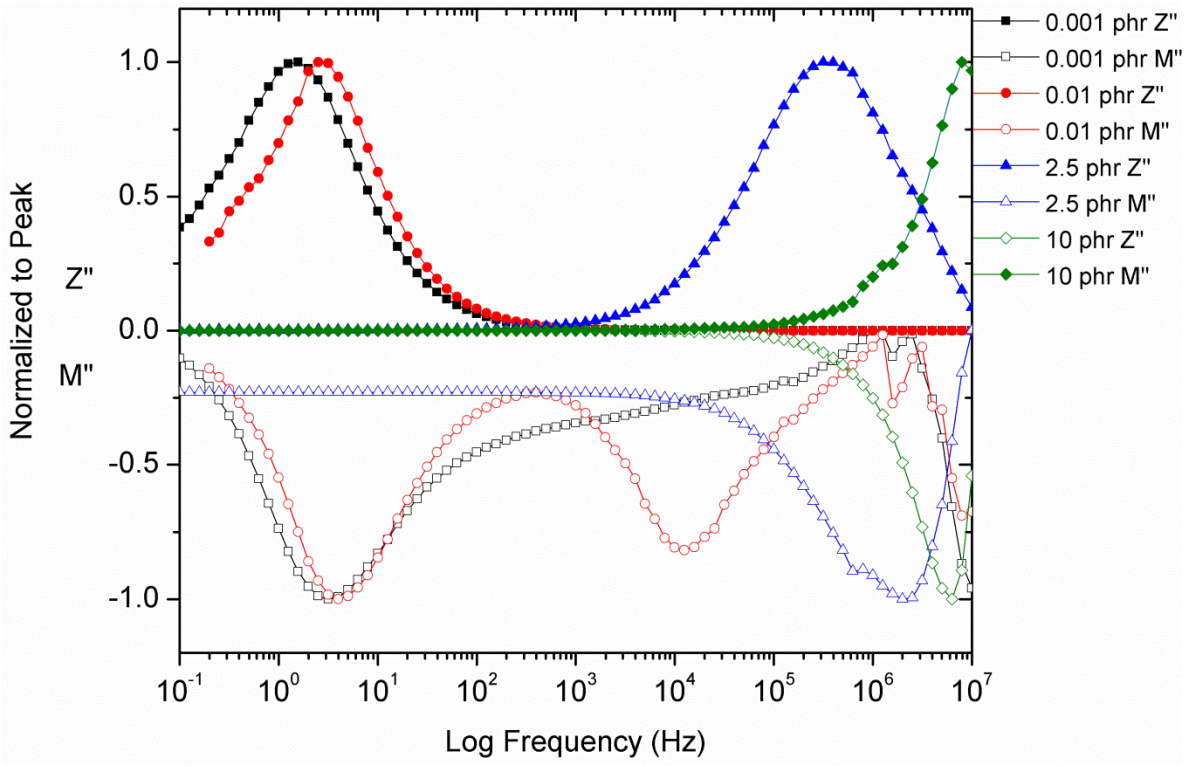

Figure 6.11. Normalized *M*" and *Z*" for select compositions for set #1 (ATO(nm)-GL0179S hot pressed at 550°C). *M*" and *Z*" peaks were normalized to +1 and -1 respectively. All samples presented here were in the middle position during hot pressing.

For set #2, similar behavior was observed across the various concentrations, which is shown in Figure 6.12. Figure 6.12(a) shows the normalized *Z*" and *M*" peaks for 0.001 phr, which is the lowest concentration composite. As expected for such a low concentration sample, the glass impedance is by far the most dominant in these composites since any ATO in the microstructure is primarily isolated. This is why for this composition the impedance behavior was modeled with just a parallel RC, just like the impedance of just the pure glass and not with the proposed circuit model that was used for the rest of the concentrations. Even so for these concentrations there are some indications of the presence of the isolated ATO clusters.

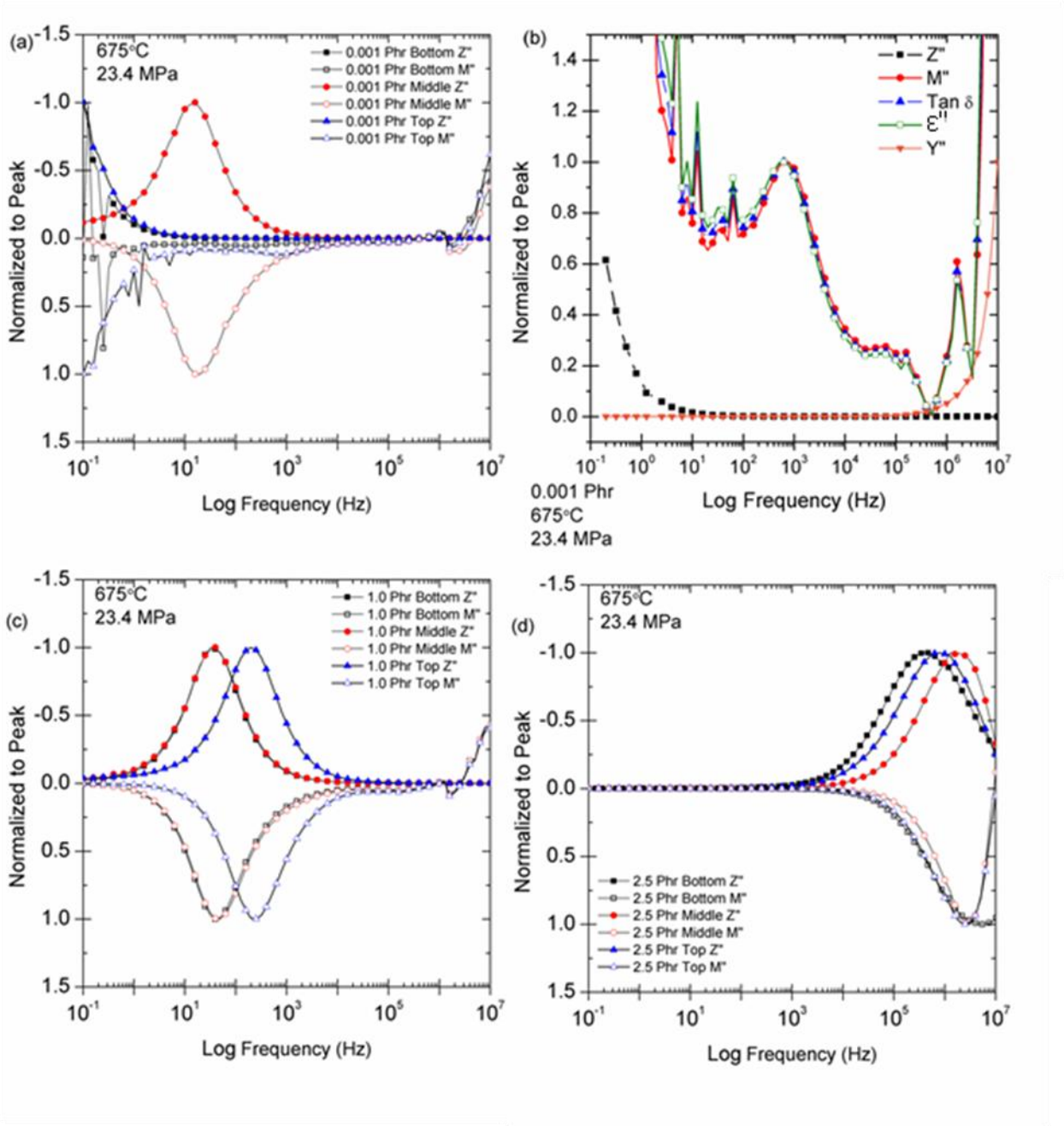

Figure 6.12. Normalized *M*" and *Z*" for select compositions for set #2 (ATO(nm)-GL0179S hot pressed at 550°C). The selected compositions were (a,b) 0.001 phr, (a) 1.0 phr, and (d) 2.5 phr. For part (b) 0.001 phr top was the sample and was normalized to the second smaller peak. (a and b) were modified from reference [113]. Additional normalized peaks in *tan δ*, *ε*", and *Y*" were included in (b). *M*" and *Z*" peaks were normalized to +1 and -1 respectively except for (b).

Figure 6.12(b) shows a secondary peak for 0.001 phr ATO (top) from part(a). This secondary peak occurs around 10^3 Hz. Much like with the frequency dependent behavior in set

#1, this secondary peak does not have a corresponding peak with *Z*", so the cause of this peak is due to short range conductivity. This is supported by the addition of normalized *tan δ*, *Y*", and ε". Like *Z*", a peak in *Y*" will be dominated by the long range conductivity mechanism.[93] For 6.12(b), there are no matching peaks between *M*" and *Y*". There is however, matching between tan δ and ε", which are indications of localized relaxations and short term conductivity.[93] For these composites this short term conductivity at these low concentrations are the small clusters of ATO networks.[113]

Much like set #1 the percolation behavior in set #2, shown in Figure 6.12(c) and (d) involves a transition of the *Z*" and *M*" peaks to higher frequencies. The same can be seen with set #3, shown in Figure 6.13. These figures show the normalized *M*" and *Z*" for compositions just before percolation (a) and after percolation (b). The frequencies and general peak behavior for these two compositions in Figure 6.13 are very similar to the ones in Figures 6.11 and 6.12. It seems that in these composites the onset of percolation is similar, and the main difference is how the processing conditions influence the impedance values once percolation has occurred.

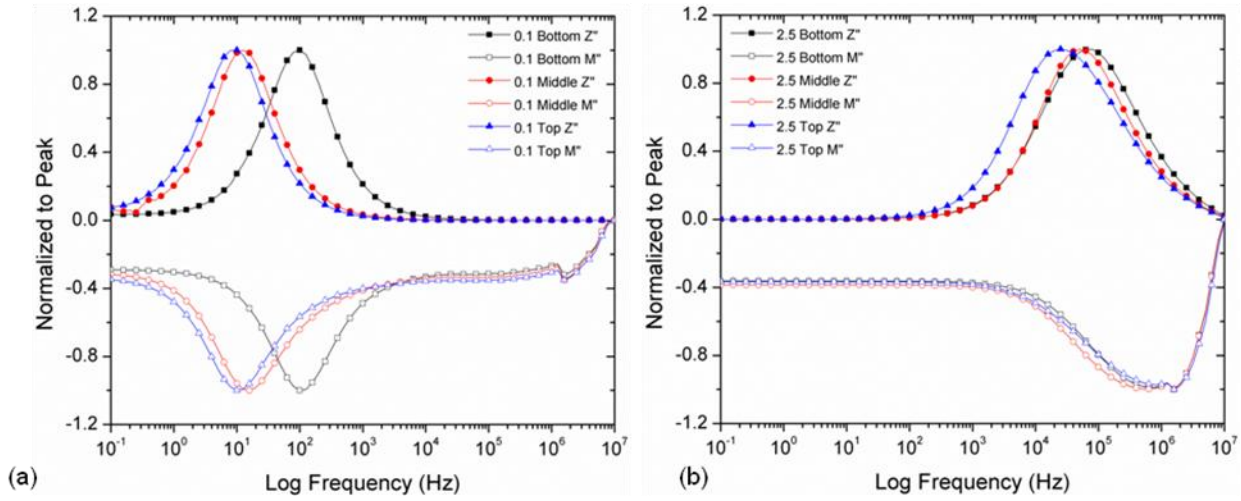

Figure 6.13. Normalized *M*" and *Z*" for (a) 0.1 phr and (b) 2.5 phr from set #3 (ATO(nm)-GL0179L hot pressed at 675°C). *M*" and *Z*" peaks were normalized to +1 and -1 respectively.

6.5. Equivalent Circuit Fitting for Set#4

Based on the microstructure of the ATO(μm)-GL0179S composites, a similar equivalent circuit model from Table 6.2 should be applicable to these composites. The main microstructural feature difference in these composites seems to be a lack of glass penetration along the ATO network. This is likely due to the larger sized ATO. The modified equivalent circuit with the removed circuit elements can be seen in Table 6.6 along with the fits for all the compositions in this study. The applied fits to Table 6.6 can be seen for select compositions in Figure 6.14. Since the percolation threshold was between 7.5 and 10.0 phr, the pre-percolation behavior was similar for all the sets with the exception of 10.0 phr. Figure 6.14(a) shows the behavior for 5.0 phr which exhibits a large semicircle in the first quadrant. The equivalent circuit fit had large resistances for R_{grain1} and R_{grain2} and the capacitances for these resistances, CPE1 and CPE2, were around 10^{-11}-10^{-12} *F* which was very similar to the capacitances for the hot pressed glass. For all the compositions before percolation, these values were obtained. Since the ATO in this study was larger, there will be less segregation initially due to the particle size ratio. This means that the ATO networks will be more susceptible to being broken up by regions of glass.

Table 6.6. Equivalent Circuit Fits For Set#4 (ATO(µm)-GL0179L Hot Pressed at 675°C).

Composition (phr)	L_{ATO} (µH)	R_{ato} (Ω)	R_{grain1} (Ω)	CPE1 (*F*)	R_{grain2} (Ω)	CPE2 (*F*)
0.001	53.70	0.05	1.48×10^{7}	7.04×10^{-12}	4.23×10^{8}	4.27×10^{-12}
0.01	44.20	0.05	1.02×10^{10}	5.54×10^{-12}	2.80×10^{8}	1.52×10^{-11}
0.1	33.53	0.05	7.43×10^{8}	1.51×10^{-11}	1.87×10^{10}	8.98×10^{-12}
1.0	46.20	0.05	1.10×10^{9}	9.04×10^{-12}	7.35×10^{9}	7.20×10^{-12}
2.5	18.13	0.05	5.31×10^{9}	1.78×10^{-11}	3.04×10^{8}	3.19×10^{-11}
5	23.13	0.05	9.18×10^{8}	3.80×10^{-11}	5.43×10^{9}	1.41×10^{-11}
7.5	22.48	0.05	2.30×10^{8}	9.14×10^{-11}	4.07×10^{7}	3.33×10^{-11}
10	10.21	0.05	1.64×10^{3}	3.23×10^{-9}	8.23×10^{2}	3.12×10^{-10}

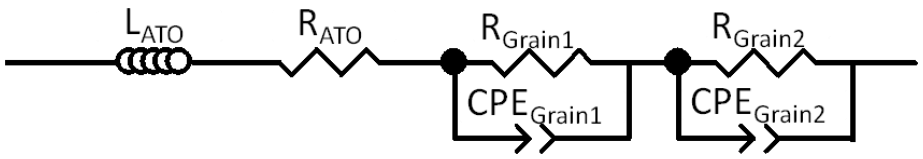

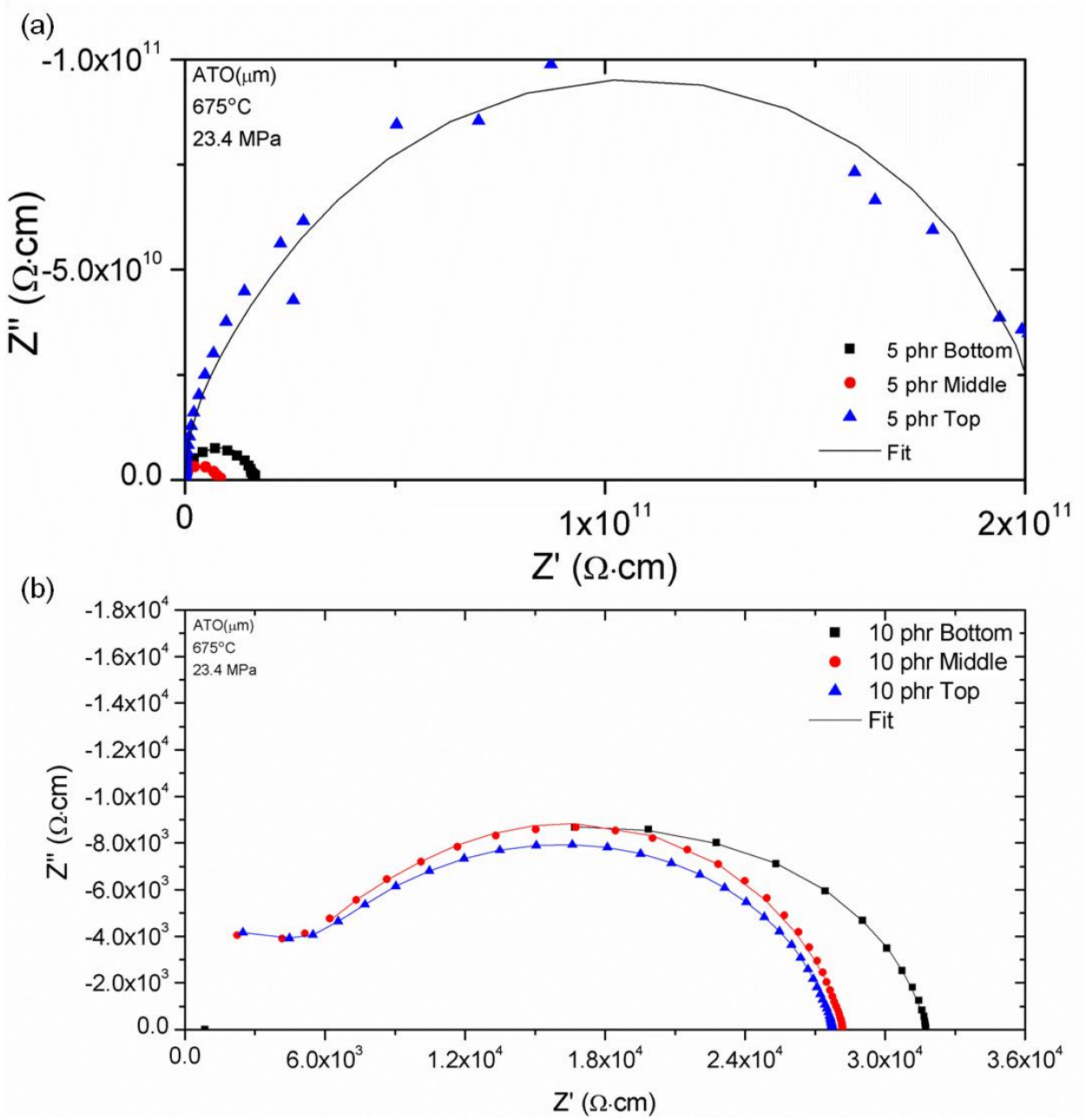

Figure 6.14. Complex impedance and equivalent circuit fits of (a) 5.0 phr and (b) 10.0 phr from set #4 (ATO(μm)-GL0179S hot pressed at 675°C). The fits were applied using the equivalent circuit fits from Table 6.6.

With the onset of percolation between 7.5 phr and 10 phr ATO, the impedance behavior changes by 8 orders of magnitude to what is shown in Figure 6.14(b). The fits shown here on this plot also show that the equivalent circuit was able to model this data. From Table 6.6 both R_{grain1} and R_{grain2} had capacitances in the nanofarad range which was similar to the capacitance

range for one of elements with the loosely compacted ATO particles. So much like set #1, the ATO network's electrical properties seems to be dictated by physically touching ATO particles and their point contacts. It is likely that the larger size of the ATO, which was around 1-5 μm in this set, was the reason why the ATO didn't partially sinter at the peak temperature of 675°C. What is significant for all these sets is that all the composites so far have exhibited some sort of physical contact, which means that along with a percolation threshold these composites are also forming a rigid network. Even though a rigid network is formed as these composites are consolidated, they all were consolidated to high relative densities, even at relatively low temperatures. This shows that this processing method is able to bypass many of the issues that have limited percolation in glass composites before. This processing method has also increased the range at which these composites can be fabricated. Instead of having to sinter at 10^6 Pa·s or lower, this method allows for processing the glass transition range to the softening temperature. For many glasses, this increases the potential processing range by 300-400°C. With the difference in ATO behavior for set #1 and #2, it was also shown that for many of the composites studied, that filler particles reacted at the higher processing temperature. So with this increased processing range, a larger control of the type of potential interfaces and resulting electrical properties opens up a wide variety of potential types of composite systems.

6.6. Impedance and Equivalent Circuit Analysis for SiC_w Alone and In Glass Composites

Since one of the main focuses of this study was to show the flexibility and potential of this processing method, it was necessary to use different types of filler material in this study. With the composites made with ATO, a large change in the electrical properties was observed and these properties were found to be dependent on several processing factors. This included the

temperature and pressure. It is important though to see how the electrical properties behave for a composite system with a different filler material. Not only do the electrical properties of SiC_w differ from ATO, but the shape and size are also very different from the ATO. From the previous chapter, it was shown that composites containing SiC_w did percolate around 10.0 phr and that there was some anisotropy depending on the electrical measurement direction.

6.6.1 Impedance Analysis of Compacted SiC_w

Similar to the composites containing ATO, it is important to obtain an estimate of the impedance of just the whiskers in order to help construct a better equivalent circuit for the composites. Since it isn't possible to get a monolithic sintered ceramic out of the whiskers by hot pressing, the dry press technique described in section 3.4.3 and 6.1 will be used.

The complex impedance of compacted SiC_w for various pressures is shown below in Figures 6.15 (a-c). A Bode plot or frequency dependent plot of the impedance magnitude is shown in Figure 6.15(d). The complex impedance shown in Figures 6.15(a-c) all have relatively the same type of behavior, which is a semicircle with a tail at the lower frequencies. As the pressure increases, these semicircles reduce in size but the shape generally remains the same. Equivalent circuit fits of the complex impedance are shown with the solid lines in Figures 6.15 (a) and (d). The fits themselves along with the equivalent circuit used are listed in Table 6.7. This circuit is an inductor in series with two parallel R-CPEs. The inductor itself decreases slightly with pressure but the biggest influences on the impedance are the two parallel R-CPEs. From the impedance magnitude in Figure 6.15(d), the change in the impedance by just changing the compaction pressure covered a range of over five orders of magnitude. While the whiskers themselves are not as conducting as the ATO, this change in the electrical properties by just

changing the applied pressure was quite substantial. It seems that the contacts and interfaces between the whiskers had a much greater influence on their impedance than it did with the ATO.

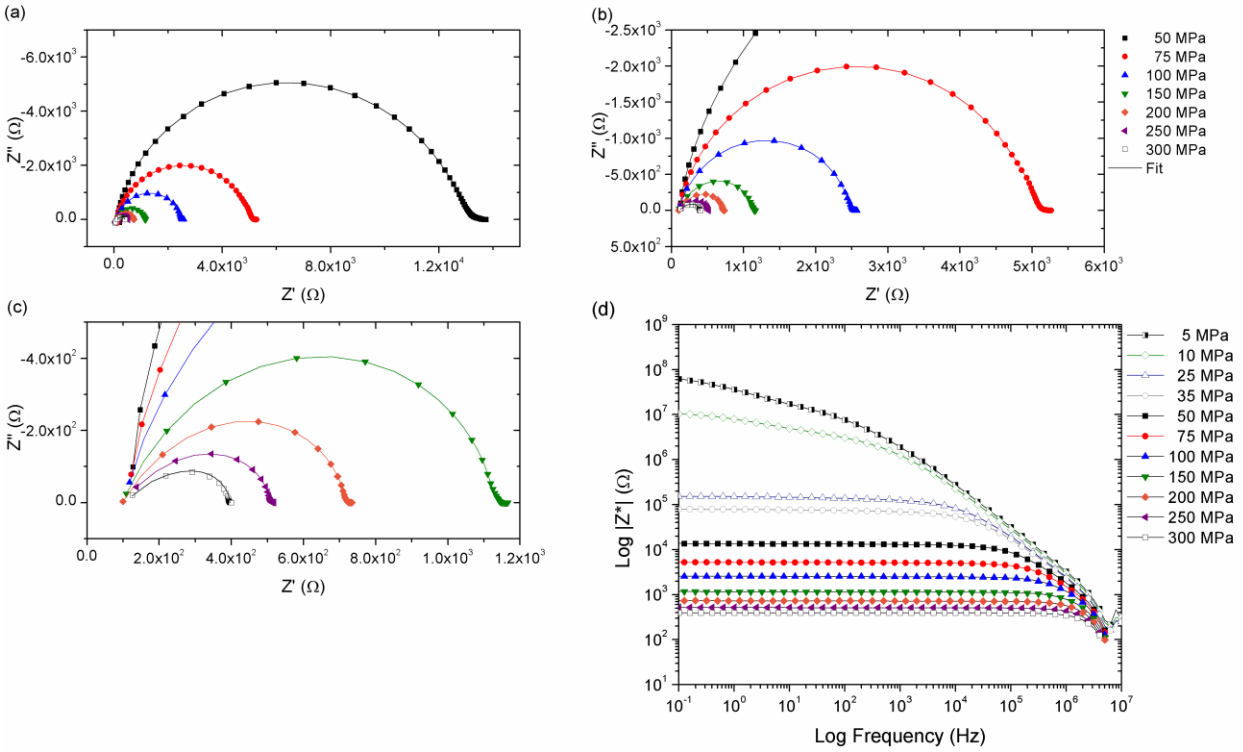

Figure 6.15. (a) Complex impedance for select pressures for dry-pressed SiC_w. (b and c) Zooms of the data presented in part (a). (d) Bode plot of the Log impedance magnitude for select pressures.

Table 6.7. Equivalent Circuit Fits for Compacted SiC_w at Various Pressures.

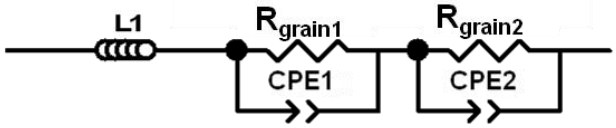

Pressure(MPa)	L1 (μH)	R_{grain1} (Ω)	CPE1 (*F*)	R_{grain2} (Ω)	CPE2 (*F*)
5	15.70	7.31×10^{6}	2.05×10^{-10}	8.18×10^{6}	4.52×10^{-8}
10	16.98	2.63×10^{6}	1.91×10^{-10}	7.20×10^{6}	1.51×10^{-8}
25	16.30	2.49×10^{5}	2.93×10^{-10}	6.84×10^{4}	7.49×10^{-8}
35	14.30	5.94×10^{4}	3.67×10^{-10}	1.80×10^{4}	1.40×10^{-7}
50	11.90	1.26×10^{4}	6.45×10^{-10}	1.03×10^{3}	1.11×10^{-5}
75	10.56	5.00×10^{3}	7.17×10^{-10}	2.18×10^{2}	8.75×10^{-5}
100	8.48	2.35×10^{3}	4.78×10^{-10}	2.15×10^{2}	7.06×10^{-5}
150	7.59	1.11×10^{3}	4.93×10^{-10}	5.03×10^{1}	2.10×10^{-5}
200	6.92	6.10×10^{2}	2.03×10^{-10}	2.09×10^{2}	2.24×10^{-7}
250	6.26	4.72×10^{2}	1.56×10^{-10}	4.27×10^{1}	1.32×10^{-5}
300	7.34	2.55×10^{2}	1.14×10^{-9}	1.41×10^{2}	1.14×10^{-9}

The complex impedance graphs for various concentrations of the whisker composites are shown in Figure 6.16. This figure includes the complex impedance measured in both the perpendicular and parallel to the hot pressing direction. Figure 6.16(a and b) shows the complex impedance for 0.001 and 0.01 phr for the perpendicular and parallel directions, respectively. This concentration of whiskers is the lowest for all these composites and should have the highest impedance. While the impedance is high, it isn't as high as expected for a composite that is

primarily glass. This could be due to some residual carbon during hot pressing as well as some carbon released by impurities in the whiskers. The equivalent circuit to fit the complex impedance in Figure 6.16 (a and b), which is shown with the solid lines, was based on the impedance and other immitance functions as well as the equivalent circuit fit from the dry pressed SiC_w. The equivalent circuit for Figure 6.16(a and b) is an inductor in series with three parallel RCs. This circuit can be seen in Table 6.8. The fit parameters for this equivalent circuit are also listed in Table 6.8.

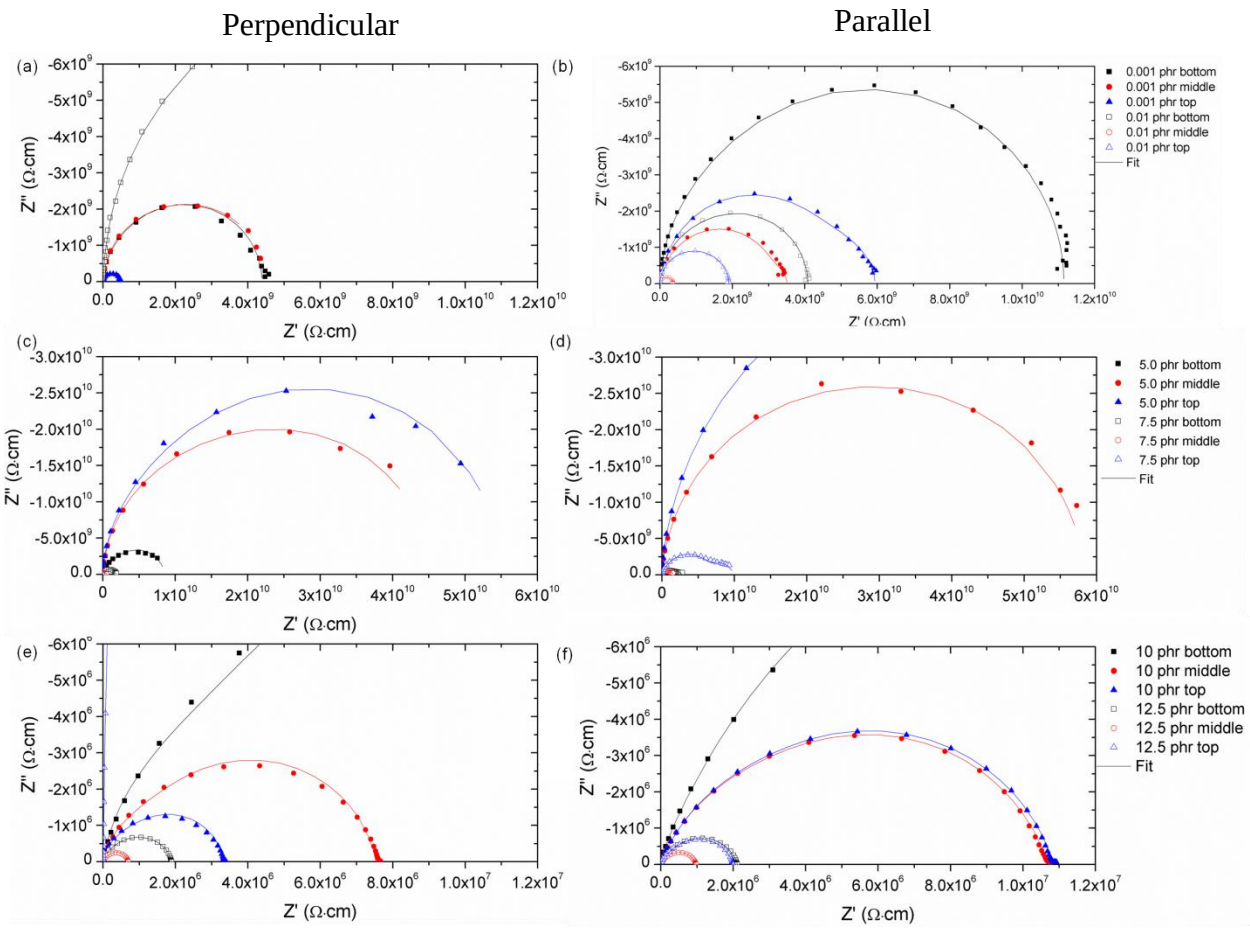

Figure 6.16. Complex impedance and equivalent circuit fits for set #5 (SiC_w-GL0179S hot pressed at 675°C). (a,b) 0.001 and 0.01 phr SiC_w along the perpendicular and parallel direction, respectively. (c,d) 5.0 and 7.5 phr SiC_w along the perpendicular and parallel direction, respectively. (e,f) 10.0 and 12.5 phr SiC_w along the perpendicular and parallel direction, respectively. The fits were applied using the equivalent circuit fits from Table 6.8.

Table 6.8. Equivalent Circuit Fits for Set#5 (SiC_w-GL0179S hot pressed at 675°C) for the Parallel and Perpendicular Direction.

Parallel

Pressure(MPa)	L1 (μH)	R_{grain1} (Ω)	CPE1 (*F*)	R_{grain2} (Ω)	CPE2 (*F*)	R_{grain3} (Ω)	CPE3 (*F*)
0.001	26.15	8.22×10^{8}	3.35×10^{-10}	2.18×10^{7}	5.51×10^{-11}	4.77×10^{8}	1.77×10^{-11}
0.01	25.19	9.90×10^{7}	2.16×10^{-11}	8.89×10^{6}	1.81×10^{-10}	2.80×10^{8}	1.50×10^{-11}
0.25	23.60	1.26×10^{9}	1.15×10^{-11}	3.56×10^{6}	1.16×10^{-10}	2.17×10^{8}	2.87×10^{-11}
2.5	22.83	1.14×10^{8}	2.36×10^{-10}	1.75×10^{8}	1.29×10^{-8}	7.63×10^{8}	1.92×10^{-11}
5.0	15.40	5.25×10^{9}	4.82×10^{-10}	6.32×10^{7}	1.53×10^{-10}	5.26×10^{9}	2.99×10^{-10}
7.5	19.50	6.85×10^{8}	7.43×10^{-11}	7.22×10^{7}	1.01×10^{-10}	4.43×10^{8}	2.29×10^{-9}
10.0	13.63	2.66×10^{5}	3.29×10^{-10}	6.21×10^{5}	4.88×10^{-10}	-	-
12.5	13.40	3.36×10^{4}	7.02×10^{-10}	2.97×10^{5}	6.85×10^{-10}	-	-

Perpendicular

Pressure(MPa)	L1 (μH)	R_{grain1} (Ω)	CPE1 (*F*)	R_{grain2} (Ω)	CPE2 (*F*)	R_{grain3} (Ω)	CPE3 (*F*)
0.001	18.35	8.21×10^{8}	1.62×10^{-11}	9.75×10^{8}	1.13×10^{-11}	6.90×10^{9}	1.77×10^{-11}
0.01	16.54	5.87×10^{9}	6.66×10^{-12}	4.02×10^{7}	2.26×10^{-11}	1.14×10^{10}	1.50×10^{-11}
0.25	13.06	8.40×10^{8}	6.54×10^{-11}	2.48×10^{6}	1.48×10^{-11}	1.23×10^{8}	2.87×10^{-11}
2.5	12.83	1.33×10^{10}	4.08×10^{-11}	7.50×10^{7}	3.14×10^{-11}	6.81×10^{9}	1.92×10^{-11}
5.0	12.10	5.18×10^{10}	1.06×10^{-11}	1.73×10^{8}	3.54×10^{-11}	1.06×10^{10}	2.99×10^{-10}
7.5	12.78	3.49×10^{8}	3.87×10^{-11}	7.24×10^{8}	1.77×10^{-11}	7.52×10^{6}	2.29×10^{-9}
10.0	11.27	2.71×10^{6}	2.59×10^{-11}	2.03×10^{7}	3.79×10^{-11}	-	-
12.5	11.82	2.58×10^{5}	1.03×10^{-11}	1.62×10^{5}	2.86×10^{-11}	-	-

For both the parallel and perpendicular directions, all the elements had a capacitance around 10^{-10} -10^{-11} *F* which was similar to the values obtained in the dry press whiskers. The parallel direction was more similar to the dry press impedance than the perpendicular direction. The dry pressed whiskers were measured parallel to the pressing direction so the whiskers likely do not have as much orientation as they would have in the perpendicular direction. The parallel

hot pressed direction also has a more random orientation of the whiskers, which is why it is more similar to the dry pressed whiskers than the perpendicular hot pressed measurement.[49, 50, 53, 111] The composites also have a combination of both whisker behavior and glass behavior so the dry pressed and composite impedance are not directly related. The glass behavior is represented mostly by the last parallel R-CPE, which consist of R_{grain3} and CPE3.

For the parallel measurement, this had the capacitance most similar to the glass capacitance and it had the largest resistance of the circuit. It is likely that overall the capacitance is influenced by the whiskers due to their polarization, which is likely causing similar behavior of elements but with a slight distribution. This also helps explain the complex behavior in the parallel direction compared to the perpendicular. In the parallel direction (b), the semicircles are not as symmetric as they are along the perpendicular measurement direction (a). Since the whiskers are not as aligned as they are in the perpendicular direction, the parallel measurements are expected to have more breaks in the network compared to that of the perpendicular. For higher concentrations, such as 5.0 and 7.5 phr, the last circuit element is the most influenced by concentration. The impedance for these concentrations is shown in Figure 6.16 for the perpendicular (c) and parallel (d) directions. These concentrations are before the onset of percolation for both the parallel and perpendicular direction. The general shape of the curve is similar to (a) and (b) but for the parallel direction, there are fewer composites that have as distorted complex impedance semicircles as it did in part (b). With the higher amounts of whiskers, the conducting network is beginning to develop and is resulting in fewer breaks in the network. These breaks still exist but the gaps are likely much smaller since the capacitance for R3 and CPE3 has increased so the whiskers are influencing this.

With the onset of percolation at 10.0 and 12.5 phr the third parallel RCPE, which was attributed to the glass breaks in the whisker network, goes away. This change in the circuit is shown in Table 6.8. With the complex impedance, shown in Figure 6.16 (e) and (f), both the perpendicular and parallel directions have a reduction in the real impedance but also the general shapes of the semicircles for both directions are similar. The perpendicular direction likely has a higher number of contacts in the whisker network, which results in a slightly lower resistance.[50] A reason why the impedance for both measurement directions is so similar to the dry pressed whisker impedance after percolation can be explained with the additional drop in density of these composites. This drop in density along with the corresponding resistivity can be seen in Figure 6.17(a). From this figure, the onset of percolation results in not only a drop in the resistivity, but also a drop in the relative density. [111] Examining the microstructure however, shows that the glass is deforming around the whiskers. An example of this is shown in Figure 6.17(b). Porosity is present in 6.17(b) within the large clusters of whiskers. It seems that many of these large clusters of whiskers have little glass penetrating inside of it. Instead it has open porosity similar to the whiskers that have been dry pressed. This is especially the case for the parallel direction. Since the whiskers are oriented more randomly, it would be harder for the glass to penetrate these clusters compared to the perpendicular direction. From the equivalent circuit fits, the perpendicular direction deviates more from the dry pressed whisker impedance. This is likely due to the greater interaction the glass has with the whiskers along this direction. This interaction is likely the cause of the behavior with the capacitance.

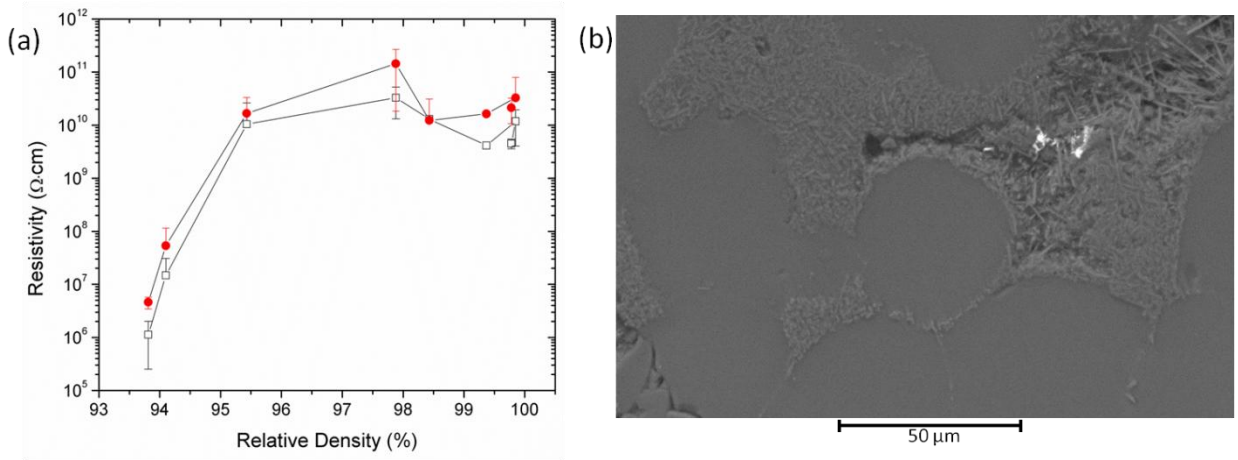

Figure 6.17. (a)Log Resistivity vs. relative density of SiC_w/borosilicate glass composites. Both the perpendicular and parallel measurement directions are shown. (b) SEM micrograph for 12.5 phr SiC_w along the parallel direction showing the porosity in the whisker clusters.[111]

While the composite has percolated around 10-12.5 phr SiC_w, the overall impedance is still quite high (10^6 Ω). Although this is comparable to hot pressed alumina-SiC_w composites at similar concentrations, the dry pressed whiskers impedance from Figure 6.15(c) suggests that the impedance of these composites can be improved.[48]

6.7. Summary of the Electrical Properties of Percolated Segregated Composites

For this study glass composites were made that percolated by forming segregated networks of the filler. The processing method involved focused on controlling the particle size ratio of the filler and matrix particles as well as the viscosity of the glass during hot pressing. The viscosity was controlled so it was low enough to allow the composites to be consolidated, but high enough that it prevented the filler from penetrating the glass particles and instead was segregated to the glass particle edges. At high enough concentrations, this segregated filler would percolate. The advantage of this method is that it bypassed many of the issues glass composites currently had with creating segregated percolated networks. These issues included composition dependences of the filler and matrix as well as the filler forming rigid networks that

resist consolidation during processing. The processing method is able to bypass these issues as well as opening up the processing range at which these composites can be fabricated by several hundred degrees. For this study, composites were made at a much lower temperature than usual. This lower temperature allowed for a range of behaviors to occur at the filler interfaces. Through impedance spectroscopy, the influence that processing conditions had on the filler interfaces and electrical properties was demonstrated. Through slight variations in these processing conditions, such as temperature and pressure, a wide range of electrical properties could result. Examples of which are shown in Figure 6.18. This figure shows a summary of the various composite sets made for the 5.0 phr (a) and 10.0 phr(b) of the ATO filler. Even though these composites all had the same concentration of filler, slight adjustments in the particle size ratio or temperature resulted in the electrical resistivity ranging about 9 orders of magnitude for 5.0 phr and about 2-3 orders of magnitude for 10.0 phr composites.

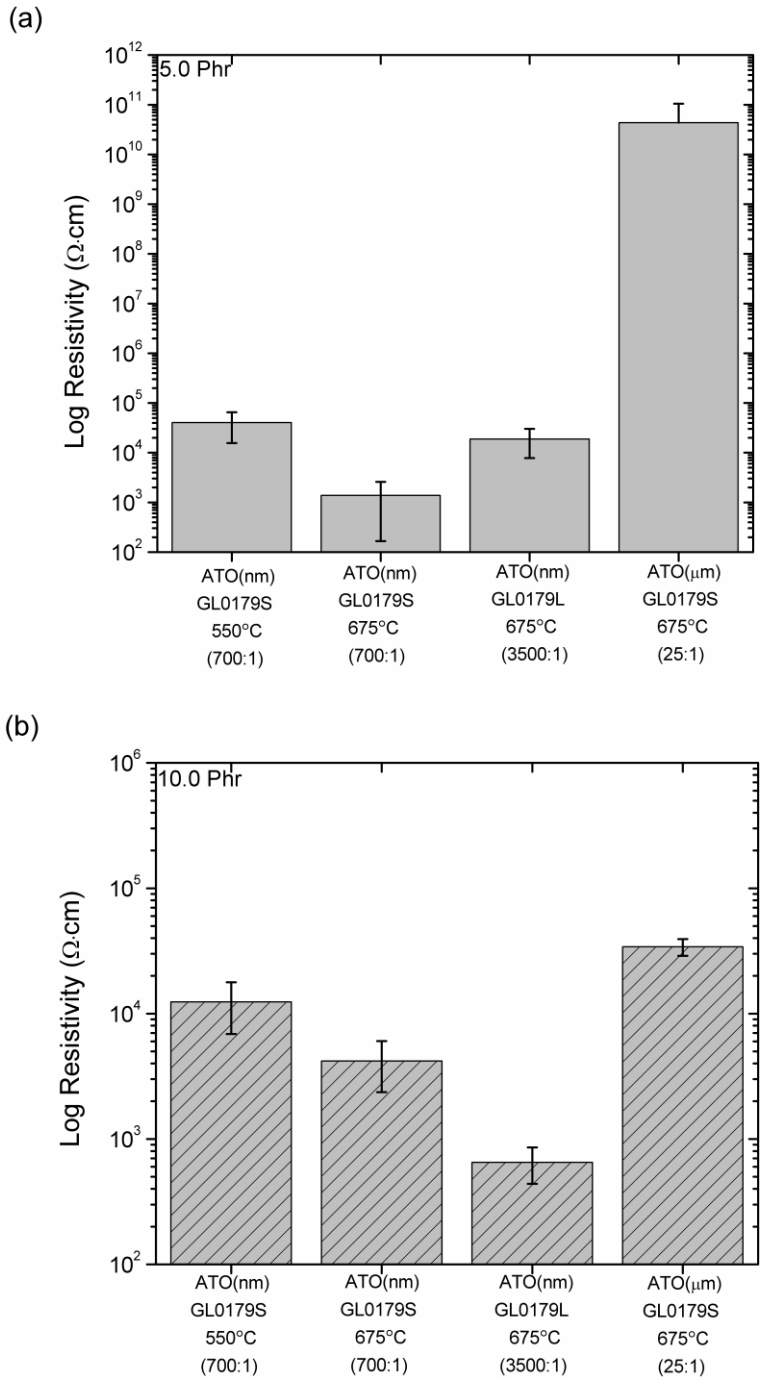

Figure 6.18. Summary of the resistivities achieved for all the primary composites sets at (a) 5.0 phr ATO and (b) 10.0 phr ATO showing the wide range of electrical properties that can be controlled by adjusting certain processing parameters.

CHAPTER 7

CONCLUSIONS AND FUTURE WORK

7.1. Conclusions

Borosilicate glass composites containing segregated and percolated networks of either ATO or SiC_w were fabricated through a hot pressing method. This hot pressing method incorporated several processing modifications originally used with polymer composites to create percolated segregated networks. The method involved fabrication around the glass transition temperature and softening point of the glass, which is substantially lower than the typical temperatures used to isothermally sinter glass (> 400°C). Because of these lower processing temperatures, the filler was segregated to the edges of the glass particles and resulted in percolated segregated networks. This processing method also allowed for a range of possible interfaces types to occur between the filler particles that controlled the resultant electrical response. This was observed primarily for the ATO composites which were studied as a function of glass/ATO size ratio, temperature, pressure, and composition. Changes were possible due to the much higher processing temperatures used with the ceramic glass composites when compared to polymer matrix composites.

In regards to percolated glass composites with segregated networks, this thesis is one of the few studies outside of the thick film resistor area that focused on electrically conducting glass composites. This thesis is also the first to apply the modified hot pressing method, to bulk ceramic glass composites in the effort to achieve percolated segregated networks of conducting fillers. The locations of these segregated networks were confirmed with a combination of AFM, I-AFM, optical, scanning electron microscopy, and EDS. The glass microspheres deformed into

faceted polyhedra with the filler primarily located at the edges, which led to the formation of the percolated networks. Depending on the size ratio between the glass and the filler and the temperature used during hot pressing, the percolation threshold could vary from 0.1 (set #1 and #2 ATO composites) to about 10 phr (SiC_w composites). For some of the composites (set #2), the drop in resistivity spanned over 12 orders of magnitude. The resistivity and the percolation threshold could be varied by adjusting the particle size ratio, temperature, and pressure. The temperature in particular could be used to control the resistivity of the percolation network. This was due to a couple of factors. With the higher temperatures, the glass was able to penetrate the network more, but even with this increased amount of glass penetration, the resistivity still decreased for composites with percolated networks of ATO.

Impedance spectroscopy was used as a technique to investigate these microstructural variations in the filler network. It was found that the glass composites that exhibited lower resistivities when processed at higher temperatures had noticeable behavior differences at the ATO interfaces. The ATO interfaces ranged primarily from a physical point contact to a partially sintered contact. The quality of contact between the filler particles had a strong influence on the overall electrical properties of the material. Overall, the partially sintered contact improved the electrical resistivity more than just the physical point contact. Through impedance spectroscopy measurements of the composites and of the individual precursor powder material, in various states, the differences in the quality of contact between filler particles and the resulting electrical properties were shown. An equivalent circuit model was created to describe how the percolated networks form and how the filler interfaces inside these networks control the electrical properties. By using this model, which consists of the arrangement and the properties of the

glass, the properties of the fillers, and the interfaces between them, the influence of the processing conditions on the electrical properties and the percolated networks was demonstrated.

7.2. Future Work

This research project demonstrated that segregated percolation can be achieved through a processing method that seemingly has little reliance on the material composition, but is more dependent on the physical arrangement of the fillers. In order to further vindicate this conclusion, additional glass and filler compositions should be studied. Along with these compositions, the entire temperature range from glass transition to close to the working point should be studied. This will show the full range of potential interfaces and electrical properties that can form as well as the viscosity range for these glass composites before the glass will break up the networks. This method would also help to show the specific hot pressing time, temperature, and pressure that can be used to optimize the composite properties.

The method described in this study involved using relatively low temperatures. While hot pressing was necessary to achieve this segregation, there were several other variables that limited the percolation threshold. Raising the temperature during hot pressing resulted in an improvement of the electrical conductivity, but also an increase in the amount of penetration of glass into the ATO network. A way to possibly improve the electrical conductivity is to form the networks at relatively low temperatures through hot pressing. Once the composite has been formed, the composite can be heat treated without pressure. This may reduce glass penetration into the network. Different atmospheres, specific for the filler, can also be used to help improve the filler-filler contacts. The rigid network percolation network of the filler that has formed is

also advantageous for this since it will resist the glass composite deforming during these heat treatments.

The current method to produce these composites with a segregated network involves hot pressing at certain temperatures and pressures in order to achieve this segregated network. With higher temperatures the electrical conductivity improved with an increase in temperature due to a change in contact (partial sintering). A method to possibly further improve these contacts while using these relatively low temperatures is to use spark plasma sintering(SPS). Like hot pressing, SPS utilizes a uniaxial force, but in addition it applies high amounts of electrical current. This method has been shown to sinter many materials at shorter times and at lower temperatures then regular hot pressing. For these composites, it could be a way to improve the contacts and charge transfer between filler particles.

With the formation of segregated networks, the electrical properties, primarily the electrical conductivity, were improved greatly. While the electrical properties improved, it would be interesting to see how the network could influence other materials science properties. Specifically, the mechanical properties. Since the networks are confined to the edges, the composite will primarily be held together by the glass. The addition of the networks should influence the mechanical properties. It has been shown that even with pure glass, the presence of boundaries has resulted in an increase of the fracture toughness.[133] With the addition of these ATO networks, an increase in the fracture toughness is therefore expected.[133]

Finally the composites made in this study were relatively thick, which contributed to percolation in three-dimensions within the composite. A reduction in the composite thickness should influence these interconnected networks and should be studied.

APPENDIX A

ADDITIONAL IMPEDANCE SPECTROSCOPY PLOTS

The other complex immitance spectra, particularly the modulus and admittance, for select composites along with the equivalent circuit fits are presented in this appendix. The immitance functions were calculated using the equations in section 2.7.2. The other functions in conjunction with the circuit fits show the accuracy of the fits and the correlation of the model to the microstructure of the composite. Both set #1 (550°C) and #2 (675°C) will be shown since these were the primary composites studied with the equivalent circuit model.

A.1. Complex Admittance and Modulus for Set #1(550°C)

The complex admittance plots of the composites and their equivalent circuit fits for select compositions during percolation, and after percolation are shown in Figures A.1-A.2, respectively. The complex modulus for select composites at various concentrations are shown in Figures A.3-5.

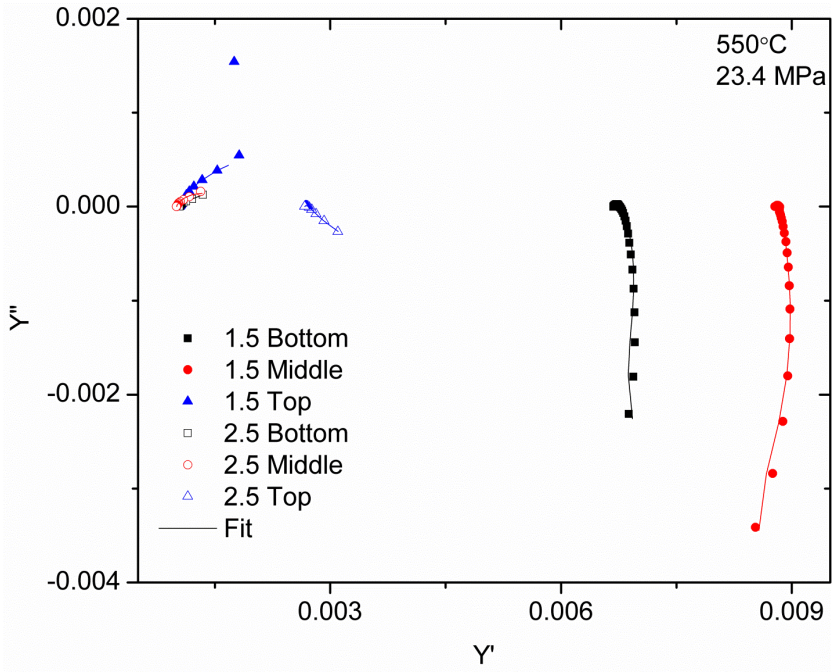

Figure A.1. Complex admittance plots and equivalent circuit fits for 1.5 and 2.5 phr ATO composites in set #1 (550°C).

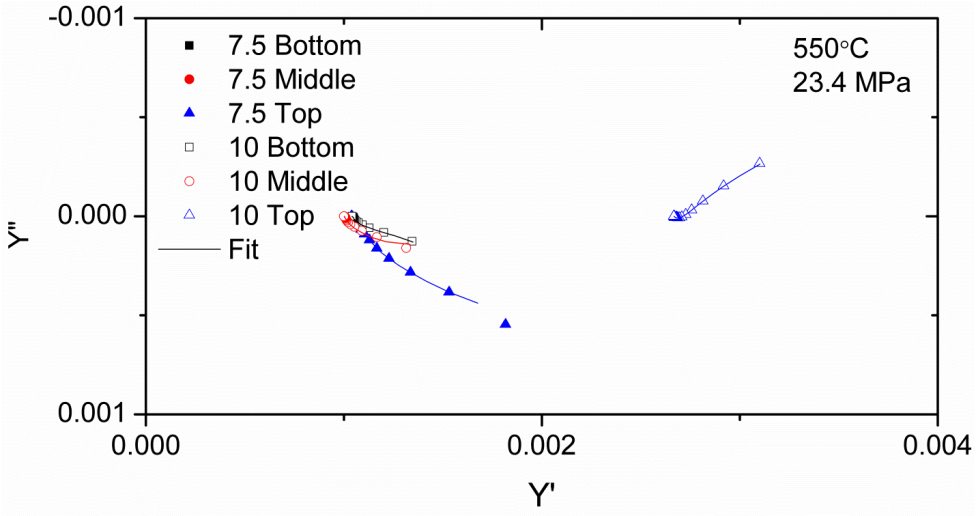

Figure A.2. Complex admittance plots and equivalent circuit fits for 7.5 and 10 phr ATO composites in set #1 (550°C).

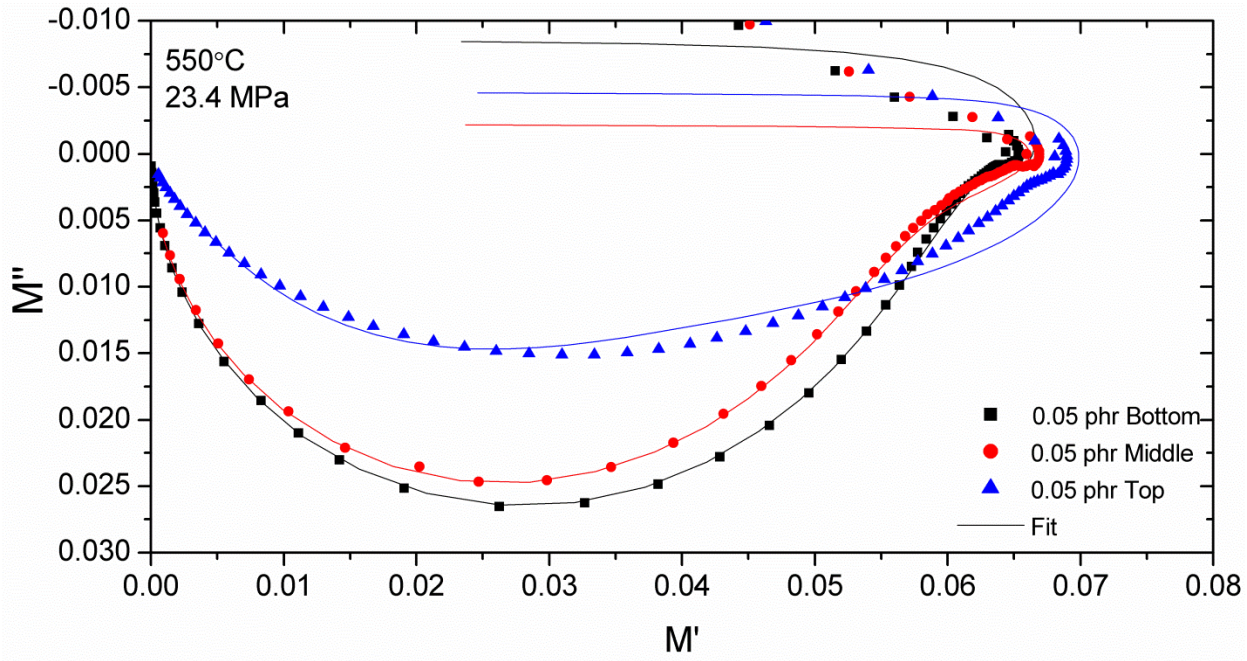

Figure A.3. Complex modulus plots and equivalent circuit fits for 0.05 phr ATO composites in set #1 (550°C).

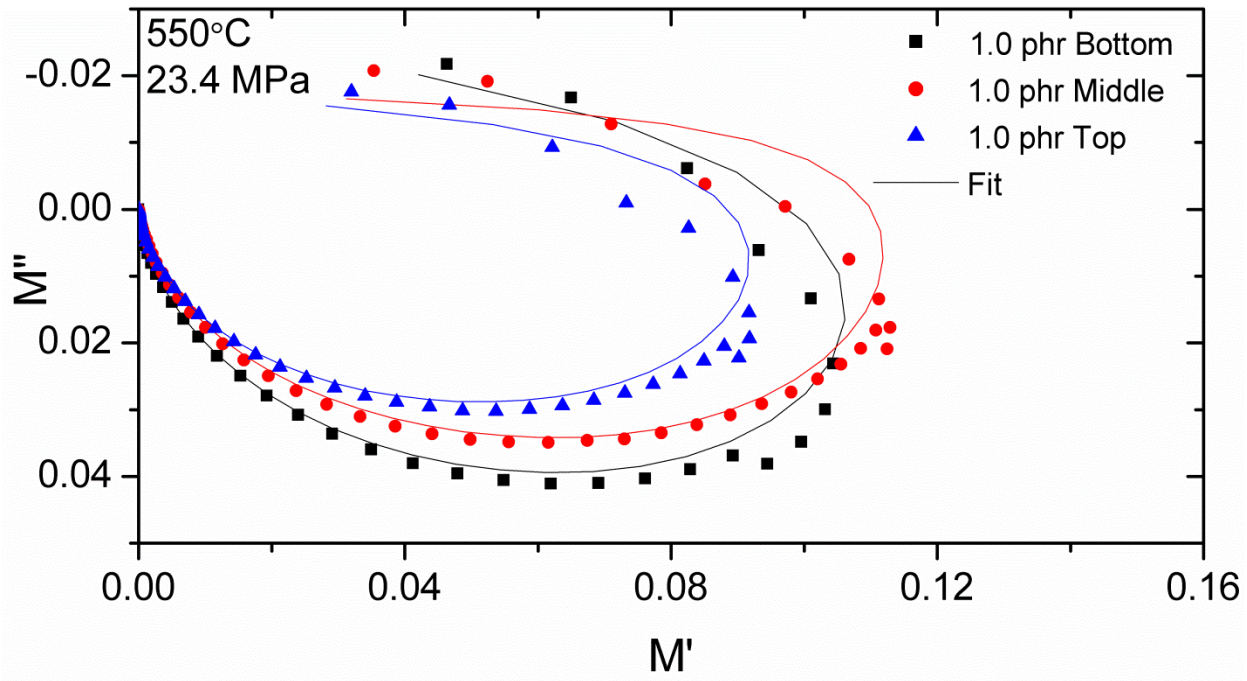

Figure A.4. Complex modulus plots and equivalent circuit fits for 1.0phr ATO composites in set #1 (550°C).

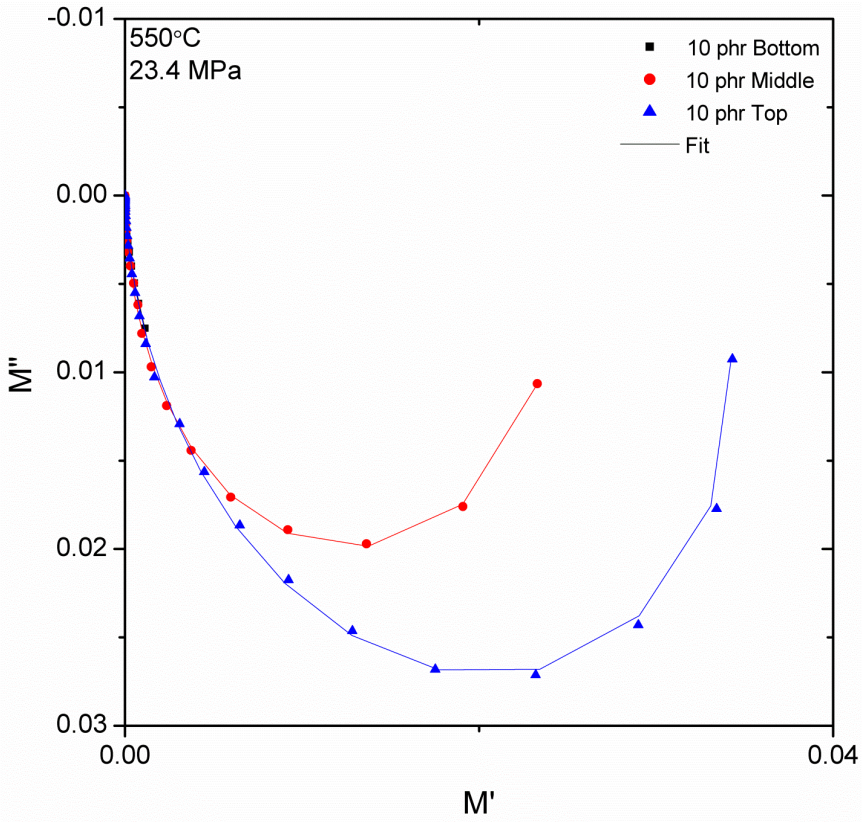

Figure A.5. Complex modulus plots and equivalent circuit fits for 10 phr ATO in set #1 (550°C).

A.2. Complex Admittance and Modulus for Set #2 (675°C)

The equivalent circuit fits for set #2 were also applied to the complex admittance, modulus, and permittivity. These fits also showed that the circuit modeling worked well with these functions. The complex admittance for various concentrations is shown in Figure A.6-8. The complex modulus is in Figure A.9-11 and the permittivity in A.12-14.

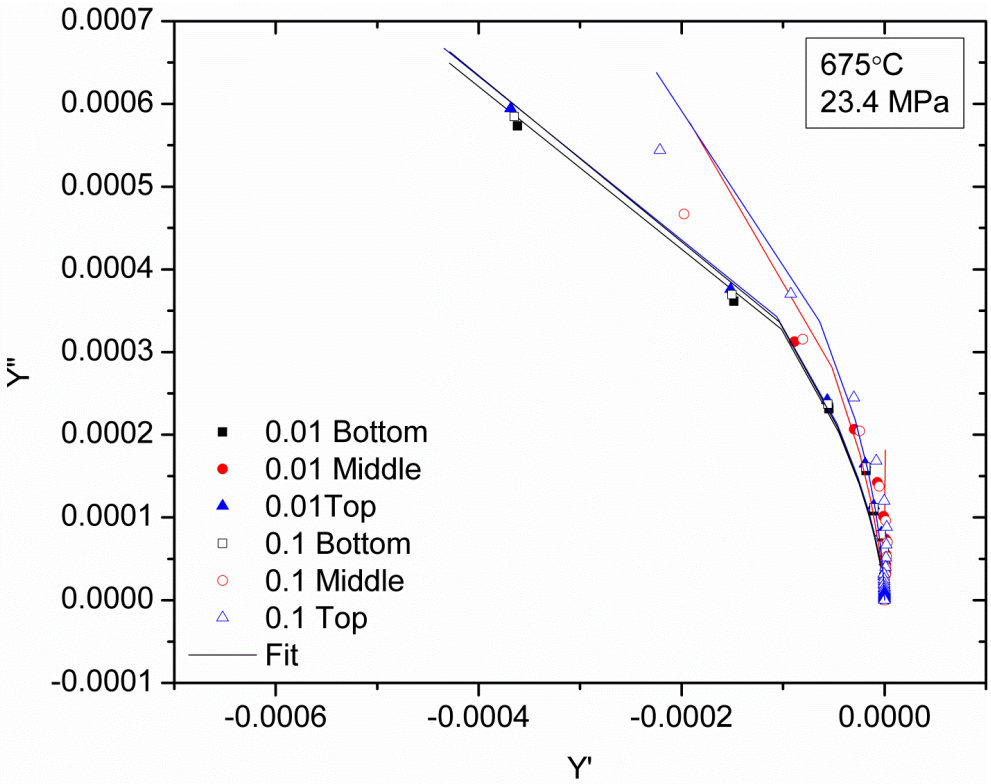

Figure A.6. Complex admittance plots and equivalent circuit fits for 0.01 and 0.1 phr ATO composites in set #2 (675°C).

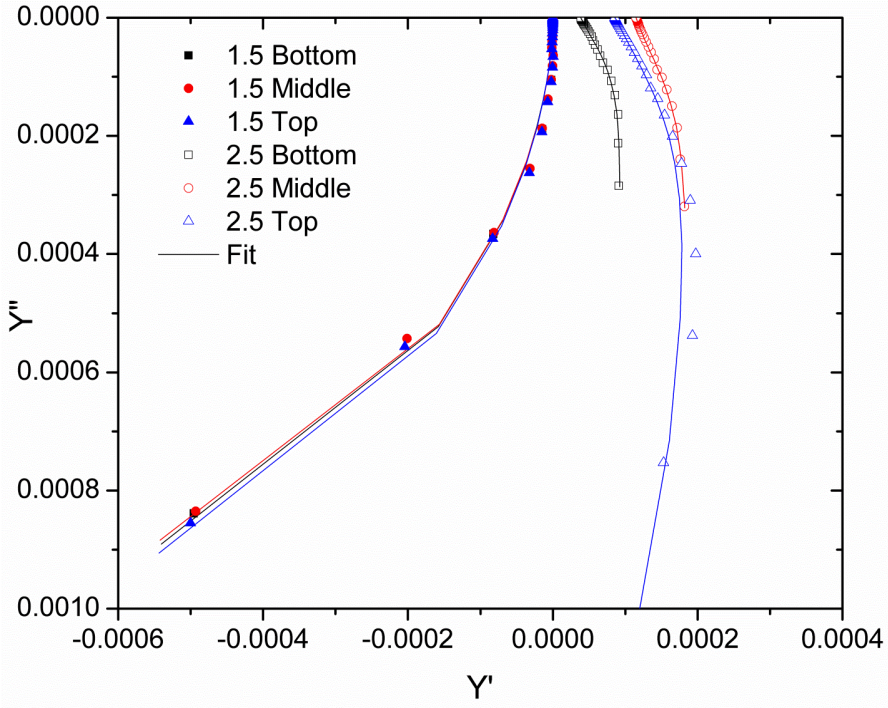

Figure A.7. Complex admittance plots and equivalent circuit fits for 1.5 and 2.5 phr ATO composites in set #2 (675°C).

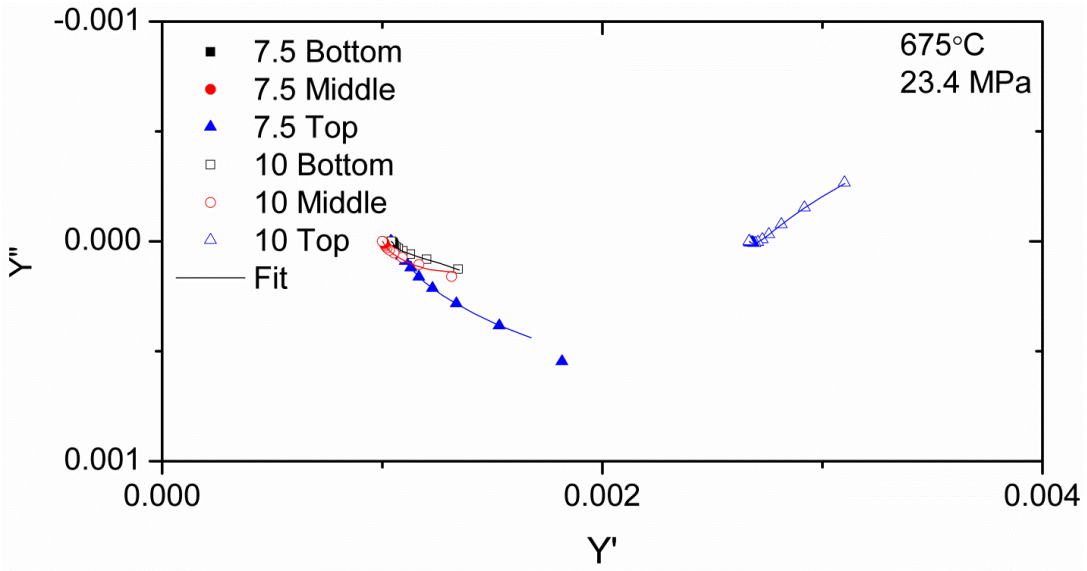

Figure A.8. Complex admittance plots and equivalent circuit fits for 7.5 and 10 phr ATO composites in set #2 (675°C).

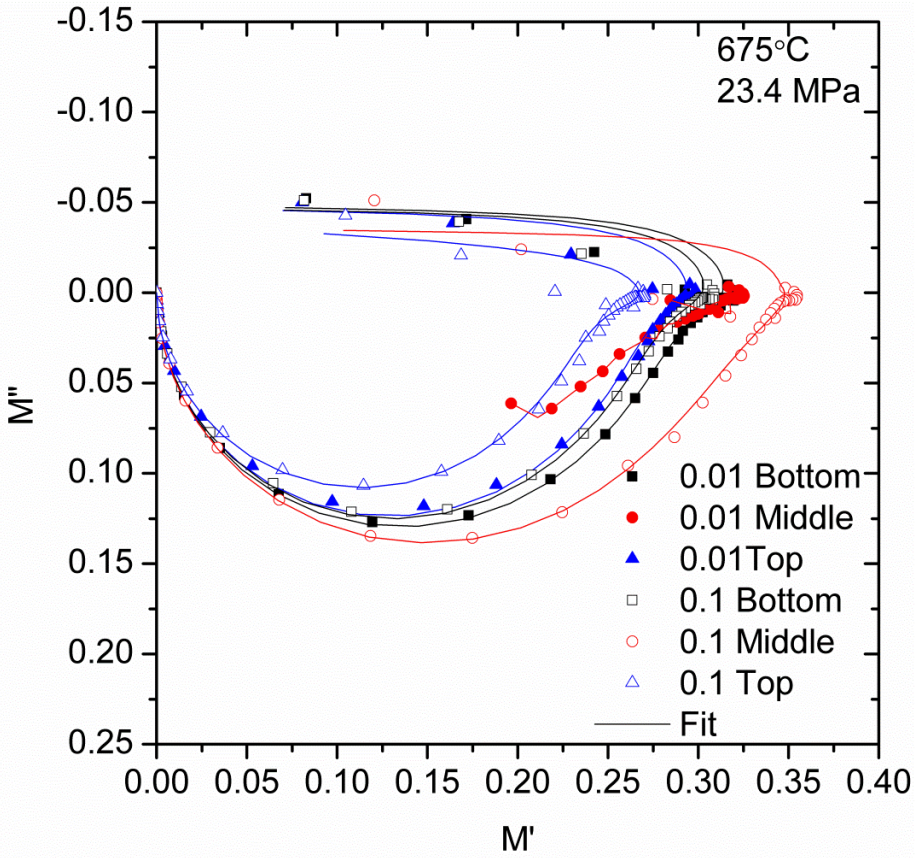

Figure A.9. Complex modulus plots and equivalent circuit fits for 0.01 and 0.1 phr ATO composites in set #2 (675°C).

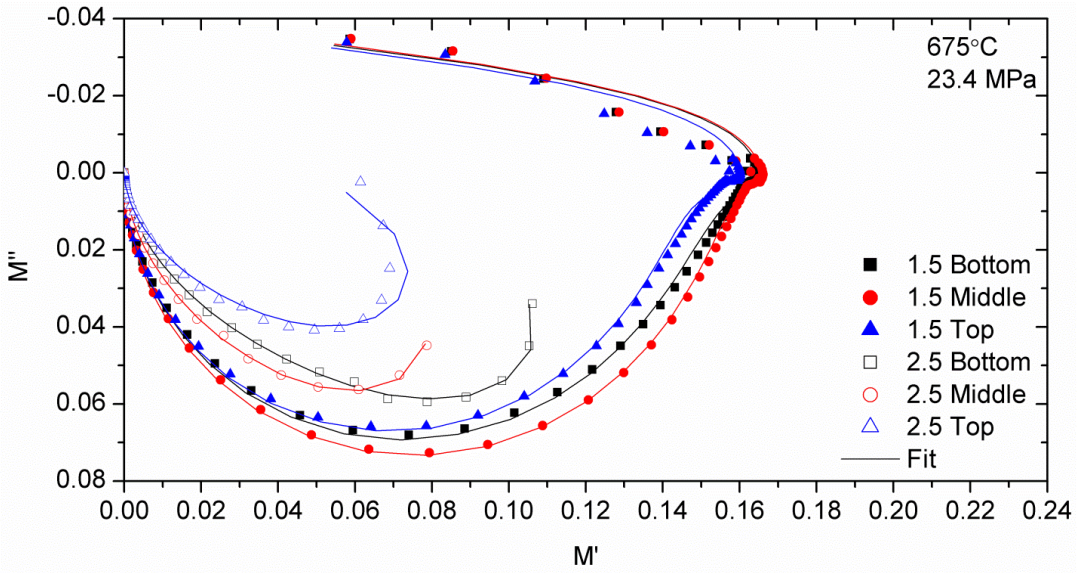

Figure A.10. Complex modulus plots and equivalent circuit fits for 1.5 and 2.5 phr ATO composites in set #2 (675°C).

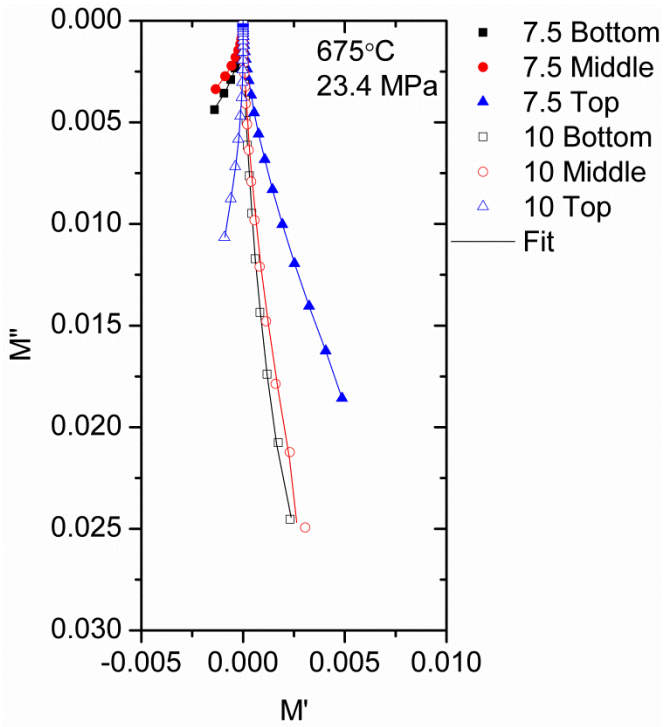

Figure A.11. Complex modulus plots and equivalent circuit fits for 7.5 and 10 phr ATO composites in set #2 (675°C).

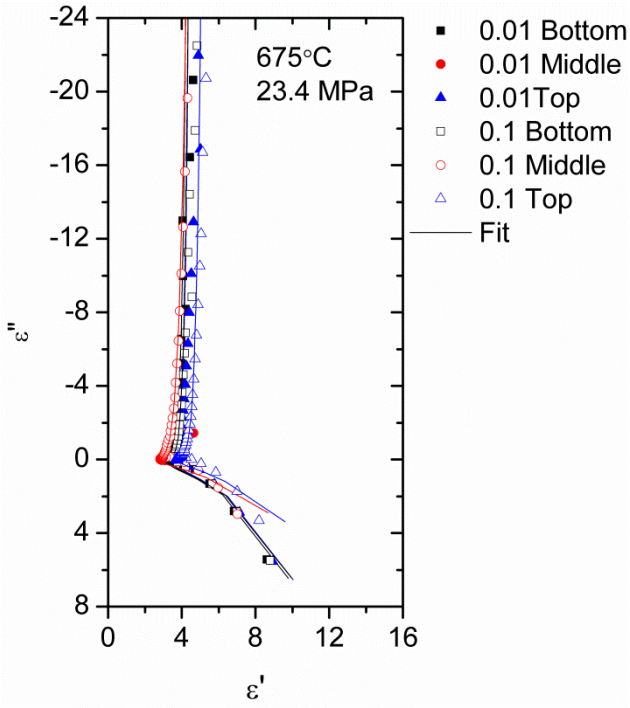

Figure A.12. Complex permittivity plots and equivalent circuit fits for 0.01 and 0.1 phr ATO composites in set #2 (675°C).

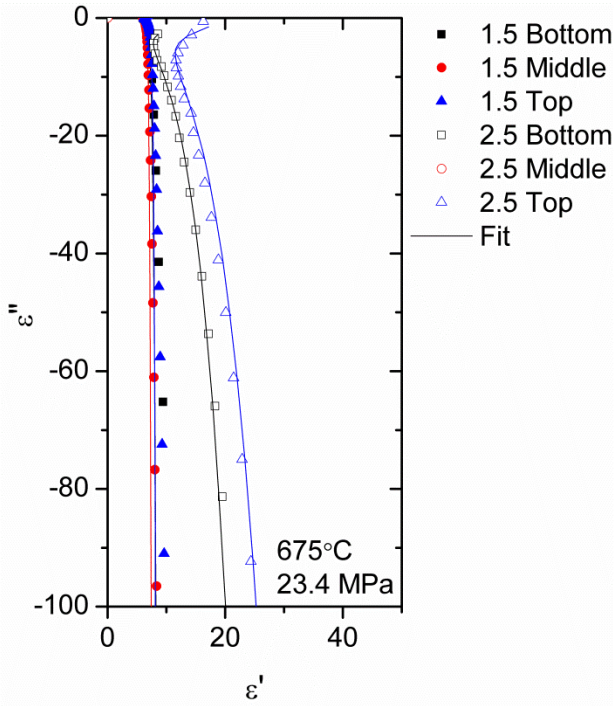

Figure A.13. Complex permittivity plots and equivalent circuit fits for 1.5 and 2.5 phr ATO composites in set #2 (675°C).

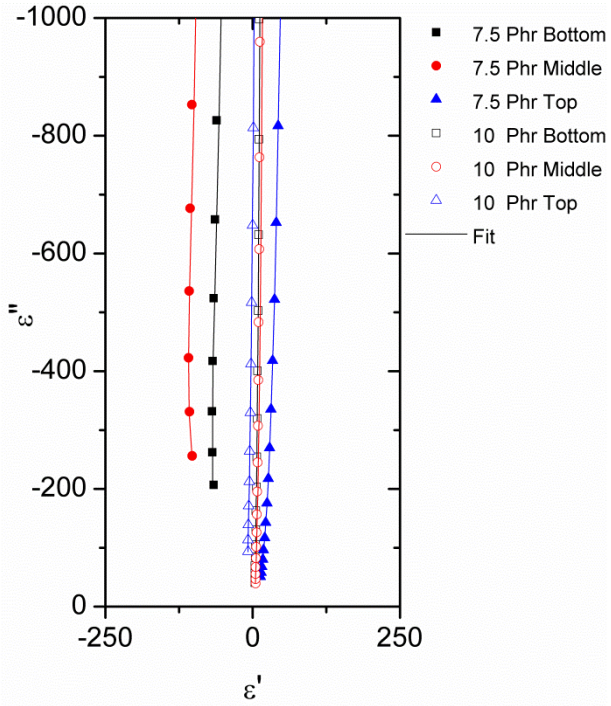

Figure A.14. Complex permittivity plots and equivalent circuit fits for 1.5 and 2.5 phr ATO composites in set #2 (675°C).

REFERENCES

1. C. W. Nan, Y. Shen, and J. Ma, "Physical Properties of Composites near Percolation," Pp. 131-51. In Annual Review Of Materials Research, Vol 40. Edited by D. R. Clarke, M. Ruhle, and F. Zok, 2010.

2. J. W. Essam, "Percolation Theory," *Reports on Progress in Physics*, 43[7] 833 (1980).

3. J. Runyan, R. A. Gerhardt, and R. Ruh, "Electrical Properties of Boron Nitride Matrix Composites: I, Analysis of McLachlan Equation and Modeling of the Conductivity of Boron Nitride–Boron Carbide and Boron Nitride–Silicon Carbide Composites," *Journal of the American Ceramic Society*, 84[7] 1490-96 (2001).

4. R. Ou, S. Gupta, C. A. Parker, and R. A. Gerhardt, "Fabrication and Electrical Conductivity of Poly(methyl methacrylate) (PMMA)/Carbon Black (CB) Composites: Comparison between an Ordered Carbon Black Nanowire-Like Segregated Structure and a Randomly Dispersed Carbon Black Nanostructure," *The Journal of Physical Chemistry B*, 110[45] 22365-73 (2006).

5. C. J. Capozzi and R. A. Gerhardt, "Novel Percolation Mechanism in PMMA Matrix Composites Containing Segregated ITO Nanowire Networks," *Advance Functional Materials*, 17[14] 2515-21 (2007).

6. J. Waddell, R. Ou, C. J. Capozzi, S. Gupta, C. A. Parker, R. A. Gerhardt, K. Seal, S. V. Kalinin, and A. P. Baddorf, "Detection of Percolating Paths in Polyhedral Segregated Network Composites Using Electrostatic Force Microscopy and Conductive Atomic Force Microscopy," *Applied Physics Letters*, 95[23] 233122, 3 pp. (2009).

7. R. K. Brow and M. L. Schmitt, "A Survey of Energy and Environmental Applications of Glass," *Journal of the European Ceramic Society*, 29[7] 1193-201 (2009).

8. R. R. Tummala, "Ceramic and Glass-Ceramic Packaging in the 1990s," *Journal of the American Ceramic Society*, 74[5] 895-908 (1991).

9. P.-F. Lu, Y. Shen, Z.-Y. Yu, L. Zhao, Q.-Y. Li, S.-J. Ma, L.-H. Han, and Y.-M. Liu, "Electronic Structure and Optical Properties of Antimony-Doped SnO_2 from First-Principle Study," *Communications in Theoretical Physics*, 57[1] 145 (2012).

10. H. Jain, "Transparent Ferroelectric Glass-Ceramics," *Ferroelectrics*, 306[1] 111-27 (2004).

11. Z. M. Jarzebski and J. P. Morton, "Physical Properties of SnO_2 Materials: III . Optical Properties," *Journal of the Electrochemical Society*, 123[10] 333C-46C (1976).

12. Z. M. Jarzebski and J. P. Marton, "Physical Properties of SnO_2 Materials: II . Electrical Properties," *Journal of the Electrochemical Society*, 123[9] 299C-310C (1976).

13. J. Zhang, L. Gao, and M. Chen, "Spark Plasma Sintering of High-Density Antimony-Doped Tin Oxide Ceramics from Nanoparticles," *Journal of the American Ceramic Society*, 89[12] 3874-76 (2006).

14. S. Geetha, K. K. Satheesh Kumar, C. R. K. Rao, M. Vijayan, and D. C. Trivedi, "EMI Shielding: Methods and Materials—A review," *Journal of Applied Polymer Science*, 112[4] 2073-86 (2009).

15. M. Sahimi, "Applications of Percolation Theory." CRC Press: Routledge, UK, (1994).

16. C.-W. Nan, "Physics of Inhomogeneous Inorganic Materials," *Progress in Materials Science*, 37[1] 1-116 (1993).

17. F. Lux, "Models Proposed to Explain the Electrical Conductivity of Mixtures Made of Conductive and Insulating Materials," *Journal of Materials Science*, 28[2] 285-301 (1993).

18. A. Bunde and W. Dieterich, "Percolation in Composites," *Journal of Electroceramics*, 5[2] 81-92 (2000).

19. Y. M. Chiang, D. Birnie, and W. D. Kingery, "Physical Ceramics." John Wiley & Sons: New York, (1997).

20. M. N. Rahaman, "Sintering of Ceramics." Taylor and Francis Group: Boca Raton, FL, (2008).

21. C. J. Capozzi and R. A. Gerhardt, "Correlation of the ac Electrical Conductivity and the Microstructure of PMMA/ITO Nanocomposites That Possess Phase-Segregated Microstructures," *The Journal of Physical Chemistry C*, 112[49] 19372-82 (2008).

22. C. J. Capozzi, Z. Li, R. J. Samuels, and R. A. Gerhardt, "Impedance Spectroscopy and Optical Characterization of Polymethyl Methacrylate/Indium Tin Oxide Nanocomposites with Three-Dimensional Voronoi Microstructures," *Journal of Applied Physics*, 104[11] 114902-02-10 (2008).

23. R. A. Gerhardt, J. Runyan, C. Sana, D. S. McLachlan, and R. Ruh, "Electrical Properties of Boron Nitride Matrix Composites: III, Observations Near The Percolation Threshold in BN-B_4C Composites," *Journal of the American Ceramic Society*, 84[10] 2335-42 (2001).

24. H. Da and N. N. Ekere, "Effect of Particle Size Ratio on the Conducting Percolation Threshold of Granular Conductive–Insulating Composites," *Journal of Physics D: Applied Physics*, 37[13] 1848 (2004).

25. R. P. Kusy and D. T. Turner, "Electrical Resistivity of a Polymeric Insulator Containing Segregated Metallic Particles," *Nature Physical Science*, 229 58-59 (1971).

26. A. K. Maity, D. Nath, and D. Chakravorty, "Electrical Conduction in Nanocomposites of Copper in Silicate Glasses," *Journal of Physics: Condensed Matter*, 8[31] 5717 (1996).

27. S. Vionnet-Menot, C. Grimaldi, T. Maeder, S. Strässler, and P. Ryser, "Tunneling-Percolation Origin of Nonuniversality: Theory and Experiments," *Physical Review B*, 71[6] 064201 (2005).

28. C. J. Capozzi, "Controlled Self-Assembly of ITO Nanoparticles into Aggregate Wire Structures in PMMA-ITO Nanocomposites"; PhD Thesis. Georgia Institute of Techonology, Atlanta, GA, 2009.

29. J. Gurland, "An Estimate of Contact and Continuity of Dispersions in Opaque Samples," *Transactions of the Metallurgical Society of AIME*, 236[5] 642-46 (1966).

30. S. Gupta, R. Ou, and R. Gerhardt, "Effect of the Fabrication Method on the Electrical Properties of Poly(Acrylonitrile-Co-Butadiene-Co-Styrene)/Carbon Black Composites," *Journal of Electronic Materials*, 35[2] 224-29 (2006).

31. P. Wei, H. Xiaowei, and C. Yan, "Preparation and Characterization of Poly (vinyl alcohol)/Antimony-Doped Tin Oxide Nanocomposites," *International Journal of Polymeric Materials and Polymeric Biomaterials*, 60[3] 223-32 (2010).

32. B. P. Grady, D. J. Arthur, and J. Ferguson, "Single-Walled Carbon Nanotube/Ultrahigh-Molecular-Weight Polyethylene Composites with Percolation at Low Nanotube Contents," *Polymer Engineering & Science*, 49[12] 2440-46 (2009).

33. F. C. Campbell, "Introduction to Composite Materials." in *Structural Composite Materials*. ASM International, Materials Park, OH, 2010.

34. C. Sana, "Modeling of Electrical Properties of Thick Film Resistors." Presentation, Georgia Institute of Technology, Atlanta, GA, 2005.

35. A. T. Ponomarenko, V. G. Shevchenko, and N. S. Enikolopyan, "Formation Processes and Properties of Conducting Polymer Composites," pp. 125-47. in *Filled Polymers I Science and Technology, Vol. 96. Advances in Polymer Science*. Edited by N. S. Enikolopyan. Springer Berlin-Heidelberg, 1990.

36. M. Zhang, W. Jia, and X. Chen, "Influences of Crystallization Histories on PTC/NTC Effects of PVDF/CB Composites," *Journal of Applied Polymer Science*, 62[5] 743-47 (1996).

37. H. Tang, J. Piao, X. Chen, Y. Luo, and S. Li, "The Positive Temperature Coefficient Phenomenon of Vinyl Polymer/CB Composites," *Journal of Applied Polymer Science*, 48[10] 1795-800 (1993).

38. F. Gubbels, R. Jerome, P. Teyssie, E. Vanlathem, R. Deltour, A. Calderone, V. Parente, and J. L. Bredas, "Selective Localization of Carbon Black in Immiscible Polymer Blends: A Useful Tool To Design Electrical Conductive Composites," *Macromolecules*, 27[7] 1972-74 (1994).

39. C. Calberg, S. Blacher, F. Gubbels, F. Brouers, R. Deltour, and R. Jérôme, "Electrical and Dielectric Properties of Carbon Black Filled Co-Continuous Two-Phase Polymer Blends," *Journal of Physics D: Applied Physics*, 32[13] 1517 (1999).

40. A. Malliaris and D. T. Turner, "Influence of Particle Size on the Electrical Resistivity of Compacted Mixtures of Polymeric and Metallic Powders," *Journal of Applied Physics*, 42[2] 614-18 (1971).

41. L. A. Prystaj, "Effect of Carbon Filled Characteristics on the Electrical Properties of Conductive Polymer Composites Possessing Segregated Network Microstructures"; Masters Thesis. Georgia Institute of Technology, Atlanta, GA, 2008.

42. R. P. Kusy and D. T. Turner, "Electrical Conductivity of a Polyurethane Elastomer Containing Segregated Particles of Nickel," *Journal of Applied Polymer Science*, 17[5] 1631-33 (1973).

43. R. Mukhopadhyay, S. K. De, and S. Basu, "Effect of Metal Concentration on the Electrical Conductivity and Some Mechanical Properties of Poly(Methyl Methacrylate)–Copper Composites," *Journal of Applied Polymer Science*, 20[9] 2575-80 (1976).

44. S. K. Bhattacharyya, S. Basu, and S. K. De, "Effect of Size, Shape and Oxide Content of Metal Particles on the Formation of Segregated Networks in PVC Composites," *Composites*, 9[3] 177-83 (1978).

45. V. R. Kolbunov, A. I. Ivon, and I. M. Chernenko, "Influence of a High Conductivity Additive on the Electrical Properties of Vanadium Dioxide-Based Ceramics," *Journal of the European Ceramic Society*, 23[9] 1435-39 (2003).

46. M. O. Lisunova, Y. P. Mamunya, N. I. Lebovka, and A. V. Melezhyk, "Percolation Behaviour of Ultrahigh Molecular Weight Polyethylene/Multi-Walled Carbon Nanotubes Composites," *European Polymer Journal*, 43[3] 949-58 (2007).

47. D. Bouvard and F. F. Lange, "Relation Between Percolation and Particle Coordination in Binary Powder Mixtures," *Acta Metallurgica et Materialia*, 39[12] 3083-90 (1991).

48. B. D. Bertram and R. A. Gerhardt, "Effects of Frequency, Percolation, and Axisymmetric Microstructure on the Electrical Response of Hot-Pressed Alumina–Silicon Carbide Whisker Composites," *Journal of the American Ceramic Society*, 94[4] 1125-32 (2011).

49. R. A. Gerhardt and R. Ruh, "Volume Fraction and Whisker Orientation Dependence of the Electrical Properties of SiC-Whisker-Reinforced Mullite Composites," *Journal of the American Ceramic Society*, 84[10] 2328-34 (2001).

50. B. D. Bertram, R. A. Gerhardt, and J. W. Schultz, "Impedance Response and Modeling of Composites Containing Aligned Semiconductor Whiskers: Effects of Dc-Bias Partitioning and Percolated-Cluster Length, Topology, and Filler Interfaces," *Journal of Applied Physics*, 111[12] 124913, 14pp (2012).

51. R. Ruh and H. M. Chizever, "Permittivity and Permeability of Mullite-SiC-Whisker and Spinel-SiC-Whisker Composites," *Journal of the American Ceramic Society*, 81[4] 1069-70 (1998).

52. D. P. H. Hasselman, K. Y. Donaldson, J. R. Thomas, and J. J. Brennan, "Thermal Conductivity of Vapor-Liquid-Solid and Vapor-Solid Silicon Carbide Whisker-Reinforced Lithium Aluminosilicate Glass-Ceramic Composites," *Journal of the American Ceramic Society*, 79[3] 742-48 (1996).

53. D.S. Mebane and R. Gerhardt, "Orientation Dependence of Resistivity In Anisotropic Ceramic Composites," *Ceramic Transaction s*[150] 265-72 (2004).

54. D. S. Mebane and R. A. Gerhardt, "Interpreting Impedance Response of Silicon Carbide Whisker/Alumina Composites Through Microstructural Simulation," *Journal of the American Ceramic Society*, 89[2] 538-43 (2006).

55. J. Bouchet, C. Carrot, J. Guillet, G. Boiteux, G. Seytre, and M. Pineri, "Conductive Composites of UHMWPE and Ceramics Based on the Segregated Network Concept," *Polymer Engineering & Science*, 40[1] 36-45 (2000).

56. A. Mierczynska, J. Friedrich, H. E. Maneck, G. Boiteux, and J. K. Jeszka, "Segregated Network Polymer/Carbon Nanotubes Composites," *Central European Journal of Chemistry*, 2[2] 363-70 (2004).

57. R. Vaish and K. B. R. Varma, "Crystallization Kinetics and Electrical Relaxation of BaO–$0.5Li_2O$–$4.5B_2O_3$ Glasses," *Journal of the American Ceramic Society*, 92[9] 1993-98 (2009).

58. M. S. Al-Assiri, M. M. El-Desoky, A. Al-Hajry, A. Al-Shahrani, A. M. Al-Mogeeth, and A. A. Bahgat, "Study of Nanostructural Behavior and Transport Properties of $BaTiO_3$ Doped

Vanadate Glasses And Glass–Ceramics Dispersed With Ferroelectric Nanocrystals," *Physica B: Condensed Matter*, 404[8–11] 1437-45 (2009).

59. K. Tapas Kumar, B. Sourish, and C. Dipankar, "Electrical Conduction in Glass Ceramics Containing Metal Nanodispersoids," *Japanese Journal of Applied Physics*, 42[3R] 1301 (2003).

60. M. Hrovat, J. Holc, and S. Glinšek, "Subsolidus Phase Equilibria in the RuO_2–ZnO–SiO_2 System," *Journal Of Materials Science*, 42[14] 5883-85 (2007).

61. R. Vest, "Materials Aspects of Thick-Film Technology," pp. 435-88 in Ceramic Materials for Electronics: Processing, Properties, and Applications. Edited by R. Buchanan. Marcel Dekker Inc., New York, 1991.

62. M. Totokawa, S. Yamashita, K. Morikawa, Y. Mitsuoka, T. Tani, and H. Makino, "Microanalyses on the RuO_2 Particle–Glass Matrix Interface in Thick-Film Resistors with Piezoresistive Effects," *International Journal of Applied Ceramic Technology*, 6[2] 195-204 (2009).

63. Y. T. T. Inokuma, and M. Haradome, "The Microstructure of RuO_2 Thick-Film Resistors and the Influence of Glass Particle-Size on Their Electrical-Properties," *IEEE Transactions on Components Hybrids and Manufacturing Technology*, 77[5] 166-75 (1984).

64. Y.-M. Chiang, L. A. Silverman, R. H. French, and R. M. Cannon, "Thin Glass Film between Ultrafine Conductor Particles in Thick-Film Resistors," *Journal of the American Ceramic Society*, 77[5] 1143-52 (1994).

65. T. Maeder, "Review of Bi_2O_3-Based Glasses for Electronics and Related applications," *International Materials Reviews*, 58[1] 3-40 (2013).

66. K. Adachi, S. lida, and K. Hayashi, "Ruthenium Clusters in Lead-Borosilicate Glass in Thick Film Resistors," *Journal of Materials Research*, 9[07] 1866-78 (1994).

67. R. Pflieger, M. Malki, Y. Guari, J. Larionova, and A. Grandjean, "Electrical Conductivity of RuO_2–Borosilicate Glasses: Effect of the Synthesis Route," *Journal of the American Ceramic Society*, 92[7] 1560-66 (2009).

68. A. K. Varshneya, "Fundamentals of Inorganic Glasses," 2 ed. John Wiley & Sons: New York, (2006).

69. K. D. Kim and G. Ondracek, "Sintering and Viscosity of Commercial Glass Powders," *Journal of Material Science Letters*, 14[6] 455-56 (1995).

70. . A. R. Boccaccini, W. Stumpfe, D. M. R. Taplin, and C. B. Ponton, "Densification and Crystallization of Glass Powder Compacts During Constant Heating Rate Sintering," *Materials Science and Engineering: A*, 219[1–2] 26-31 (1996).

71. A.R. Boccaccini, G. Ondracek, "Viscous Sintering of Non-Spherical Borosilicate-Glass Powder," *Glastechnische Berichte*, 65[3] 73-8 (1992).

72. J. E. Shelby, "Introduction to Glass Science and Technology," 2 ed. Royal Society of Chemistry: Cambridge, (2005).

73. T. J. Clark and J. S. Reed, "Kinetic Processes Involved in the Sintering and Crystallization of Glass Powders," *Journal of the American Ceramic Society*, 69[11] 837-46 (1986).

74. E. M. Rabinovich, "Preparation of Glass by Sintering," *Journal of Materials Science*, 20[12] 4259-97 (1985).

75. G. W. Scherer, "Viscous Sintering under a Uniaxial Load," *Journal of the American Ceramic Society*, 69[9] C-206-C-07 (1986).

76. R. M. German and S. J. Park, "Handbook of Mathematical Relations in Particulate Materials Processing." John Wiley & Sons: New York, (2008).

77. M. N. Rahaman and L. C. De Jonghe, "Effect of Rigid Inclusions on the Sintering of Glass Powder Compacts," *Journal of the American Ceramic Society*, 70[12] C-348-C-51 (1987).

78. A. R. Boccaccini, "On the Viscosity of Glass Composites Containing Rigid Inclusions," *Materials Letters*, 34[3–6] 285-89 (1998).

79. R. K. Bordia and R. Raj, "Analysis of Sintering of a Composite with a Glass or Ceramic Matrix," *Journal of the American Ceramic Society*, 69[3] C-55-C-57 (1986).

80. M. Eberstein, S. Reinsch, R. Müller, J. Deubener, and W. A. Schiller, "Sintering of Glass Matrix Composites with Small Rigid Inclusions," *Journal of the European Ceramic Society*, 29[12] 2469-79 (2009).

81. A. Tewari, V. S. R. Murthy, and G. S. Murty, "Rheological Behaviour of SiC (particulate)-Borosilicate Composites at Elevated Temperatures," *Journal of Materials Science Letters*, 15[3] 227-29 (1996).

82. L. C. De Jonghe, M. N. Rahaman, and C. H. Hsueh, "Transient Stresses in Bimodal Compacts During Sintering," *Acta Metallurgica*, 34[7] 1467-71 (1986).

83. M. A. Lima and R. C. Monteiro, "Shrinkage Behaviour of Borosilicate Glass-Al_2O_3 Composites During Isothermal Sintering," *Materials Science Forum*, 514-516 648-52 (2006).

84. H. K. Lee, S. Zerbetto, P. Colombo, and C. G. Pantano, "Glass–Ceramics and Composites Containing Aluminum Borate Whiskers," *Ceramics International*, 36[5] 1589-96 (2010).

85. A. Jagota and G. W. Scherer, "Viscosities and Sintering Rates of a Two-Dimensional Granular Composite," *Journal of the American Ceramic Society*, 76[12] 3123-35 (1993).

86. R. E. Dutton and M. N. Rahaman, "Creep Viscosity of Glass-Matrix Composites near the Percolation Threshold," *Journal of Materials Science Letters*, 12[18] 1453-56 (1993).

87. C.-H. Kuo and P. K. Gupta, "Rigidity and Conductivity Percolation Thresholds in Particulate Composites," *Acta Metallurgica et Materialia*, 43[1] 397-403 (1995).

88. E. A. Holm and M. J. Cima, "Two-Dimensional Whisker Percolation in Ceramic Matrix–Ceramic Whisker Composites," *Journal of the American Ceramic Society*, 72[2] 303-05 (1989).

89. F. F. Lange, "Constrained Network Model for Predicting Densification Behavior of Composite Powders," *Journal of Materials Research*, 2[01] 59-65 (1987).

90. D. Han and G. Choi, "Impedance Spectra for a 2-D Conductor-Insulator Composite by Computer Simulation," *Journal of Electroceramics*, 2[1] 57-66 (1998).

91. E. Barsoukov and J. R. Macdonald, "Impedance Spectroscopy: Theory, Experiment, and Applications," 2 ed. Wiley-Interscience: New York, (2005).

92. R. A. Gerhardt, "Impedance Spectroscopy and Mobility Spectra," pp. 350-63. in *Encyclopedia of Condensed Matter Physics*. Edited by G. Bassani, G. Liedl, and P. Wyder. Elsevier, Oxford, 2005.

93. R. Gerhardt, "Impedance and Dielectric Spectroscopy Revisited: Distinguishing Localized Relaxation from Long-Range Conductivity," *Journal of Physics and Chemistry of Solids*, 55[12] 1491-506 (1994).

94. R. Gerhardt, A. S. Nowick, M. E. Mochel, and I. Dumler, "Grain-Boundary Effect in Ceria Doped with Trivalent Cations: II, Microstructure and Microanalysis," *Journal of the American Ceramic Society*, 69[9] 647-51 (1986).

95. R. Gerhardt and A. S. Nowick, "Grain-Boundary Effect in Ceria Doped with Trivalent Cations: I, Electrical Measurements," *Journal of the American Ceramic Society*, 69[9] 641-46 (1986).

96. M. Kleitz, L. Dessemond, and M. C. Steil, "Model for Ion-Blocking at Internal Interfaces in Zirconias," *Solid State Ionics*, 75[0] 107-15 (1995).

97. J. Fleig, "Impedance Spectroscopy on Solids: The Limits of Serial Equivalent Circuit Models," *Journal of Electroceramics*, 13[1-3] 637-44 (2004).

98. T. G. Conti, A. J. Chiquito, R. O. da Silva, E. Longo, and E. R. Leite, "Electrical Properties of Highly Conducting SnO_2:Sb Nanocrystals Synthesized using a Nonaqueous Sol-Gel Method," *Journal of the American Ceramic Society*, 93[11] 3862-66 (2010).

99. Z. M. Jarzebski and J. P. Marton, "Physical Properties of SnO_2 Materials: I . Preparation and Defect Structure," *Journal of the Electrochemical Society*, 123[7] 199C-205C (1976).

100. T. Krishnakumar, R. Jayaprakash, N. Pinna, A. R. Phani, M. Passacantando, and S. Santucci, "Structural, Optical and Electrical Characterization of Antimony-Substituted Tin Oxide Nanoparticles," *Journal of Physics and Chemistry of Solids*, 70[6] 993-99 (2009).

101. H. S. Ahn and D. J. Choi, "Fabrication of Silicon Carbide Whiskers and Whisker-Containing Composite Coatings Without using a Metallic Catalyst," *Surface and Coatings Technology*, 154[2–3] 276-81 (2002).

102. J. V. Milewski, F. D. Gac, J. J. Petrovic, and S. R. Skaggs, "Growth of Beta-Silicon Carbide Whiskers by the VLS Process," *Journal of Materials Science*, 20[4] 1160-66 (1985).

103. L. Chen, C. Leonelli, T. Manfredini, and C. Siligardi, "Processing of a Silicon-Carbide-Whisker-Reinforced Glass-Ceramic Composite by Microwave Heating," *Journal of the American Ceramic Society*, 80[12] 3245-49 (1997).

104. T. E. Quantrille, ‘‘Ceramic Composites for Microwave Grilling and Speed Cooking’’; pp. 1–6 in *42nd Annual Microwave Symposium Proceedings*, International Microwave Power Institute, New Orleans, LA, 2008.

105. L. M. Porter and R. F. Davis, "A Critical Review of Ohmic and Rectifying Contacts for Silicon Carbide," *Materials Science and Engineering: B*, 34[2–3] 83-105 (1995).

106. "Antimony tin oxide, 99.5%." Accessed on: January 2011. Available at <http://www.alfa.com/en/catalog/44930>

107. "GL-0179 Data Sheet." Accessed on: February 2014. Available at < http://www.mo-sci.com/uploads/PDF_documents/Documents/GL_Data_Sheets/GL-0179_Borosilicate%20Glass%20Spheres.pdf>

108. "Silar(R) SC-9M Deagglomerated Silicon Carbide Whiskers." Accessed on: February 2014. Available at < http://acm-usa.com/site/user/files/1/Product_Datasheet__SC_9M.pdf>

109. A. Sharma, Sulzer Ltd., Westbury,NY, July 2012, Private Communication.

110. T. L. Pruyn and R. A. Gerhardt, "Percolation in Borosilicate Glass Matrix Composites Containing Antimony-Doped Tin Oxide Segregated Networks. Part I: Fabrication of Segregated Networks," *Journal of the American Ceramic Society*, 96[11] 3544-51 (2013).

111. T. L. Pruyn and R. A. Gerhardt, "Fabrication and Characterization of Conductive Glass Composites with Networks of Silicon Carbide Whiskers," *Ceramic Transactions*, accepted (2014).

112. T. L. Pruyn and R. A. Gerhardt, "Fabrication of Conductive Glass Nanocomposites with Networks of Antimony Tin Oxide," *MRS Online Proceedings Library*, 1552 65-70 (2013).

113. T. L. Pruyn and R. A. Gerhardt, "Percolation in Borosilicate Glass Matrix Composites Containing Antimony-doped Tin Oxide Segregated Networks Part II: Examination of Electrical Behavior Using Impedance Spectroscopy," *Journal of the American Ceramic Society*, DOI: 10.1111/jace.12902 (2014).

114. B. D. Bertram and R. A. Gerhardt, "Room Temperature Properties of Electrical Contacts to Alumina Composites Containing Silicon Carbide Whiskers," *Journal of Applied Physics*, 105[7] 074902, 10*pp* (2009).

115. M. J. Pascual, A. Durán, and L. Pascual, "Sintering Process of Glasses in the System Na_2O–B_2O_3–SiO_2," *Journal of Non-Crystalline Solids*, 306[1] 58-69 (2002).

116. Y.-J. Wang, Y. Pan, X.-W. Zhang, and K. Tan, "Impedance Spectra of Carbon Black Filled High-Density Polyethylene Composites," *Journal of Applied Polymer Science*, 98[3] 1344-50 (2005).

117. B. Bertram, "Effects of Interfaces and Preferred Orientation on the Electrical Response of Composites of Alumina and Silicon Carbide Whiskers." PhD Thesis. Georgia Institute of Technology, Atlanta, GA, 2011.

118. B. D. Bertram, R. A. Gerhardt, and J. W. Schultz, "Extruded and Pressureless-Sintered Al2O3–SiC_w Composite Rods: Fabrication, Structure, Electrical Behavior, and Elastic Modulus," *Journal of the American Ceramic Society*, 94[12] 4391-98 (2011).

119. R. P. Kusy, "Influence of Particle Size Ratio on the Continuity of Aggregates," *Journal of Applied Physics*, 48 5301-05 (1977).

120. D. Chakravorty, S. Basu, P. K. Mukherjee, S. K. Saha, B. N. Pal, A. Dan, and S. Bhattacharya, "Novel Properties of Glass–Metal Nanocomposites," *Journal of Non-Crystalline Solids*, 352[6–7] 601-09 (2006).

121. B. Nigro, C. Grimaldi, and P. Ryser, "Tunneling and Percolation Transport Regimes in Segregated Composites," *Physical Review E*, 85[1] 011137 (2012).

122. M. G. Busana, M. Prudenziati, and J. Hormadaly, "Microstructure Development and Electrical Properties of RuO_2-Based Lead-Free Thick Film Resistors," *Journal of Materials Science: Materials in Electronics*, 17[11] 951-62 (2006).

123. O. Millo, D. Azulay, D. Toker, And I. Balberg, "Percolation and Tunneling in Composite Materials," *International Journal of Modern Physics B*, 18[15] 2091-121 (2004).

124. M. T. Connor, S. Roy, T. A. Ezquerra, and F. J. Baltá Calleja, "Broadband Ac Conductivity of Conductor-Polymer Composites," *Physical Review B*, 57[4] 2286-94 (1998).

125. S. M. Joshi, "Effect of Heat and Plasma Treatments on the Electrical and Optical Properties of Colloidal Indium Tin Oxide Films." PhD Thesis. Georgia Institute of Technology, Atlanta, GA, 2013.

126. T. Pruyn and R. A. Gerhardt, "Characterization of Ceramic Powders During Compaction Using Electrical Measurements," pp. 199-209. in *Advances in Bioceramics and Porous Ceramics IV*. John Wiley & Sons, Inc., 2011.

127. L. Bakueva, G. Konstantatos, S. Musikhin, H. E. Ruda, and A. Shik, "Negative Capacitance in Polymer-Nanocrystal Composites," *Applied Physics Letters*, 85[16] 3567-69 (2004).

128. G. B. Parravicini, A. Stella, M. C. Ungureanu, and R. Kofman, "Low-Frequency Negative Capacitance Effect in Systems of Metallic Nanoparticles Embedded in Dielectric Matrix," *Applied Physics Letters*, 85[2] 302-04 (2004).

129. M. Ershov, H. C. Liu, L. Li, M. Buchanan, Z. R. Wasilewski, and A. K. Jonscher, "Negative Capacitance Effect in Semiconductor Devices," *Electron Devices, IEEE Transactions*, 45[10] 2196-206 (1998).

130. B. S. Doyle, "Anomalous Low-Frequency Resonance-Type Behaviour and Negative Capacitance in Doped Glasses," *Journal of Physics D: Applied Physics*, 19[6] 1129 (1986).

131. W. Cao and R. Gerhardt, "Calculation of Various Relaxation Times and Conductivity for A Single Dielectric Relaxation Process," *Solid State Ionics*, 42[3–4] 213-21 (1990).

132. I. M. Hodge, M. D. Ingram, and A. R. West, "Impedance and Modulus Spectroscopy of Polycrystalline Solid Electrolytes," *Journal of Electroanalytical Chemistry*, 74[2] 125-43 (1976).

133. L. Ramond, G. Bernard-Granger, A. Addad, and C. Guizard, "Sintering of Soda-Lime Glass Microspheres Using Spark Plasma Sintering," *Journal of the American Ceramic Society*, 94[9] 2926-32 (2011).